The role of steroid hormones, GREB1, and reproductive status in ovarian cancer progression

Kendra M. Hodgkinson

Department of Cellular and Molecular Medicine
University of Ottawa
Ottawa, Ontario, Canada

This thesis is submitted to the Faculty of Graduate and Postdoctoral Studies as a partial fulfillment of the Ph.D. program in Cellular and Molecular Medicine.

Authorization and contributions

Published data, reproduced with permission:
Hodgkinson KM and Vanderhyden BC. 2014. Consideration of GREB1 as a potential therapeutic target for hormone-responsive or endocrine-resistant cancers. *Expert Opin Ther Targets* 18(9):1065-76.
(Figures 1 and 2)

Laviolette LA, Hodgkinson KM, Minhas N, Perez-Iratxeta C, Vanderhyden BC. 2014. 17beta-estradiol upregulates GREB1 and accelerates ovarian tumor progression in vivo *Int J Cancer* 135(5):1072-84.
(Figures 5-7, 10AB, 18, 25AB, 36A, 37, 40, 41, 43AC, 48, 56A)

Contributions by students under supervision of K. Hodgkinson:
L. Forrest: Figure 46B
S. Scaffidi Argentina: Figures 47-48
P. Charette: Figures 18 (*Kdr*, *Ednra* only), 19-24

Contributions by others:
Dr. K. Garson: Figures 4, 50C
L. Laviolette: Figures 10AB, 25A, 43C
N. Vuong: Figures 11B-D, 25C, 42A
O. Collins: Figures 35A, 36B,D

Abstract

Estrogenic hormone replacement therapy increases the risk of developing ovarian cancer, and 17-β estradiol accelerates tumour growth in mouse models of this disease. One possible mediator of estrogen action is Growth Regulation by Estrogen in Breast Cancer 1 (GREB1), an estrogen receptor alpha (ESR1)-upregulated protein. GREB1 is required for hormone-driven proliferation of several breast and prostate cancer cell lines, but its role in tumour progression is unknown and its mechanism of action remains unclear. To determine the role of GREB1 in ovarian cancer, its expression and function were examined in ovarian cancer cell lines and mouse models. GREB1 was upregulated by estradiol, and overexpression and/or knockdown of GREB1 showed that GREB1 promotes proliferation and migration in ovarian cancer cells. GREB1 knockdown also slowed tumour growth and prolonged survival in mice engrafted with ovarian cancer cells. GREB1 expression was detected in human ovarian tumours of all major histotypes, with moderate to strong expression in 75-85% of serous, endometrioid, mucinous, and clear cell carcinomas. GREB1 mRNA levels correlated with ESR1 transcripts, but protein levels of GREB1 and ESR1 did not show a correlation in tumours. Serous, endometrioid and mucinous ovarian cancers were almost always positive for either ESR1 or GREB1 (59/60 tumours), which may imply a dependence on estrogen signalling pathways. GREB1 expression in normal tissues is mainly confined to the reproductive tract, suggesting that it may be useful as a diagnostic biomarker. GREB1 combined with PAX8 showed high efficacy in differentiating mucinous tumours of gastrointestinal vs. ovarian origin. Targeting GREB1 may inhibit tumour-promoting pathways downstream of ESR1 and could therefore prove more effective than current anti-estrogen therapies.

Table of Contents

List of Tables

List of Figures

List of abbreviations

°C	degrees Celsius
α-MEM	alpha minimum essential medium
ACTB	beta actin
AdCre	adenovirus expressing Cre recombinase
AIP	aryl hydrocarbon receptor interacting protein
AKT	v-akt murine thymoma viral oncogene homolog 1 (aka AKT1)
AMHR2	anti-Mullerian hormone receptor type II
ANOVA	analysis of variance
AR	androgen receptor
ARID1A	AT-rich interaction domain 1A
B6	C57BL/6N mouse strain
BCL2	B-cell CLL/lymphoma 2
bp	base pair(s)
BMP7	bone morphogenetic protein 7
BRCA	BRCA1 and/or BRCA2
BRCA1	breast cancer 1
BRCA2	breast cancer 2
CA125	cancer antigen 125
CAG	cytomegalovirus early enhancer and chicken beta-actin
CAG-TAg	tgCAG-LS-TAg transgenic mouse model of ovarian cancer
CAMK2N1	calcium/calmodulin-dependent protein kinase II inhibitor 1
CCDN1	cyclin D1
CD31	platelet/endothelial cell adhesion molecule 1 (aka PECAM1)
cDNA	complementary DNA
CDH1	E-cadherin
CDH2	N-cadherin
cDNA	complimentary DNA
CHD1	chromodomain helicase DNA binding protein 1
CMV	cytomegalovirus
COL1A2	collagen type I alpha 2
CREB	cAMP response element-binding
CREBBP	CREB binding protein, aka CBP
CRISPR	clustered regularly-interspaced short palindromic repeats
CSS	charcoal-stripped serum
CTNNB1	catenin beta 1
CYP	cytochrome P450 family
CYP11A1	cytochrome P450 family 11 subfamily A member 1
CYP1A1	cytochrome P450 family 1 subfamily A member 1
CYP1A2	cytochrome P450 family 1 subfamily A member 2
CYP1B1	cytochrome P450 family 1 subfamily B member 1
DAB	diaminobenzidine
DAPI	4',6-diamidino-2-phenylindole
DICER1	dicer 1 ribonuclease III
DMBA	7,12-dimethylbenz[a]anthracene

DMEM/F12	Dulbecco's Modified Eagle Medium: Nutrient Mixture F-12
DNA	deoxyribonucleic acid
DSC2	desmocollin 2
E2	17β-estradiol
EBI	European Bioinformatics Institute
EDN1	endothelin 1
EDNRA	endothelin receptor type A
EMBL	European Molecular Biology Laboratory
EMT	epithelial-to-mesenchymal transition
EOC	epithelial ovarian cancer(s)
EP300	E1A binding protein p300, aka p300
ER	estrogen receptor(s)
ERBB2	erb-b2 receptor tyrosine kinase 2 (aka HER2)
ERK	extracellular signal-regulated kinase family (aka MAPK1)
ESR1	estrogen receptor 1 (aka alpha)
ESR2	estrogen receptor 2 (aka beta)
ERE	estrogen response element(s)
FACS	fluorescence-activated cell sorting
FBS	fetal bovine serum
FGF7	fibroblast growth factor 7
fl/fl	both alleles floxed
floxed	flanked by loxP sites
FSH	follicle stimulating hormone
FSHR	follicle stimulating hormone receptor
FTE	fallopian tube epithelium
GAPDH	glyceraldehyde-3-phosphate dehydrogenase
GATA3	GATA binding protein 3, aka globin transcription factor
GFP	green fluorescent protein
GNG11	guanine nucleotide binding protein (G protein), gamma 11
GO	gene ontology
GPER1	G protein-coupled receptor 1 (aka GPR30)
GREB1	growth regulation by estrogen in breast cancer 1
GTEx	Genotype-Tissue Expression
H&E	hemotoxylin and eosin
h	hours
HIF1A	hypoxia inducible factor 1 alpha subunit
hOSE	human OSE
HRT	hormone replacement therapy
ICC	immunocytochemistry
IGFBP4	insulin like growth factor binding protein 4
IHC	immunohistochemistry
IL6	interleukin 6
i.b.	intrabursal
i.p.	intraperitoneal
JAK2	Janus kinase 2
JNK	c-Jun N-terminal kinase (aka MAPK8)

KDR	vascular endothelial growth factor receptor 2
Ki67	marker of proliferation Ki-67, aka MKI67
KPNA2	karyopherin subunit alpha 2
KRAS	v-Ki-ras2 Kirsten rat sarcoma viral oncogene homolog
KRT7	keratin 7
KRT19	keratin 19
LH	luteinizing hormone
LHR	luteinizing hormone receptor
LIV-1	solute carrier family 39 member 6 (aka SLC39A6)
logFC	logarithmic fold change
LoxP	locus of X-over P1
LS	Lox-stopped (stop sequence flanked by loxP sites)
M	molar
min	minute(s)
MAPK	mitogen-activated protein kinase(s)
MAS	mouse ascites-derived ovarian cancer cell line
MASE	MAS line derived from an E2-treated mouse
MASEL	MAS line derived from a low-dose E2-treated mouse
MASC	MAS line derived from a control mouse
MASP	MAS line derived from a P4-treated mouse
MEK	mitogen-activated protein kinase kinase (aka MAP2K) family
MEM	minimum essential media
MF	mifepristone
miRNA	micro RNA
MISIIR	Mullerian inhibitory substance type II receptor
MMP9	matrix metallopeptidase 9
mOSE	mouse ovarian surface epithelium
MPP	methyl-piperidino-pyrazole
mRNA	messenger RNA
MTU	mouse tumour-derived ovarian cancer cell line
MTUE	MTU line derived from an E2-treated mouse
MTUEL	MTU line derived from a low-dose E2-treated mouse
MTUC	MTU line derived from a control mouse
MYB	v-myb avian myeloblastosis viral oncogene homolog
MYBBP1A	MYB binding protein (P160) 1a
MYC	v-myc avian myelocytomatosis viral oncogene homolog
NCBI	National Center for Biotechnology Information
NCoR	nuclear receptor co-repressor
NOTCH1	notch 1
OCP	oral contraceptive pills
OSE	ovarian surface epithelium
OVX	ovariectomized
OVGP1	oviductal glycoprotein 1
P4	progesterone
PARP	poly(ADP-ribose) polymerase family
PAX8	paired box 8

PBS	phosphate-buffered saline
PCR	polymerase chain reaction
PDX	patient-derived xenograft
PGR	progesterone receptor
PI3K	phosphoinositide-3-kinase(s)
PPIA	peptidylprolyl isomerase A
PTEN	phosphatase and tensin homolog
QPCR	quantitative reverse transcriptase polymerase chain reaction
RB1	retinoblastoma 1 (aka RB)
RIA	radioimmunoassay
RNA	ribonucleic acid
RT-PCR	reverse transcription polymerase chain reaction
s.c.	subcutaneous
SCID	severe combined immunodeficiency
SDF1	stromal-cell derived factor 1
SEM	standard error of the mean
siRNA	short interfering RNA
shRNA	short hairpin RNA
SNAI1	snail family zinc finger 1
SRC1	steroid receptor coactivator 1
STAT3	signal transducer and activator of transcription 3
STC2	stanniocalcin 2
STIC	serous tubal intraepithelial carcinoma
SV40	Simian vacuolating virus 40
TAF4B	TATA-box binding protein associated factor 4b
TAg	SV40 large and small T-antigens
TCF4	transcription factor 4
TCGA	The Cancer Genome Atlas
TMA	tissue microarray
TP53	tumour protein p53
VCD	4-vinylcyclohexene diepoxide
VEGFA	vascular endothelial growth factor A (aka VEGF)
vs.	versus
wt/wt	both alleles wildtype

Acknowledgements

I would like to thank everyone who has helped me successfully complete (and enjoy!) my graduate studies. Above all, I am very grateful to have had such a fantastic supervisor, Dr. Barbara Vanderhyden. She puts an impressive amount of energy every day into mentoring her students, and helps us become the best scientists we possibly can be. Her scientific guidance, personal encouragement, and life wisdom have contributed immeasurably to my success in this program and I can't imagine where I would be today without all her help. She has also put together an amazing research team, including Dr. Ken Garson, Olga Collins, and Elizabeth Macdonald, who have all taught me so much about science and life. Ken's expertise was critical for getting the lentiviral constructs functioning properly, and my mouse experiments were made much easier by all of Liz's hard work maintaining our mouse colonies. I am also grateful to Olga for all her advice about cell culture issues and help with last-minute experiments.

I would like to thank my graduate student friends in the Vanderhyden lab and elsewhere for all your help, including teaching me new techniques, thoughtfully critiquing my results, and helping me relax and stay sane. Special thanks to Laura Laviolette, who set the stage for my research project with her own doctoral research and whose advice greatly contributed to my success at the start of my graduate studies.

I would like to thank all of my other collaborators, including Dr. Carolina Perez-Iratxeta (microarray analysis), Dr. Bojana Djordjevic (histology analysis), Rose Vuong (ChIP experiment), Pascale Charette (angiogenesis data), Sarina Scaffidi Argentina (GREB1 induction by E2 in human cell lines), Laura Forrest (*Greb1* induction by E2 in ESR1-deleted cells), and Olga Collins (colony formation). I am also grateful to my thesis advisory committee, Drs. McKay, Pratt and Tsang, for all of their thoughtful comments, constructive criticism and advice, and to the animal care staff at the University of Ottawa for all their assistance and advice on my mouse studies.

Finally, I have to thank my friends and family for all of their support and encouragement that helped me persist when things got the hardest. Special thanks to Marc for helping me stay motivated, listening patiently to my endless complaining, and always believing in me.

Chapter 1: Introduction

1.1: Ovarian cancer overview

1.1.1. Disease characteristics and treatment

Ovarian cancer is the fifth highest cause of cancer mortality in Canadian women, despite a relatively low incidence (2800 diagnosed per year; Canadian Cancer Statistics 2015). This high mortality is often attributed to delayed diagnosis; 75% of patients are diagnosed at advanced stages, suggesting that many ovarian cancers grow undetected for a long time (Ebell et al. 2016). Warning signs of ovarian cancer are subtle and include appetite loss, an abdominal mass, distension, pain or bloating; notably, many ovarian cancers show few or none of these symptoms (Ebell et al. 2016). CA125 and ultrasounds have shown some utility as a diagnostic aid, but no screening methods have yet altered ovarian cancer mortality (Sundar et al. 2015).

First-line treatment for ovarian cancer has remained unchanged for many years: cytoreductive surgery followed by paclitaxel and carboplatin chemotherapy (Kampan et al. 2015). Many ovarian cancers initially respond well, but resistance develops rapidly leading to aggressively metastatic disease with no effective second-line therapies (Kampan et al. 2015). Genetic instability and heterogeneity are very high in ovarian cancer (Blagden 2015), increasing resistance to cancer therapies. Targeted therapies are particularly impaired by this heterogeneity; only two have been approved for ovarian cancer. Bevacizumab targets angiogenesis by inhibiting VEGFA (also known as VEGF) and has shown modest efficacy for some patients, in combination with conventional chemotherapies. However, further research is needed to predict sensitive tumours

(Symeonides and Gourley 2015). Olaparib is the only therapy targeting a subtype of ovarian cancer: BRCA-deficient high-grade serous ovarian tumours (Walsh 2015). These cancers are already more sensitive to DNA-damaging chemotherapies due to faulty mechanisms for repairing double-stranded DNA breaks (Pennington et al. 2014). Olaparib exploits this weakness by inhibiting PARP, which recruits repair enzymes for single-strand DNA breaks. This forces cancer cells to accumulate DNA damage or use faulty mechanisms for DNA repair, resulting in synthetic lethality (Walsh 2015).

1.1.2. Ovarian cancer histological subtypes and genetics

Most research on ovarian cancer focuses on epithelial tumours, which account for more than 95% of all ovarian cancers. Epithelial ovarian cancers (EOC) are divided into five subtypes (low-grade serous, high-grade serous, endometrioid, mucinous, and clear cell), which have distinct histology, molecular profiles, and disease characteristics. High-grade serous tumours almost always have *TP53* mutations and many also have germline or sporadic *BRCA* deficiencies; the other four subtypes rarely have mutated *TP53*, and instead frequently have mutations in *BRAF/KRAS* (low-grade serous), *CTNNB1/PTEN/ARID1A* (endometrioid), *KRAS/ERBB2* (mucinous), or *ARID1A* (clear cell; Shih and Kurman 2011, Mungenast et al. 2014). These histological subtypes are often grouped into slow-growing, genetically stable type I tumours and aggressive, genetically unstable type II tumours (Shih and Kurman 2004, Kurman and Shih 2011). Type I tumours include low-grade serous, endometrioid, mucinous and clear cell subtypes, whereas type II tumours are high-grade serous tumours, which comprise the majority of EOC (Shih and Kurman 2004). However, some argue that grouping four histological subtypes together as "Type I" is misleading due to large differences in

genetics and disease characteristics (Prat 2012). Type II tumours can be further divided into 4 molecular subtypes: immunoreactive, differentiated, proliferative, and mesenchymal (Tothill et al. 2008, Cancer Genome Atlas Research Network 2011), which have shown some prognostic differences (Konecny et al. 2014). However, the clinical utility of these subtypes is currently limited by the lack of effective alternatives to conventional therapy.

1.1.3. Tissues of origin and preneoplastic lesions

The tissues of EOC origin remain controversial because EOC subtypes resemble various Müllerian tissues despite seemingly arising in the ovary. The ovarian surface epithelium (OSE) has long been believed to be the source of EOC, but recent evidence suggests alternative origins including mislocalized uterine tissue (endometriosis) and fallopian tube epithelium (FTE; Lim and Oliva 2013). Moreover, metastatic mucinous EOC is often difficult to distinguish from metastatic gastrointestinal cancers due to similar histology and disease characteristics (Lim and Oliva 2013). However, like other EOC subtypes, mucinous cancers are sometimes diagnosed when still confined to the ovary, suggesting that at least some of these cancers arise from the ovary.

Endometriosis-derived preneoplastic lesions on the ovary have been linked to endometrioid and clear cell EOC subtypes, which show a strong histological similarity to uterine endometrial cancers (Lim and Oliva 2013). Molecular evidence indicates that these lesions progress to EOC through activation of oncogenes such as *KRAS* and inactivation of tumour suppressor genes including *PTEN* and *ARID1A* (Anglesio et al. 2015). However, only 20-40% of endometrioid EOC and 30-70% of clear cell EOC

tumours are accompanied by endometriosis (Lim and Oliva 2013), suggesting that some have a different origin.

OSE preneoplastic lesions (including stratification, hyperplasia, pleomorphism, invaginations, and inclusion cysts) have been observed adjacent to EOC, in contralateral ovaries of stage I EOC patients, and in prophylactically-removed ovaries from *BRCA* mutation carriers (Plaxe et al. 1990, Salazar et al. 1996, Chene et al. 2009, Chene et al. 2014). Similarly, ovaries from women with a high genetic risk of EOC showed higher OSE proliferation, TP53 expression, and dysplasia scores relative to normal controls (Schlosshauer et al. 2003).

Systemic examination of prophylactically-removed fallopian tubes from high-risk women began after full serial sectioning revealed neoplastic lesions in up to 10% of these tissues (Colgan et al. 2001, Leeper et al. 2002). Larger follow-up studies have confirmed that occult invasive cancers or serous tubal intraepithelial carcinomas (STICs) are present in 2-10% of fallopian tube fimbria from *BRCA* mutation carriers (Powell et al. 2005, Medeiros et al. 2006, Finch et al. 2006, Callahan et al. 2007, Reitsma et al. 2013, Wethington et al. 2013). Recent initiatives to examine fallopian tubes removed for all benign reasons have also revealed STICs in a low percentage (<1%) of women without *BRCA* mutations or other significant risk factors (Wethington et al. 2013, Rabban et al. 2014, Seidman et al. 2015). STICs are characterized by abnormal morphology, rapid proliferation, and TP53 expression (Lim and Oliva 2013) and are present in 30-50% of EOC patients (Chene et al. 2014). This suggests that roughly half of EOCs originate in the fallopian tube. Next-generation sequencing has shown that STICs are frequently clonally related to an associated high-grade serous EOC, but also revealed one case where a STIC was actually a micrometastasis from a primary uterine carcinoma

(McDaniel et al. 2015). This suggests that some STICs coinciding with EOC could be metastases from a tumour originating in the ovary.

While the current evidence indicates that EOC can develop from FTE and endometriotic lesions, there is still debate whether the OSE is also a tissue of origin. Some researchers believe that the FTE is the source of all high-grade serous or even all EOC subtypes, through fallopian tissue "sloughing" and transplanting to the ovary (Kurman and Shih 2011, Wang et al. 2015). However, there is substantial experimental evidence for the OSE as an additional tissue of origin, including spontaneous OSE transformation and mouse models displaying preneoplastic lesions and cancers closely resembling EOC (see section 1.2.3).

1.2: Models of epithelial ovarian cancer

1.2.1. Cell models of ovarian cancer

Dozens of EOC cell lines have been isolated from tumours or ascites fluid, but published studies overwhelmingly focus on the NIH:OVCAR-3 (also known as OVCAR3, OVCAR-3; Hamilton et al. 1983), SK-OV-3 (also known as SKOV3, SKOV-3), and A2780 cell lines (Domcke et al. 2013). OVCAR-3 cells most resemble high-grade serous cancers, with mutated *TP53* and high copy number variation; SKOV3 and A2780 are most likely Type I cancers, but their precise histological origin is unclear (Domcke et al. 2013). A less frequently used cell line, OVCA 432 (also known as OV432, OVCA432; Bast et al. 1981), also closely resembles high-grade serous EOC, based on TP53 status and molecular profiling (Domcke et al. 2013, Bourgeois et al. 2015). OVCAR-3 and OVCA 432 cells express receptors for estrogen, androgen, and

progesterone (Hamilton et al. 1983, Lau et al. 1999). Notably, recent drives to authenticate cell line identities using short tandem repeat profiling have revealed alarmingly frequent misidentification (Hughes et al. 2007). A screen of 51 EOC cell lines revealed that 10 were misidentified, including the commonly used OV2008 and BG-1 lines (ME-180 and MCF7 cervical and breast cancer cells, respectively; Korch et al. 2012). Therefore, experimental data from OV2008 and BG-1 are not included in this review.

Cancer cell lines cultured in vitro have many critical differences from primary tumours. Some factors, such as hypoxia, three-dimensional growth, and influences from other cell types or extracellular matrix, can be modelled in vitro but are routinely ignored for simplicity. More complex interactions such as angiogenesis, immune response, and metastasis are not possible to accurately model in vitro. Furthermore, intratumoural heterogeneity makes it difficult to isolate a representative cell line, and genetic drift and selection pressure associated with extended passaging induce many molecular changes (Goodspeed et al. 2016). Therefore, cell culture experiments require confirmation in more accurate models.

1.2.2. Xenograft and PDX models

Cell line xenograft models, where immune-deficient mice are injected with cancer cells, are the most common way to model cancer growth in vivo due to their relative ease and low cost. EOC xenografts are typically intraperitoneal (i.p.) injections to model cancer dissemination throughout the peritoneal cavity as in advanced EOC. Subcutaneous (s.c.) injections can also be used to facilitate monitoring of tumour volume, and intrabursal (i.b.) injections can be used to model disease dissemination from a localized

ovarian tumour. For these orthotopic injections, the ovaries are surgically exposed and cells are injected into the space between the bursal membrane and the ovary. Xenograft models have been characterized for many EOC lines, including transformed OSE and FTE (Shaw et al. 2004, Zheng et al. 2010, Jazaeri et al. 2011, McCloskey et al. 2014).

Patient-derived xenograft (PDX) models are becoming increasingly popular as evidence accumulates that the molecular profile of the original tumour is recapitulated far more accurately in PDX models than in cell line xenografts (Boone et al. 2015). In PDX models, primary tumours or ascites are isolated and immediately implanted into immune-deficient mice, then expanded with serial passages in mice and frozen to generate a "living tumour bank" (Boone et al. 2015, Weroha et al. 2014, Pepin et al. 2015). Extensive validation has confirmed that histology, proliferative index, genetic profile, intratumour heterogeneity, and chemoresistance closely resemble the primary tumours (Weroha et al. 2014). Although it remains unclear whether PDX models have high predictive value for unrelated patients, the genetic profiles of high-grade serous PDX tumours closely resemble tumours in The Cancer Genome Atlas (TCGA; Weroha et al. 2014).

Cell line xenografts remain useful for preliminary studies but share many of the drawbacks of cell lines, including major genetic differences from primary tumours. PDX models are far more histologically and genetically accurate, but are difficult and expensive to generate, validate, and maintain. The accuracy of all xenograft models is restricted by the impaired immune system, which can significantly alter tumour growth and response to treatment (Cekanova et al. 2014). Species differences between the tumour and host may also affect blood vessel formation and microenvironment interactions, resulting in altered tumour growth. Immune reactions can be modelled in

xenografts with "humanized" mice, which develop human immune components (Rongvaux et al. 2014). However, xenograft models are incapable of modelling transformation or early tumour growth because tumours develop from fully transformed cancer cells rather than progressing gradually in situ.

1.2.3. Syngeneic and spontaneous models

Allograft models are similar to xenograft models but have one notable difference: the injected cancer cells are murine, derived from mouse OSE (mOSE) or transgenic mouse models. Mouse cancer cells can often be injected into mice sharing the same genetic background, allowing a normal immune response and species-consistent interactions with the microenvironment. Several allograft mouse models of ovarian cancer have been characterized (Roby et al. 2000; Laviolette et al. 2010, McCloskey et al. 2014, Szabova et al. 2014). These models are useful for examining syngeneic tumour growth, but share the other limitations of xenograft models.

Many transgenic models of ovarian cancer have been developed by inducing mutations in the OSE. Models for endometrioid (Dinulescu et al. 2005, Wu et al. 2007), low-grade serous (Mullany et al. 2011), and high-grade serous EOC (Szabova et al. 2012), show progression from precursor OSE lesions to metastatic cancer with significant histological and genetic similarity to the human disease. Three of these models use i.b. injections of adenovirus expressing Cre recombinase (AdCre) to induce genetic changes specifically in the OSE. Another useful model based on i.b. AdCre is the tgCAG-LS-TAg (CAG-TAg) mouse, which forms estrogen-responsive tumours with mixed histology and disease progression resembling human EOC (Laviolette et al. 2010). Tumours are driven by the oncogene TAg (SV40 T-antigen), which induces transformation by inhibiting

TP53 and RB1 (Pipas 2009). Many other models of OSE-derived cancer have been developed, with most including alterations of *Tp53* and at least one other gene (Orsulic et al. 2002, Flesken-Nikitin et al. 2003, Xing and Orsulic 2006, Tirodkar et al. 2014).

As evidence accumulates that the majority of high-grade serous "ovarian" cancers likely originate in the FTE (Kurman and Shih 2011), additional transgenic mouse models have been developed targeting the oviductal epithelium. *Pten* and *Dicer1* deletion via *Amhr2-Cre* induced high-grade serous tumours that originated in the oviduct (Kim et al. 2012). However, these tumours arose in the stroma rather than the epithelium, and did not follow the transformation process believed to result in high-grade serous EOC in humans (Kim et al. 2012). A more accurate model used *Pax8-Cre* to delete *Pten* and *Tp53* in secretory FTE cells; 4/6 mice developed oviduct lesions resembling STICs by 40 weeks (Perets et al. 2013). When *Brca1* or *Brca2* was also deleted, the mice formed aggressive metastatic tumours that closely resembled high-grade serous EOC both histologically and genetically (Perets et al. 2013). Notably, the majority of these tumours appeared in the ovary with an apparently normal oviduct, but salpingectomy prevented tumour development (Perets et al. 2013). *Ovgp1*-driven TAg expression in the oviducts also induces high-grade serous tumours and STIC-like lesions (Sherman-Baust et al. 2014).

Unlike most animals, hens predictably develop spontaneous ovarian tumours due to their very high ovulation frequency (Johnson and Giles 2013). These tumours recapitulate all histological subtypes of EOC, have similar mutations including changes in *TP53* and *KRAS*, and are often seen with ascites and widespread metastasis (Johnson and Giles 2013). This model has been useful to study the early stages of tumourigenesis and to test preventative strategies such as flax seed supplementation (Hales et al. 2014).

Mouse models are limited by their lack of spontaneous EOC and the rapid progression of oncogene-driven models. This decreases tumour heterogeneity and limits the extent to which transgenic models can be used to examine cancer prevention and early disease progression. Many transgenic models also initiate tumours in juvenile or even fetal mice, whose ovaries are very different structurally and hormonally from the human perimenopausal ovary. Hen models overcome these problems, but have additional challenges. Reagents, cell culture and transgenic techniques are very limited for chickens relative to mouse models, and large numbers of hens must be maintained for several years to generate an adequate sample size of spontaneous tumours (Johnson and Giles 2013). Furthermore, genetics are a limitation of all animal models; even the minority with highly genetically similar tumours are likely to have some functional changes caused by species-specific differences in gene function.

Although all cell and animal models of EOC have flaws, each model also has well-defined uses. Cell lines are invaluable for basic research exploring molecular mechanisms of cancer growth and identifying potential therapeutic targets. Genetically manipulated cell lines can be used for xenograft models to confirm that results seen in cell experiments are also applicable in vivo. PDX models are critical for testing new therapeutic targets in tumours with high genetic similarity to human EOC. Syngeneic mouse and hen models are useful for exploring early events in EOC, testing preventative strategies, determining the relative contribution of various mutations, and elucidating signalling pathways and therapy efficacy in an immunocompetent setting.

1.3: Drivers of ovarian tumourigenesis

1.3.1. Hormone-related risk factors and prevention

Oral contraceptive pills (OCP) containing synthetic estrogen and progestins have a well-defined protective effect, reducing the risk of EOC by 4-5% per year of use with a maximum effect after approximately 10 years (Collaborative Group on Epidemiological Studies of Ovarian Cancer 2008, Braem et al. 2010). Pregnancy also has a clear protective effect, with the first child decreasing the EOC risk by 10-40% (Whittemore et al. 1992, Braem et al. 2010). The impact of breastfeeding is more subtle, but many studies show a protective effect; breastfeeding decreases the risk of EOC by about 5-25% relative to other parous women (Whittemore et al. 1992, Luan et al. 2013, Schuler et al. 2013).

Infertility and the associated fertility treatments have been linked to EOC, but reports are inconsistent. Currently available data do not indicate a harmful effect but are insufficient to rule one out (Ness et al. 2002, Whittemore et al. 1992; Diergaarde et al. 2014). Similarly inconsistent and limited data links EOC to polycystic ovarian syndrome, which can cause infertility. A recent meta-analysis showed that polycystic ovarian syndrome did not increase risk overall, but increased risk 2-fold when women over 54 were excluded, suggesting a higher risk for premenopausal women (Barry et al. 2014). However, these data should not be considered conclusive due to a low sample size. Endometriosis, which can also cause infertility, increases the risk of endometrioid and clear cell EOC (Kim et al. 2014).

Most women with EOC are diagnosed after menopause, with incidence closely following the sharp rise in gonadotropins (Chakravarti et al. 1976, Choi et al. 2007). Increased gonadotropin levels and other changes associated with menopause have been proposed to trigger EOC growth (Salehi et al. 2008). Estrogenic hormone replacement

therapy (HRT) after menopause increases the risk of EOC by approximately 20-40% depending on duration of use and time since stopping HRT (Pearce et al. 2009; Collaborative Group on Epidemiological Studies of Ovarian Cancer 2015). It is unclear whether estrogen promotes transformation or simply accelerates the growth of existing tumours; both mechanisms have been demonstrated in EOC cell lines and mouse models (see section 1.4).

1.3.2. Mechanisms of hormonal risk factors

Ovarian tumourigenesis was long believed to be triggered by physical damage from ovulatory wounding and the associated hormone-induced OSE proliferation (Fathalla 1971, Cramer and Welch 1983). Extended proliferation of murine OSE through repeated passaging can lead to spontaneous transformation (Godwin et al. 1992, Roby et al. 2000, McCloskey et al. 2014). However, these mechanisms do not explain FTE transformation, so the "incessant menstruation" theory was developed, where high iron from retrograde menstruation causes oxidative stress in FTE (Vercellini et al. 2011). Ovulation is also associated with inflammation, which promotes EOC tumourigenesis through oxidative stress that could affect both the OSE and the fimbrial FTE (Ness and Cottreau 1999, Modugno et al. 2003). These interconnected mechanisms are difficult to evaluate separately, but it is clear that reproductive cycles are a major risk factor.

Follicle depletion has also been proposed to promote EOC (Salehi et al. 2008), although follicle depletion increases gonadotropin levels due to decreased negative feedback and the relative risk effects are therefore difficult to distinguish. Follicle depletion and other structural changes associated with menopause could alter the ovarian response to exogenous hormones, explaining the differential response to estrogenic OCP

pre-menopause and estrogenic HRT post-menopause (Salehi et al. 2008). The physiological importance of the follicle-depleted postmenopausal ovary can be investigated using the VCD (4-vinylcyclohexene diepoxide) chemical model of menopause. VCD injections induce follicle depletion by accelerating atresia (Kappeler and Hoyer 2012). The resulting premature ovarian failure decreases serum estrogen levels, increases serum gonadotropin levels, and decreases ovary size, closely paralleling menopause in humans (Lohff et al. 2005). In the CAG-TAg model, treatment with VCD alters tumour histology but not survival time; notably, the combined effect of exogenous hormones (simulating HRT) was not examined in this study (Laviolette et al. 2010).

Gonadotropins are increased by menopause, fertility treatments, and ovulation, but lowered by pregnancy and OCP use (Salehi et al. 2008). Luteinizing hormone (LH) and follicle-stimulating hormone (FSH) have been suggested to promote EOC by stimulating OSE proliferation (Cramer and Welch 1983, Choi et al. 2007). LH and FSH receptors are expressed in OSE cells and in some EOC tumours and cell lines (Zheng et al. 1996, Parrott et al. 2001, Lu et al. 2000). Gonadotropin levels in ovarian cysts are higher when malignant tissue is present, although serum levels show no consistent changes (Kramer et al. 1998, Choi et al. 2007). Gonadotropin treatment or overexpression stimulate proliferation, migration and/or invasion of many OSE and EOC cell lines and stimulate OSE proliferation in many animal models (Choi et al. 2007). OSE dysplasia and inclusion cysts were observed after long-term gonadotropin treatment (Celik et al. 2004). Furthermore, gonadotropin treatment increased the severity of rat ovarian lesions in a chemical model of ovarian cancer (Stewart et al. 2004).

Estrogen promotes tumourigenesis and growth of several cancers including breast, endometrial, and ovarian. The nuclear receptor ESR1 (also known as ERα, ER)

mediates the majority of estrogen-stimulated proliferation and tumour progression in hormone-responsive cancers (Ribeiro et al. 2014). The G-protein coupled estrogen receptor GPER1 (also known as GPER, GPR30) also promotes tumour growth, whereas another nuclear receptor, ESR2 (also known as ERβ), has a protective effect, antagonizing the effects of ESR1 and GPER1 (Bossard et al. 2012, Ribeiro et al. 2014). Local 17β-estradiol (E2) production occurs in many breast, endometrial and ovarian cancers, faciliating E2-driven growth even with very low circulating E2 levels (Mungenast and Thalhammer 2014). Therefore, the higher serum E2 levels observed in some EOC patients could be either a cause or effect of the cancer (Kirilovas et al. 2007). ESR1 expression does not correlate with clinical outcome of EOC patients; however, a better prognosis was seen with PGR expression, which antagonizes ESR1 signalling (Jönsson et al. 2015). Antiestrogen therapy has limited efficacy in EOC, although some patients have responded (Ribeiro et al. 2014).

Gonadotropins induce ovulation and E2 production, making it difficult to distinguish the relative effects of these risk factors. E2 production and an associated increase in proliferation have been observed in OVCAR-3 cells following gonadotropin treatment (Kraemer et al. 2001), suggesting that some of the observed effects of gonadotropins may actually be an E2 response. However, E2-induced proliferation and gonadotropin-induced proliferation responded differently to a surgical injury mimicking ovulation, implying that the hormones can stimulate proliferation separately (Stewart et al. 2004).

1.3.3. Mechanisms of hormonal protective factors

Ovulation suppression is seen with all of the major protective factors (pregnancy, breastfeeding, OCP). Menstruation is reduced or eliminated by the same protective factors, so this also supports the incessant menstruation theory of tumourigenesis. However, the risk reduction per year of prevented ovulations varies. An earlier menopause decreases the risk by 2% per year whereas OCP and pregnancy decrease it by 4-5% and 10-40% per year respectively, implying additional protective mechanisms (Collaborative Group on Epidemiological Studies of Ovarian Cancer 2008, Braem et al. 2010, Whittemore et al. 1992).

Progesterone (P4) may be one of those protective mechanisms (Risch 1998). High levels of P4 are produced by the corpus luteum and placenta during pregnancy, and OCP pills contain various progestins. P4 or synthetic progestins reduce proliferation, slow migration, and/or increase apoptosis in OSE, FTE and EOC cells (Bareither and Verhage 1981, Wollenhaupt et al. 2002, Ivarsson et al. 2001, Syed et al. 2001, Syed et al. 2007, Hua et al. 2008). These effects appear to be mediated by downregulating cyclin-dependent kinase and AKT activity and activating TP53 and the caspase 8 pathway (Zhou et al. 2002, Zheng et al. 2007, Hua et al. 2008).

Progestins also increased apoptosis and/or eliminated preneoplastic changes of OSE in animal models (Rodriguez et al. 1998, Gotfredson and Murdoch 2007). In hens, a progestin profoundly reduced spontaneous EOC incidence, although this was likely mediated by ovulation inhibition (Barnes et al. 2002, Treviño et al. 2012). Exogenous progestins inhibited growth of progesterone receptor-expressing (PGR+) but not PGR- EOC cells in one xenograft study (Langdon et al. 1998) but have shown little effect in other mouse models (Sawada et al. 1990, Armaiz-Pena et al. 2009, Laviolette et al. 2010). One study showed that P4 treatment initiated before xenograft injection reduced

peritoneal dissemination and increased survival whereas P4 treatment of established xenografts had no effect, suggesting that the main protective effect of P4 occurs before tumourigenesis (McDonnel et al. 2005). Surprisingly, the PGR antagonist mifepristone significantly decreased tumour growth of SKOV3 xenografts (Goyeneche et al. 2007).

Adding P4 to a platinum-based chemotherapy regime increased 3-year survival of stage III EOC patients from 42.9 to 85.7% (Chen and Feng 2003), but this has not yielded any approved therapies. Low PGR expression in ovarian tumours is associated with a poor diagnosis and more advanced stages (Ho 2003, Jönsson et al. 2015).

Progestins may have a protective effect by abrogating E2 actions. In FTE, P4 inhibits E2-stimulated proliferation (Oka and Schimke 1969). In SKOV3ip1 and HeyA8 xenograft models, P4 attenuated E2-stimulated tumour growth despite having no effect alone (Armaiz-Pena et al. 2009). Therefore, high progestin levels associated with protective factors such as pregnancy may be preventing the tumour-promoting effects of high E2 levels. Supporting this theory, adding a progestin lowers the risk of EOC relative to estrogen-only HRT (Pearce et al. 2009). Additional experimental studies are badly needed to clarify the interaction between E2 and P4 in ovarian cancer.

1.3.4. Nonhormonal preventative and risk factors

Few lifestyle risk factors for EOC have been identified. Unlike other cancers, ovarian cancer is not clearly linked to diet or exercise, although obesity has shown inconsistent risk increases (Webb 2015). Smoking increases the risk of mucinous EOC (Faber et al. 2013), and perineal use of talcum powder may (Terry et al. 2013) or may not (Houghton et al. 2014) increase the risk of serous, endometrioid and clear cell EOC.

Obstructing the path between the ovaries and the rest of the reproductive tract by tubal ligation, hysterectomy, or similar surgical interventions decreases the risk of EOC by limiting ovarian (and fallopian tube) exposure to carcinogens and/or retrograde menstruation (Green et al. 1997, Cibula et al. 2011, Webb 2015). Salpingectomy was infrequently performed until evidence emerged implicating the fallopian tube as an origin of EOC, but surgeons have recently begun to remove fallopian tubes for women at high risk of EOC and all women undergoing abdominal surgeries as a preventative strategy (Daly et al. 2015). Preliminary studies indicate that salpingectomy has a protective effect (Falconer et al. 2015, Daly et al. 2015), although there is not yet enough long-term data to accurately determine its extent.

BRCA mutations are the predominant genetic risk factor and confer a lifetime EOC risk of 11-60% (George and Shaw 2014). BRCA1 and BRCA2 are critical proteins for repairing double-stranded DNA breaks through homologous recombination (Walsh 2015). Although faulty DNA repair is the main mechanism leading to BRCA-related tumours, it remains unclear why these cancers are limited to hormone-responsive tissues such as breast and ovary; additional tissue-specific mechanisms are likely (George and Shaw 2014). BRCA1 and E2 have a complex interaction in breast cancer; *BRCA1* is induced by E2 and induces transcription of *ESR1* in return, but also inhibits ESR1 signalling (Gorski et al. 2009). Due to their faulty DNA repair, BRCA-deficient tissues would be expected to have increased sensitivity to DNA damage induced by E2. This was confirmed in both BRCA1 and BRCA2-deficient breast epithelial cells, but BRCA1 loss had an additional, unexpected effect: the initial DNA damage was increased (Savage et al. 2014). This was caused by the upregulation of several enzymes catalyzing the formation of genotoxic E2 metabolites (Savage et al. 2014). *BRCA* mutation carriers are

not only more sensitive to the damaging effects of E2, they also have higher serum E2 levels (Widschwendter et al. 2013). This is likely caused by the role of BRCA1 in suppressing aromatase, which catalyzes E2 production from androgens (Hu et al. 2005); prophylactically-removed breast and ovarian tissue from *BRCA1* mutation carriers had high aromatase levels (Chand et al. 2009). This association between BRCA1 and E2 was similarly evident in transgenic mice; *Brca1* deletion in the granulosa cells resulted in higher circulating E2 levels and the development of serous ovarian cystadenomas (Chodanker et al. 2005, Hong et al. 2010).

1.4: Effects of estrogen on epithelial ovarian cancer growth

1.4.1. E2 production and signalling

The ovary is the main source of circulating estrogens in premenopausal women; after menopause, estrogen production shifts to peripheral tissues (Mungenast and Thalhammer 2014). The primary estrogen in premenopausal women, E2, is produced in granulosa cells from androgens produced in the nearby theca cells (Mungenast and Thalhammer 2014). The critical developmental, reproductive, and systemic functions of E2 are mediated through various receptors. Canonical estrogen signalling involves E2 binding to the nuclear receptors ESR1 and ESR2, which dimerize and bind (with various cofactors) to estrogen response element (ERE) sequences in order to drive transcription; the receptors are then degraded by ubiquitination (Welboren et al. 2009). Transcription is regulated by coactivators and corepressors which are highly dependent on tissue type, ligand, and chromatin modifications (Welboren et al. 2009). Many additional noncanonical E2 signalling pathways have been described, including E2-independent

receptor activity, interaction with other transcription factors, and rapid nongenomic activation of MAPK/ERK and PI3K/AKT/MAPK pathways (Welboren et al. 2009, Ribeiro et al. 2014). This noncanonical signalling appears to be mediated by ESR1 and/or GPER1 (Welboren et al. 2009).

1.4.2. E2 effects on ovarian cancer initiation

The ovarian surface and the fallopian tube fimbria are exposed to high endogenous E2 levels after ovulation (Wu et al. 1977). This may promote tumourigenesis by stimulating growth; exogenous E2 treatment in vivo induces OSE proliferation, benign tumours and/or preneoplastic lesions in various small mammal species (Bai et al. 2000, Silva et al. 1998, Stewart et al. 2004, Gotfredson and Murdoch 2007, Perniconi et al. 2008, Laviolette et al. 2010). Surgical injury to the ovary increased the mitogenic actions of E2, suggesting that OSE are particularly sensitive to E2 during ovulation (Stewart et al. 2004. FTE proliferation is also increased by ovulation-associated E2 in many animals (Oka and Schimke 1969, Bareither and Verhage 1981, Wollenhaupt et al. 2002) including primates (Verhage et al. 1990), although not in mice (King et al. 2011). Interestingly, rabbit OSE cells isolated as tissue fragments remained responsive to E2 in vitro, whereas OSE isolated by trypsin digestion did not, suggesting that the stroma plays an important role in E2 response (Bai et al. 2000). While E2-induced proliferation of OSE and FTE has been reported by many studies, some reports are inconsistent (Syed et al. 2001, Wright et al. 2002).

E2 also induces DNA damage after hydroxylation by cytochrome p450 enzymes (particularly CYP1A1, CYP1A2, and CYP1B1) to form catechol estrogens, which can then be converted to quinones (Mungenast and Thalhammer 2014). Quinones react with

DNA to form genotoxic DNA adducts; quinone conversion back to catechol estrogens produces free radicals, causing additional DNA damage (Mungenast and Thalhammer 2014). This process has been shown in mOSE (Symonds et al. 2008) as well as breast epithelial cells (Cavalieri et al. 2006). Higher levels of DNA adducts are found in the urine of EOC patients, who often have activity-increasing polymorphisms in CYP1B1 (Zahid et al. 2014) that increase the risk of EOC (Goodman et al. 2001). Higher CYP1B1 levels were seen in hen ovarian cancers (Zhuge et al. 2009) and human breast cancers (Singh et al. 2005) relative to normal controls, implying that catechol estrogens contribute to both ovarian and breast tumourigenesis.

1.4.3. E2 effects on ovarian cancer growth in vitro

E2 increases proliferation of many EOC cell lines. For at least five cell lines, including OVCA 432 and OVCAR-3, this is mediated by ESR1-dependent activation of the IL6/STAT3 pathway (Syed et al. 2002, Yang et al. 2009, Li et al. 2014). There are also several reports where E2 did not change (Nash et al. 1989, Shi et al. 2008) or decreased OVCAR-3 proliferation (Chao et al. 2013); this discrepancy could be caused by culture differences, cell line misidentification, or other unknown factors. Proliferation was not increased by E2 in SKOV3 cells, which express a mutated ESR1 reported as both functional (Hua et al. 1995) and nonfunctional (Lau et al. 1999). E2 also increased proliferation in ESR1- OVCAR5 cells through GPER1 (Liu et al. 2014), and E2 metabolites increased OVCAR-3 proliferation in an ESR1-independent manner (Li et al. 2014).

E2 decreases apoptosis in transformed OSE by increasing BCL2 (Choi et al. 2001) and in paclitaxel-treated Caov-3 cells by stimulating the AKT/JNK pathway

(Mabuchi et al. 2004). E2 also decreased anoikis in Caov-3 cells through ESR1-dependent PI3K pathway activation (Zheng et al. 2014). In ES-2 and SKOV3 cells, E2 increases migration and invasion through ESR1-independent activation of PI3K/AKT signalling (Hua et al. 2008, Yan et al. 2015). E2 also induced EMT in these cells, shown by morphology, SNAI1 induction and decreased CDH1 (E-cadherin; Ding et al. 2006, Lu et al. 2014). GPER1 mediated E2-stimulated migration and invasion in ESR1- OVCAR5 cells (Yan et al. 2013). Surprisingly, E2 effects on migration, invasion and EMT have not been reported in ESR1+ cell lines.

Ligand-bound ESR1 drives transcription of many tumour-promoting genes in EOC cells, including *MYC*, survivin, cyclins, *HIF1A*, and *BCL2* (Chien et al. 1994, Zhu et al. 2012, Gery et al. 2005, Hua et al. 2008, Hua et al. 2009, Choi et al. 2001). Furthermore, E2 signalling activates many interconnected tumour-promoting pathways, including IL6/STAT3, PI3K/AKT and MAPK/ERK (Ribeiro et al. 2015). In EOC cells, IL6-mediated STAT3 activation promotes cisplatin resistance by preventing apoptosis (Han 2013) and increases resistance to antiestrogen therapy, likely by increasing E2-independent ESR1 signalling (Wang et al. 2014). The PI3K/AKT and MEK/ERK pathways are linked to cell proliferation, survival, metastasis and invasion in EOC and other cancers, and AKT is often overexpressed in EOC (Mabuchi et al. 2015).

1.4.4. E2 effects on ovarian cancer growth in vivo

Acceleration of tumour growth by exogenous E2 has been shown in various ESR1+ EOC xenograft models (SKOV3, SKOV3ip1, HEYA8, PE04, OVA-5 and OVCAR-3; Sawada et al. 1990, Armaiz-Pena et al. 2009, Laviolette et al. 2010, Spillman et al. 2010). ESR1- cell line xenografts are nonresponsive to E2 in vivo (Spillman et al.

2010). Endogenous E2 also promotes tumour growth; SKOV3ip1 xenografts grew faster when they were initiated during proestrus, a high-estrogen phase of the ovulatory cycle (Armaiz-Pena et al. 2009). Furthermore, antiestrogen therapy or ovariectomy slowed the growth of PE04 and OVA-5 xenografts respectively (Sawada et al. 1990, Langdon et al. 1994). In SKOV3 xenografts, VEGFA levels and microvessel density were increased in tumours from mice injected during proestrus, suggesting that enhanced angiogenesis may be partially responsible for the increased growth (Armaiz-Pena et al. 2009). E2 also promoted angiogenesis in ESR1- breast and prostate cancer xenografts, suggesting systemic angiogenic actions (Gupta et al. 2007).

Exogenous E2 also stimulates tumour growth and/or onset in syngeneic models (Lee et al. 1992, Laviolette et al. 2010, Mullany et al. 2014). In CAG-TAg mice, median survival was 50 days with E2 treatment but microscopic ovarian lesions were not detected until 80 days in control mice (Laviolette et al. 2010). In hens, E2 did not alter spontaneous tumour incidence but showed trends for altered stage and histology (Treviño et al. 2012).

1.5: GREB1 expression and function

1.5.1. GREB1 discovery and expression in breast cancer

The gene *KIAA0575* was initially sequenced from human brain tissue (Nagase et al. 1998). *KIAA0575* was renamed "growth regulation by estrogen in breast cancer 1" (*GREB1*) when the first clue about its function was revealed: GREB1 is highly upregulated by E2 in MCF7 breast cancer cells (Ghosh et al. 2000). Three isoforms for human GREB1 have been identified (Figure 1), whereas the mouse homolog has 2

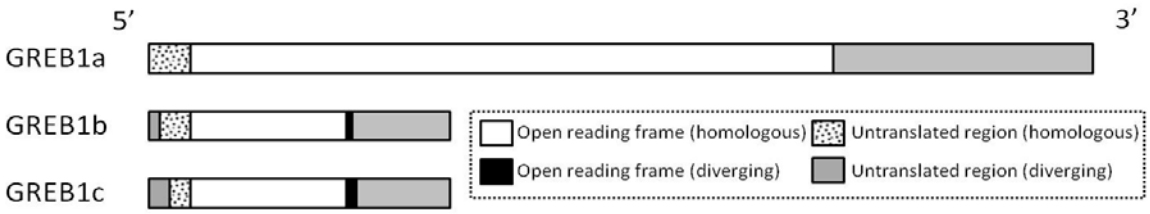

Figure 1. Human GREB1 transcripts. The *GREB1a* isoform encodes the longest protein (1949 amino acids). *GREB1b* encodes a C-terminal truncated isoform (457 aa) with 8 final amino acids that are distinct from *GREB1a*. *GREB1c* also encodes a C-terminal truncated isoform (409 aa) with 23 final amino acids that are distinct from both *GREB1a* and *GREB1b*. The 3 isoforms have unique 3' untranslated regions and partially unique 5' untranslated regions as depicted above. Figure drawn based on RefSeq data accessed May 1, 2014 (Hodgkinson and Vanderhyden 2014).

isoforms (Pruitt et al. 2014). Western blot and immunohistochemistry (IHC) analyses in breast and endometrial cancer cell lines and tissues have shown that GREB1 appears at 216 kilodaltons and is predominantly, but not exclusively, located in the nucleus (Pellegrini et al. 2012, Hnatyszyn et al. 2010, Mohammed et al. 2013).

In MCF7 and T47D breast cancer cells, *GREB1* is induced by 1-100 nM E2 as early as 2 hours with expression persisting for at least 72 hours of treatment (Ghosh et al. 2000, Rae et al. 2005). GREB1 expression correlates with ESR1 positivity in both breast cancer cell lines and primary breast tumours (Rae et al. 2005, Ghosh et al. 2000, Hnatyszyn et al. 2010, Mohammed et al. 2013). *GREB1* levels in breast tumours correlate with serum E2 levels and change throughout the menstrual cycle (Dunbier et al. 2010, Haakensen et al. 2011, Haynes et al. 2013). No overall differences were observed between *GREB1* mRNA levels in normal breast vs. cancer tissue (Haakensen et al. 2011). *GREB1* induction is suppressed by tamoxifen and the estrogen receptor antagonist ICI 182,780, which both inhibit ESR1 activity (Rae et al. 2005).

Transcriptional induction of *GREB1* is not dependent on protein synthesis (Ghosh et al. 2000, Deschenes et al. 2007), suggesting direct upregulation by ESR1. This has been confirmed in MCF7 cells, where *GREB1* is induced through ligand-dependent binding of ESR1 to three EREs located 1.6, 9.5, and 21.2 kb upstream of the *GREB1* transcriptional start site (Figure 2A; Sun et al. 2007, Deschenes et al. 2007). Luciferase reporter assays showed that all three EREs are functional and act synergistically (Sun et al. 2007). Furthermore, E2 induces histone acetylation and polymerase II binding in the promoters for all three *GREB1* isoforms (Sun et al. 2007). A chromatin conformation capture assay showed that E2 induces *GREB1* by transient colocalization of the

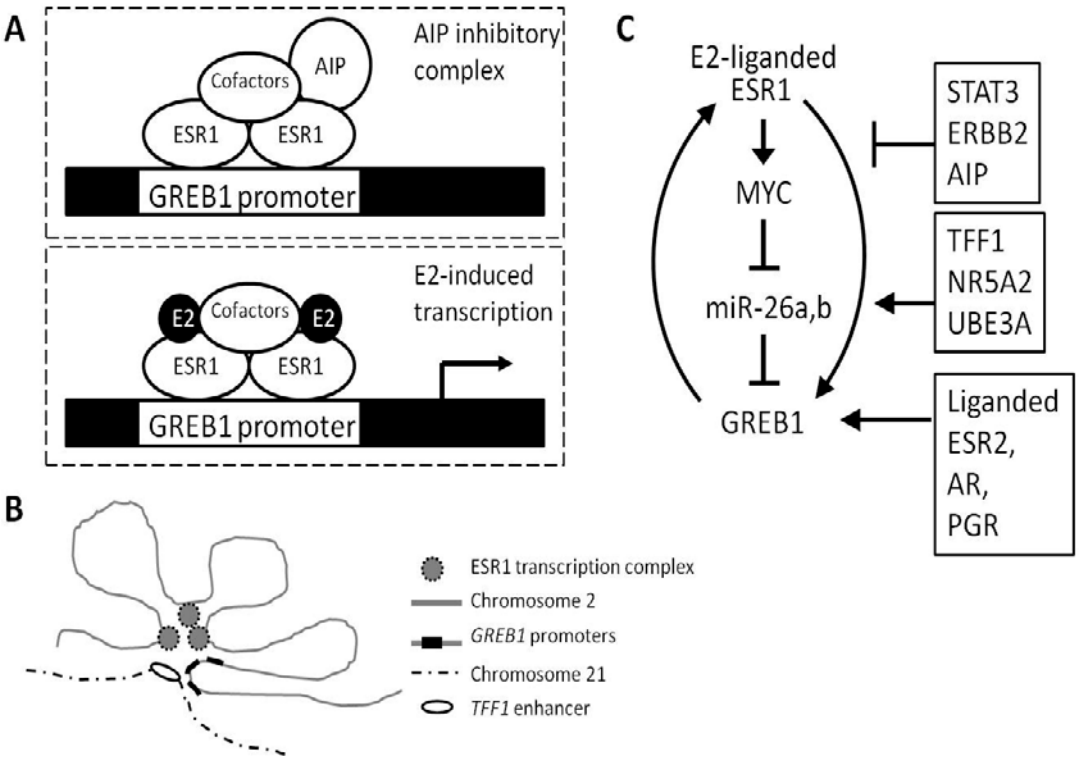

Figure 2. Regulation of *GREB1* expression in ESR1+ breast cancer cells. A) AIP inhibits ESR1-mediated *GREB1* transcription, and is displaced from the *GREB1* promoter in the presence of E2. E2 increases the recruitment of ESR1 and the coactivators NR5A2 and NCOA3 to the *GREB1* promoter region, promoting transcription. STAT3 and UBE3A have also been implicated as cofactors, although their binding at the GREB1 promoter has not yet been confirmed. B) *GREB1* transcription is initiated by ESR1 following synergistic activity from 3 EREs via chromosomal looping, and colocalization with the TFF1 enhancer. C) Overview of *GREB1* regulation though ESR1. ESR1 upregulates *GREB1* through downregulation of miR-26a and miR-26b (left pathway) as well as directly promoting its transcription by binding to its three EREs (right pathway). Several factors have been identified as regulators of GREB1 transcription, as shown on the right. *GREB1* upregulation through ESR2, AR and PGR has also been observed but has not yet been characterized (Hodgkinson and Vanderhyden 2014).

promoters with the ESR1-bound EREs, through DNA looping (Figure 2B; Sun et al. 2007).

Recent evidence suggests that microRNA (miRNA) regulation also plays a key role in *GREB1* induction by E2. In MCF7 and T47D cells, E2 decreases miR-26 through upregulation of *MYC* (Jang et al. 2006, Tan et al. 2014). Expressing mimics for miR-26, which targets the *GREB1* 3' untranslated region, eliminated *GREB1* induction by E2 and greatly reduced E2-stimulated proliferation (Tan et al. 2014). *GREB1* is also upregulated through other steroid receptors including ESR2, PGR, and AR (Rae et al. 2006, Stossi et al. 2004, Jacobsen et al. 2005). In fact, AR binds to an androgen response element in the *GREB1* promoter in prostate cancer cells (Rae et al. 2006). Although ESR1 appears to be the main regulator of *GREB1* levels, and in fact, *GREB1* is commonly reported as a marker of ESR1 activity, the relative contributions of these additional regulators remain unclear. Furthermore, GREB1 influences the transcription of many ESR1 target genes (Mohammed et al. 2013), making it difficult to distinguish factors specifically altering GREB1 from factors that simply affect overall ESR1 activity (Figure 2C; Hodgkinson and Vanderhyden 2014).

1.5.2. Experimental evidence of GREB1 function in breast cancer

GREB1 is a critical mediator of estrogen-stimulated proliferation in breast cancer cells. When MCF7 cells were transfected with siRNA targeting *GREB1*, proliferation in the presence of E2 was reduced to E2-deprived levels, but proliferation under E2-deprived conditions was not changed by GREB1 knockdown (Rae et al. 2005). Indirect induction of *GREB1* by depletion of miR-26 in E2-deprived MCF7 or T47D cells increased proliferation, mimicking the effects of E2; GREB1 knockdown abrogated this

increase (Tan et al. 2014). Silencing GREB1 also significantly impaired the ability of MCF7 cells to form colonies in soft agar (Mohammed et al. 2013).

Purification of ESR1-associated proteins revealed that GREB1 is not only regulated by ESR1, it also regulates ESR1 activity in return (Mohammed et al. 2013). GREB1 binding closely paralleled ESR1 binding, and most GREB1 DNA binding locations were co-occupied by EP300 (also known as p300) and CREBBP (also known as CBP), suggesting that they form a cofactor complex (Mohammed et al. 2013). GREB1 contains two LXXLL motifs, which mediate binding of many nuclear receptor coactivators (including CREBBP/EP300 and the MYBBP1A, also known as p160, family) to the ligand binding domain of nuclear receptors (Mohammed et al. 2013). In MCF7 cells, 739 genes were upregulated by E2, and silencing of GREB1 with siRNA eliminated the induction of half of these genes (Mohammed et al. 2013). In this study, GREB1 knockdown did not alter ESR1 DNA binding activity, but decreased binding of the EP300 and CREBBP coactivators, suggesting that GREB1 promotes ESR1 transcription by recruiting these cofactors to the ERE.

Few studies have examined the function of GREB1 in animal models, but preliminary evidence suggests that the proliferative effects seen in vitro translate to increased tumour growth in vivo. *GREB1* was induced in MCF7-derived tumours when mice were treated with slow-release E2 pellets; pellet removal decreased *GREB1* (Rae et al. 2005). Furthermore, MCF7 cells expressing miR-26 mimics had slower tumour growth in E2-treated mice (Tan et al. 2014). GREB1 was decreased by these mimics both in the original cell lines and in the resulting tumours, but it is unclear whether other targets of miR-26 also contribute to the observed effects (Tan et al. 2014).

1.5.3. GREB1 expression in cancer and other pathologies

Interestingly, GREB1 expression correlated with good prognostic outcome in ESR1+ breast cancer patients (Mohammed et al. 2013). It is difficult to draw conclusions about the clinical significance of GREB1 without knowing the disease characteristics or treatment regimens for these patients. However, GREB1 correlates with ESR1 status in breast cancer (Hnatyszyn et al. 2010), and ESR1+ patients typically receive endocrine therapy. An earlier study showed that a combination of 36 estrogen-regulated genes including *GREB1* predicted tamoxifen response with greater accuracy than PGR (Lippman et al. 2008). Recent experimental evidence suggests that GREB1 directly affects endocrine sensitivity; a tamoxifen-resistant subclone of MCF7 cells showed a decrease in GREB1 expression relative to the parental line, and re-expression of GREB1 restored sensitivity to tamoxifen (Mohammed et al. 2013).

Although the vast majority of studies examining GREB1 have been done in breast cancer, it is also expressed in other hormone-responsive cancers. GREB1 is induced by androgens in AR+ prostate cancer cell lines, and GREB1 knockdown prevented androgen-stimulated proliferation (Rae et al. 2006). Surprisingly, GREB1 levels were higher in prostate tumours with favourable characteristics such as low stage and low prostate-specific antigen (Antunes et al. 2012). However, there is no research directly comparing GREB1 levels to clinical outcomes in prostate cancer. In EOC, a small study found that GREB1 hypomethylation correlated with progression-free survival (Bauerschlag et al. 2011). Because all patients had late-stage serous cancer treated with carboplatin and taxol, GREB1 was suggested to play a role in chemosensitivity. Increased chemosensitivity could be caused by increased proliferation in GREB1-expressing tumours, but proliferation markers were not assessed in this study so it is difficult to draw

conclusions about GREB1 actions. GREB1 has not been examined in endometrial cancer, but it is induced by E2 in the ECC-1 endometrial carcinoma cell line (Ghosh et al. 2000). Only two studies have reported *GREB1* expression in cancers that are not hormone-responsive. *GREB1* was increased 3-fold in normal bronchiole epithelial cells after a low dose of mainstream cigarette smoke (Parsanejad et al. 2008), and a 5-gene panel including *GREB1* showed promise as a biomarker screen for lung cancer in saliva samples, with better sensitivity and specificity than current blood-based screening methods (Zhang et al. 2012).

GREB1 may play a role in endometriosis, which is E2-responsive and increases the risk of developing EOC. GREB1 expression was higher in endometriosis than in eutopic uterine tissue from the same patient or healthy controls (Pellegrini et al. 2012). GREB1 localization also changed from mixed cytoplasmic and nuclear in normal tissue to strong nuclear staining in epithelial cells of ectopic tissue (Pellegrini et al. 2012). A *GREB1* polymorphism has been associated with endometriosis in several large genome-wide association studies; its odds ratio was higher in advanced stages, suggesting a link with disease progression (Rahmioglu et al. 2014). However, it is unclear what the functional significance of this polymorphism is and how it, or GREB1, may contribute to endometriosis.

1.6: Rationale, hypothesis and objectives

Rationale:

E2 promotes EOC tumour growth through a complex signalling network, much of which remains unclear. There are many similarities between breast and ovarian cancers,

despite their large differences in clinical progression and response to antiestrogens and other cancer therapies. Major ESR1 transcriptional targets driving E2-stimulated proliferation in breast cancer include *CCND1*, *MYC*, and *GREB1*. Although CCND1 and MYC have been examined in EOC, the role of GREB1 is unknown. Considerable correlational evidence implicates GREB1 in tumour growth and response to cancer therapeutics, but few experimental studies have been done to clarify this link, even in the comparatively well-studied breast cancer. The links to endocrine sensitivity are particularly interesting considering the large numbers of breast cancer patients currently treated with endocrine-targeting therapies, many of whom will eventually develop resistance. Endocrine therapy is not routinely used in EOC due to high resistance, but an apparent response has been seen in a subset of patients. Therefore, a biomarker to identify sensitive patients or a therapeutic target that increases the response to endocrine therapy would be extremely valuable in both breast and ovarian cancers. Mechanistic studies are badly needed to investigate the role of GREB1 in cancer initiation and progression and to determine whether measuring or targeting GREB1 has clinical utility.

Hypothesis:

E2 promotes ovarian cancer progression through ESR1-mediated upregulation of GREB1. GREB1 expression promotes tumour progression primarily by increasing cell proliferation.

Objectives:

1) Characterize E2 responsiveness of mouse ovarian cancer cells in vitro and in mouse models

2) Investigate modulators of tumour growth in the CAG-TAg model

3) Elucidate the mechanisms of E2 action in mouse ovarian cancer cells in vitro and in vivo by identifying E2 target genes, investigating the role of angiogenesis, and determining the importance of ESR1

4) Determine GREB1 expression and function in mouse cancer cell lines and in vivo models of ovarian cancer

5) Examine GREB1 expression and function in EOC cancer lines, normal tissues, and primary tumours

Chapter 2: Materials and methods

2.1: Mouse experiments

Housing and veterinary monitoring

All mouse experiments were performed in accordance with the *Guidelines for the Care and Use of Animals* established by the Canadian Council on Animal Care, with protocols approved by the University of Ottawa Animal Care Committee. Mice were housed in the standard University of Ottawa animal care facilities which meet or exceed all relevant Canadian and international standards (cages of 2-5 mice, 12:12 light:dark cycle, free access to food and water). Veterinarian technicians who were blinded to experimental groups monitored mice regularly throughout tumour progression, with veterinarian assistance as needed, to identify mice requiring euthanasia (or in rare cases, medical treatment). This was based on an overall health assessment including criteria such as severe weight loss, impaired mobility, respiratory distress, ulcerated tumours, jaundice, or other signs indicating pain or distress. If no humane endpoint was reached, mice were euthanized at experimentally defined endpoints (15 months after surgery for survival studies). Animal Research: Reporting of In Vivo Experiments recommendations (Kilkenny et al. 2010) were followed whenever possible.

Breeding and genotyping

Experimental CAG-TAg mice were generated from a stable breeding colony which did not require genotyping. For the ESR1 deletion study, CAG-TAg (FVB/N background) mice were crossed with conditional ESR1 knockout mice (C57BL/6N, also

known as B6; floxed Exon 3) kindly provided by Dr. Korach. This yielded mice that simultaneously express TAg and delete ESR1 after exposure to Cre recombinase (localized to the OSE by i.b. AdCre). Because the B6 background inhibited tumour progression, mice were bred to >99% FVB/N strain markers using the MAX-BAX accelerated back-crossing protocol (Charles River, USA). Breeding pairs used to generate experimental mice were $ESR1^{wt/fl}$ and $TAg^{+/+}$ in order to obtain $ESR1^{wt/wt}$ and $ESR1^{fl/fl}$ siblings that were both $TAg^{+/+}$. TAg-homozygosity of breeding pairs was confirmed by test mating. ESR1 genotype was assessed by polymerase chain reaction for wildtype and mutant ESR1 in the genomic DNA isolated from ear punches (Hewitt et al. 2010).

Experimental grouping, necropsy and analysis

Mice were divided into experimental groups with an even distribution between cages and surgery dates. All surgeries were done at the same time of day, on a maximum of two consecutive mice of any group, and group order was alternated each surgery day. At necropsy, mice were euthanized with carbon dioxide and weighed, then ascites fluid was removed and measured, tumours were dissected and weighed, metastasis locations noted, and tumour tissues were collected (frozen for quantitative real-time RT-PCR (QPCR) and western blots and/or formalin-fixed and paraffin-embedded for IHC). Mice were excluded from survival analyses only in cases where humane endpoint was reached for reasons unrelated to cancer growth, or where ovarian tumours could not be confirmed at necropsy. Mice were excluded from other analyses for the same reasons or when data collection was not possible despite confirmed ovarian tumours (e.g. animals found dead or not enough tumour tissue to collect).

Hormone pellet implants

For hormone treatments, mice were anaesthetized then implanted s.c. with a 60-day slow-release hormone pellet (E2, P4, the PGR antagonist mifepristone, or placebo; Innovative Research of America, USA). E2 pellets were verified by measuring serum E2 levels with a Coat-a-Count radioimmunoassay kit (Diagnostic Products, USA). To collect serum, blood was withdrawn from the inferior vena cava at necropsy, allowed to clot for 30-60 min at room temperature, then spun for 10 min to isolate the supernatant, which was stored at -20°C until analysis. Serum samples and kit calibrators (100 µL; 0-2600 pg/ml) were loaded into tubes coated with antibodies against E2, then incubated with ^{125}I-E2 for 3h. Tubes were then decanted and radioactivity measured with a Wizard 1470 Automatic Gamma Counter (Wallac, USA) to determine ^{125}I-E2 binding. E2 levels in samples were determined by comparing ^{125}I-E2 binding to the standard curve generated by the kit calibration samples.

Tumour initiation

For xenograft experiments, 6-8 week old mice with severe combined immunodeficiency (SCID), either ovariectomized or intact, were ordered from Charles River (USA). After waiting 1 week to allow recovery from shipping, mice were anaesthetized then injected i.p. with 10 million cells suspended in 0.5 mL sterile phosphate-buffered saline (PBS). For experiments with the CAG-TAg mouse model, tumourigenesis was initiated with bilateral i.b. AdCre injections. Mice were anaesthetized with isofluorane and ovaries were exposed through a dorsal peritoneal incision. Under a microscope, 2 µL AdCre ($4x10^7$ plaque forming units per µL in PBS; Vector Development Laboratory, USA) was injected into each bursal space with a repeated

injector (2 clicks/ovary; Hamilton, USA). If hormone treatments were given, pellets were implanted immediately after cancer cell or AdCre injection.

VCD injections

For the menopause study, CAG-TAg mice were transferred from the breeding colony at 6 months and injected i.p. daily with VCD (240 mg/kg) or vehicle (1:1 dimethyl sulfoxide:saline) for 5 consecutive days (Sahambi et al. 2008). After waiting 60 days for ovarian failure due to follicle depletion (Hoyer et al. 2007), surgeries were done to activate TAg and implant hormone pellets as described above.

2.2: Cell line experiments

Cell line isolation and authentication

Mouse ascites-derived (MAS) ovarian cancer cell lines were isolated by L. Laviolette (MASE1, MASE2, MASC1, MASC2), or by K. Hodgkinson (MASE3, MASC3, MASE-L, MASE-ESR1del, MASC-ESR1del, MASE-L-ESR1del; see Table 1). MASE lines were derived from estrogen-treated mice, whereas MASC lines were derived from control mice receiving no exogenous hormones. Ascites were collected with a syringe through the peritoneal membrane, incubated with an erythrocyte lysis buffer, then centrifuged to collect intact cells. Cells were washed with sterile PBS, then plated in α-MEM (Invitrogen, USA) containing 10% FBS (Cansera, Canada), 1X gentamicin (Gibco, Thermo Fisher Scientific, USA) and 0.1X penicillin/streptomycin (pen/strep; Sigma-Aldrich, USA). The following day, cells were washed with PBS and given fresh media. After cells grew enough to freeze down, antibiotics were discontinued and cells were

Table 1. Mouse ovarian cancer cell lines isolated from ascites (MAS lines) or solid tumours (MTU lines) of CAG-TAg mice at endpoint.

Cell line name	Cell line ID	ESR1 status	Isolated by	Date isolated
MASC lines, derived from control-treated mice (implanted with placebo pellet)				
MASC1	3527A	wildtype	L. Laviolette	2005
MASC2	1140A	wildtype	L. Laviolette	2005
MASC3	4528A	wildtype	K. Hodgkinson	Sept. 8, 2014
MASC-ESR1del -1	3471A	deleted	K. Hodgkinson	Sept.5, 2014
MASC-ESR1del -2	4533A	deleted	K. Hodgkinson	Oct. 3, 2014
MASE lines, derived from E2-treated mice (implanted with 60d-release 0.25 mg E2 pellet)				
MASE1	6406A	wildtype	L. Laviolette	2007
MASE2	2068A	wildtype	L. Laviolette	2005
MASE3	4790A	wildtype	K. Hodgkinson	Dec. 10, 2014
MASE-ESR1del -1	4610A	deleted	K. Hodgkinson	Sept. 11, 2014
MASE-ESR1del -2	4646A	deleted	K. Hodgkinson	Oct.10, 2014
MASL lines, derived from low-dose E2-treated mice (implanted with 60d-release 0.05 mg E2 pellet)				
MASL1	4624A	wildtype	K. Hodgkinson	Nov. 11, 2014
MASL2	4741A	wildtype	K. Hodgkinson	Dec.19, 2014
MASL-ESR1del -1	4537A	deleted	K. Hodgkinson	Sept.6, 2014
MASL-ESR1del -2	4678A	deleted	K. Hodgkinson	Nov. 11, 2014
MTU lines, derived from solid tumours of control (MTUC), E2-treated (MTUE), or low-dose E2-treated (MTUL) mice				
MTUC	4528T	wildtype	K. Hodgkinson	Sept. 8, 2014
MTUE	4742T	wildtype	K. Hodgkinson	Oct. 12, 2014
MTUL	4624T	wildtype	K. Hodgkinson	Nov. 11, 2014
MTUC-ESR1del	3471T	deleted	K. Hodgkinson	Sept.5, 2014
MTUE-ESR1del	4720T	deleted	K. Hodgkinson	Nov. 28, 2014
MTUL-ESR1del	4537T	deleted	K. Hodgkinson	Sept.6, 2014

tested for mycoplasma. Mouse ovarian surface epithelial (mOSE) cell lines were isolated from whole ovaries by O. Collins and used at passages 20-50. Human cancer lines were obtained from ATCC (OVCAR-3), G. Mills (OVCA 432), M. Molepo (OV2008), or I. Lorimer (MCF7). The OVCA 432 and OV2008 cell lines were authenticated by the Genetic Analysis Facility, The Centre for Applied Genomics, The Hospital for Sick Children (Toronto, Canada) using short-tandom repeat sequencing. Notably, our OV2008 cells were identified as the ME-180 cervical cancer cell line, consistent with literature reports that the OV2008 and its derived C13 cell line are not ovarian cancer cells, but rather the ME-180 cervical cancer cell line (Korch et al. 2012).

Cell culture

Cell lines were stored at -80°C in fetal bovine serum (FBS; Cansera, Canada) with 10% dimethyl sulfoxide added. Frozen aliquots were thawed rapidly, plated in 25 cm^2 flasks (Corning, USA) with 5 mL media, and incubated at 37°C with standard oxygen and carbon dioxide levels. All cell lines except OVCAR-3 were normally cultured in α-MEM (Invitrogen, USA) containing 10% FBS; OVCAR-3 cells were cultured in RPMI (Invitrogen, USA) + 20% FBS. Cells were split when 90-100% confluent; otherwise media was changed weekly. Antibiotics were not used for routine culture (exceptions are noted). Mycoplasma testing was performed by O. Collins every 3 months of culture or when cells were frozen down, whichever happened first, and no cells described in this thesis ever tested positive.

Hormone treatments

E2-free media was used for all experiments involving E2 treatments: phenol-red-free DMEM/F12 (Invitrogen), with 1.2 g/L sodium bicarbonate and 5-10% charcoal-stripped serum (CSS). CSS was made by stirring fetal bovine serum with 50 mg/mL charcoal overnight at 4°C followed by several centrifuges to remove charcoal. Cells were plated in regular media for optimum attachment; fully attached cells were washed with PBS then switched to E2-free media a minimum of 24h prior to E2 treatment. For E2 treatments, E2 stock solutions (Sigma; suspended in 100% ethanol, then stored in glass vials at -20°C) were diluted with ethanol as necessary and added to E2-free media for a final concentration of no more than 0.1% ethanol. Most experiments used an E2 dose of 10 nM; the remainder used 500 nM.

GREB1 knockdown and overexpression

Lentiviruses encoding two GREB1-targeted shRNA constructs based on the GIPZ vector, which co-expresses GFP and puromycin resistance sequences, were obtained from Open Biosystems (now Dharmacon; USA; Figure 3). Cells transduced with the knockdown constructs were allowed to recover in fresh media for 72h before selection with puromycin. Puromycin-resistant cells were GFP-sorted using fluorescence-activated cell sorting (FACS) for high GFP expression, at the Ottawa Hospital Research Institute StemCore Flow Cytometry facility.

A lentivirus encoding the full length isoform of human GREB1 was based on the pWPI vector, with an IRES-GFP expression cassette (Figure 4). Lentivirus was produced in transfected 293T cells by Dr. K. Garson (Ottawa, Canada). Cells transduced with the overexpression construct were GFP-sorted 72h after transduction. Because FACS is a frequent source of bacterial contamination, all sorted cells were cultured with 1X

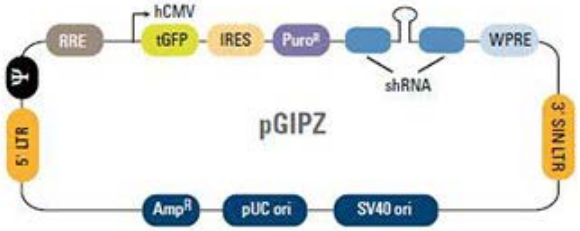

Vector Element	Utility
hCMV	Human cytomegalovirus promoter drives strong transgene expression
tGFP	TurboGFP reporter for visual tracking of transduction and expression
Puro^R	Puromycin resistance permits antibiotic-selective pressure and propagation of stable integrants
IRES	Internal ribosomal entry site allows expression of TurboGFP and puromycin resistance genes in a single transcript
shRNA	microRNA-adapted shRNA (based on miR-30) for gene knockdown
5' LTR	5' long terminal repeat
3' SIN LTR	3' self-inactivating long terminal repeat for increased lentivirus safety
Ψ	Psi packaging sequence allows viral genome packaging using lentiviral packaging systems
RRE	Rev response element enhances titer by increasing packaging efficiency of full-length viral genomes
WPRE	Woodchuck hepatitis posttranscriptional regulatory element enhances transgene expression in the target cells

Figure 3. Lentiviral constructs used for shRNA-based GREB1 knockdown. A) Map of pGIPZ vector. Note the miR-30-based shRNA, GFP and puromycin resistance elements.

(from Open Biosystems, now Dharmacon; http://dharmacon.gelifesciences.com)

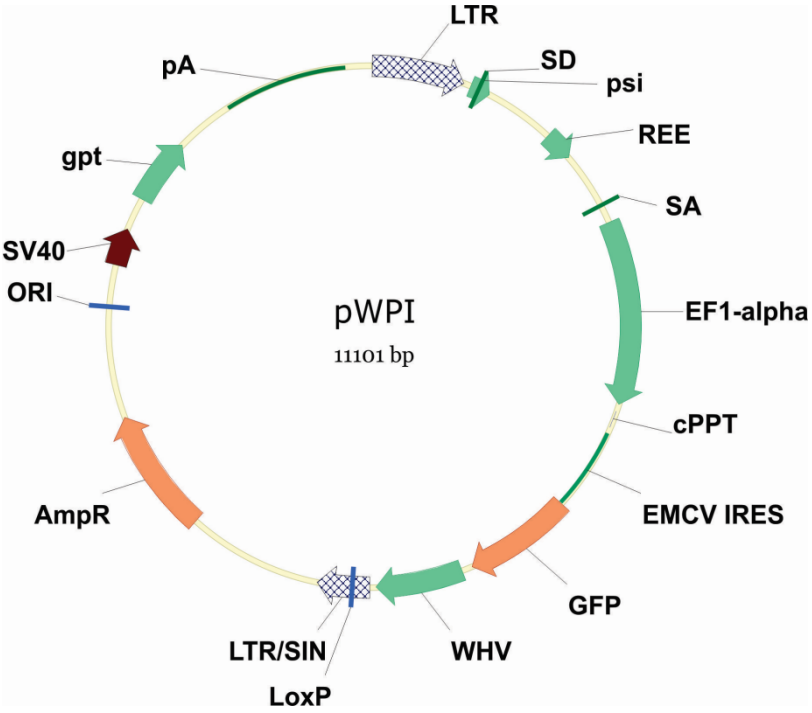

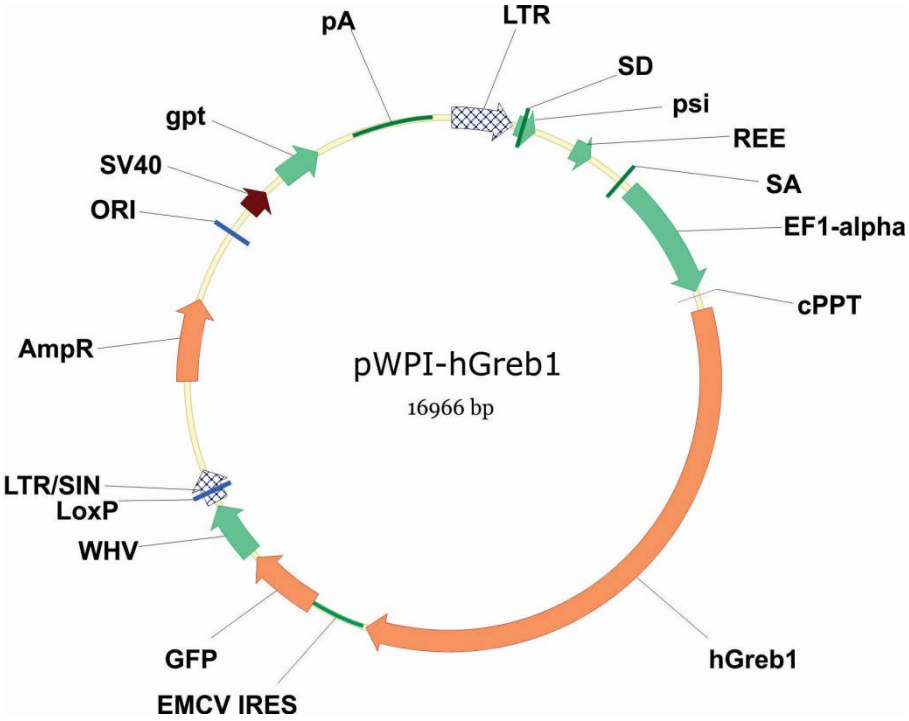

Figure 4. Lentiviral constructs for GREB1 overexpression. Maps of pWPI vector (top) and pWPI-based human GREB1 construct (bottom).

(from Dr. K. Garson)

pen/strep and 3X gentamicin until they could be preserved in frozen aliquots. Cells were then switched to normal media (no antibiotics) and tested for mycoplasma to confirm the absence of contamination. Knockdown and overexpression were confirmed by QPCR for all cell lines, as well as by western blot analysis of MASE lines. Mouse cell lines are listed in Table 2; human cell lines are listed in Table 3.

Cell proliferation

Cells were plated in 6-well plates in their regular culture media, with time=0 set when the media was changed to the experimental media after cells were fully attached (overnight for OSE and human ovarian cancer cell lines, or 4-6h for ascites cell lines). Based on different growth rates and time to confluence, mOSE were plated at 200,000 cells/well, mouse ascites cells were plated at 50,000 cells/well, and human ovarian cancer cells were plated at 300,000/well. At each time point, cells were trypsinized for 5-10 minutes (min) at 37°C, then resuspended in 1mL of their regular media, and examined with the ViCell automated counter (Vi-CELL TM XR Cell Viability Analyzer; Beckman Coulter Inc, USA). For each experiment, treatment groups were assessed in triplicate wells (with the exception of the OVCA 432 WPI-GREB1 proliferation experiment in E2-free vs. E2-containing media, which used duplicate wells). In all proliferation experiments, viability was compared between groups to ensure that viable cell count was correctly assessing proliferation rather than changes in viability; most experiments had viability consistently higher than 90%.

Cell migration

Table 2. Mouse ovarian cancer cell lines (MAS) generated with GREB1 knockdown or overexpression.

Cell line name	Lentiviral construct	Date transduced
GREB1 knockdown: MASE cells transduced with GIPZ-based constructs		
MASE-NS-1	Non-silencing	2011
MASE-shGREB1#1-1	shGREB1#1	2011
MASE-shGREB1#2-1	shGREB1#2	2011
MASE-shGREB1#3-1	shGREB1#3	2011
MASE-NS-2	Non-silencing	2013
MASE-shGREB1#1-2	shGREB1#1	2013
MASE-shGREB1#2-2	shGREB1#2	2013
MASE-shGREB1#3-2	shGREB1#3	2013
GREB1 overexpression: MASE cells transduced with WPI-based constructs		
MASE-WPI-1	WPI (empty)	2014
MASE-GREB1-1	WPI-GREB1	2014
MASE-WPI-2	WPI (empty)	Sept 12, 2014
MASE-GREB1-2	WPI-GREB1	Sept 12, 2014
GREB1 overexpression: MASC cells transduced with WPI-based constructs		
MASC-WPI-1	WPI (empty)	Sept 12, 2014
MASC-GREB1-1	WPI-GREB1	Sept 12, 2014

All cells have been sorted by FACS for GFP; cells transduced with the GIPZ construct were also selected with puromycin before GFP sorting.

Table 3. Human ovarian cancer cell lines generated with GREB1 knockdown or overexpression.

Cell line name	Working cell line name	Lentiviral construct	Date generated
GREB1 knockdown: cells transduced with GIPZ-based constructs			
OVCAR3-NS	OVCAR3-NSAS	Non-silencing	2013
OVCAR3-shGREB1#1	OVCAR3-SH1AS	shGREB1#1	2013
OVCAR3-shGREB1#2	OVCAR3-SH2AS	shGREB1#2	2013
OVCAR3-shGREB1#3	OVCAR3-SH3AS	shGREB1#3	2013
GREB1 overexpression: cells transduced with WPI-based constructs			
OVCAR3-WPI	OVCAR3-WPI	WPI (empty)	Sept 12, 2014
OVCAR3-GREB1	OVCAR3-GREB1	WPI-GREB1	Sept 12, 2014
OVCA432-WPI	OVCA432-WPI	WPI (empty)	Sept 16, 2014
OVCA432-GREB1	OVCA432-GREB1	WPI-GREB1	Sept 16, 2014

All cells have been sorted by FACS for GFP; cells transduced with the GIPZ construct were selected with puromycin before GFP sorting.

Cells were plated in their regular media at 15,000/well in 96-well ImageLock tissue culture plates (Essen BioScience, USA). When cells were 95-100% confluent (around 20 hours later), identical scratch wounds were made in every well using the IncuCyte WoundMaker according to the manufacturer's protocol (Essen BioScience, USA). Wells were immediately washed twice with regular culture media before adding treatment media and incubating cells in the IncuCyte automated monitoring system, which photographed all wells every 2 hours. IncuCyte ZOOM software was used to quantify wound width and calculate wound density (cell confluence in wound relative to cell confluence outside the wound).

Colony formation

Cells for colony formation assay were plated in soft agar by O. Collins according to standard protocols (Laviolette et al. 2014). Briefly, cells in single suspension were mixed with 37°C low-melting-point soft agar, and plated in 24-well tissue culture plates with 3 replicate wells per group (Corning, USA). Cells were counted with a phase contrast microscope (EVOS, Thermo Fisher Scientific, USA) when colonies were large enough to distinguish from single cells (7d after plating for MASE lines, 14d for OVCAR3 and OVCA 432). To reduce bias from unevenly distributed cells, the objective was centred on each well and visible colonies were counted in all planes without moving the objective. In each experiment, colony counts were averaged across the 3 replicate wells. All group identities were hidden until statistical analysis was completed to minimize potential bias.

2.3: Molecular techniques

Quantitative real-time RT-PCR (QPCR)

Cells were trypsinized, resuspended, and washed with PBS before freezing as cell pellets. Small pieces of tumours (20-100 mg) were cut with a clean razor blade on a surface cooled by dry ice, then immediately homogenized in lysis buffer from the RNA extraction kit. RNA was extracted using commercial centrifugation-based kits (RNeasy, Qiagen, USA or GenElute, Sigma-Aldrich, USA) and cDNA was generated with 500 ng RNA using a commercial reverse transcription kit (Qiagen Quantitect or Bio-Rad iScript; Qiagen, USA). RNA quantity and quality was assessed with a NanoDrop ND-1000 spectrophotometer (Thermo Fisher Scientific, USA). Water used for RNA, cDNA and QPCR reactions was RNase and DNase-free (Qiagen, USA or autoclaved double-distilled water). All RT reactions included two negative controls to be added to each QPCR plate: a "no-RT control" with water replacing the RT enzyme and a "no template control" with water replacing the cDNA sample. In addition to these negative controls, every QPCR plate included a positive control (tissue or cell line expected to highly express the gene of interest). If amplification was seen in negative controls earlier than cycle 35, the QPCR was redone with a new aliquot of RNase/DNase-free water.

All QPCRs were run on an ABI 7500 FAST machine (Applied Biosystems, USA) with a commercial mastermix (TAqMan; Applied Biosystems, USA; RT^2 SYBR green; Qiagen, USA; SsoFAST SYBR green; BioRad, USA). QPCR primers are listed in Table 4; primer design and initial validation (showing a clean melt curve and amplification of a single product near the predicted size) was done by L. Laviolette. Major primers (*mGreb1*, *mEsr1*, *mTbp*, *mPpia*, *hGREB1, hPPIA)* were further validated to confirm

Table 4. Primers for QPCR with SYBR green mastermix.

Target	Forward sequence	Reverse sequence
mGreb1	GCAACACGGTGCCTCCACCA	GAGGCGCCTGCTGGTACTGC
mEsr1	TCTGCAGCAGCAGCATCGCC	GGCATGAAGGCGGTGGGCAT
mEsr2	CGTTCTGGACAGGGATGAGGGGA	GGCTTGCGGTAGCCAAGGGG
mCyp11a1	CATGCGAGGGTCCCAACCCG	CACCTTCCAGCAGGGGCACG
mStc2	GAGCGGCTGGGCCAGTTTGT	CCACGTCCCCGGCATTGACC
mPgr	CGCAGCACCCGCCATCTACC	ACTGTGGGCTCTGGCTGGCT
mKdr	GTGCTCGTACCGGGACGTCG	ACCCTCGGCAGGGGATCACC
mEdnra	CGCCACCCTCGTTCTCCAGC	CGCCTCCCATGGTCAGC
mEdn1	TCCTTGATGGACAAGGAGTGT	CCCAGTCCATACGGTACGA
mTbp	GGCGGTTTGGCTAGGTTT	GGGTTATCTTCACACACCATGA
mPpia	AGGGTGGTGACTTTACACGC	GATGCCAGGACCTGTATGCT
hGREB1	TAGCGACCCCTGGCCAGACC	GCCGTCTGACGCCGCACATA
hESR1	CCTGATGGCCAAGGCAGGCC	CGGTGGGCGTCCAGCATCTC
hPPIA	CCTAAAGCATACGGGTCCTG	TTTCACTTTGCCAAACACCA

m, mouse; h, human

adequate primer efficiency (close to 100%), relative efficiency (similar efficiency as the housekeeping genes), and dynamic range (linear range of dilution curves).

Western blots

Cells were cultured in 10 cm dishes and lysed in the dish with a commercial cell lysis buffer when 70-100% confluent (ProteoJet or M-PER; Thermo Fisher Scientific, USA) following the manufacturer's protocol but with the addition of a 15-30 second sonication (Sonic Dismembrator Model 300; Fisher Scientific, Canada) before the final spin for increased yield. Frozen tissues were homogenized then added to the same cell lysis buffer for protein extraction. Protein was stored at -80°C until use. Protein was quantified using a Bio-Rad Protein Assay commercial assay (Bio-Rad Laboratories, Canada) and an equal amount of protein (30-60 µg, depending on the blot) was prepared for each lane. The NuPAGE electrophoresis system (Invitrogen, USA) was used for all blots. For blots probed for GREB1, the tris-acetate gel protocol in the NuPAGE Technical Guide was followed using the commercial buffers recommended in the protocol and precast 10% tris-acetate gels (Invitrogen, USA). For all other blots, buffers were prepared in the lab and samples were loaded on precast 4-12% graduated tris-glycine gels (Invitrogen, USA) following the tris-glycine gel protocol described in the NuPAGE Technical Guide. Gels were run for 1.5-2h at 120-140V with 1X NuPage MOPS running buffer (20X: 1 M MOPS, 1 M Tris, 69.3 mM SDS, 54.8 mM EDTA).

Gels were transferred to nitrocellulose (Hybond-C Extra; Amersham Biosciences, UK) with 1X NuPage Transfer Buffer (20X: 500 mM bicine, 500 mM Bis-Tris, 20.5 mM EDTA) for 2h at 30V. Blots were then blocked with blocked for at least 1 hour in 5% skim milk in 1X Tris-buffered saline with 0.1% Tween-20, probed with primary antibody

for 30 min-1h, washed 3x5 min with PBS, probed with the relevant HRP-conjugated secondary antibody for 1h, washed 3x5 min with PBS, and developed with ECL Advance Western Blotting Detection Kit (Amersham Biosciences, UK). Primary antibodies used include GREB1 (1:500; Sigma HPA024616, USA), ESR1 (1:200; Santa Cruz, USA), GAPDH (Abcam, USA), ACTB (Abcam), KDR (Abcam), and EDNRA (Abcam). The SuperSignal Western Blot Enhancer kit (Thermo Fisher Scientific, USA) was used for blots examining GREB1.

Chromatin Immunoprecipitation (ChIP)

MASE cells were treated with 100 nM E2 for 45 min then cross-linked with 1% formaldehyde for 30min at room temperature. Cross-linking was quenched by adding 125 mM glycine for 10 minutes at RT. Cells were sonicated with Diagenode's Bioruptor® for 30sec on HIGH and 60sec off for 80 cycles at 4°C to produce 150-200 bp fragments. To bind antibody to Dynabeads® magnetic beads, 5µg of ESR1 anti-body (Santa Cruz, sc-542) or normal mouse IgG (control for non-specific interactions) (Millipore, USA) was incubated with 20µl of magnetic beads O/N at 4°C the day prior to IP. 250µg of DNA was used per IP and DNA was pre-cleared using 1µl/ml salmon sperm (Sigma, USA), 10µl/ml ovalbumin (Sigma), and 10µl/ml Dynabeads® magnetic beads for 1H at 4°C. 10% of pre-cleared chromatin was saved as "Input" and IP of DNA with antibody-bound beads occurred O/N at 4°C. Next day, the beads bound by immune-complexes were collected using a Magna GrIP™ Rack (Millipore, USA) and washed twice with low-salt, high-salt, and LiCl washes. The immuneprecipitated materials were eluted from the beads by incubating the samples with elution buffer at 65°C for 10mins at 1400 rpm in an Eppendorf Thermomixer. Reverse cross linking and protease treatment was performed on

each sample including input. The immunoprecipitated genomic DNA fragments were isolated via phenol:chloroform:isoamyl alcohol extraction, precipitated with ethanol, then pelleted. Air-dried DNA pellet was resuspended in nuclease-free water. A HotStarTaq DNA Polymerase Kit (Qiagen, USA) was used to amplify DNA with primers spanning the mouse *Greb1* ERE1 and ERE2. Amplified PCR products were ran on a 4% agarose gel containing RedSafe™ Nucleic Acid Staining Solution (Intron Biotechnology) and bands were visualized with a EpiChem II Darkroom transilluminator (UVP Laboratory).

Immunohistochemistry (IHC) and hematoxylin and eosin (H&E)

Tissues were fixed in formalin for 24-72h then processed and embedded in paraffin by the University of Ottawa pathology lab. Sections were cut 3-5 µm thick and allowed to dry for 24-96h at room temperature. Tissue microarray (TMA) slides were obtained from the Cooperative Human Tissue Network (University of Virginia, USA) or The Ottawa Hospital (Canada). For H&E, slides were stained with Harris Modified Haematoxylin (Thermo Fisher Scientific, USA) and eosin (Surgipath, USA) according to standard protocols. For IHC, slides were deparaffinized with xylene, rehydrated with ethanol, incubated with a citrate antigen retrieval buffer (Antigen Unmasking Solution, Vector, USA) for 10 min at 100°C, then allowed to cool for 60-90 min. Slides were incubated with serum-free Dako protein block (30-60 min; Agilent, USA) to reduce nonspecific staining, then incubated with the relevant antibody at RT for 30m (ESR1; Abcam, USA) or 1-2h (GREB1; Millipore, USA). Primary antibodies were diluted in Dako Antibody Diluent (Agilent, USA; GREB1 1:25; ESR1 1:200). Staining was visualized with Dako Envision secondary reagents (anti-rabbit or anti-mouse as applicable; Agilent, USA) followed by a 5 min incubation in a 0.2% diaminobenzidine

(DAB)/0.001% hydrogen peroxide solution (Sigma-Aldrich, USA). After fully drying, slides were scanned with a Scanscope (Aperio Technologies Inc., USA) and examined with Aperio ImageScope software.

Immunocytochemistry (ICC)

Cells were plated on sterilized glass cover slides, treated with E2 if applicable, then fixed with 4% paraformaldehyde for 30 min. Slides were then washed, permabilized with 0.2% Triton X-100 (10 min), washed, and blocked with 5% normal goat serum in PBS (1h). Slides were incubated with primary antibody (GREB1, 1:200 Abcam or 1:100 Millipore; Ki67 1:100) for 1h at room temperature or overnight at 4°C, washed, and incubated with the relevant secondary antibody for 1h in the dark (AlexaFluor 488, 1:1000). For imaging, slides were washed and mounted onto slides with a mounting media containing a DAPI stain (ProLong Gold Antifade Mountant, Thermo Fisher Scientific, USA), allowed to dry overnight, and then examined with a fluorescence microscope.

2.4: Statistical analysis

The sample size for each group is listed in the relevant figure legend; in most cases, 3 replicate experiments were used for cell studies and 6-8 replicate animals were used in mouse studies. Kaplan-Meier survival curves were compared using log-rank tests. Cell proliferation curves were compared with a linear regression of log-transformed cell counts throughout the exponential growth phase. Parametric tests (t-tests for 2 groups, ANOVA for 3 or more independent groups) were chosen when possible. Nonparametric

alternatives (Mann-Whitney U-test or Wilcoxon test) were used in cases of nongaussian distribution and/or off-scale values which precluded parametric tests. To avoid assuming equal variance, Welch's t-tests were used instead of Student's t-tests (Ruxton et al. 2006). Multiple comparisons corrections were chosen based on experiment goals and design; p values are directly reported whenever possible for maximum transparency.

Chapter 3: Results

3.1: Estrogen responsiveness of ovarian cancer models in vivo and in vitro

3.1.1. E2 accelerates tumour progression and decreases body weight

To clarify the actions of E2 in ovarian cancer, we investigated its impact on survival, tumour and ascites development, and body weight in several mouse models of ovarian cancer. We found that E2 treatment decreased survival time in all three models examined (Figure 5). Ovariectomized (OVX) SCID mice engrafted i.p. with MAS mouse ovarian cancer cell lines (MASE2 and MASC2; Table 1) had 55% ($p=0.0013$) and 14% ($p=0.0052$) lower median survival times respectively when a slow-release E2 pellet (0.25 mg/60d) was implanted s.c. in the neck. Disease-free survival (based on first tumour detection by palpation) was not significantly altered by E2 in either cell line, although a trend for decreased disease-free survival was seen in the MASE study ($p=0.1308$). This suggests that E2 is predominantly increasing growth of established tumours rather than promoting initial cell engraftment. To confirm these results in an immune-competent mouse model of ovarian cancer, we treated CAG-TAg transgenic mice with the same E2 pellets. In this model, E2 decreased median survival by 43% ($p=0.0003$) in one study and by 61% ($p<0.0001$) in a later study (Figure 5). Methodology was similar for both CAG-TAg studies; the main differences were that the methodology was optimized before the second study (a repeating device was introduced to standardize the volume of injected AdCre), and that mice were 8 months old at tumour initiation in the first study vs. 8-10 weeks in the second study.

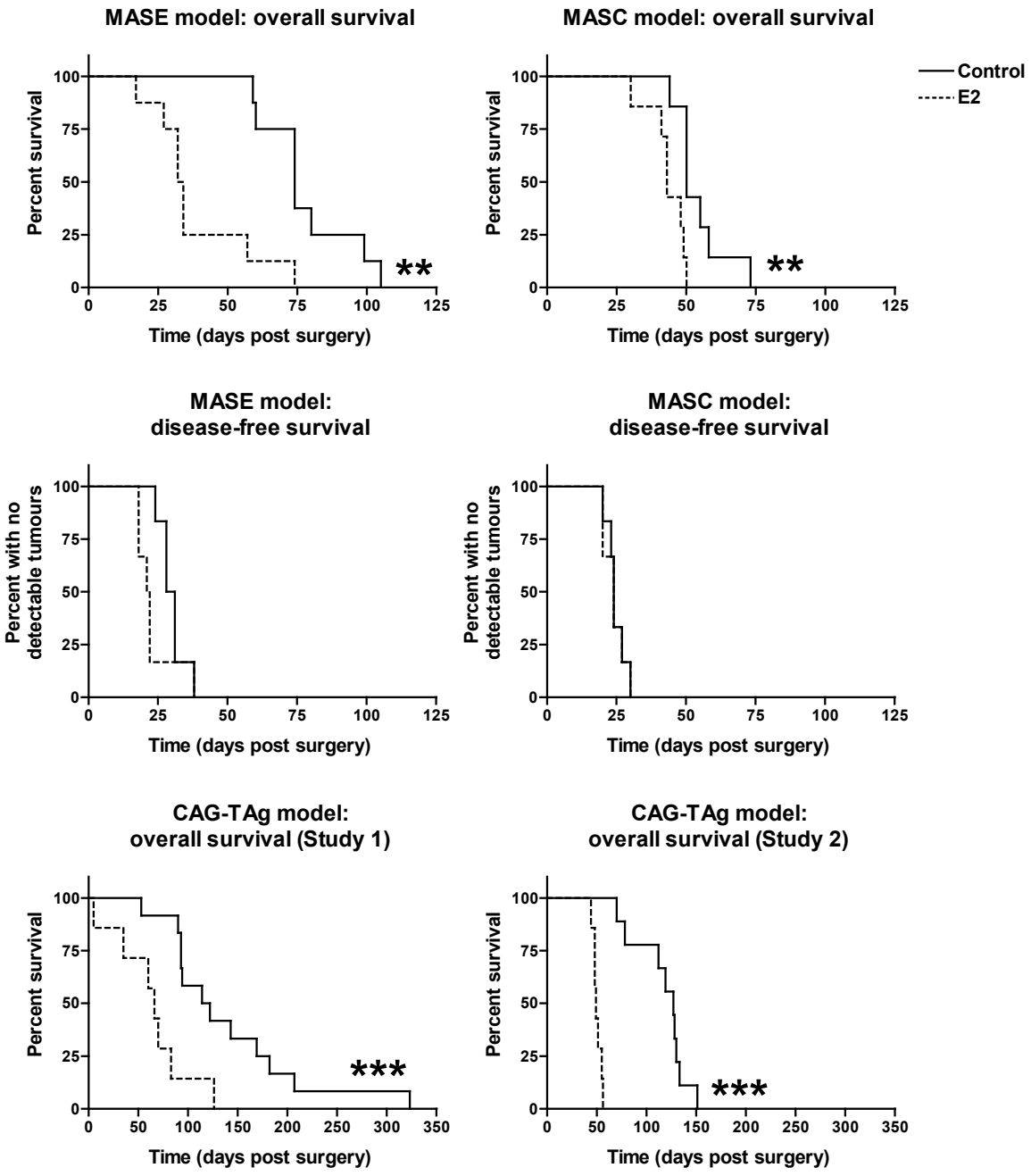

Figure 5. Survival time after E2 treatment for several mouse models of ovarian cancer. For allograft models, OVX SCID mice were injected i.p. with 10^7 MASE or MASC cells and implanted with a slow-release pellet containing 0.25 mg E2 or placebo (N=7-8 per group). For CAG-TAg models, TAg was activated with bilateral i.b. AdCre injections and hormone pellets were implanted at 8 months (Study 1; N=7-12) or 6-8 weeks (Study 2; N=7-9). Survival was prolonged by E2 in both allograft and CAG-TAg models; disease-free survival, defined as the time before tumours are first detected by palpation, was not altered by E2.**: $p<0.01$, ***: $p<0.001$; log-rank test.

E2 had an inconsistent effect on tumour burden at endpoint (Figure 6). On average, tumour weight was increased 300% by E2 in mice engrafted with MASE cells ($p=0.0487$) but was not altered in mice engrafted with MASC cells. In CAG-TAg mice, E2 did not alter tumour weight in the first study but decreased tumour weight by 85% in the second study ($p=0.0182$). Ascites volume and incidence were not altered by E2 in any mouse model examined (Figure 7).

E2 decreased body weight in both the allograft and transgenic mouse models (Figure 8). Body weight at endpoint was decreased 22% by E2 in MASE-engrafted mice ($p=0.0249$) and 15% in MASC-engrafted mice ($p=0.0015$). The first CAG-TAg study showed a near-significant trend for decreased body weight (16%; $p=0.0852$) whereas the second CAG-TAg study showed a small but significant decrease ($p=0.0116$). E2 pellet function was confirmed by radioimmunoassay (Figure 9); mice engrafted with E2 pellets had significantly higher serum E2 levels at endpoint than mice implanted with placebo pellets ($p<0.0001$). There was surprisingly high variability in the E2-treated group, with E2 levels ranging from 8 to 178 pg/ml (vs. controls ranging from undetectable to 10 pg/ml). This wide range in E2 may have been caused by a loss of pellet function over time, as E2 levels in serum (collected at endpoint) inversely correlated with survival time ($p=0.0107$, $R^2=0.5779$).

3.1.2. E2 actions are subtle in mOSE and mouse ovarian cancer cell lines

Despite the important role of E2 in vivo, few effects were seen on mouse ovarian cell lines in vitro. MAS ovarian cancer cells did not show any change in proliferation, colony formation or migration with E2 treatment in vitro (Figure 10). E2 did not alter proliferation or viability of mOSE in short-term serum starvation conditions (Figure 11A)

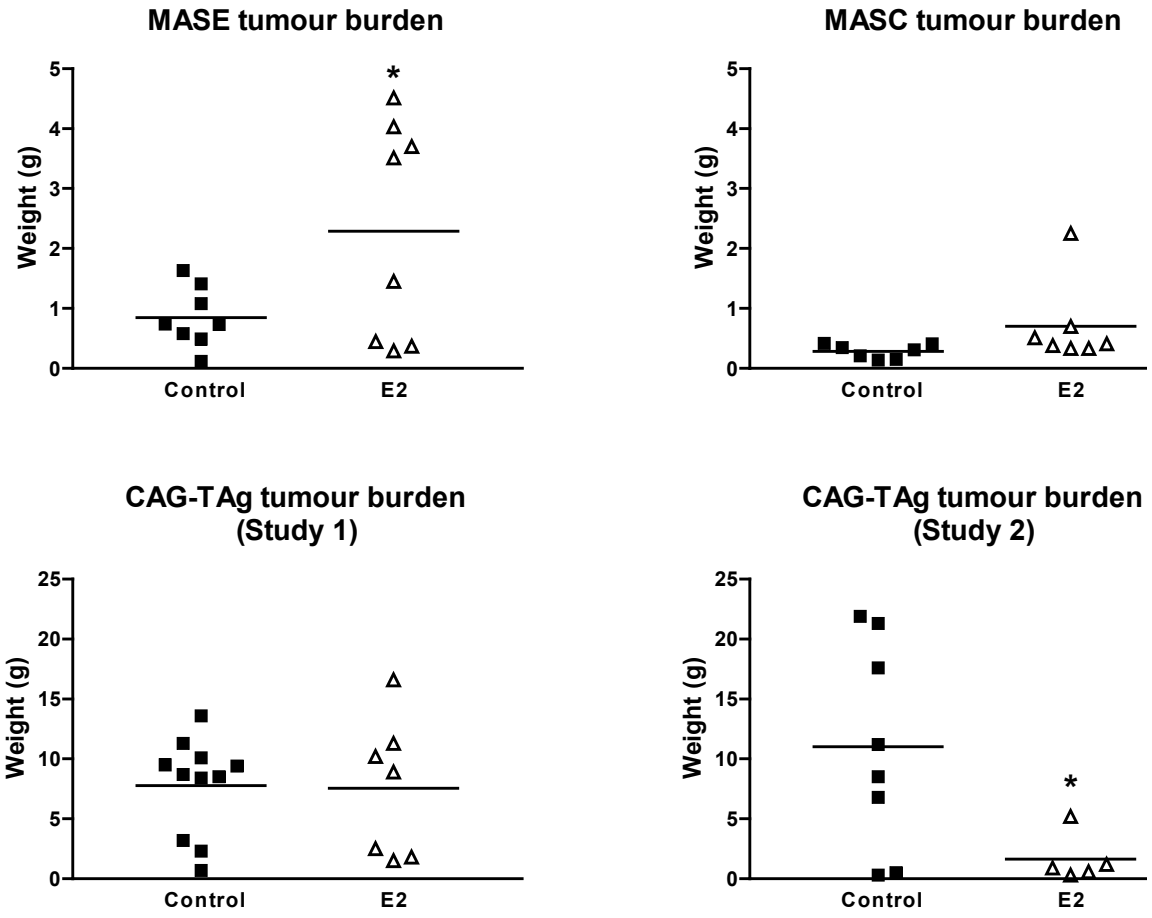

Figure 6. Effect of E2 on tumour weight in several mouse models of ovarian cancer. Tumours of mice described in Figure 5 were dissected after euthanasia and total tumour mass was weighed. E2 increased tumour burden in MASE-engrafted mice but not in MASC-engrafted mice (N=7-8). In the CAG-TAg model, E2 did not alter tumour burden in one study but decreased tumour burden in a second study (N=5-11). The only major difference between these two studies is that the mice were 8 months old at AdCre injection in the first study and 8-10 weeks old in the second study. *: $p<0.05$; t-test.

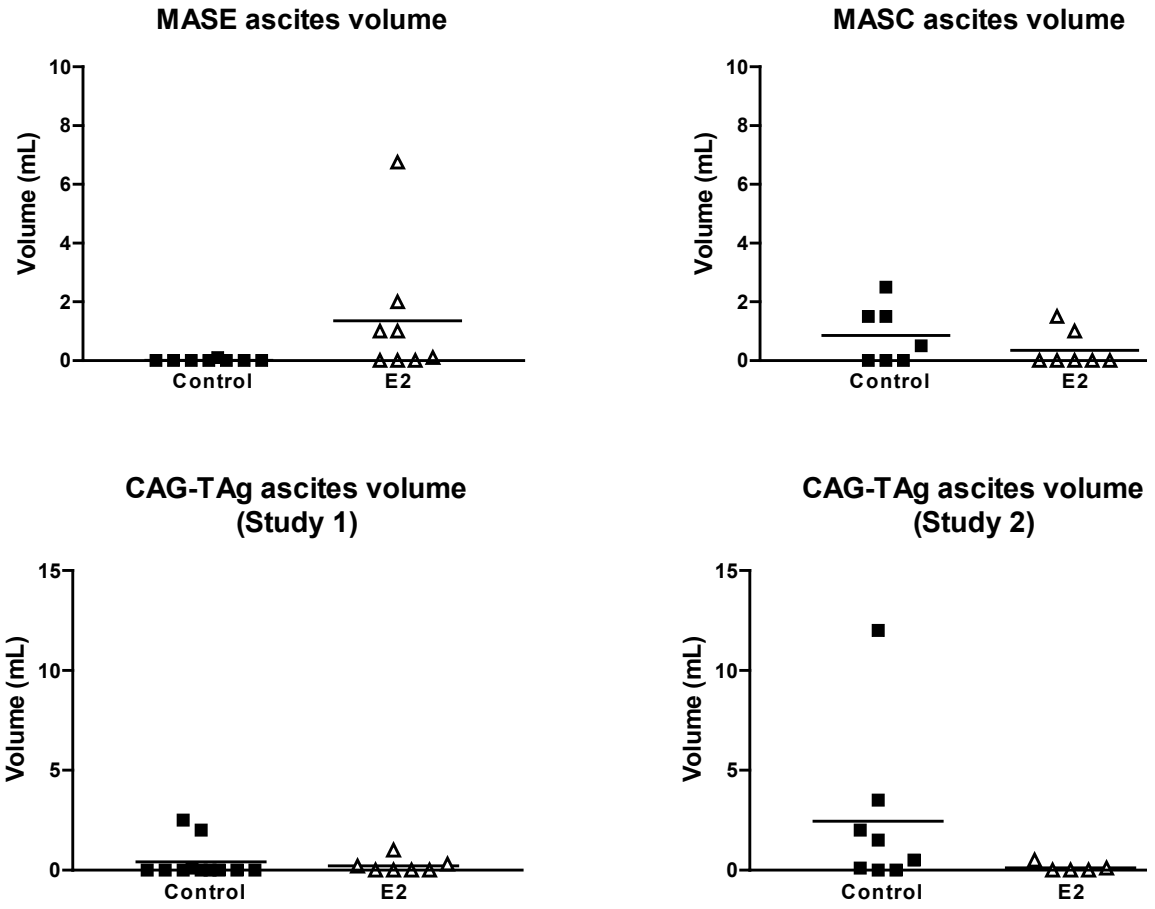

Figure 7. Effect of E2 on ascites in several mouse models of ovarian cancer. Ascites fluid of mice described in Figure 5 was extracted with a large-gauge needle and syringe through the peritoneal membrane immediately after euthanasia. Ascites volume was not altered by E2 in any mouse model examined (N=5-11; $p>0.05$; Mann-Whitney U-test). Ascites incidence was also unchanged by E2 (Chi-square test).

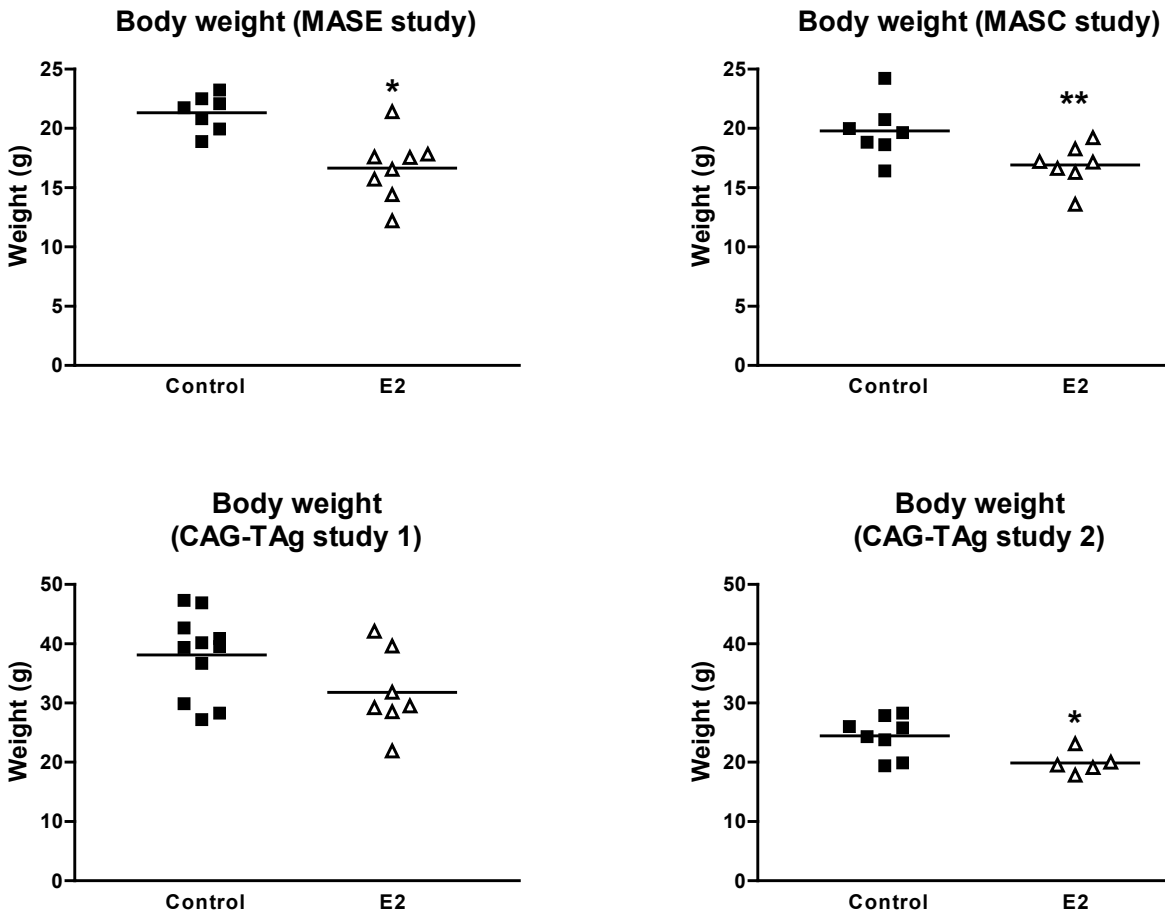

Figure 8. Effect of E2 on body weight in several mouse models of ovarian cancer. Mice described in Figure 5 were weighed immediately after euthanasia and body weight was calculated by subtracting tumour weight and ascites weight (approximated from volume at 1 g/mL) from this initial body weight measurement. Body weight was decreased by E2 in both MASE and MASC allograft models (N=7-8). In the CAG-TAg model, a trend for decreased body weight was seen in the first study and body weight was decreased by E2 in the second study (N=5-11). The only major difference between these two studies is that the mice were 8 months old at AdCre injection in the first study and 8-10 weeks old in the second study. *: $p<0.05$; **: $p<0.01$; t-test.

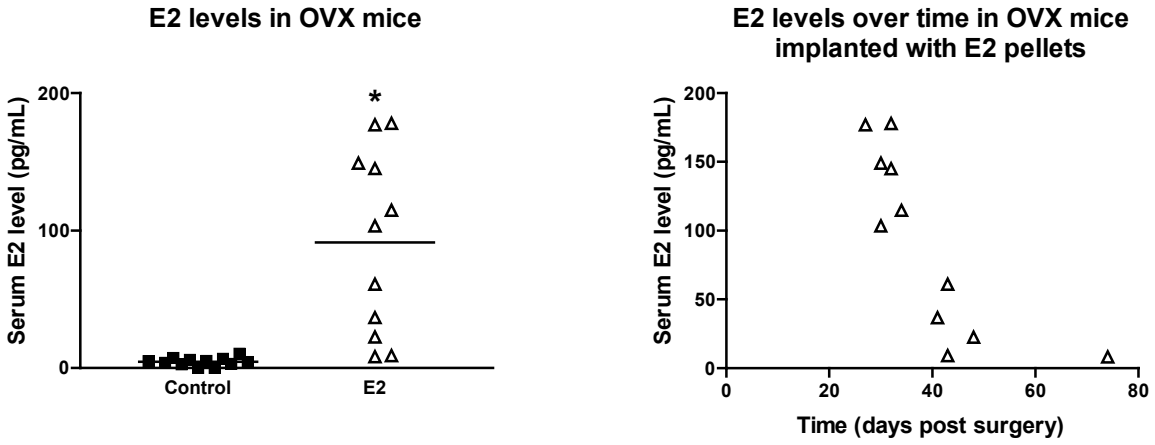

Figure 9. Efficacy of E2 pellets. E2 pellets were validated by measuring E2 levels in the serum of OVX mice engrafted with MASE or MASC cells. Blood was collected from the inferior vena cava at endpoint and serum was isolated by centrifuging clotted blood and collecting the supernatant. E2 levels were measured by radioimmunoassay. A) Mice implanted with E2 pellets had higher serum E2 levels at endpoint than mice implanted with placebo pellets (N=11-12; *: $p<0.0001$; Mann-Whitney U-test). B) E2 serum levels at endpoint inversely correlated with survival time for mice implanted with E2 pellets (N=11; $p<0.05$; $R^2=0.5779$; Pearson's correlation analysis).

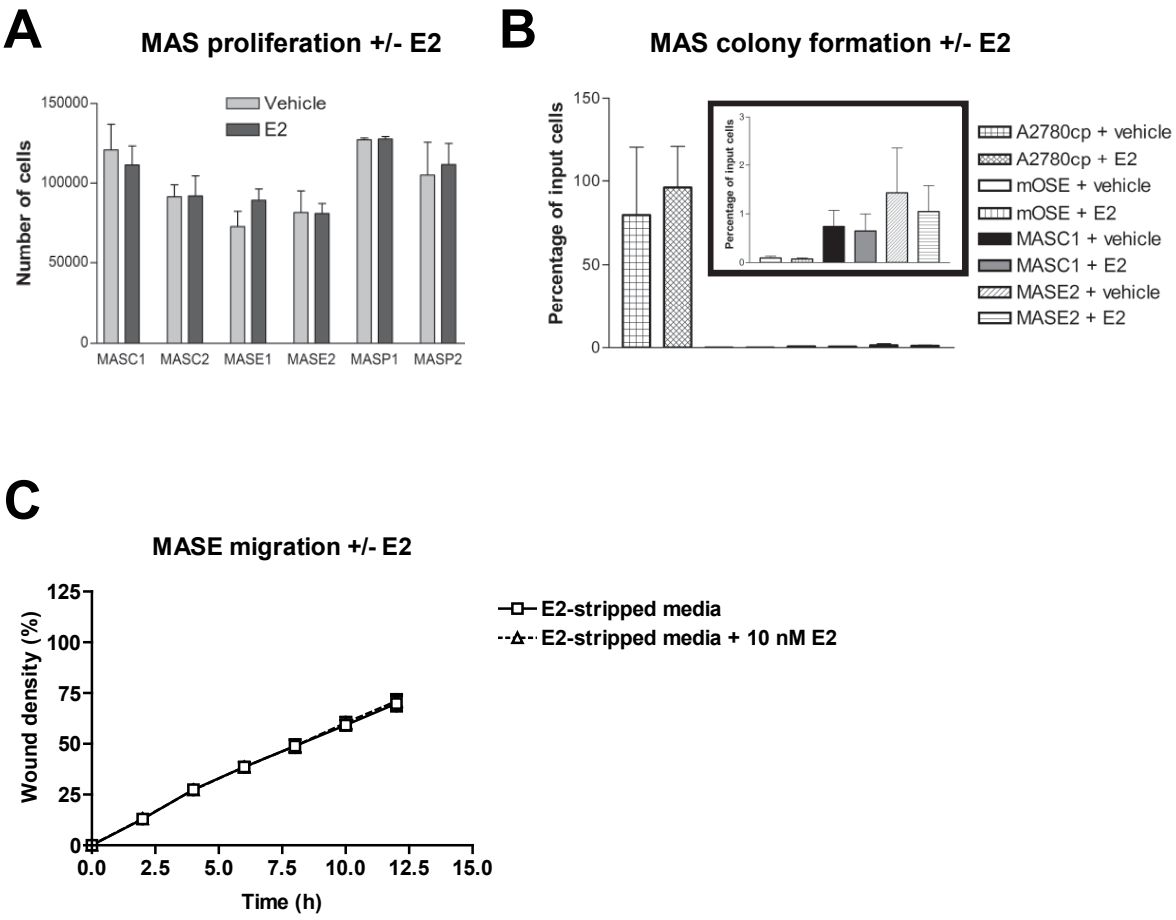

Figure 10. Effect of E2 on proliferation, colony formation, and migration of mouse ascites (MAS) cell lines. A) MAS cells (described in Table 1) were plated at 15,000/well and treated with 500 nM E2, then counted 48h later. Proliferation was not altered by E2 in any cell line (n=3). B) To assess tumourigenicity, MAS cells were plated in E2-free media with 1% agarose and 250 nM E2 or vehicle control. Colony formation was not altered by E2 in any cell line (n=3; positive control: A2780cp; negative control: mOSE). C) Migration was examined by plating MASE cells in 96-well ImageLock plates and using an Essen Biosciences Woundmaker when 100% confluent. Plates were then washed twice with PBS and replenished with E2-free media containing 10 nM E2 or vehicle control and cultured in the IncuCyte incubator system with images taken every 2h. Wound density was determined by IncuCyte ZOOM software (see Figure 33). Rate of wound closing was not altered by E2 (n=3).

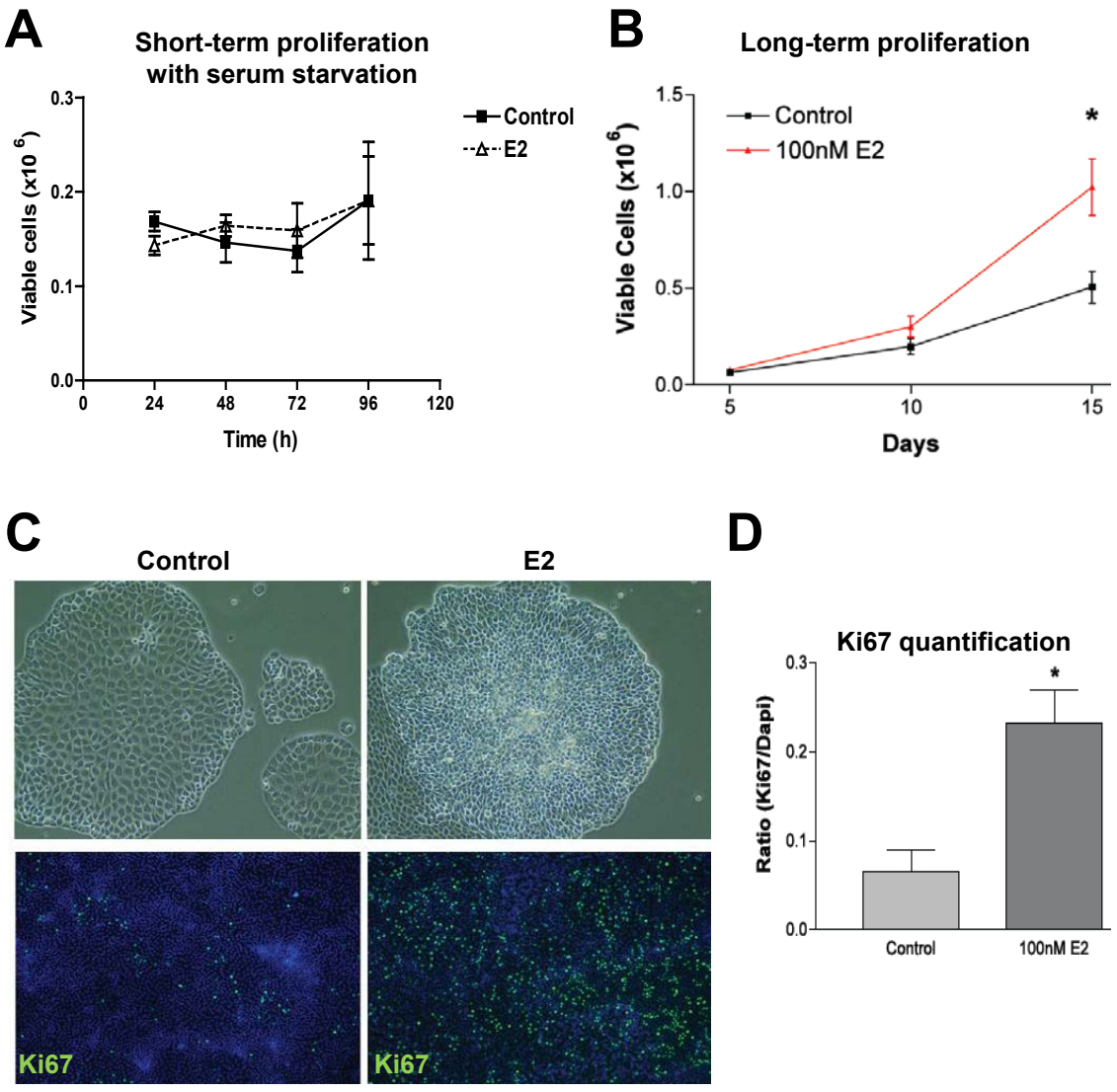

Figure 11. Effect of E2 on proliferation of normal mouse ovarian surface epithelial cells (mOSE). A) Proliferation and (not shown) viability of mOSE in serum starvation conditions (0.1% serum) were assessed with a ViCell automated counter over 4d of treatment with 500 nM E2; E2 did not alter proliferation or survival (n=3). B) When mOSE cells were assessed over a longer time frame (15d), E2 increased proliferation (n=3; *: $p<0.05$; t-test). C) After being treated with 100 nM E2, mOSE cells showed a loss of contact-inhibition, forming multi-layered growths. ICC for Ki67 indicated that cells in these growths remained highly proliferative. D) In confluent areas, Ki67 was higher in E2-treated cells (n=3; *: $p<0.05$; t-test).

or in normal serum conditions (not shown). However, long-term E2 treatment increased mOSE proliferation (Figure 11B) and caused cells to build up into dense, multi-layered structures expressing high Ki67 (Figure 11C), suggesting that E2 can override cell cycle arrest signals such as contact-inhibition. In confluent areas, the proportion of Ki67+ cells was increased 3.3-fold by E2 ($p=0.0182$; Figure 11D). The resulting disorganized cell growth may be a mechanism of action for the E2-stimulated tumour growth and preneoplastic lesions seen in our mouse models.

3.2: Elucidation of factors modulating tumour progression in CAG-TAg mice

3.2.1. P4 has no effect on tumour growth in CAG-TAg mice

To investigate whether P4 either directly inhibits ovarian cancer growth or abrogates the deleterious effects of E2 in the CAG-TAg model, two studies were done in 8-month old mice (to model ovarian cancer occurring after many reproductive cycles in women). In the first study, mice were treated with inert placebo pellets, pellets releasing P4 or E2, or a combination treatment (implanting both pellets). Surgeries were done for 12 mice per group based on the prediction that several mice would need to be excluded for health problems unrelated to tumour growth, including the bladder complications known to occur occasionally in E2-treated CAG-TAg mice (L. Laviolette, unpublished data). P4 did not alter survival, tumour burden, ascites volume or incidence, or body weight relative to controls (Figure 12). Similarly, adding P4 to E2 treatments did not alter any of these outcomes relative to mice treated with E2 alone, although the combined E2+P4 treatment did show a trend for a decreased tumour burden ($p=0.0589$). To confirm that P4 does not affect tumour progression, a pilot study was done using a longer

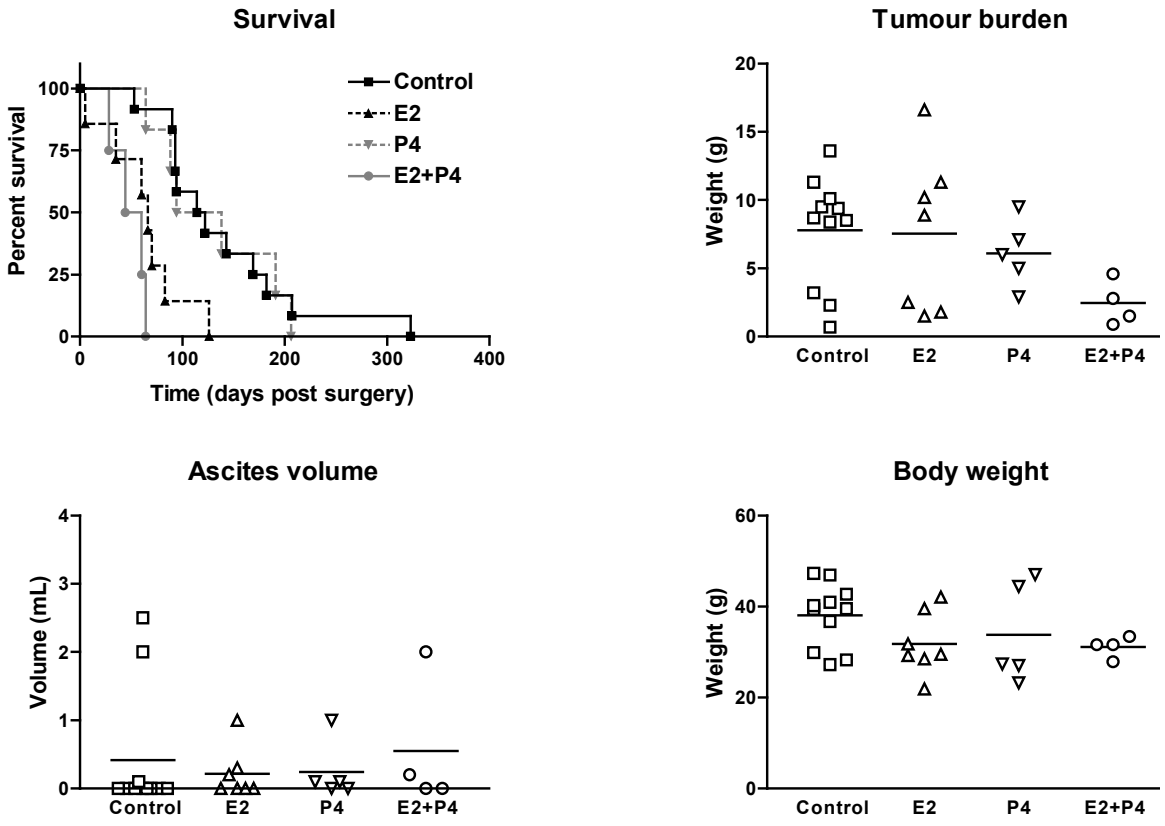

Figure 12. Effect of P4 on CAG-TAg tumour progression with and without E2. Immediately after bilateral i.b. AdCre injections, 8 month old CAG-TAg mice were implanted s.c. with a slow-release E2 pellet (0.25 mg), P4 pellet (50 mg), both pellets (E2+P4 combined treatment), or a placebo pellet. Survival curves were compared by log-rank tests (control vs. P4 and E2 vs. E2+P4; N=4-12; both $p>0.05$). Tumour weight, ascites volume, and body weight were measured at endpoint and compared by two-way ANOVA; P4 caused a trend for decreased tumour burden ($p=0.0589$) but no significant differences were observed (N=4-11; all $p>0.05$).

P4 treatment (2 serial doses) in 4 mice. For this study, P4 pellets were removed after 60d and replaced with a fresh hormone pellet, enabling exposure to the hormone for at least 120d. The effect of P4 inhibition was also examined using slow-release pellets containing the PGR antagonist mifepristone (MF; 50 mg/60d). No survival difference was seen with either long-term P4 treatment or MF treatment (Figure 13). Similarly, no changes in tumour burden, ascites volume, or body weight were observed with either treatment relative to controls.

3.2.2. Menopause does not alter tumour progression in CAG-TAg mice

To examine the impact of menopause on ovarian cancer growth, the VCD-induced chemical model of menopause was previously combined with the CAG-TAg model of ovarian cancer in young mice (Laviolette et al. 2011). To better simulate human menopause, which occurs in older women after many reproductive cycles, mice were aged to 6 months before initiating VCD injections. Mice were injected with 240 mg/kg VCD (or vehicle control) for 5 consecutive days to induce follicular atresia. After 60d, ovarian failure was confirmed by examining ovarian histology. Few or no follicles were seen in the ovaries of VCD-treated mice (Figure 14A), whereas age-matched control mice had many obvious follicles (Figure 14B). Induction of ovarian failure with VCD had no effect on CAG-TAg mouse survival regardless of hormone treatment (Figure 14C). Similarly, VCD did not alter tumour burden, ascites volume, or body weight in any treatment group (Figure 15).

3.2.3. A lower dose of E2 has little to no effect on tumour progression

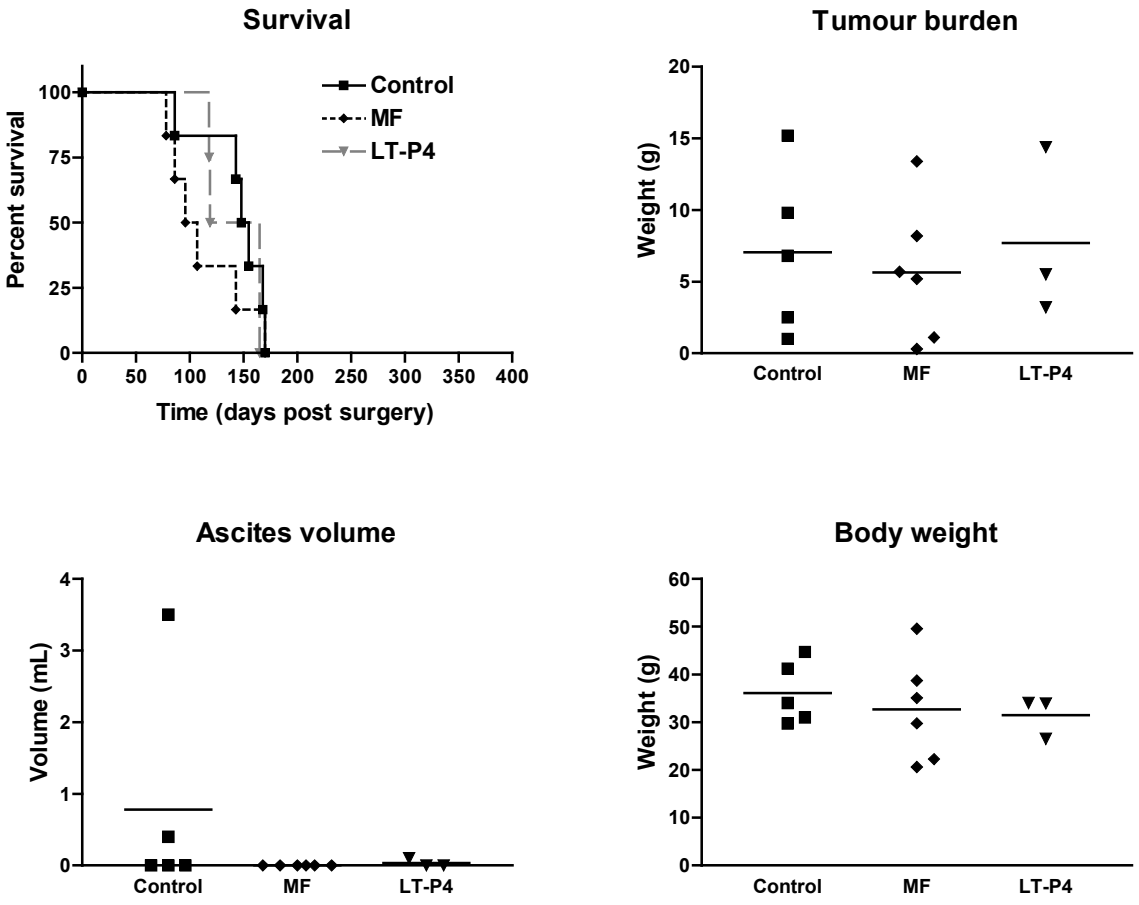

Figure 13. Effect of P4 inhibition or long-term treatment on CAG-TAg tumour progression. Immediately after bilateral i.b. AdCre injections, 6-8 month old CAG-TAg mice were implanted s.c. with a slow-release pellet containing a progesterone receptor antagonist (mifepristone; MF; 50 mg), P4 (50 mg), or placebo pellet (N=4-6). Unlike the previous P4 study (Figure 12), P4 pellets were replaced after 60d with a fresh P4 pellet for a long-term treatment (LT-P4). Survival curves were compared by log-rank tests (control vs. MF and control vs. LT-P4; N=4-6; both $p>0.05$). Tumour weight, ascites volume, and body weight were measured at endpoint and compared by one-way ANOVA, but no significant differences were observed (N=4-11; all $p>0.05$).

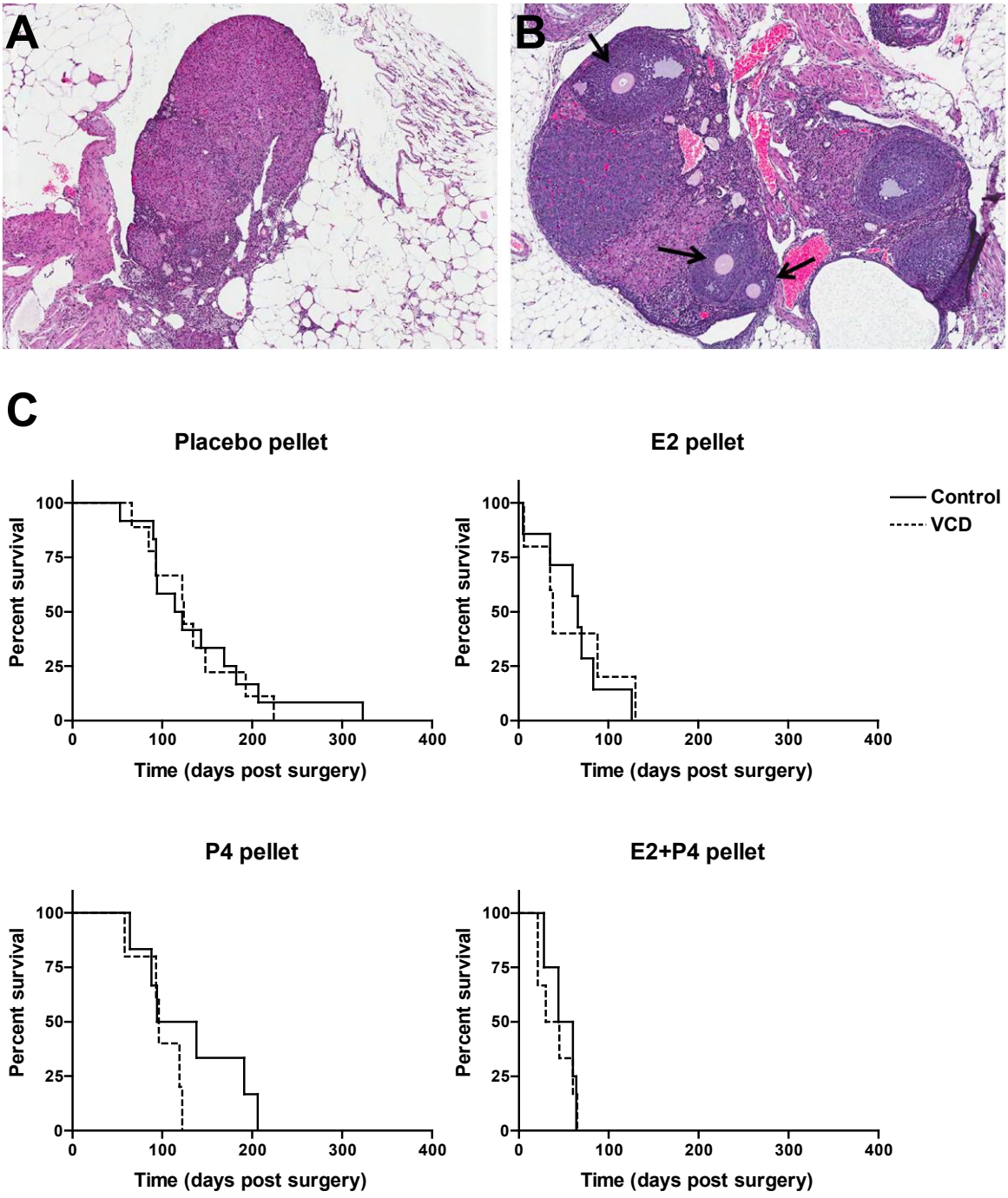

Figure 14. Effect of VCD-induced ovarian failure ("menopause") on CAG-TAg tumour progression and response to hormones. Ovarian failure was induced in 6 month old CAG-TAg mice by i.p. VCD injections; 60d later, surgeries were done to activate TAg and implant hormone pellets. A) No follicles are seen in the ovary of a VCD-treated mouse 60d after injections. B) Growing follicles (arrows) are easily seen in the ovary of an age-matched control mouse. C) VCD treatment did not alter survival in any of the four hormone contexts examined (N=4-12, $p>0.05$, log-rank test).

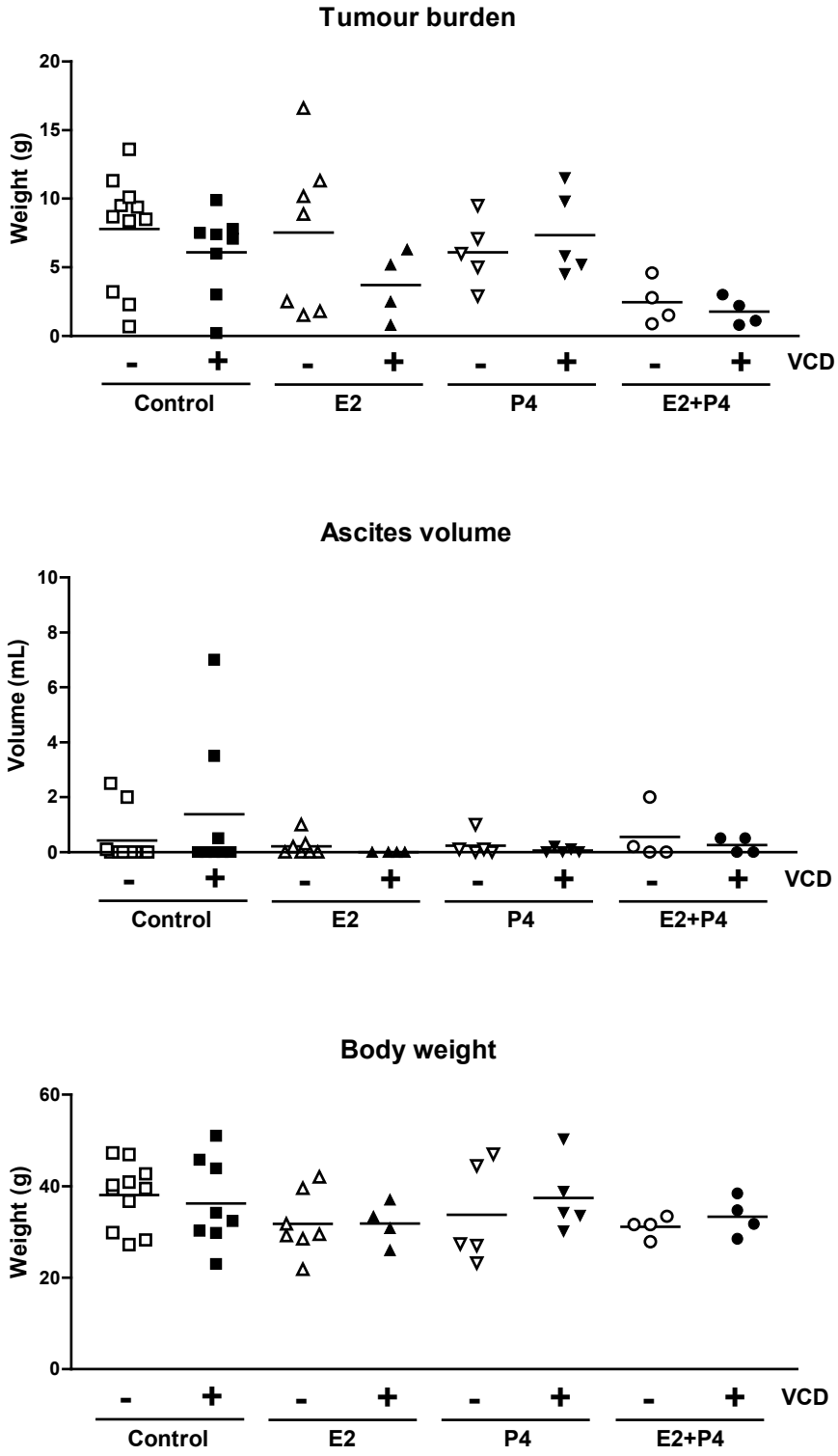

Figure 15. Effect of VCD-induced ovarian failure ("menopause") on CAG-TAg endpoint characteristics. For the mice described in Figure 14, VCD treatment did not alter tumour burden, ascites volume, or body weight at endpoint in any hormone context (N=4-11; $p>0.05$, two-way ANOVA).

To investigate whether E2 acts in a dose-dependent manner, and in an attempt to reduce the bladder complications seen previously with E2 treatment, an additional low-dose E2 (0.05 mg/60d) treatment group was compared to the higher regular dose of 0.25 mg/60d. Surprisingly, no mice in this study developed bladder problems with either low-dose E2 or the higher-dose E2. The lower dose of E2 showed a trend for decreased survival but was not significantly different from control mice due to high variability (41% shorter median survival; p=0.1091; Figure 16). Decreases in tumour burden and body weight seen at the higher E2 dose were not seen with the lower dose, and ascites volume and incidence were unchanged by E2 at either dose (Figure 16).

3.2.4. Both alleles of TAg contribute to tumour progression in a mouse strain-specific manner

To determine if some of the variability in animal survival in the previous experiments might be due to the number of alleles in which TAg was activated, we tested whether tumour progression is maximally driven with one allele of TAg. CAG-TAg mice were crossed with wildtype mice of the same strain (FVB/N) and given i.b. AdCre injections to activate TAg. Although all resulting TAg hemizygous mice formed tumours, median survival was prolonged by 47% relative to normal TAg-homozygous CAG-TAg mice (p=0.0036; Figure 17A).

Surprisingly, when CAG-TAg mice were crossed with mice of a different background (ESR1-floxed mice; C57BL/6N; B6) in another study using identical methodology to induce tumour formation, no tumours developed in any of the resulting 47 mixed-background (F3; $ESR1^{wt/wt}$ and $ESR1^{fl/fl}$) TAg-hemizygous mice by up to 150 days, even with E2 treatment (data not shown). To confirm that the mixed B6 background

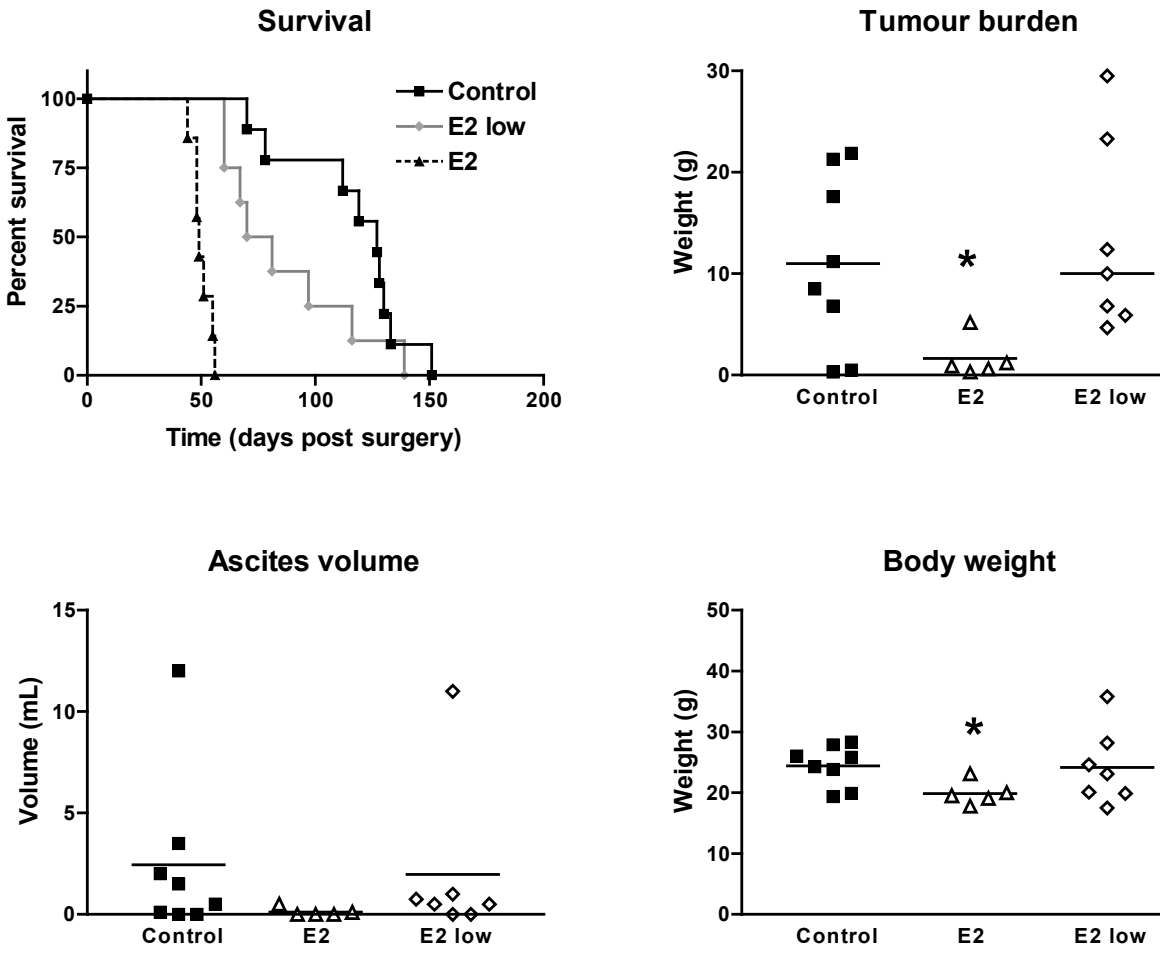

Figure 16. Effect of low-dose E2 on CAG-TAg tumour progression. CAG-TAg mice were implanted with hormone pellets immediately following i.b. AdCre injections. Mice treated with a low-dose E2 pellet (0.05 mg; "E2 low") showed a trend for intermediate survival time between mice treated with placebo and mice treated with the higher E2 dose used in previous studies (0.25 mg; "E2"), but this did not reach statistical significance due to large variability ($p>0.05$, log-rank test vs. control). Unlike mice treated with the higher E2 dose, the tumour burden and body weight of mice treated with low-dose E2 were no different from control mice (N=5-9; *: $p<0.05$; t-test vs. control). Ascites volume and incidence were not altered by either E2 dose (Mann-Whitney U-test and chi-square test respectively).

A

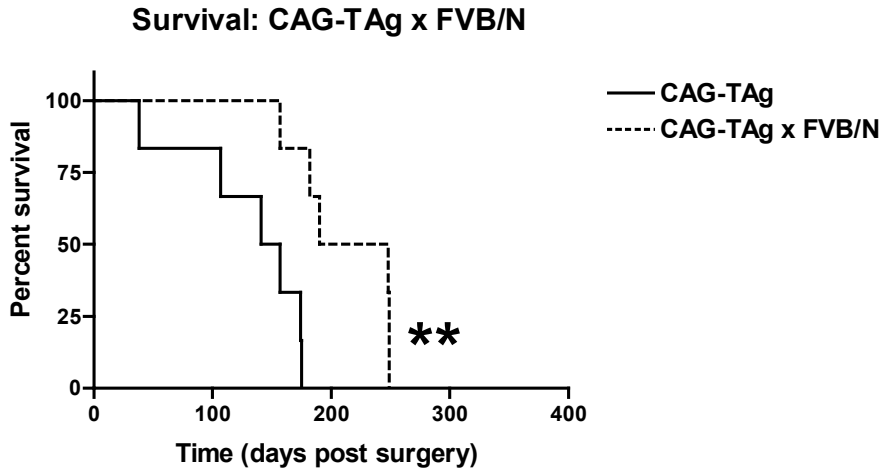

B

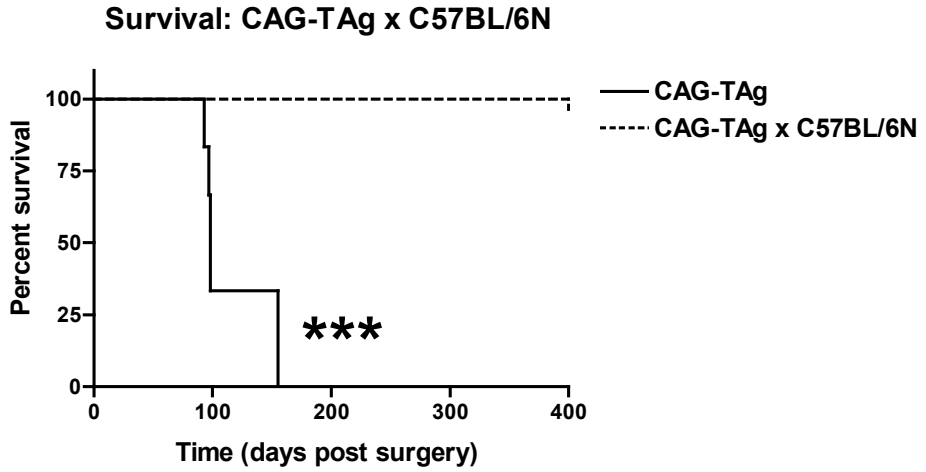

Figure 17. Changes in tumour development with different numbers of TAg alleles and mouse strains. A) When CAG-TAg mice were crossed with wildtype FVB/N mice, the resulting TAg-hemizygous offspring had prolonged survival time after i.b. AdCre relative to normal CAG-TAg mice (N=6; **: $p<0.01$; log-rank test). B) When CAG-TAg mice were crossed with wildtype C57BL/6N mice, i.b. AdCre did not induce any tumours in the resulting TAg-hemizygous offspring after being monitored for over a year (N=6; ***: $p<0.001$; log-rank test).

was the problem, an additional study was done comparing mixed-background TAg-hemizygous mice to regular (FVB/N background and TAg-homozygous) CAG-TAg mice. F1 mixed background mice were generated by crossing CAG-TAg mice with wildtype B6 mice. In this study, FVB/N CAG-TAg mice formed tumours normally with a median survival time of 98 days after AdCre injections, whereas the mixed-background mice were euthanized after more than 400 days with no tumours ($p<0.0001$; Figure 17B).

3.3: Mechanisms of E2 action in ovarian cancer models

3.3.1. E2 regulates many genes in tumours from the MASE allograft mouse model

To determine possible mechanisms by which E2 accelerates tumour progression, microarray analyses were done comparing MASE-derived tumours from E2-treated vs. control mice, identifying 197 upregulated and 55 downregulated genes. The full list is available on the Gene Expression Omnibus database (accession number GSE45271). Based on expression level and known function, several E2-upregulated "genes of interest" were selected for further analysis (Table 5). Six of these were examined by QPCR in MASE-derived tumours to confirm their upregulation by E2 (*Greb1*, *Stc2*, *Pgr*, *Cyp11a1*, *Kdr*, and *Ednra*; Figure 18). A collaborator confirmed E2-upregulation of a seventh gene (*Taf4b*) as well as the estrogen receptors *Esr1* and *Esr2* in the same tumour samples (Wardell et al. 2013).

3.3.2. E2 upregulates angiogenesis-related genes but does not alter microvessel density in MAS allograft models

Table 5. Subset of interesting E2-upregulated genes identified in a microarray of tumours from MASE-engrafted mice.

Gene		Gene Ontology Pathway(s)	logFC	P value
Cyp11a1	Cytochrome P450 (scc)	Steroid metabolic process	4.26	0.0006
Greb1	Growth regulation by estrogen in breast cancer 1	Unknown	3.41	0.0015
Fgf7	Fibroblast growth factor 7	Cell proliferation Cell division	2.65	0.0044
Pgr	Progesterone receptor	Reproduction Transcription Cell proliferation Cell differentiation	2.64	0.0446
Cdh2	N-cadherin	Cell differentiation Cell migration	2.18	0.0044
Ednra	Endothelin receptor type A	Cell differentiation Angiogenesis	2.11	0.0281
Kdr	Vascular endothelial growth factor receptor 2	Cell proliferation Cell migration Cell differentiation Angiogenesis	2.07	0.0170
Stc2	Stanniocalcin 2	Biological process	1.90	0.0201
Bmp6	Bone morphogenetic protein 6	Cell differentiation Inflammatory response	1.31	0.0375

(Laviolette et al. 2014)

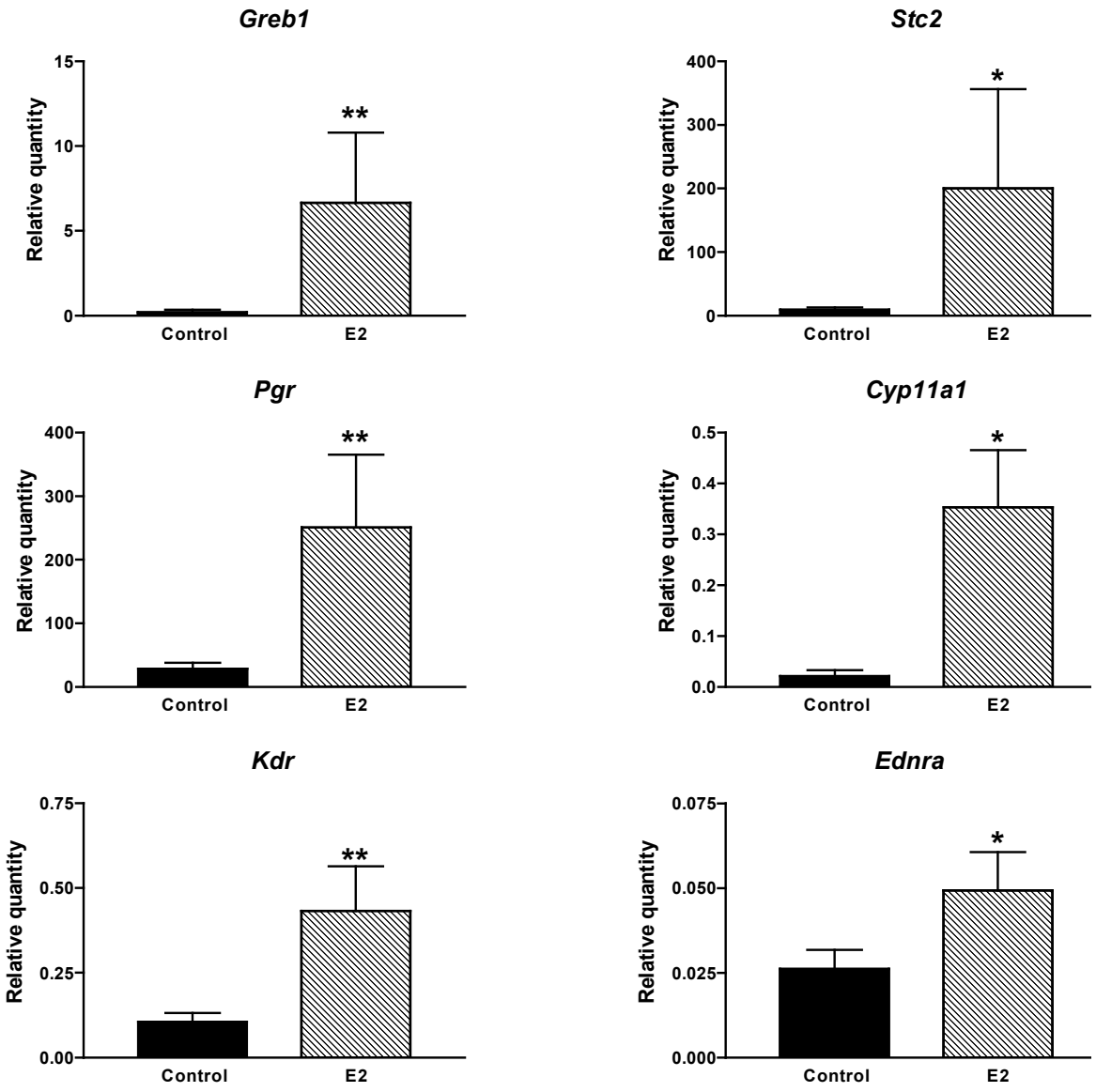

Figure 18. Validation of a microarray comparing tumours from E2 vs. placebo-treated mice injected with MASE cells. Six E2-regulated genes identified by the microarray were examined by QPCR in snap-frozen tumours of OVX mice injected with MASE cells (described in Figure 5). Data were normalized to *18S* or *Ppia* and log-transformed for statistical analysis. Upregulation by E2 treatment in vivo was confirmed for all six genes (N=3-8; *: $p<0.05$; **: $p<0.01$; one-tailed t-test).

Two E2-upregulated genes are closely linked to angiogenesis (*Kdr* and *Ednra*, which encode VEGF receptor type II and endothelin receptor type A, respectively), suggesting that increased angiogenesis may be a mechanism of E2 action in the MASE allograft model. To determine whether the upregulation of *Kdr* and *Ednra* was specific to MASE-derived tumours, MASC-derived tumours were also examined. Surprisingly, E2 did not upregulate either gene (Figure 19A) in MASC-derived tumours. In fact, E2 decreased *Ednra* by 63% (p=0.0129) and *Kdr* also showed a trend for a 61% decrease with E2 (p=0.0701). Consistent with the mRNA differences, KDR and EDNRA were increased at the protein level by E2 in MASE- but not MASC-derived tumours (Figure 19B). To confirm that E2 can act directly on MASE tumour cells rather than simply upregulating angiogenesis-related genes in the stroma, E2 induction of *Kdr* and *Ednra* was examined in MASE cells in vitro. Both genes were consistently upregulated by E2 at all doses examined (10-500 nM), but statistics could not be done with *Ednra* due to technical problems with one replicate, and *Kdr* showed high replicate variability in the magnitude of upregulation by E2 (2.4 to 25-fold increase), reducing the statistical significance of the observed effects (10 nM p=0.046; 100 nM p=0.0765; 500 nM p=0.0824; Figure 20A). KDR was also upregulated at the protein level by all doses of E2, although EDNRA was not changed by E2 (Figure 20B). This suggests that the observed upregulation of *Kdr* and perhaps also *Ednra* in MASE-derived tumours was caused by E2 acting directly on MASE tumour cells.

To further clarify the role of *Kdr* and *Ednra* in the MAS allograft models, the genes encoding their most relevant ligands (*Vegfa* and *Edn1*, respectively) were examined in MASE cells and in MASE- and MASC-derived tumours (Figure 21). *Vegfa* was not significantly changed by E2 in MASE-derived tumours, although a trend for a

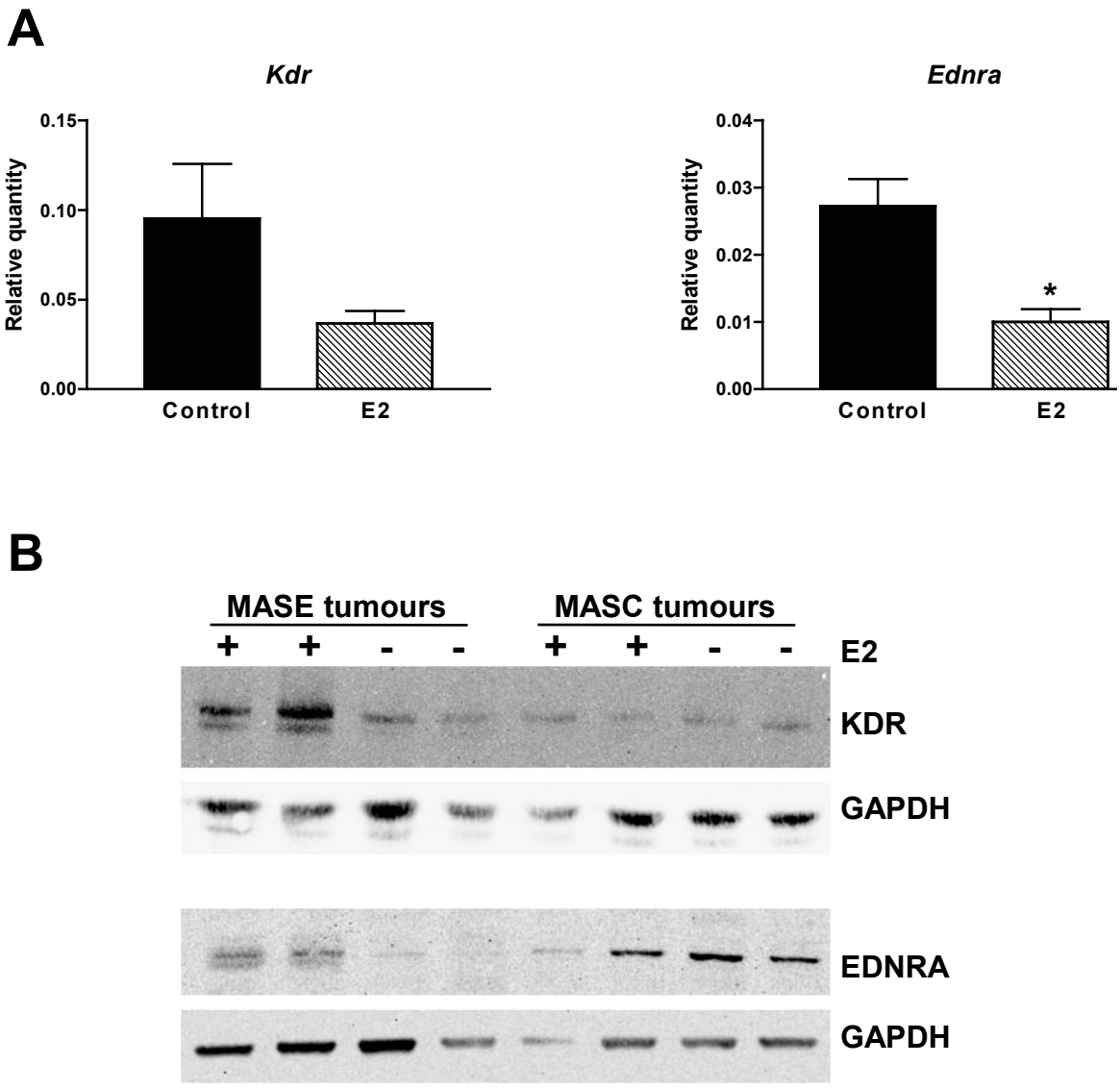

Figure 19. Validation of E2 induction for two angiogenesis-related receptors in MAS-derived tumours. A) *Kdr* and *Ednra* were examined by QPCR in snap-frozen tumours from E2-treated and control OVX mice injected with MASC cells (see Figure 5). QPCR data were normalized to *Ppia* and log-transformed for statistical analysis. *Ednra* was decreased by E2 in MASC-derived tumours and *Kdr* showed a nearly-significant trend for a similar decrease ($p=0.0701$; N=4; *: $p<0.05$; t-test). B) KDR and EDNRA protein levels were examined by western blot in MAS-derived tumours. KDR and EDNRA were both increased by E2 in MASE but not in MASC tumours.

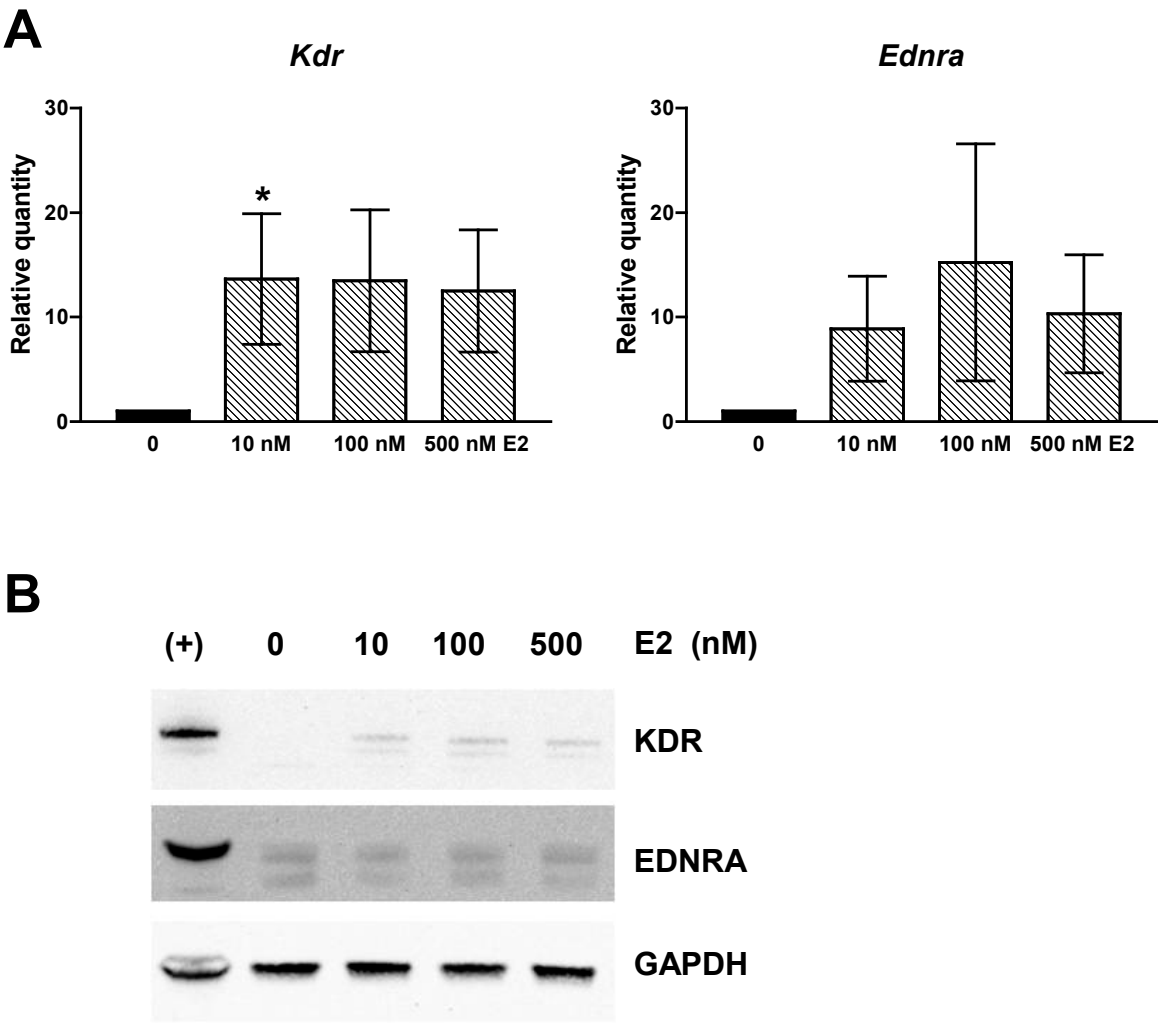

Figure 20. Validation of KDR and EDNRA induction by E2 in MASE cells. MASE cells were treated with 10-500 nM E2 and collected after 48h for analysis by QPCR and western blot. Gene expression was quantified relative to the E2-free sample for each replicate, normalized to *Ppia,* and log-transformed for statistical analysis. A) *Kdr* and *Ednra* were consistently upregulated by E2 at all doses examined, but statistical analysis was not possible for *Ednra* (n=2) and large variability in the magnitude of upregulation reduced the statistical power of *Kdr* (n=3; 100 nM p=0.0765; 500 nM p=0.0824; *: $p<0.05$, one-sample t-test vs. control). B) E2 upregulated KDR but not EDNRA at the protein level at all three doses examined. Mouse heart was used as a positive control.

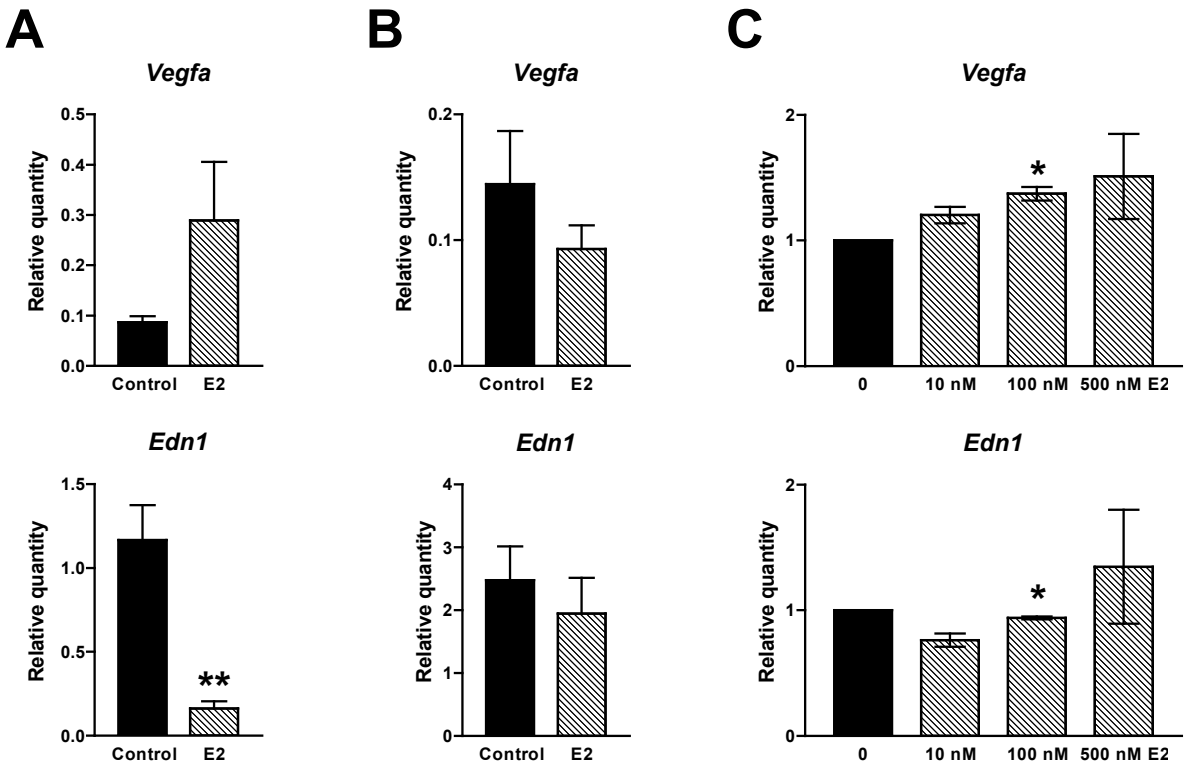

Figure 21. E2-induced changes in expression of KDR and EDNRA ligands in MAS-derived tumours and MASE cells. E2 regulation of *Vegfa* and *Edn1* was examined by QPCR in MAS tumours and MASE cells. MAS tumours were quantified relative to the positive control (mouse heart); MASE cells were quantified relative to the E2-free sample for each replicate. Expression was normalized to *Ppia* and relative quantities were log-transformed for statistical analysis. A) Tumours from mice injected with MASE cells showed a trend for increased *Vegfa* ($p=0.1752$) whereas *Edn1* was reduced by E2 treatment (N=4-8; **: $p<0.01$, t-test). B) *Vegfa* and *Edn1* were not altered by E2 treatment in tumours from mice injected with MASC cells (N=4). C) MASE cells showed a trend for a dose-dependent increase in *Vegfa*, but only the 100 nM dose was statistically significant (n=3; *: $p<0.05$, one-sample t-test vs. control). *Edn1* was decreased by 100 nM E2.

3.3-fold increase by E2 (p=0.1752) was seen (Figure 21A). *Edn1* was downregulated 86% (p=0.0019) by E2 in MASE-derived tumours (Figure 21A). In MASC tumours, *Vegfa* and *Edn1* were not changed by E2 (Figure 21B). In MASE cells, *Vegfa* was increased by 100 nM E2 (p=0.0153) and showed a trend for a dose-dependent increase between 10 nM (20% increase; p=0.0787) and 500 nM E2 (51% increase; p=0.2415) (Figure 21C). *Edn1* was highly variable, showing a trend for decrease at lower doses of E2 (10 nM p=0.0571 and 100 nM p=0.0372).

To determine the localization of KDR in tumour and stroma cells, paraffin-embedded tumours were examined by IHC (Figure 22). KDR was expressed in both the endothelial cells and tumour cells of MASE- (Figure 22) and MASC-derived tumours (Figure 23). No changes were seen with E2 treatment in either model (not quantified). For a functional measure of angiogenesis, microvessel density was assessed by IHC for CD31 in paraffin-embedded tumours (Figure 24A). No differences were seen between tumours from placebo- vs. E2-treated mice in either MAS model (Figure 24B).

3.4: GREB1 expression and function in cell and mouse models of ovarian cancer

3.4.1. GREB1 is induced by E2 in several mouse cell lines and allograft models

Greb1 was highly upregulated in the microarray (Table 5), and is a particularly interesting target due to its critical role in E2-stimulated breast cancer cell proliferation. Initial experiments showed that *Greb1* was induced 58-fold in MASE cells by a 48h treatment with 500 nM E2 (p=0.0230, Figure 25A). In the same study, *Greb1* showed a trend for upregulation in MASC cells, but the difference did not reach significance (6.7-fold increase; p=0.0990). GREB1 was upregulated in MASE-derived tumours at the

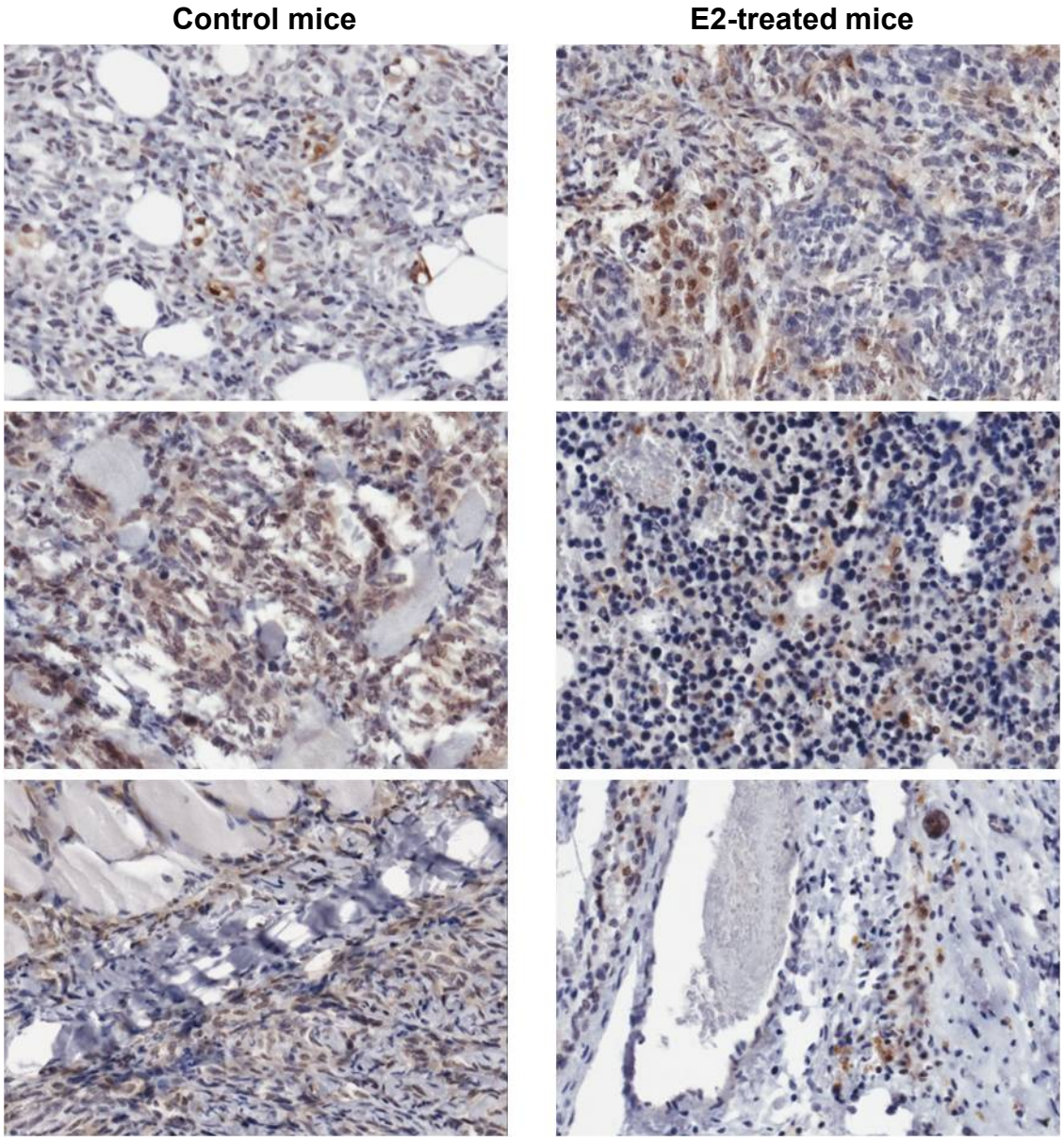

Figure 22. KDR localization in MASE-derived tumours. KDR expression was examined by IHC in paraffin-embedded tumours from mice injected with MASE cells (see Figure 5). Stained slides were scanned with a ScanScope and 40x images were taken with ImageScope software. Representative images are shown for three control-treated mice (left) and three E2-treated mice (right). KDR staining was seen in some tumour cells as well as endothelial cells; staining was variable and no obvious increase was seen in E2-treated mice.

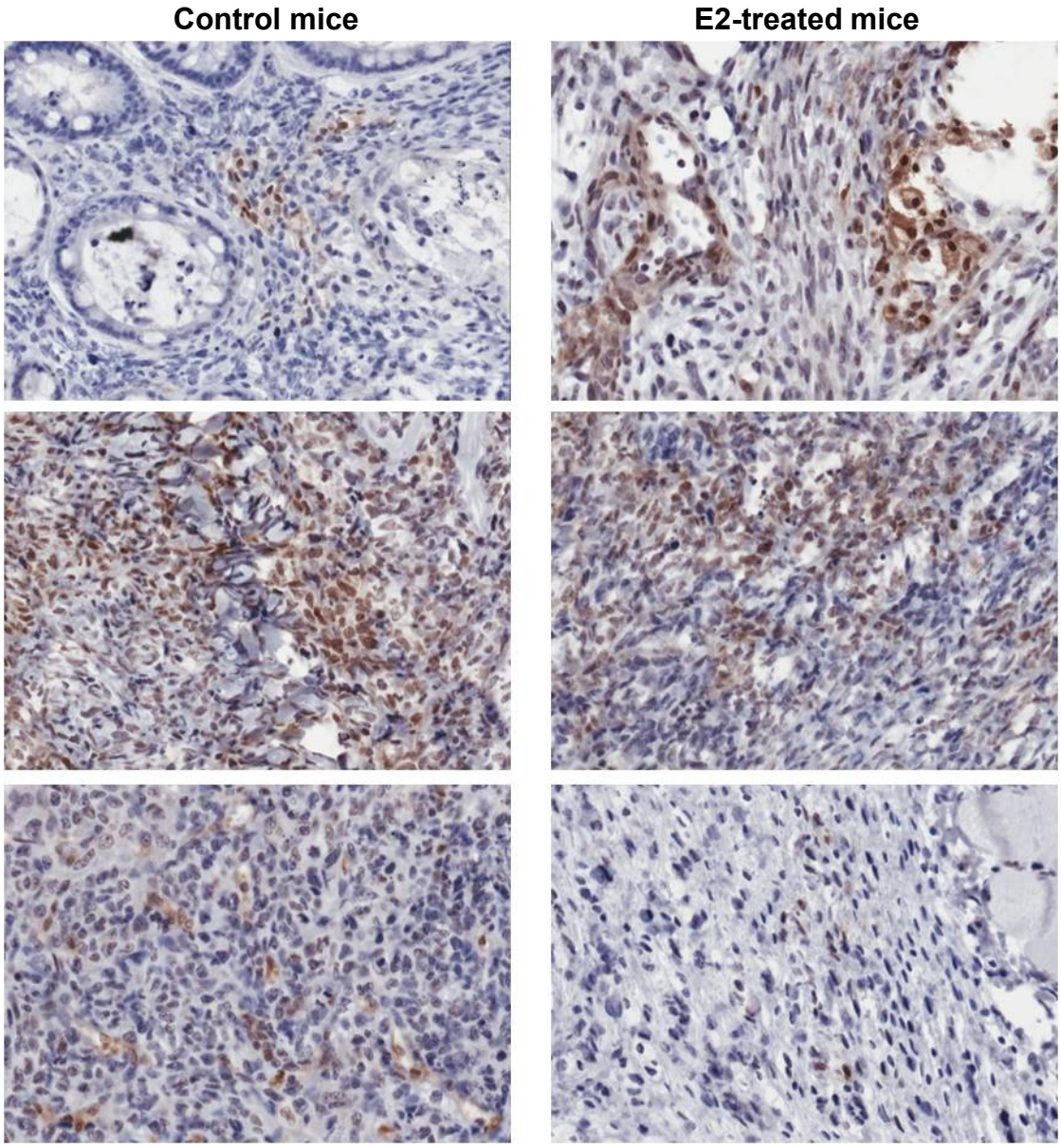

Figure 23. KDR localization in MASC-derived tumours. KDR expression was examined by IHC in paraffin-embedded tumours from mice injected with MASC cells (see Figure 5). Stained slides were scanned with a ScanScope and representative 40X images were generated for three control-treated mice (left) and three E2-treated mice (right). As in MASE-derived tumours (Figure 22), KDR staining was seen in both tumour and endothelial cells, and staining was highly variable with no obvious increase in E2-treated mice.

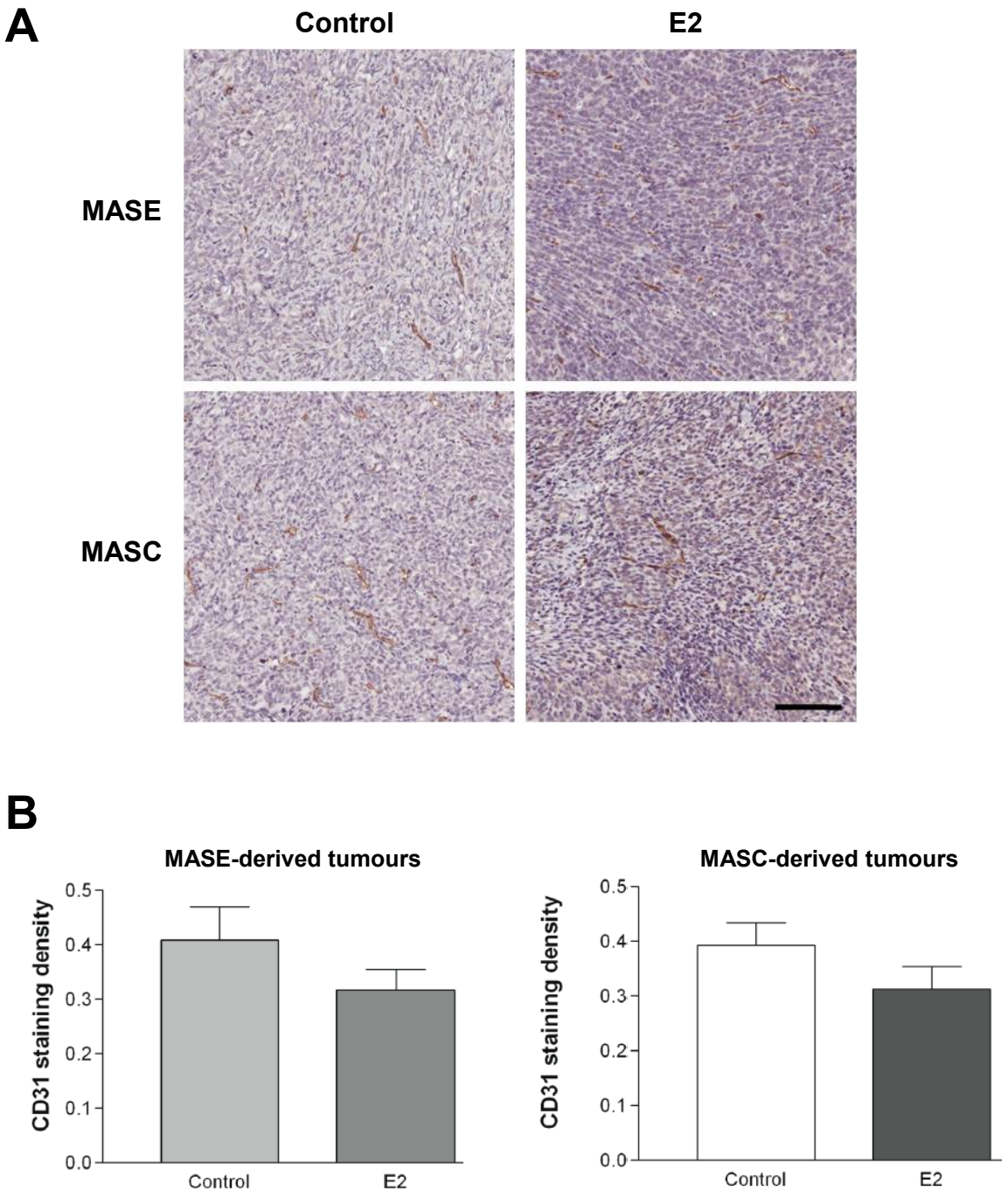

Figure 24. Effect of E2 on microvessel density in MAS-derived tumours. Paraffin-embedded tumours from MAS-engrafted mice (see Figure 5) were stained for the endothelial marker CD31 by IHC. Microvessel density was determined by quantifying DAB staining with ImageScope software. A) Representative images are shown for MAS-derived tumours from E2-treated and control mice. B) Quantification of CD31 staining. E2 did not alter microvessel density in either model (N=4; $p>0.05$; t-test). Scale bar: 100 μm.

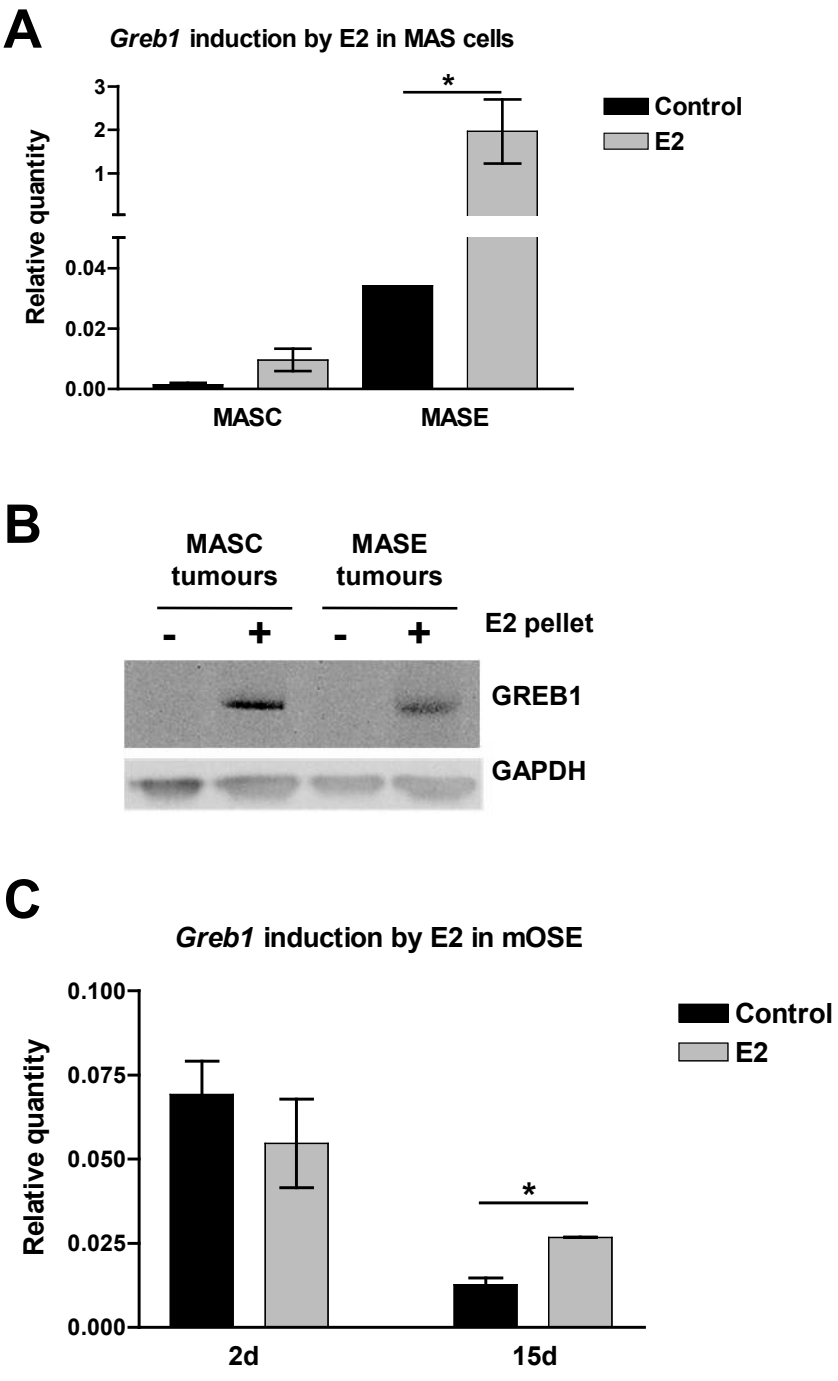

Figure 25. GREB1 expression in MAS cells, MAS-derived tumours, and mOSE cells. A) MAS cells were treated with 500 nM E2 for 48h, then RNA was collected for QPCR analysis. *Greb1* was induced by E2 in MASE cells but not in MASC cells (n=3, t-test). B) Tumours from mice engrafted with MAS cells (see Figure 5) were examined by western blot; GREB1 was induced by E2 in both MASC- and MASE-derived tumours. C) Normal mOSE cells were treated with 100 nM E2 for up to 15d (see Figure 11B-D) and RNA was collected at 2d and 15d time points for QPCR analysis. *Greb1* was induced by E2 only after long-term treatment (n=3; *: $p<0.05$; t-test).

mRNA level (Figure 18) and at the protein level (Figure 25B). GREB1 was also upregulated in MASC-derived tumours (Figure 25B).

Interestingly, *Greb1* decreased with culture time in mOSE cells; this decrease was partially abrogated by E2 treatment (Figure 25C). This may be related to the E2-induced loss of contact-inhibition seen in mOSE, which resulted in a proliferation difference visible after 15d of treatment (Figure 11B-D). It remains unclear whether *Greb1* drives mOSE proliferation or whether it is simply upregulated in proliferating cells.

To examine the pattern of GREB1 upregulation by E2 in MASE cells, a dose response and time course were done in MASE cells. After 24h of culture in E2-stripped media, 10-500 nM E2 was added for 48h, then cells were collected for QPCR and western blots. GREB1 upregulation was observed at both the mRNA and protein level with all three E2 doses (Figure 26). Two lower E2 doses (0.1 and 1 nM) showed inconsistent *Greb1* induction at the mRNA level (not shown) and GREB1 protein levels were not examined at these doses, so the 10 nM dose was used for all subsequent experiments. The time course showed *Greb1* upregulation beginning with a 1.7-fold increase at 2h and increasing to a 7.5-fold increase by 48h (Figure 26).

3.4.2. GREB1 is detectable in both the nucleus and cytoplasm of MASE cells

ICC showed that GREB1 expression is highly variable in MASE ovarian cancer cells, with little to no expression in most cells but high expression in a small subset of cells (Figure 27). This subpopulation had very distinct morphology: cells appeared small, fibroblastic or mesenchymal-looking, and rounded under phase contrast, and showed bright DAPI staining indicating condensed chromatin. This morphology suggests that these highly GREB1-expressing cells may have recently completed mitosis. Supporting

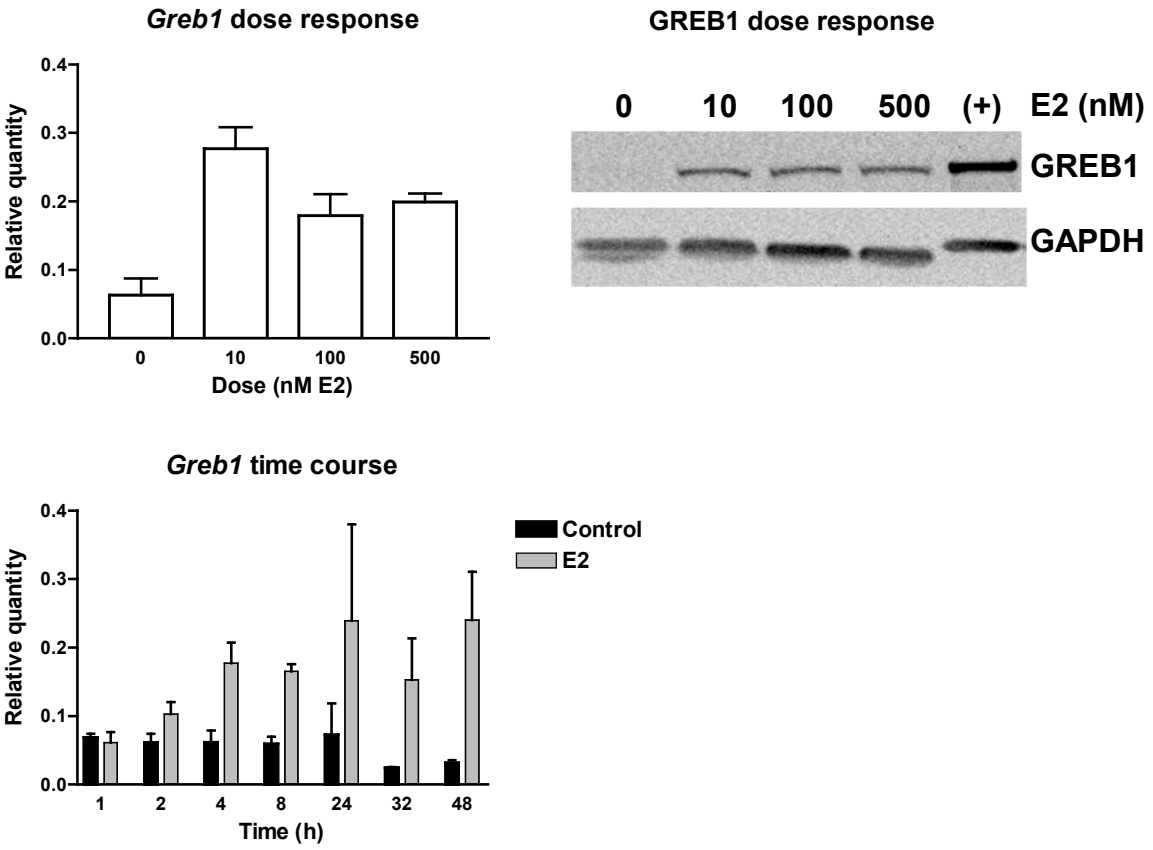

Figure 26. Validation of GREB1 induction by E2 in MASE cells. To examine whether GREB1 induction by E2 is dose-dependent, MASE cells were treated with 10-500 nM E2 and RNA and protein were collected after 48h (n=2). For the time course, MASE cells were treated with 10 nM E2 or vehicle control (an equal volume of 100% ethanol) for 1-48h and cells were collected at each time point for QPCR analysis (n=3). MCF7 cells were used as a positive control for western blots and mouse ovary was used as a positive control for QPCR. QPCR data were normalized to *Ppia*. *Greb1* upregulation was observed as early as 2h and reached a plateau at 24-48h. Graphs depict means +/- SEM.

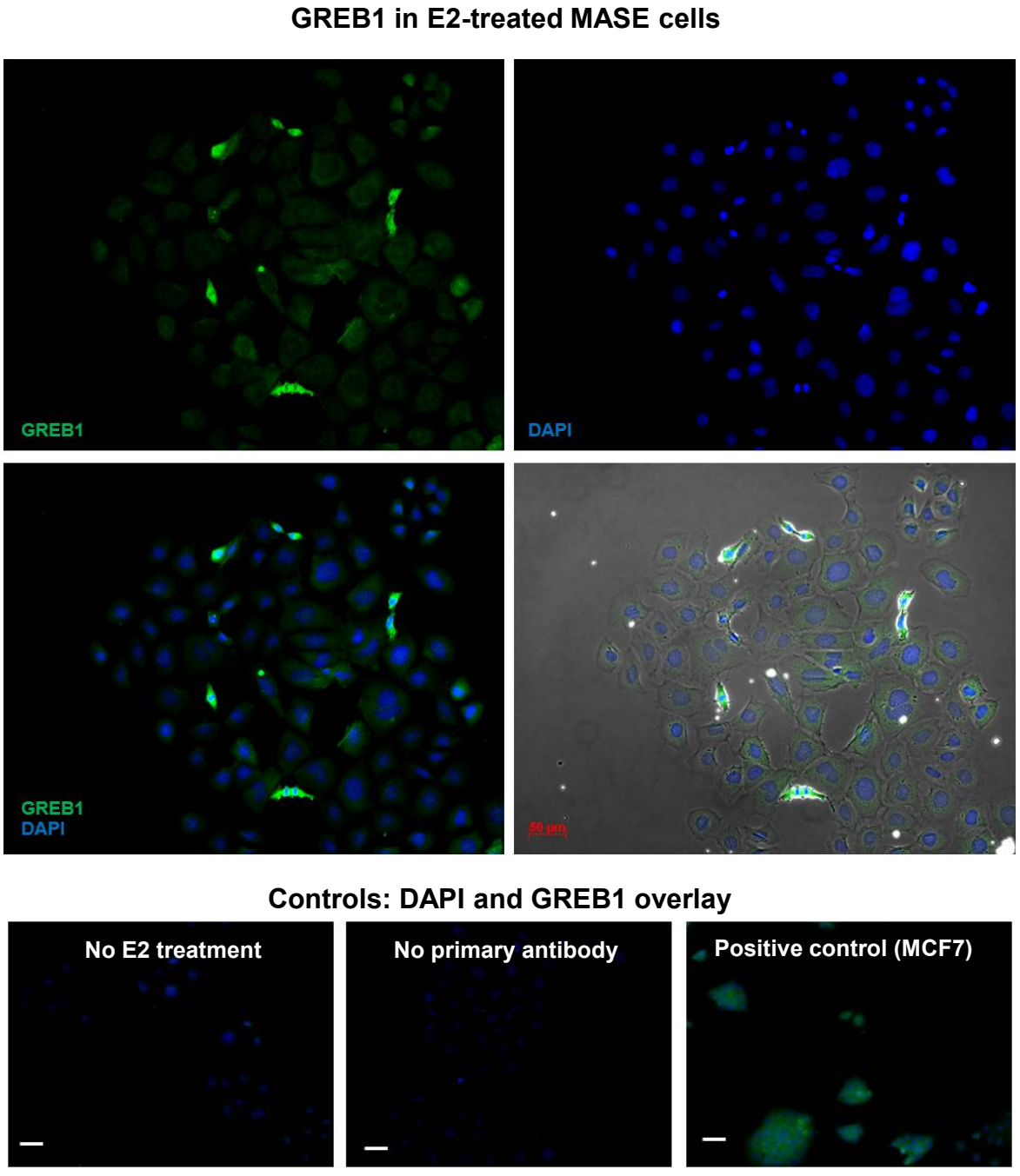

Figure 27. GREB1 localization in MASE cells. After treatment with 10 nM E2 for 24h, a subpopulation of MASE cells had high cytoplasmic GREB1 expression by ICC. These cells (arrows) had a small, rounded morphology and their DAPI staining indicated highly condensed DNA. A lower level of GREB1 was visible in both the nucleus and cytoplasm of most other cells. Negative controls had low fluorescence and the positive control (MCF7 cells) had consistent nuclear and cytoplasmic expression. Scale bar: 50 µm.

this theory, these cells were frequently seen in pairs. GREB1 expression was mainly cytoplasmic but some nuclear expression was also seen, particularly in the low-expressing cells. It is unclear from this experiment whether higher levels of GREB1 in these cells may be driving rapid mitosis, or whether all cells undergoing mitosis upregulate GREB1 temporarily. E2 treatment appeared to increase the proportion of highly GREB1-expressing cells without changing the intensity of expression in most cells (not quantified). This suggests that the increases in GREB1 mRNA and protein observed after E2 treatment (Figures 25-26) may be caused by an increased number of cells expressing high levels of GREB1 rather than an increased amount of GREB1 expressed in every cell. Alternatively, GREB1 expression may be linked with mitosis, with E2 treatment accelerating the rate of the cell cycle, resulting in an increased proportion of GREB1-expressing cells at any given time.

3.4.3. GREB1 knockdown and overexpression in MASE cells

To more directly investigate GREB1 function, lentiviral constructs were used to achieve stable knockdown and overexpression of GREB1 in MASE cells. For GREB1 knockdown, GIPZ-based lentivirus particles encoding a miR-30-based short hairpin (shRNA) targeting mouse and human GREB1 were obtained from Open Biosystems (Figure 3). For GREB1 overexpression, WPI-based lentivirus particles encoding full-length human *GREB1* were generated (Figure 4). Following transduction, cells were selected with puromycin (GIPZ constructs only), then successfully transduced cells were enriched by FACS for GFP-positive cells. Stable knockdown and overexpression were confirmed after several passages by QPCR and/or western blot (Figure 28).

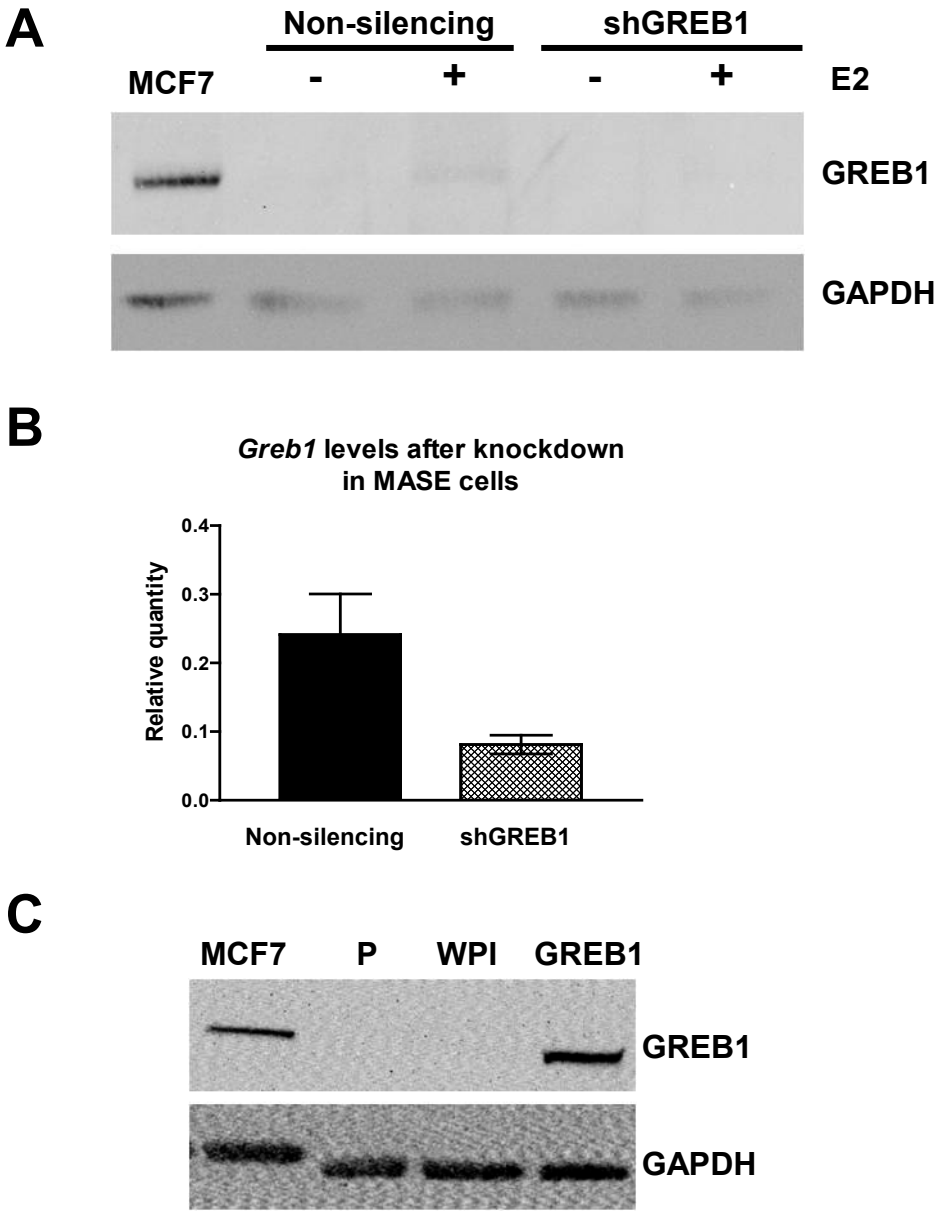

Figure 28. GREB1 knockdown and overexpression in MASE cells. Cells were transduced with a GIPZ-based lentiviral vector containing a short hairpin directed at GREB1 or with a WPI-based lentiviral vector containing the full-length human GREB1 sequence (Figure 4). Control cell lines were transduced with a non-silencing short hairpin or an empty WPI construct, respectively. Following drug selection, GREB1 baseline levels and induction by E2 were assessed by QPCR and western blot. A) GREB1 was induced by 500 nM E2 within 48h in non-silencing control MASE cells but not in cells transduced with the knockdown construct (shGREB1). B) *Greb1* mRNA levels were decreased in cells transduced with shGREB1 (n=2). C) GREB1 was highly expressed in MASE cells transduced with the overexpression construct (GREB1) and undetectable in the control-transduced cells (WPI) or parental MASE (P). MCF7 cells were used as a positive control.

3.4.4. GREB1 alters MASE cell morphology and decreases cell volume

Following selection, a stable difference in morphology was seen with both GREB1 knockdown and overexpression. Although all cell lines remained a mix of morphologies, clear changes were observed in the proportion of each phenotype. Cells with GREB1 knocked down became more epithelial-looking, with an increased proportion of large, flat cells in tight clusters and decreased proportion of small, mesenchymal-looking cells (Figure 29A). GREB1 overexpression caused a shift in the opposite direction, with an increased number of small mesenchymal-looking cells relative to the larger epithelial-looking cells. Supporting these observations, average cell volumes were decreased 32% by GREB1 overexpression ($p=0.0016$) and showed a trend for a 48% increase with GREB1 knockdown ($p=0.0756$; Figure 29B). In cells transduced with the GIPZ construct, GFP expression was seen in both subpopulation morphologies, indicating that the mixed morphology was not caused by poor transduction efficiency (Figure 30).

3.4.5. GREB1 promotes migration of MASE cells

To determine whether the morphological changes observed after GREB1 knockdown and overexpression translated to a functional effect, migration was examined using the IncuCyte system for scratch wound assays. GREB1 knockdown did not alter migration; both cell lines took approximately 24h to close the wound ($n=3$; Figure 31). Cells overexpressing GREB1 migrated more rapidly, closing the wound approximately 2h faster on average than control cells transduced with the empty WPI vector ($n=3$; Figure 32). The migration of the WPI control cells closely paralleled the migration of parental MASE cells. Migration was quantified by wound density, which was generated

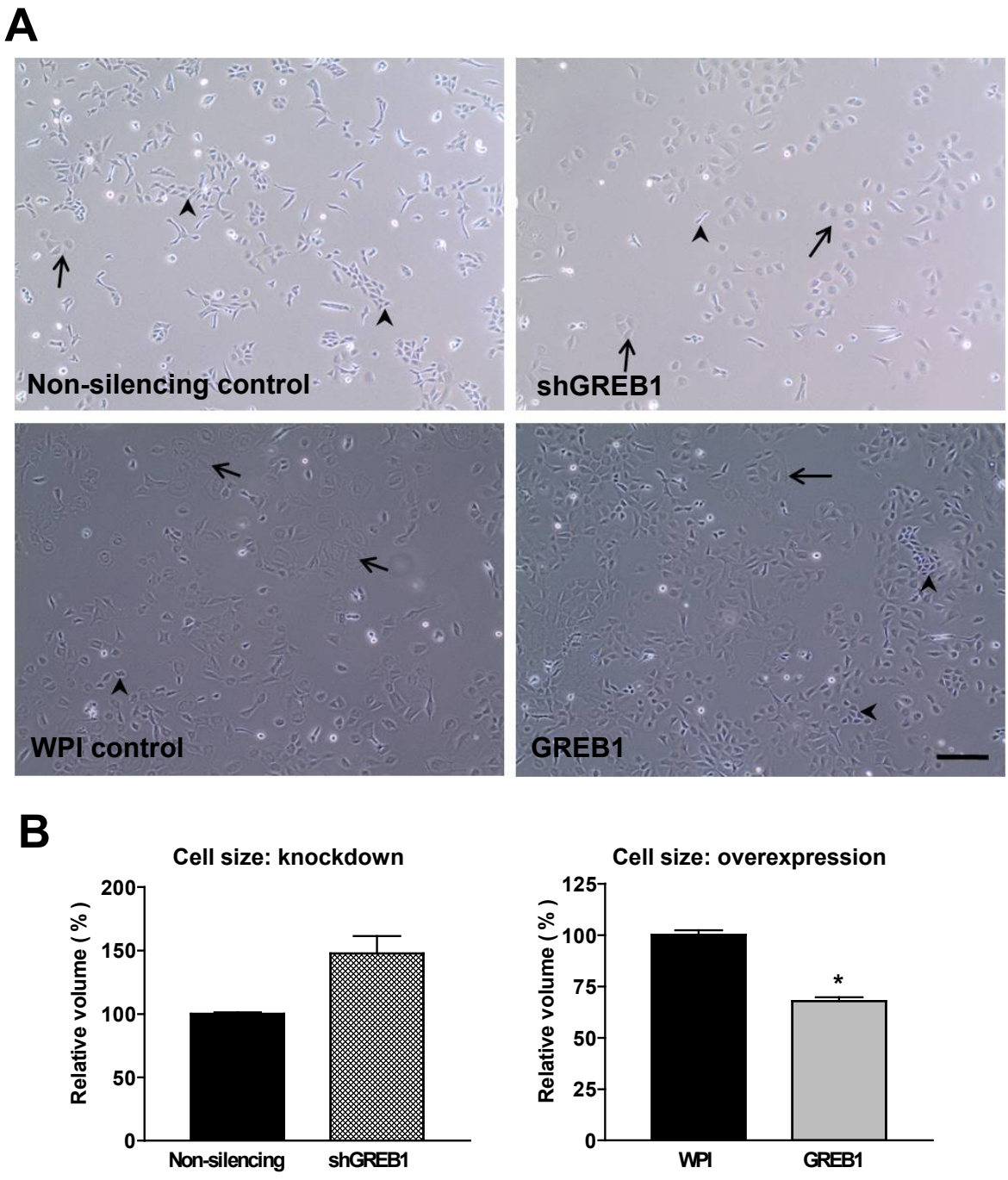

Figure 29. Effect of GREB1 knockdown and overexpression on MASE morphology. A) MASE cells with GREB1 knocked down (shGREB1) had a higher proportion of large, cobblestone "epithelial-like" cells (arrows) vs. small, fibroblastic "mesenchymal-like" cells (arrowheads) than seen in non-silencing control cells. GREB1 overexpression caused an opposite shift in these subpopulations. Scale bar: 100 µm. B) Diameter of cells in suspension was measured with a ViCell automated counter and used to calculate volume. GREB1 knockdown showed a trend for increased cell volume (n=3; p=0.0756) whereas GREB1 overexpression decreased cell volume (n=3; *: $p<0.01$; t-test).

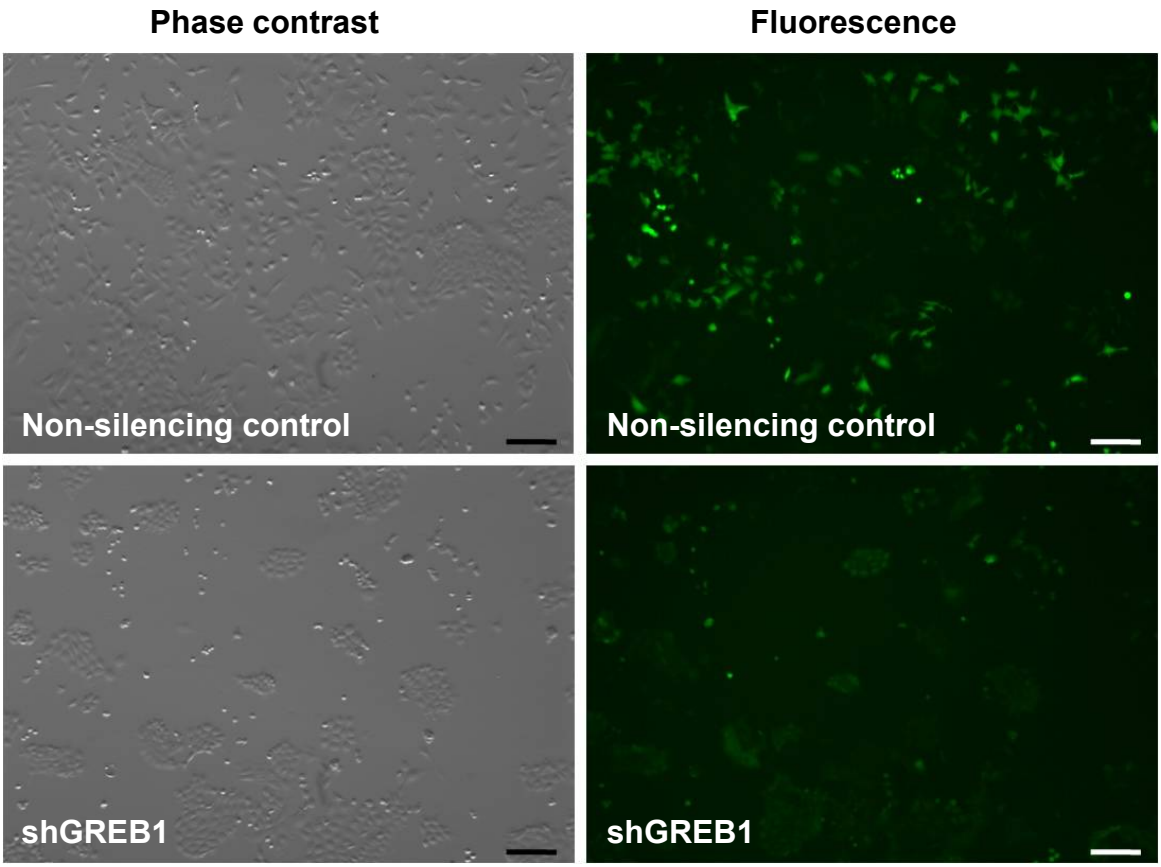

Figure 30. GFP expression in MASE cells with GREB1 knocked down. Cells were transduced with a pGIPZ-based vector encoding a short hairpin directed at GREB1 (shGREB1) or a non-silencing control hairpin (see Figure 28). GFP was examined with a fluorescence microscope several weeks after puromycin selection and fluorescence-activated cell sorting for GFP. GFP expression was variable but clearly present in both morphological subpopulations described in Figure 29. Non-silencing control cells showed higher GFP levels than shGREB1-transduced cells, but both cell lines were clearly GFP-positive relative to (not shown) non-transduced parental MASE cells. Scale bar: 100 μm.

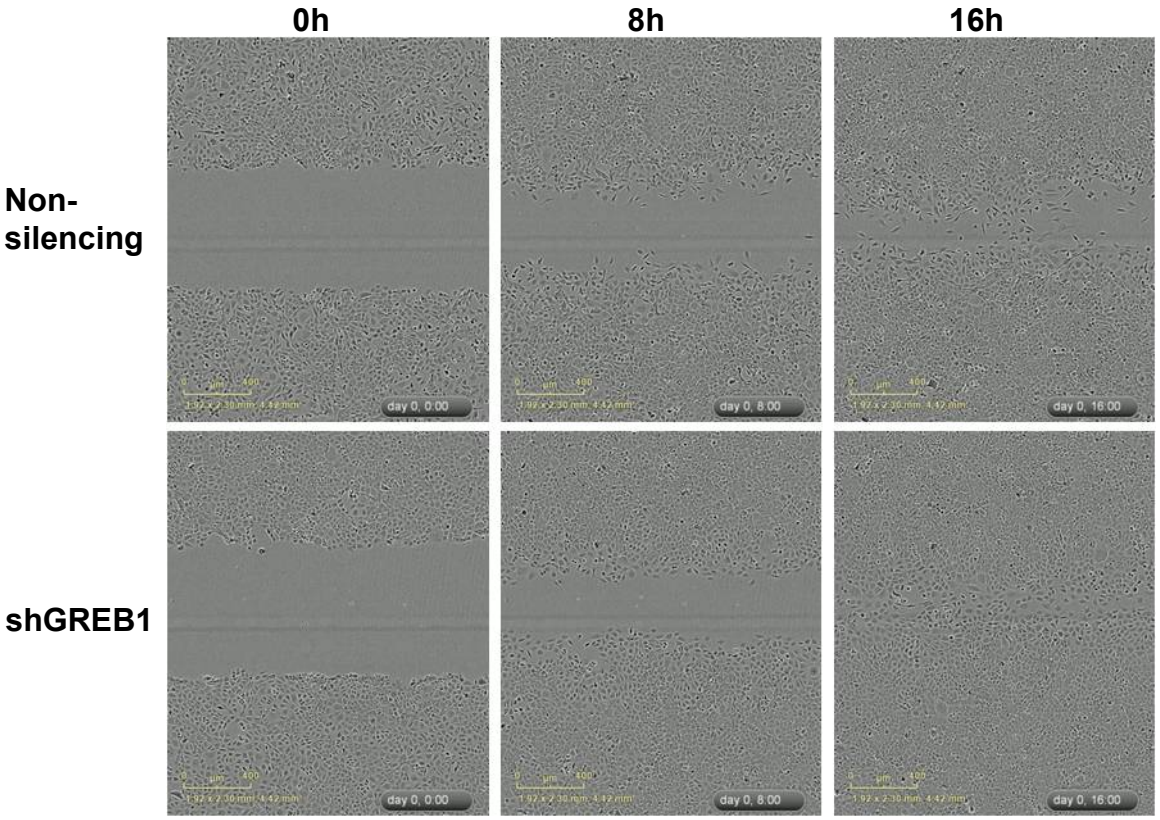

Figure 31. Effect of GREB1 knockdown on MASE cell migration. MASE cells stably expressing a short hairpin targeting GREB1 (shGREB1) or a non-silencing control were plated in 96-well ImageLock plates. When cells were 100% confluent, identical scratch wounds were made in each well using the Essen Biosciences Woundmaker. Wells were washed twice with PBS, replenished with their normal media (αMEM + 10% serum), and cultured in the IncuCyte incubator system with photos taken every 2h. Images were generated with IncuCyte ZOOM software. GREB1 knockdown did not alter the rate of wound closure.

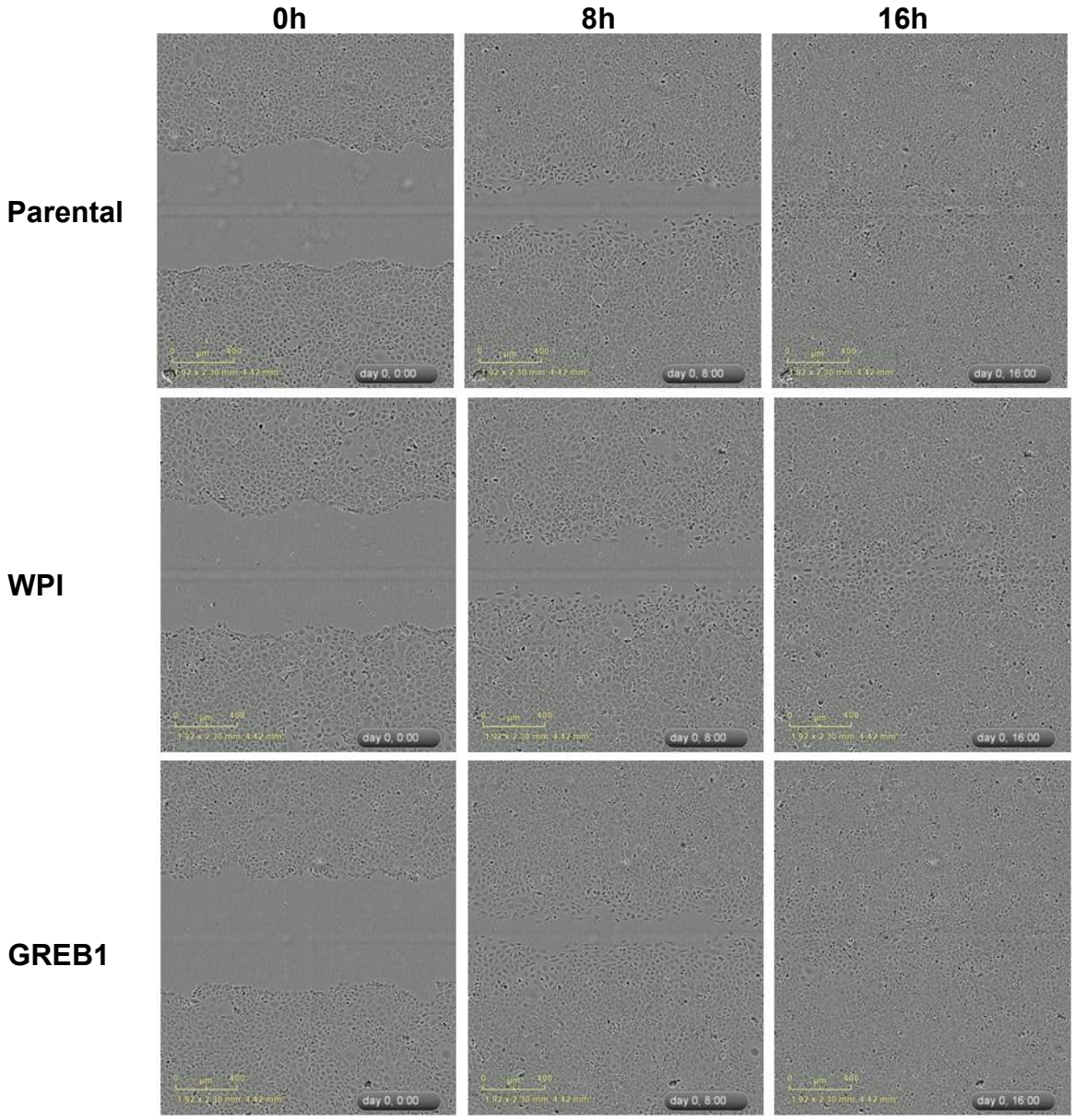

Figure 32. Effect of GREB1 overexpression on migration. MASE cells overexpressing GREB1 and two control lines (WPI vector control and parental MASE cells) were plated in 96-well ImageLock plates. When cells were 100% confluent, identical scratch wounds were made with the Essen Biosciences Woundmaker. Wells were washed twice with PBS and replenished with their normal media, then cultured in the IncuCyte incubator system with photos taken every 2h and images generated with IncuCyte ZOOM software. Scratch wounds closed faster with GREB1 overexpression.

using IncuCyte ZOOM software. Wound density was defined as cell confluence inside the initial scratch wound area normalized to cell confluence outside the wound area, and was determined for each time point by comparing the confluence mask to the wound mask from the first time point (Figure 33A). Supporting the visual observations, quantification showed that GREB1 knockdown did not alter migration rate in either normal media or low-serum media (Figure 33B). GREB1 overexpression increased average migration rate (slope, Figure 33C) by 20% in regular media ($p=0.04422$) and by 45% in low-serum media ($p<0.0001$). Similar results were seen in E2-free media; GREB1 knockdown did not alter migration rate with or without 10 nM E2 (Figure 34A), but GREB1 overexpression increased migration rate by 57% in E2-free media ($p<0.0001$), and by 27% when 10 nM E2 was added to the media ($p=0.03111$; Figure 34B). These results suggest that pro-migration effects of GREB1 are more apparent in less favourable culture conditions.

3.4.6. GREB1 does not alter most EMT-related genes in MASE cells

To determine whether these effects on morphology and migration were caused by an epithelial-to-mesenchymal transition (EMT), the common EMT marker *Snai1* was examined by QPCR (Figure 35A). No significant changes were seen with GREB1 knockdown or overexpression. To confirm the lack of EMT, a panel of EMT-related genes were examined with the QPCR-based RT^2 profiler array. Heat maps generated with the online RT^2 profiler analysis platform showed few major changes, although six genes showed opposite effects with GREB1 knockdown vs. overexpression (*Bmp7*, *Col1a2*, *Gng11*, *Krt19*, *Notch1*, and *Tcf4*; Figure 35B). Only one of these, *Col1a2*, showed significant changes in both cases. GREB1 knockdown downregulated *Col1a2* more than

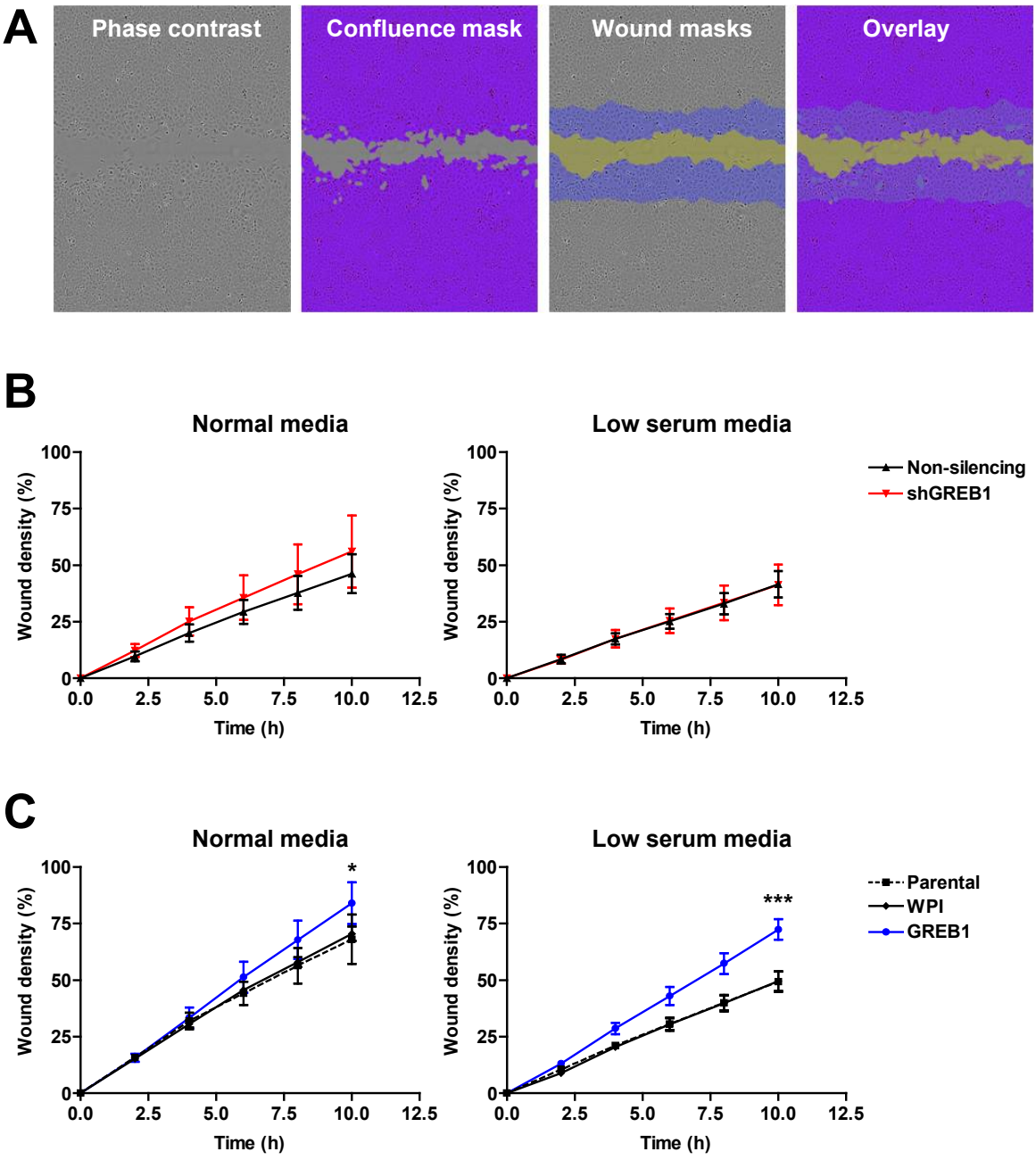

Figure 33. Quantification of migration after GREB1 knockdown and overexpression. Scratch wounds were analyzed with IncuCyte ZOOM software; examples of software-generated masks are shown in (A). To calculate wound density at each time point, confluence within the original wound area was compared to confluence outside the wound. B) GREB1 knockdown did not alter the rate of wound closing in either media (n=3). C) Wound density for cells overexpressing GREB1 increased faster than WPI control cells in both regular media (αMEM + 10% serum; n=3) and low-serum media (αMEM + 1% serum; n=3). *: $p<0.05$, ***: $p<0.0001$; linear regression.

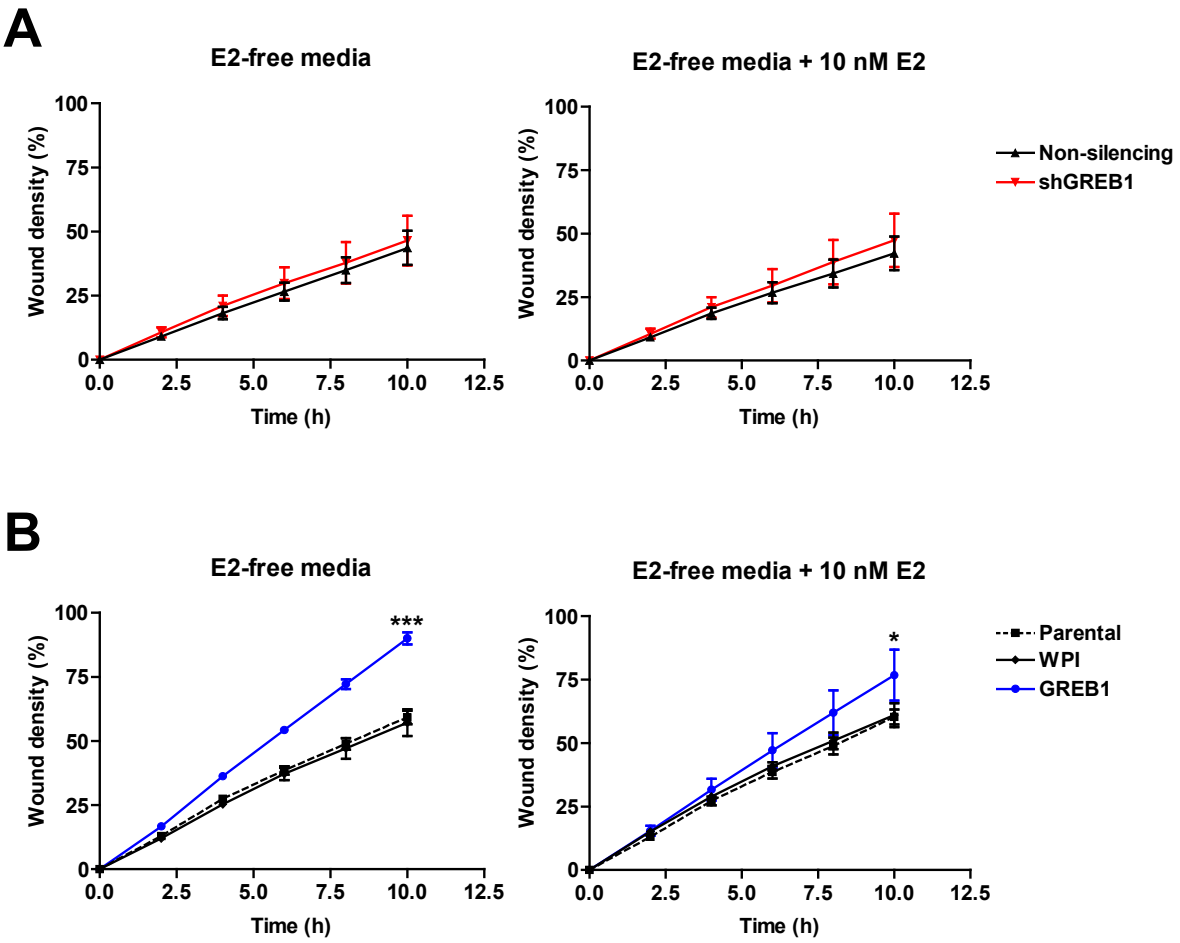

Figure 34. Effect of GREB1 knockdown and overexpression on migration +/- E2. MASE cells with GREB1 knocked down (shGREB1) or overexpressed (GREB1) were plated in 96-well ImageLock plates and scratched with the Essen Biosciences Woundmaker when 100% confluent. Scratches were washed twice with PBS, replenished with E2-free media (phenol-red-free DMEM/F12 + 5% CSS), and cultured in the IncuCyte incubator system with images taken every 2h. Wound closing was analyzed with IncuCyte ZOOM software (see Figure 33). A) Migration was unchanged by GREB1 knockdown in either media condition (n=3; $p>0.05$; linear regression). B) Migration was increased by GREB1 overexpression in both media conditions, but a more clear separation was seen in the absence of E2 (n=3; *: $p<0.05$, ***: $p<0.0001$; linear regression).

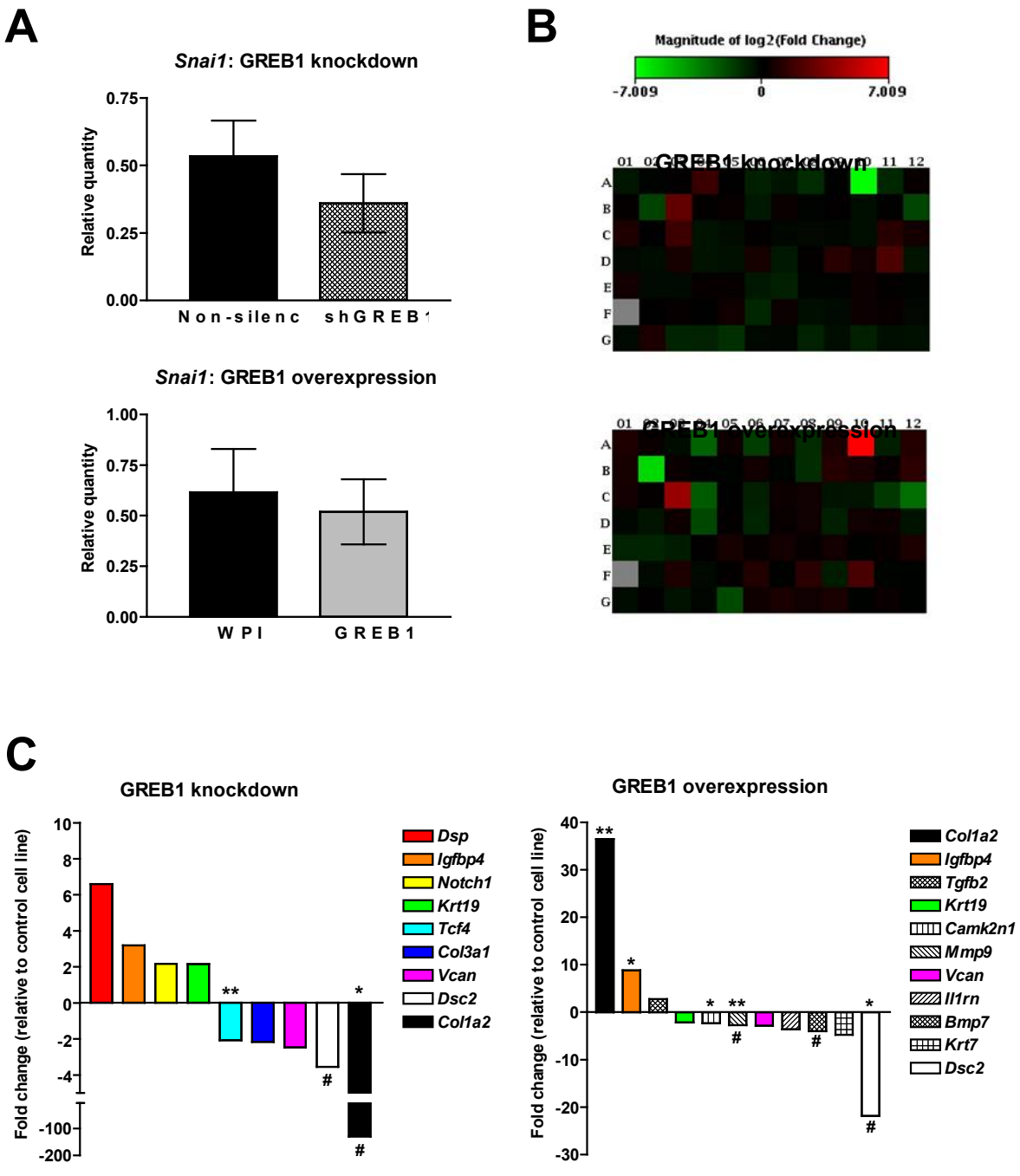

Figure 35. Effect of GREB1 knockdown and overexpression on EMT in MASE cells. MASE-shGREB1, MASE-NS, MASE-WPI, and MASE-GREB1 cells in regular culture conditions were examined by QPCR and a RT^2 Profiler PCR array of EMT markers. A) *Snai1* was not altered by GREB1 knockdown or overexpression. B) Heat maps show reciprocal changes in 6 genes from the PCR array: *Bmp7*, *Col1a2*, *Gng11*, *Krt19*, *Notch1*, and *Tcf4* (A4, A10, B12, C11, D9, and F6). C) Waterfall plots of fold changes from the PCR array (n=3; *: $p>0.05$, **: $p<0.01$; t-test). *Snai1* QPCR by O. Collins. #: Cycle threshold above 30 after GREB1 knockdown or overexpression.

99%, to a threshold cycle (Ct) below 30 (p=0.011717), whereas GREB1 overexpression increased *Col1a2* 37-fold (p=0.001515; Figure 35C). *Tcf4* was decreased 52% by GREB1 knockdown (p=0.008716) but unchanged by GREB1 overexpression. *Bmp7*, *Gng11*, *Krt19*, and *Notch1* were not significantly altered by either GREB1 knockdown or overexpression due to high variability, but their reciprocal expression patterns suggest that they might also be altered by GREB1. GREB1 overexpression also upregulated *Igfbp4* 9-fold (p=0.038291) and decreased *Camk2n1, Mmp9* and *Dsc2* by 57% (p=0.049877), 64% (p=0.001441), and 95% (p=0.042585) respectively, but none of these four genes showed reciprocal changes with GREB1 knockdown (Figure 35C). The overall results from this PCR array indicate that GREB1 does not significantly affect EMT, as most of the 79 EMT-related genes in the PCR array remained unchanged after GREB1 knockdown or overexpression. The canonical markers of EMT, *Snai1* and *Cdh1*, were not altered by GREB1 knockdown or overexpression in this assay. Notably, this experiment examined gene expression in the overall population rather than attempting to isolate the subpopulations showing altered morphology. As a result, changes in these subpopulations may have been masked by gene expression patterns of the overall population.

3.4.7. GREB1 promotes MASE cell proliferation

The effect of GREB1 on proliferation was examined by measuring viable cell counts over time in regular and low-serum culture conditions. In low-serum conditions, MASE cells with GREB1 knocked down had more rapid proliferation (p=0.0460; Figure 36A) and MASE cells overexpressing GREB1 had slower proliferation (p=0.0435; Figure 36B). In regular serum, GREB1 knockdown did not alter proliferation (data not shown).

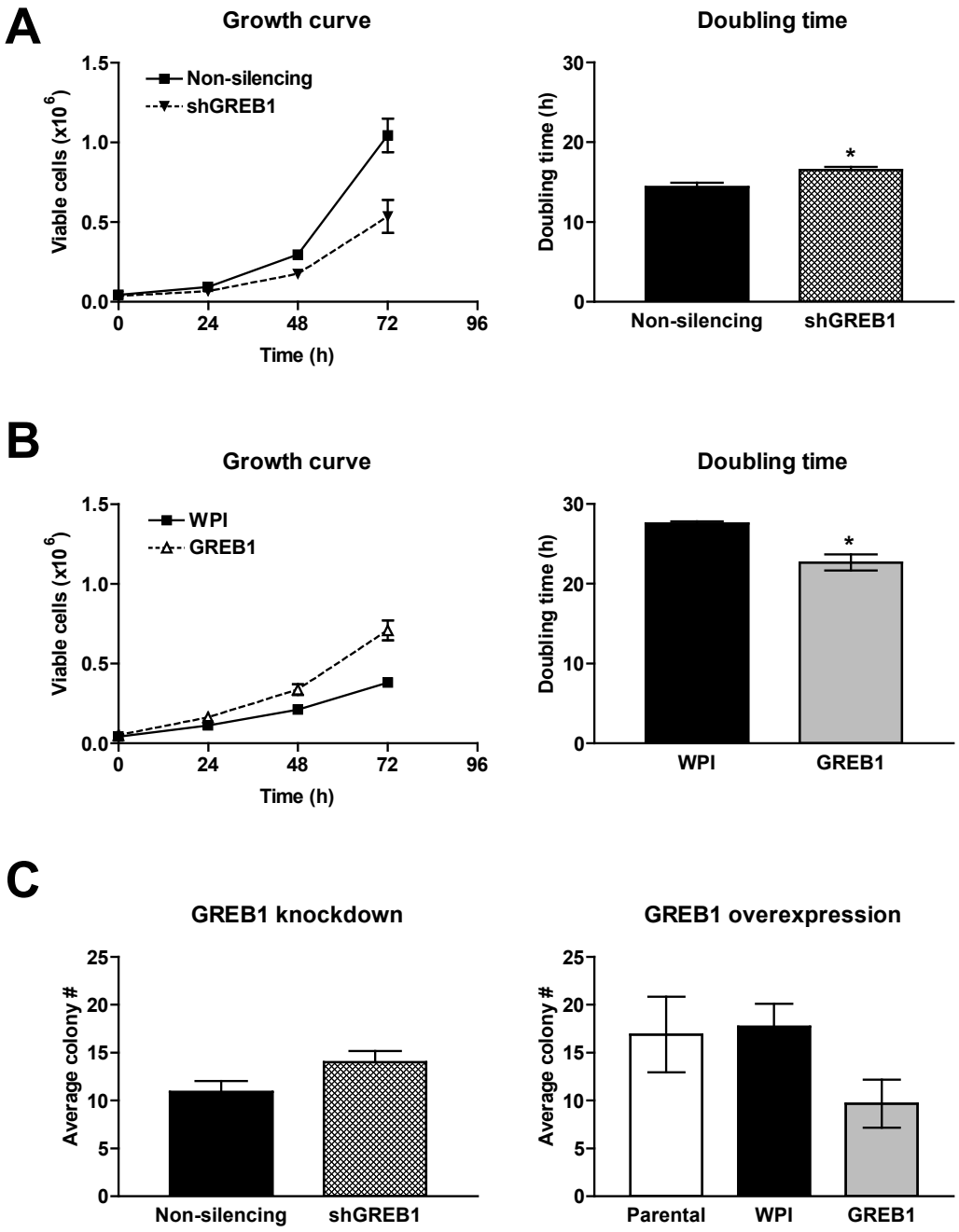

Figure 36. Effect of GREB1 on proliferation and colony formation of MASE cells. For proliferation assays, cells were plated at 50,000/well and switched to low-serum media (αMEM + 1% serum) after 4-6h. Viable cells were counted at each time point with a ViCell automated counter. Doubling times were calculated during the exponential growth phase (24-72h). A) Proliferation was decreased by GREB1 knockdown, causing an increased doubling time (n=3; *: $p<0.05$; t-test). B) Proliferation was increased by GREB1 overexpression, causing a decreased doubling time (n=3). C) Cells in single suspension were plated in E2-free media with 1% agarose. After 14d, colonies in all planes of a single field of 3 replicate wells were counted by a blinded observer. Colony formation was not altered by GREB1 knockdown (left) or overexpression (right; n=3).

Tumourigenicity was assessed by growth of single cells plated in soft agar; colony formation was not altered by GREB1 knockdown or overexpression (Figure 36C).

3.4.8. GREB1 accelerates MASE-derived tumour growth in mice

When MASE cells with GREB1 knocked down were engrafted into SCID mice, median survival was prolonged by 83% ($p<0.0001$) relative to mice engrafted with control cells expressing a non-silencing shRNA construct (Figure 37). Surprisingly, the tumour response to E2 was not altered by GREB1 knockdown. Cells with GREB1 knocked down showed a trend for fewer metastases ($p=0.1419$) which disappeared with E2 treatment; no changes in tumour burden, ascites volume or incidence were seen with GREB1 knockdown, regardless of E2 treatment.

To determine whether GREB1 overexpression would have an opposite effect, MASE-WPI and MASE-GREB1 cells were engrafted into SCID mice and monitored until reaching a humane endpoint. Overexpression of GREB1 did not alter survival or tumour dissemination of mice engrafted with MASE cells (Figure 38). However, GREB1 overexpression still seemed to be promoting tumour growth, as tumour burden was higher at endpoint ($p=0.0458$). Ascites volume was decreased by GREB1 overexpression ($p=0.0079$), indicating that the control mice were reaching endpoint primarily due to ascites accumulation whereas mice engrafted with GREB1-overexpressing cells were reaching endpoint primarily due to tumour growth. No significant differences were seen in body weight with GREB1 overexpression (data not shown).

To confirm GREB1 knockdown and overexpression remained stable in tumours, RNA and protein were collected from snap-frozen tumours from each study and examined by QPCR and/or western blot for GREB1. Although knockdown was

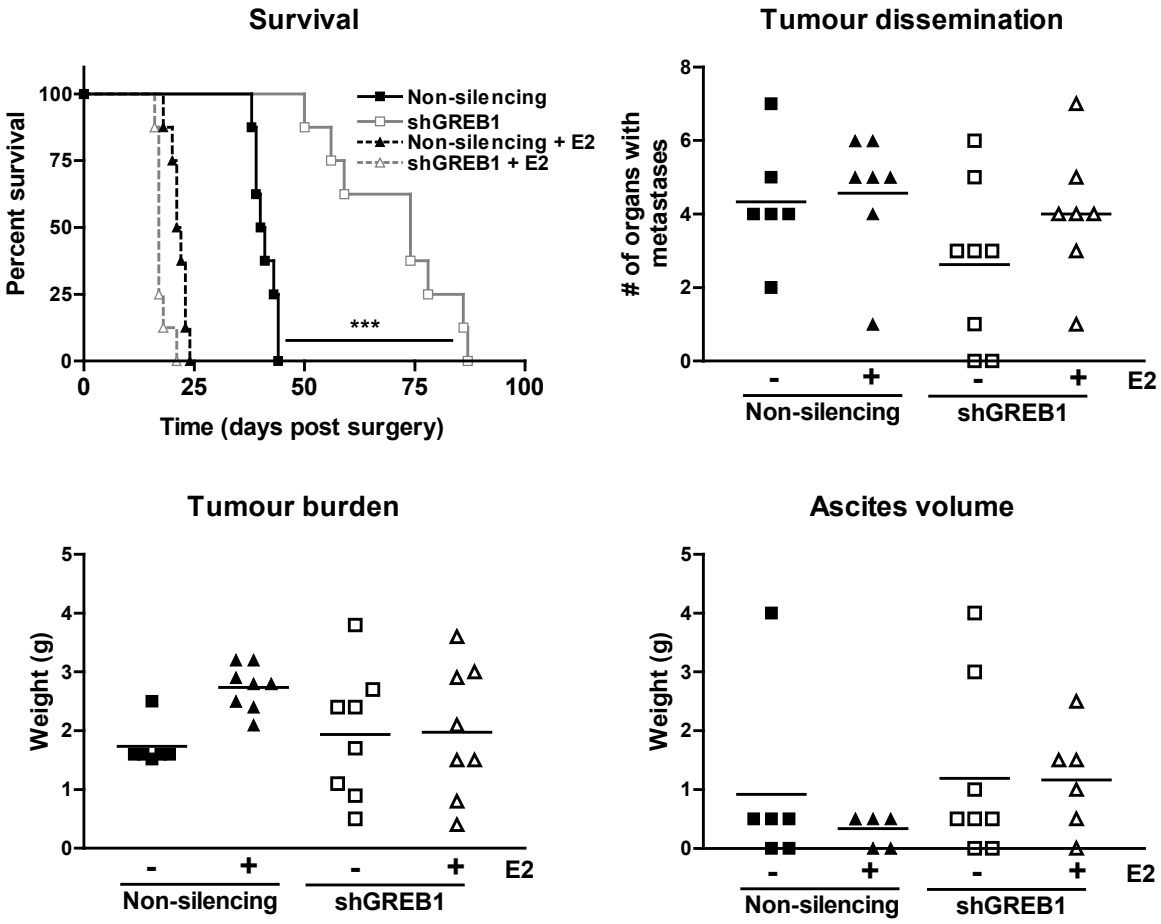

Figure 37. Growth of GREB1-deficient MASE cells in vivo. SCID mice were injected i.p. with 10^7 MASE cells stably expressing a short hairpin targeting GREB1 (shGREB1) or a non-silencing control. At the same time, mice were implanted with a 60-day slow-release pellet containing 0.25 mg E2 or placebo (N=8). Mice were monitored until loss of wellness required a humane endpoint, then euthanized and tumour characteristics examined. GREB1 knockdown in MASE cells significantly prolonged survival of mice treated with a placebo pellet, but not mice treated with an E2 pellet (***: $p<0.0001$; log-rank test). No significant differences were seen in tumour dissemination, tumour burden or ascites volume after GREB1 knockdown, regardless of E2 treatment (two-way ANOVA).

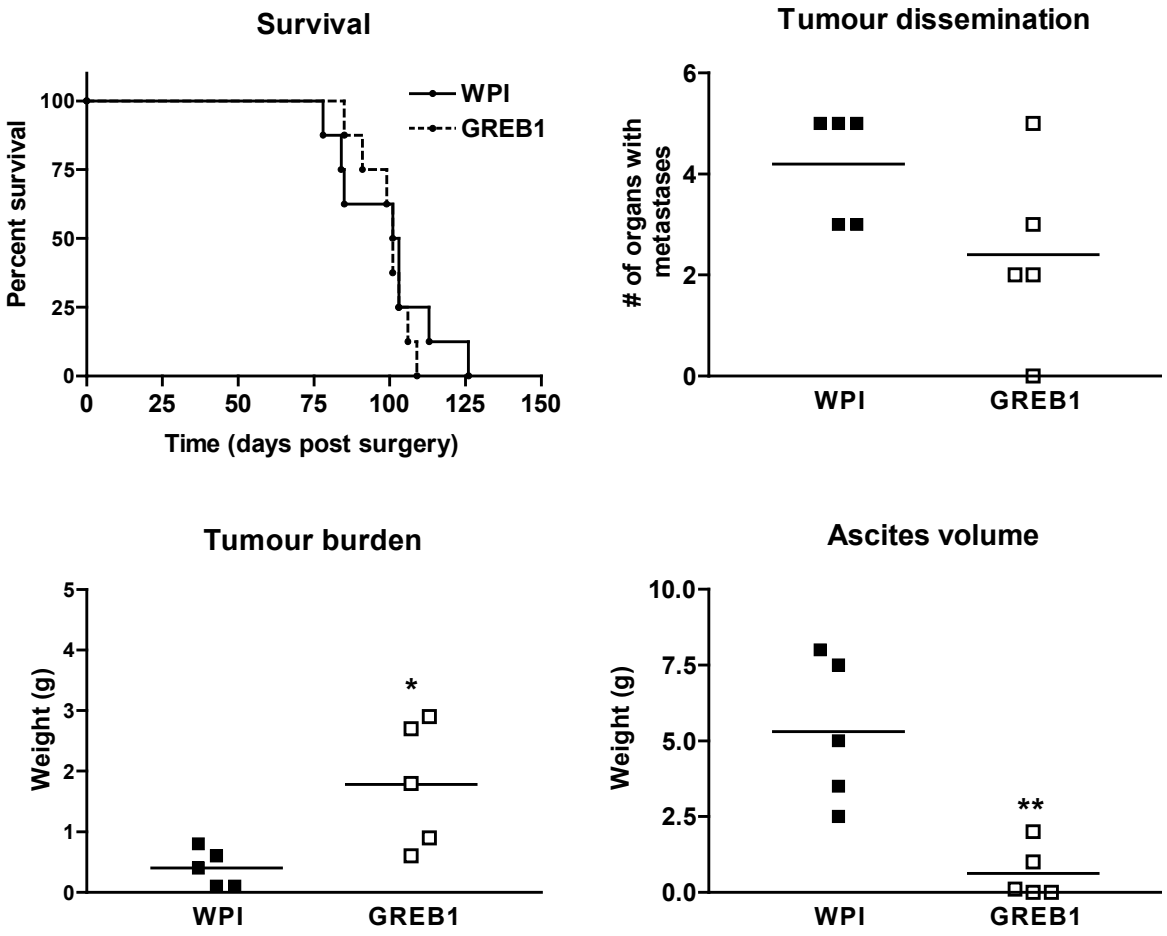

Figure 38. Growth of GREB1-overexpressing MASE cells in vivo. SCID mice were injected i.p. with 10^7 MASE cells stably expressing a GREB1 overexpressing construct (GREB1) or the vector control (WPI). Mice were monitored until loss of wellness required a humane endpoint, then euthanized and tumour characteristics examined. GREB1 overexpression in MASE cells did not change mouse survival time (N=8; $p>0.05$; log-rank test) or tumour dissemination ($p>0.05$; Mann-Whitney U-test). Mice injected with GREB1-overexpressing cells had a higher tumour burden (N=5; *: $p<0.05$; t-test) and lower ascites volume (**: $p<0.01$; Mann-Whitney U-test) relative to WPI-transduced control cells.

confirmed previously in the MASE-shGREB1 cell line in vitro (Figure 28), *Greb1* transcripts were not decreased in tumours derived from those cells, beyond a small, non-significant trend in E2-treated mice (35% decrease; p=0.1017; Figure 39A). However, GREB1 knockdown was visible at the protein level in E2-treated mice engrafted with MASE-shGREB1 cells (Figure 39B). As shown previously in MASE cells (Figure 23), GREB1 was undetectable in placebo-treated mice and therefore knockdown could not be assessed at the protein level for those mice. Surprisingly, GREB1 was undetectable in tumours derived from MASE-GREB1 cells (Figure 39C), despite strong expression in MASE-GREB1 cells in vitro (Figure 28).

It is unclear why GREB1 knockdown and overexpression were no longer detectable in tumours collected at endpoint; the most likely explanations include stroma effects and/or loss of construct expression in vivo. GFP was expressed in tumours from all mice at endpoint, indicating that the knockdown constructs retained some level of function (Figure 40). Tumours from mice engrafted with MASE-NS cells (Figure 40A) typically expressed higher GFP than tumours derived from MASE-shGREB1 cells (Figure 40B), reflecting the differential GFP expression seen in vitro (Figure 30). Notably, GFP expression rapidly declined over time in vivo, with large GFP-negative areas visible in isolated tumours from mice collected several months after cell injection (Figure 40C). This suggests that the short hairpin construct was expressed at very low levels in placebo-treated mice at endpoint, which would explain the lack of knockdown observed in those tumours.

3.4.9. ESR1 partially mediates E2 action in vivo and is necessary for GREB1 induction

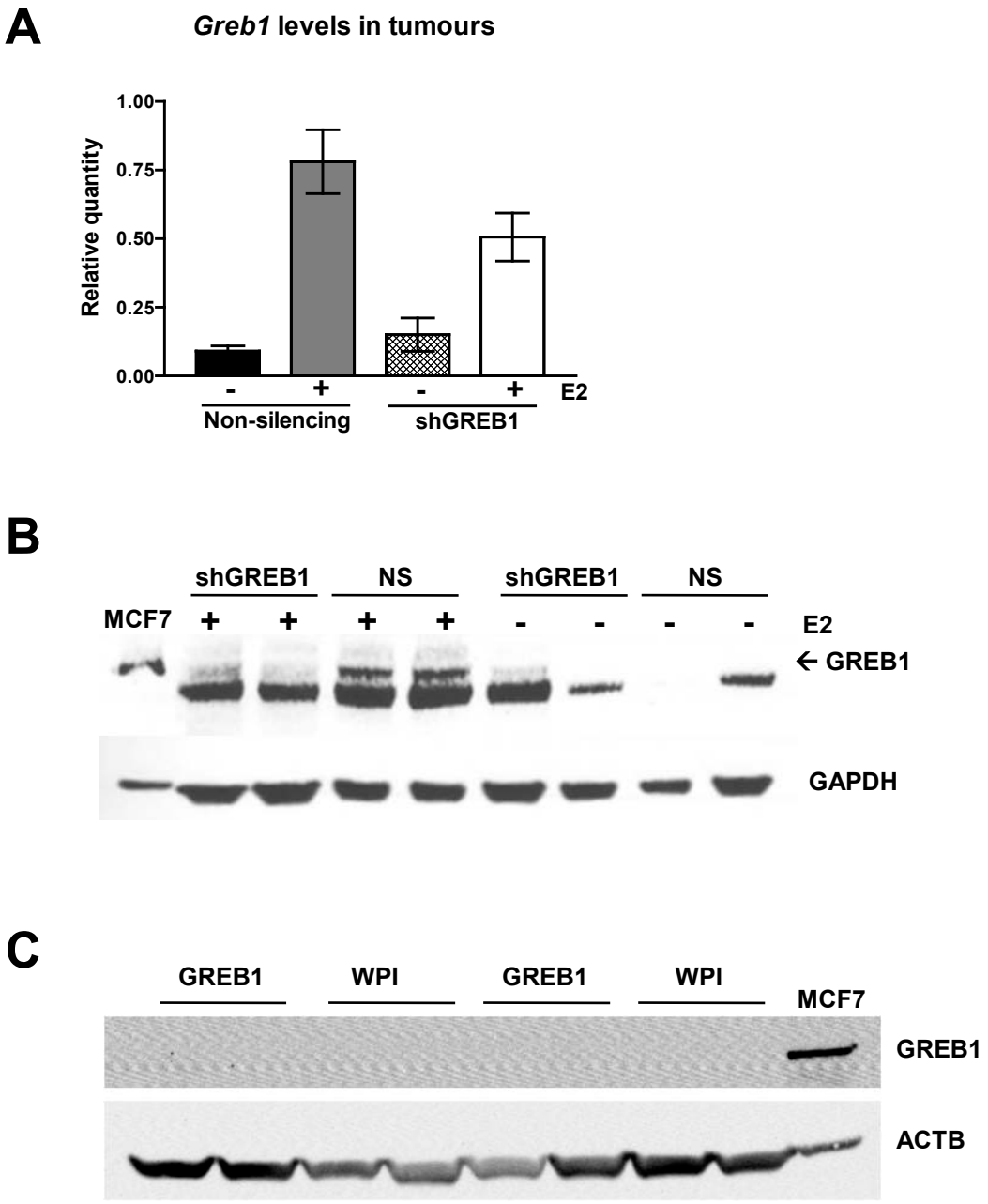

Figure 39. GREB1 levels in tumours derived from MASE cells with GREB1 knockdown or overexpression. GREB1 was assessed by QPCR and western blot in snap-frozen tumours from mice described in Figures 37-38. A) *Greb1* mRNA levels were similar in MASE-NS and MASE-shGREB1, regardless of E2 treatment. B) GREB1 induction by E2 was lower in tumours from MASE-shGREB1 cells, but GREB1 was not consistently detected in placebo-treated mice. It is unclear whether the bottom band is also a form of GREB1. C) GREB1 was undetectable in tumours from either MASE-WPI or MASE-GREB1 cells. MCF7 cells were used as a positive control.

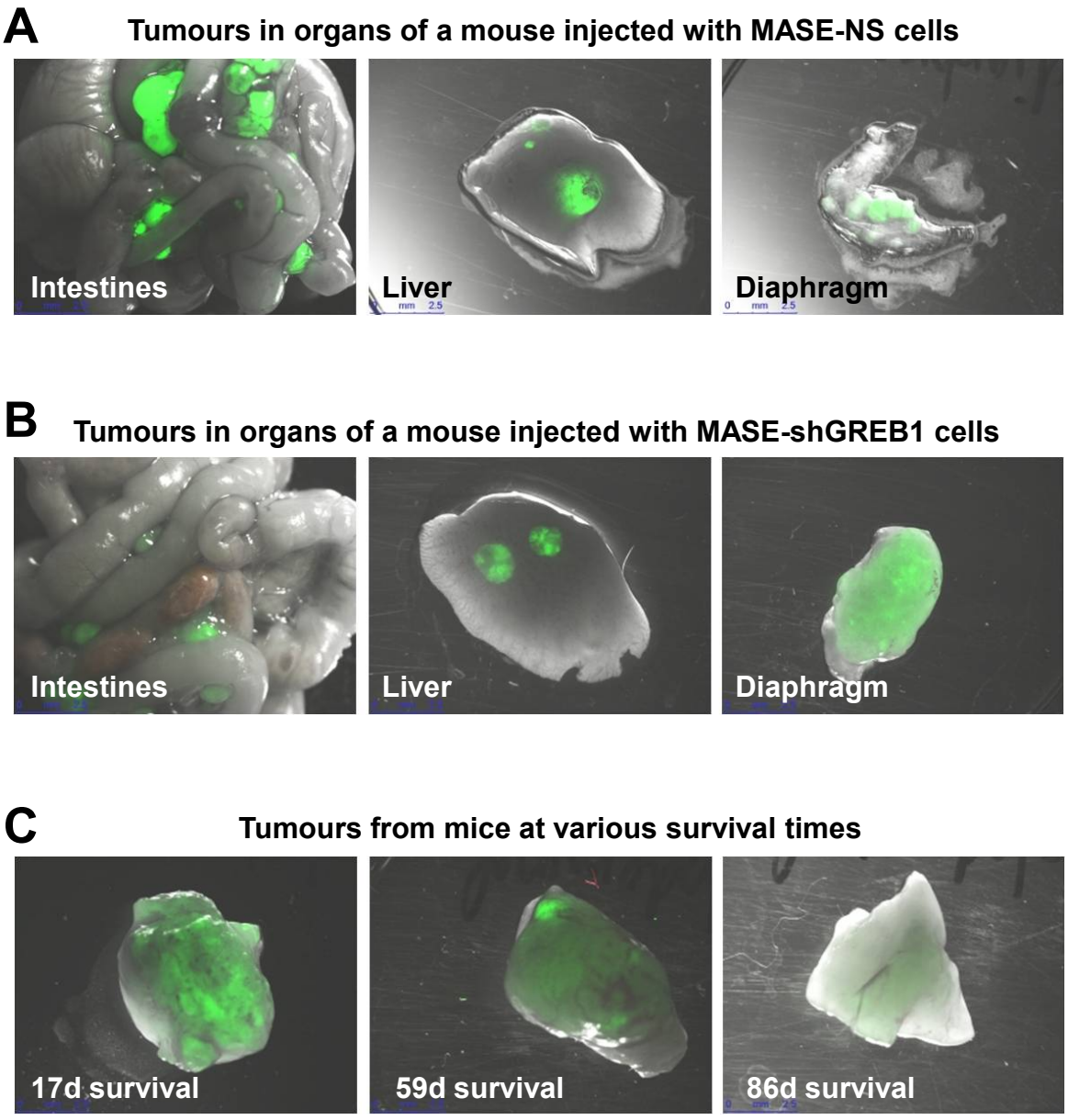

Figure 40. GFP expression of tumours developing in the organs of mice injected with MASE-NS and MASE-shGREB1 cells. Major organs of mice described in Figure 34 were removed at endpoint and examined with a fluorescence microscope. GFP was clearly visible in tumours derived from both MASE-NS (A) and MASE-shGREB1 cells (B). These two mice were both treated with E2 and had similar survival times. C) GFP expression in tumours decreased over time; far lower GFP was observed in the tumours of mice surviving longer after injection. These three examples are from mice injected with MASE-shGREB1 cells; a similar trend was seen in tumours from MASE-NS cells.

ESR1 is known to be a critical mediator of estrogen-induced transcriptional activity in human ovarian cancer cells, so we investigated its importance in our mouse models and associated cell lines. *Esr1* was highly expressed in MASE-derived tumours relative to the normal ovary positive control, whereas *Esr2* was expressed at much lower levels in MASE-derived tumours relative to the ovary. Both receptors showed non-significant trends for upregulation with E2 treatment (2.2-fold increase; p=0.0936 and 3.3-fold increase; p=0.2075 respectively; Figure 41).

Among its many tumour-promoting actions, ESR1 upregulates *GREB1* in MCF7 breast cancer cells through three EREs located upstream of the *GREB1* promoter (Sun et al. 2007, Deschenes et al. 2007). Chromatin immunoprecipitation was done to investigate whether similar regulation occurs in mouse ovarian cancer cells. Both EREs examined showed clear ligand-dependent ESR1 binding in MASE cells (Figure 42A). To determine whether ESR1 is necessary for *Greb1* induction, ESR1 activity was inhibited with a specific antagonist (methyl-piperidino-pyrazole; MPP). MPP completely prevented *Greb1* mRNA induction by E2 in MASE cells (2 or 5 μM added 30 min before a 48h treatment with 10 nM E2; Figure 42B). GREB1 induction by E2 was also significantly inhibited at the protein level by MPP treatment (Figure 42C).

The MASC ovarian cancer cell line expresses far lower levels of ESR1 than the MASE in regular culture conditions (Figure 43A) or in E2-free media with or without 500 nM E2 added (Figure 43B-C). *Greb1* was not significantly induced by E2 in MASC cells (Figure 25A), and MASC allografts are less responsive to E2 in vivo (Figure 5). When GREB1 was overexpressed in MASC cells, no change in proliferation was seen (Figure 43D) despite strong expression levels (Figure 28), suggesting that high ESR1 levels may be required for GREB1 function as well as its upregulation. This supports

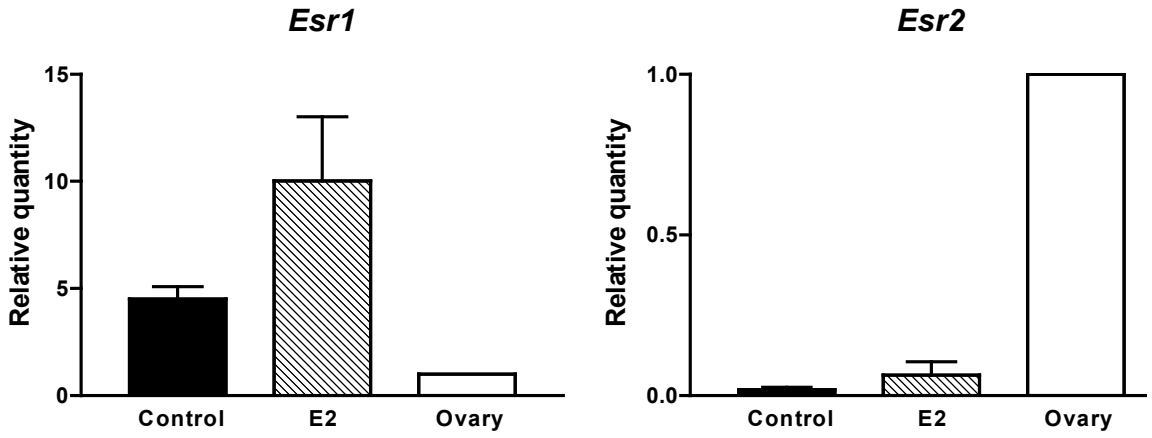

Figure 41. Estrogen receptor expression in MASE-derived tumours. Estrogen receptors were examined by QPCR in snap-frozen MASE-derived tumours from mice described in Figure 5. *Esr1* levels were high relative to the ovary reference sample, and showed a trend for increased expression with E2 treatment (N=4-5; $p>0.05$; t-test). *Esr2* levels were very low relative to the ovary sample, and showed a similar trend for increased expression with E2 (N=4-5; $p>0.05$; t-test).

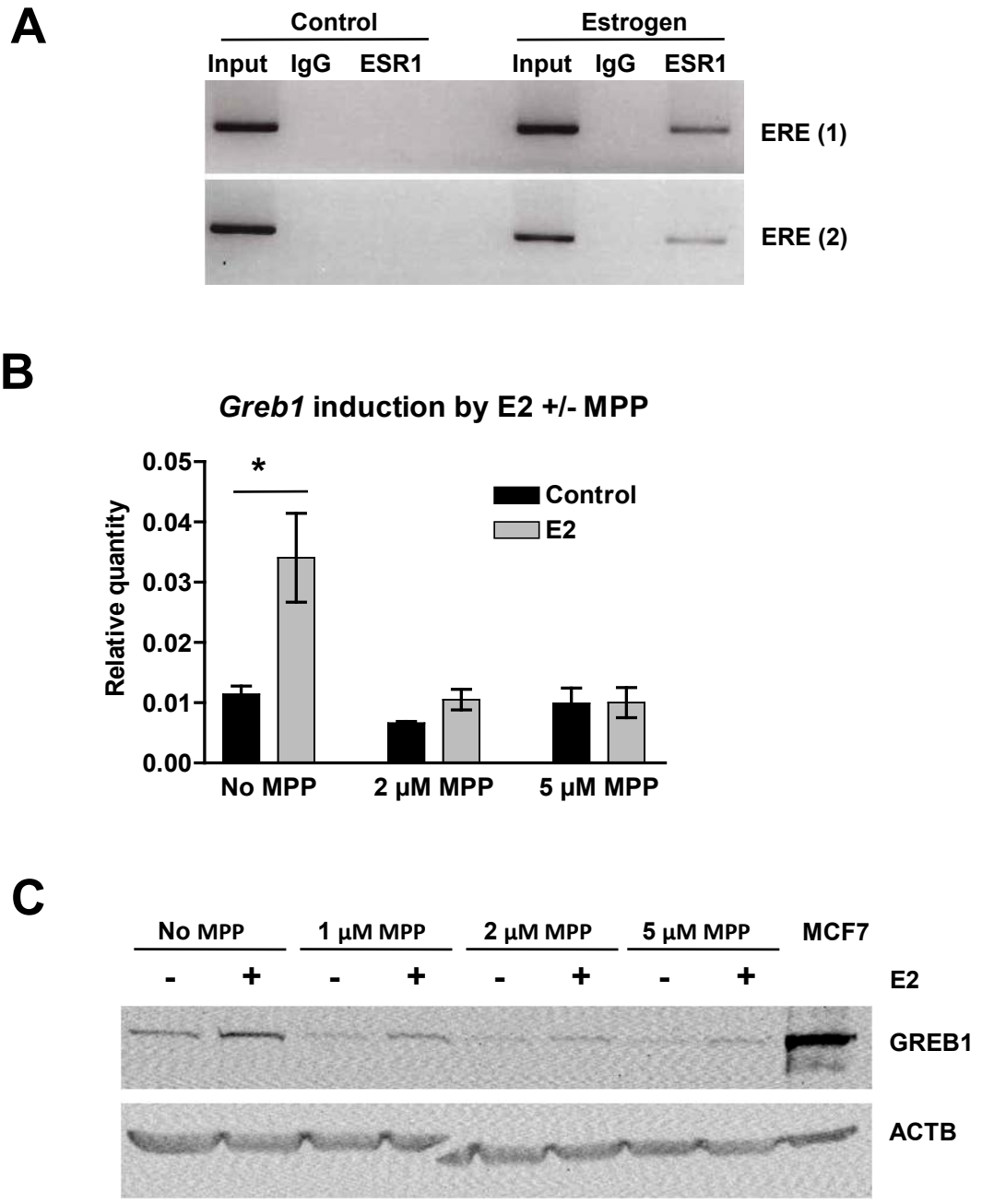

Figure 42. GREB1 regulation by ESR1 in MASE cells. A) Chromatin immunoprecipitation showed ESR1 binding to two estrogen response element (ERE) sequences upstream of the *Greb1* promoter in MASE cells treated with 100 nM E2. To confirm the importance of ESR1 in GREB1 induction by E2, MASE cells were E2-deprived for 24h, and treated with MPP for 30 min before adding 10 nM E2 to each well. Protein and RNA were collected after 24h of E2 treatment and GREB1 levels were measured by QPCR and western blot. B) Both doses of MPP blocked *Greb1* upregulation by E2 at the mRNA level (n=3; *: $p<0.05$; t-test vs. E2-free control). C) MPP similarly inhibited GREB1 protein induction by E2 (n=2).

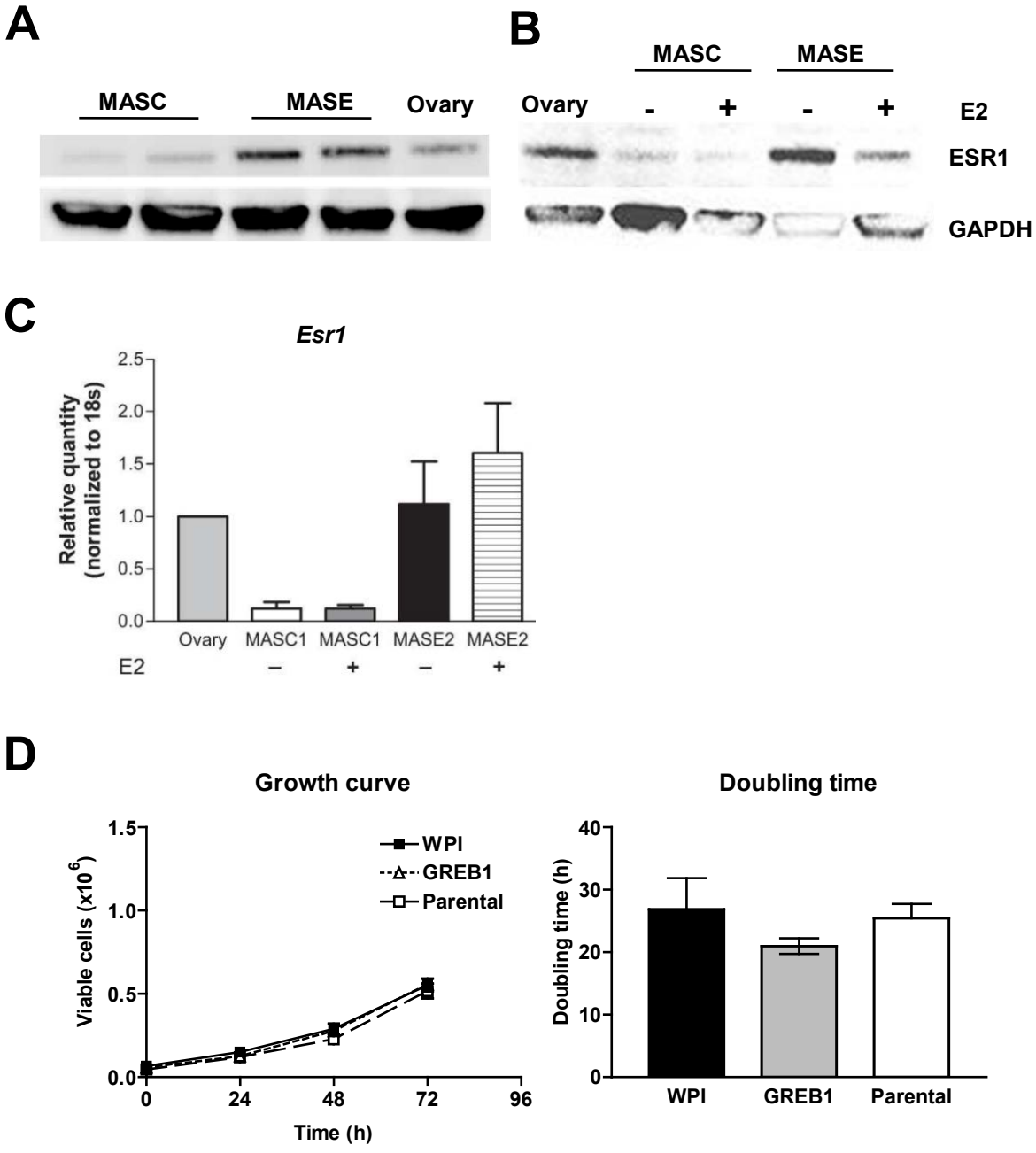

Figure 43. ESR1 levels and GREB1-responsiveness of the MASC cell line. Protein was isolated from MAS cells in regular culture conditions (A) or after 48h in E2-free media +/- 500 nM E2 (B) and ESR1 was examined by western blot (positive control: mouse ovary). MASE cells showed higher ESR1 than MASC cells both in regular culture (A) and in E2-free media +/- 500 nM E2 (B). ESR1 levels decreased with E2 treatment, but MASE cells maintained higher ESR1 levels than MASC. C) QPCR analysis showed that *Esr1* mRNA levels were also higher in MASE cells (n=3; 500 nM/48h). D) MASC cells were less responsive to GREB1 than MASE cells; proliferation was not altered by GREB1 overexpression (t-test).

published data identifying one function of GREB1: acting as a cofactor for ESR1-mediated transcription (Mohammed et al. 2013).

To determine how much of the effect of E2 on accelerated tumourigenesis is mediated by ESR1, the CAG-TAg transgenic mouse model of ovarian cancer was crossed to mice with floxed ESR1. ESR1 inactivation by i.b. AdCre-mediated exon 3 deletion prolonged median survival by 94% in E2-treated mice ($p<0.0001$) and by 20% in mice implanted with placebo pellets ($p=0.0003$; Figure 44A). A similar trend was seen in mice treated with low-dose E2, with median survival prolonged 50% by ESR1 deletion, but the difference was not statistically significant due to high variability ($p=0.0942$). Tumour burden, ascites volume and ascites incidence were not changed by ESR1 deletion (Figure 44B). A two-way ANOVA indicated that body weight was altered by E2 ($p=0.0019$); ESR1 deletion had a nearly-significant effect ($p=0.0766$), and no interaction of E2 and ESR1 status was detected. Post-hoc analysis showed that body weight was significantly decreased by E2 in both ESR1-wildtype ($p<0.05$) and in ESR1-deleted ($p<0.001$) mice. Low-dose E2 did not significantly alter body weight, but showed a trend for intermediate body weight between E2- and control-treated mice of both genotypes.

Several ovarian cancer cell lines were derived from the tumours or ascites of ESR1-wildtype or ESR1-deleted mice from this study (Table 1). Ascites-derived lines from ESR1 wildtype mice had much higher *Esr1* levels, with the highest expression in lines derived from E2-treated mice (MASE; Figure 45A). This supports the ESR1 differences seen previously in ESR1-wildtype MASE and MASC cells (MASC1 and MASE2; Figure 43). *Greb1* expression roughly correlated with *Esr1* but showed smaller differences between ESR1-wildtype and ESR1-deleted cell lines and lower induction by E2 treatment in vivo than *Esr1* (Figure 45A). Cell lines derived from solid tumours

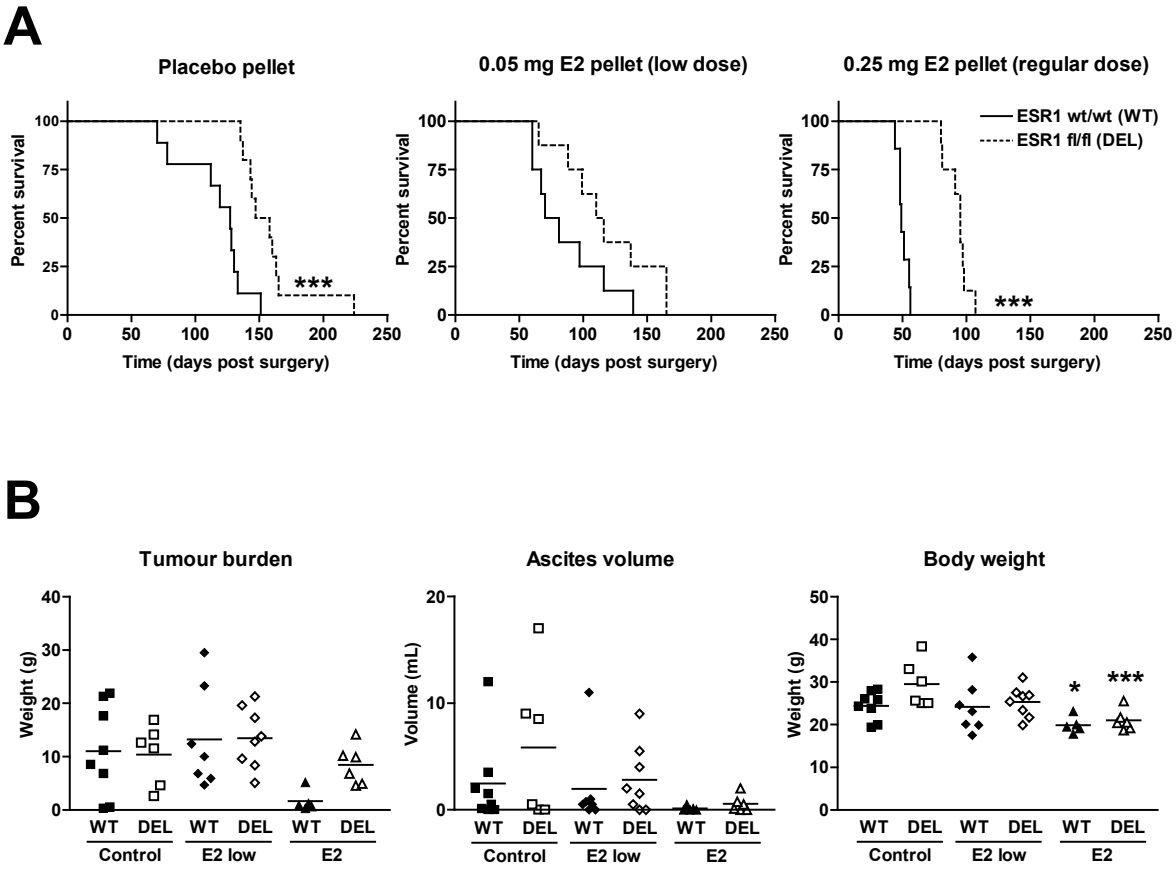

Figure 44. CAG-TAg survival and tumour characteristics after ESR1 deletion. CAG-TAg mice were crossed with *Esr1*-floxed mice to generate TAg-homozygous *Esr1*$^{wt/wt}$ and *Esr1*$^{fl/fl}$ siblings. At 8-10 weeks, mice were injected i.b. with AdCre to activate TAg and delete ESR1 in the OSE, then implanted s.c. with an E2 (0.05 or 0.25 mg) or placebo pellet. Mice were monitored until they required a humane endpoint, then euthanized and tumour characteristics were examined. A) Survival was increased by ESR1 deletion in mice treated with regular-dose E2 or placebo pellets (***: $p<0.001$; log-rank test). A trend for prolonged survival was seen in mice treated with low-dose E2. B) ESR1 deletion (DEL) did not alter tumour weight, ascites volume or ascites incidence relative to ESR1-wildtype (WT) controls. Body weight was decreased by 0.25 mg but not 0.05 mg E2 in both ESR1-wildtype and ESR1-deleted mice (*: $p<0.05$; ***: $p<0.001$ vs. control-treated mice of the same genotype; two-way ANOVA with Bonferroni post-hoc test). ESR1 deletion caused a nearly-significant trend for increased body weight ($p=0.0766$, two-way ANOVA).

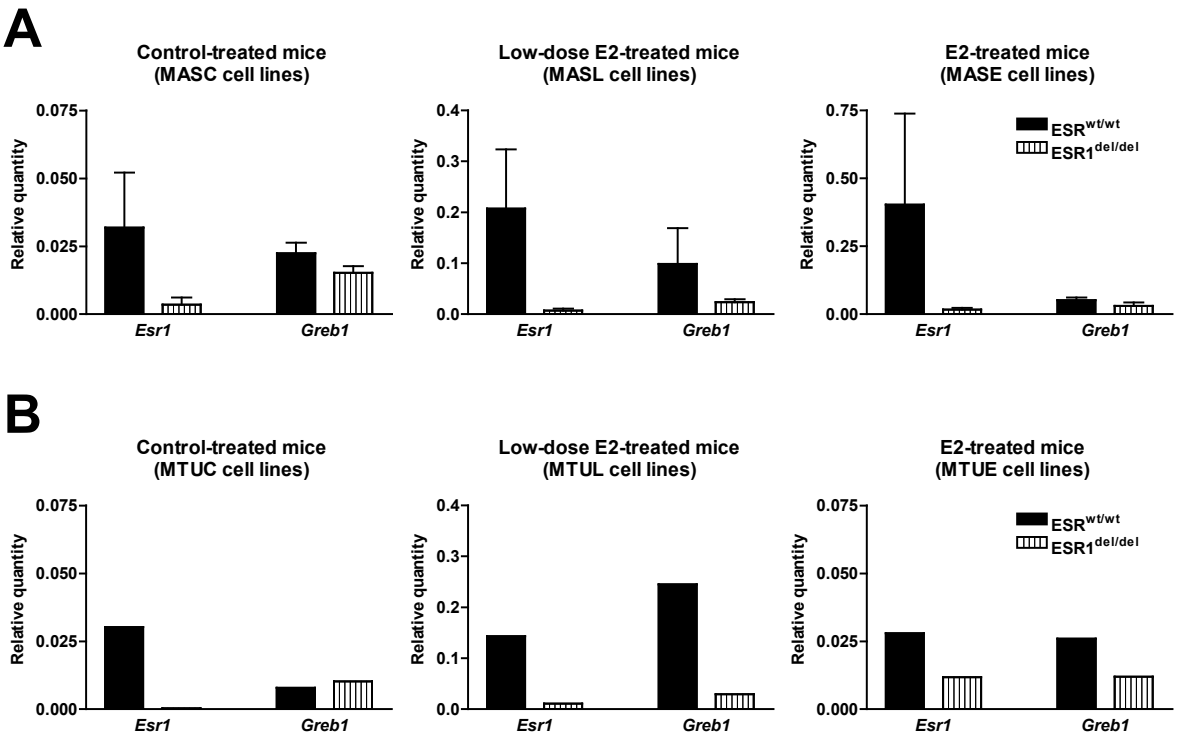

Figure 45. *Esr1* and *Greb1* expression in early-passage cell lines isolated from solid tumours and ascites fluid of CAG-TAG mice. Cell lines were derived from ascites (MAS) or tumours (MTU) of CAG-TAg mice with wildtype or floxed (deleted by AdCre) ESR1. RNA was collected when cells were growing in regular media without antibiotics and baseline *Esr1* and *Greb1* levels were examined by QPCR. Note that the relative quantities are plotted on different scales. A) *Esr1* was much lower in cell lines derived from the ascites of ESR1-deleted mice regardless of E2 treatment; *Esr1* was highest in MASE lines derived from ESR1-wildtype mice (n=2). *Greb1* was slightly lower in ESR1-deleted mice, with highest expression in MASL and MASE cells from ESR1-wildtype mice. B) Cell lines derived from the tumours of ESR1-deleted mice also had lower *Esr1* and *Greb1* than ESR1-wildtype mice (n=1).

showed similar *Esr1* and *Greb1* expression patterns (Figure 45B). In the 4 cases where a tumour line and ascites line were derived from the same mouse (see Table 1), *Esr1* and *Greb1* expression were similar (data not shown). Therefore, ascites lines were used in all subsequent experiments to stay consistent with previous experiments in MASE and MASC cell lines.

To examine the role of ESR1 in GREB1 induction in vivo, GREB1 levels in snap-frozen tumours from ESR1-wildtype and ESR1-deleted mice were examined by western blot. GREB1 was clearly expressed in both tumours examined from E2-treated ESR1-wildtype mice (Figure 46A). A faint band was seen for one E2-treated ESR1-deleted mouse; the other mouse had no detectable GREB1. No GREB1 was detected in mice of either genotype treated with low-dose E2 or (not shown) placebo pellets. To confirm the importance of ESR1 in *Greb1* upregulation by E2 in vitro, *Greb1* induction was compared in two MASE lines (one ESR1-wildtype and one ESR1-deleted) after 48h treatment with 10 nM E2. *Greb1* was increased 2.6-fold by E2 in the ESR1-wildtype MASE line but was unchanged by E2 in the ESR1-deleted MASE line (Figure 46B). Failure of ESR1-dependent GREB1 induction is likely to be partially responsible for the decreased E2 responsiveness seen in vivo after ESR1 deletion.

3.5: GREB1 expression and function in human cell lines and tissues

3.5.1. GREB1 is induced by E2 in human ovarian and cervical cancer cell lines

Two ESR1+ human ovarian cancer cell lines were used to investigate whether GREB1 is regulated by E2 in human ovarian cancer. The OV2008 cell line was also examined, but was later discovered to be a cervical cancer cell line (Korch et al. 2012).

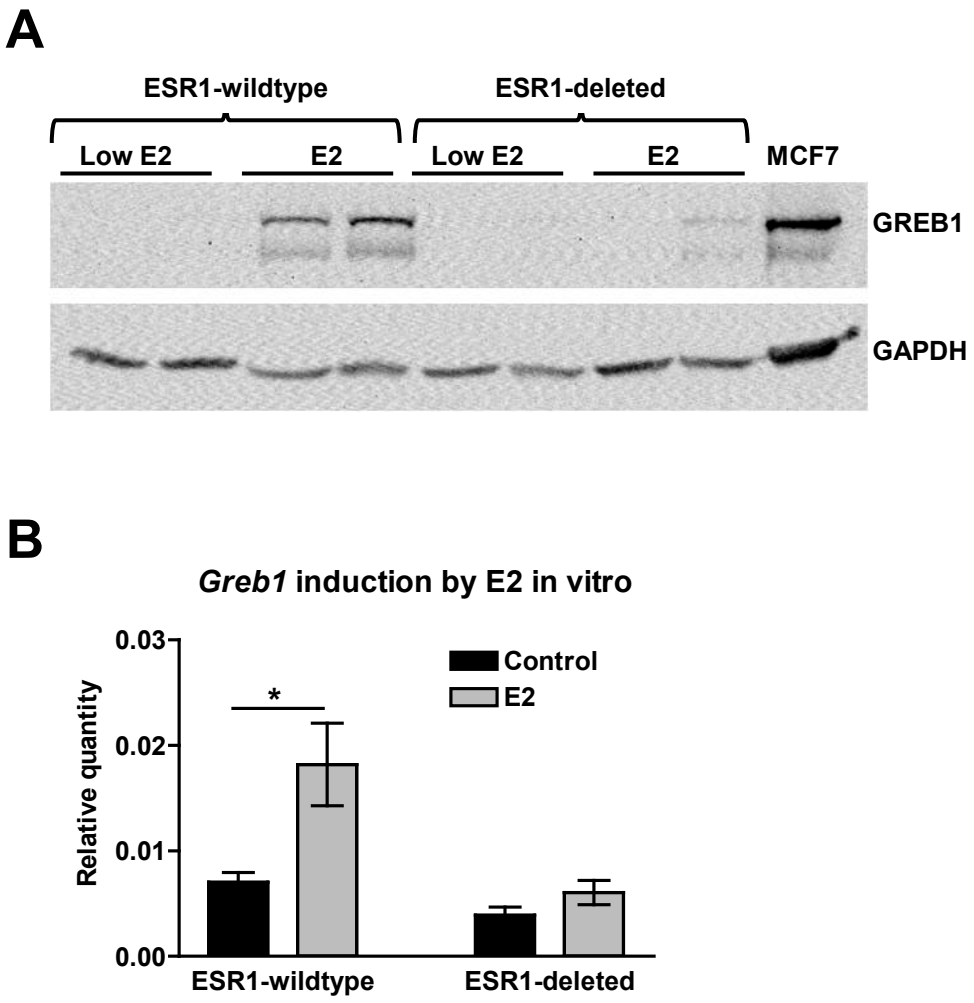

Figure 46. GREB1 induction in ESR1-deleted tumours and ascites cell lines. A) Protein was isolated from snap-frozen tumours of the ESR1-wildtype and ESR1-deleted mice described in Figure 44 and GREB1 levels were examined by western blot. GREB1 was highly expressed in tumours from ESR1-wildtype mice treated with 0.25 mg E2, but barely any GREB1 was detected in tumours from ESR1-deleted mice treated with E2. No GREB1 was visible in either genotype of mice treated with low-dose E2 (0.05 mg) or (not shown) placebo pellets. MCF7 cells were used as a positive control. B) Two MASE lines derived from ESR1-wildtype and ESR1-deleted mice (MASE3 and MASE-ESR1del-1 respectively; see Table 1) were E2-deprived for 24h, then treated with 10 nM E2 for 48h. QPCR for *Greb1* showed induction by E2 in the ESR1-wildtype but not in the ESR1-deleted MASE cells (n=3; *: $p<0.05$; two-way ANOVA with Bonferroni post-hoc test) .

To determine the optimum dose for GREB1 upregulation, a dose-response experiment was done with 24h and 48h treatments of 0.1-500 nM E2. OVCA 432 cells consistently upregulated *GREB1* after 24h treatment with 1-500 nM E2 and after 48h with all doses (n=2; Figure 47A). OVCAR-3 cells consistently upregulated *GREB1* after 24h or 48h treatment with 0.1-500 nM E2 (n=2; Figure 47B). C) OV2008 consistently upregulated *GREB1* only after a 48h treatment with 500 nM (n=2; Figure 47C). Little to no protein was detected in western blots at any E2 dose (not shown).

To determine how early GREB1 is upregulated, a time course was done with 500 nM E2. *GREB1* upregulation was first consistently seen by 8h in OVCA 432 cells (p=0.0302), 24h in OVCAR-3 cells (p=0.0494), and 8h in OV2008 cells (p= 0.0153). By 24h, *GREB1* mRNA levels were increased 8.3-fold in OVCA 432 cells (p= 0.0766), 7.0-fold in OVCAR-3 cells (p=0.0494), and 28.9-fold in OV2008 cells (p=0.0044). A faint GREB1 band was visible after 30h of E2 treatment in the OVCAR-3 cell line (500 nM; Figure 48B).

To determine whether GREB1 upregulation would be detectable at the protein level in tumours derived from these cell lines, a pilot xenograft study was done. SCID mice were injected with 10^7 OVCA 432 or OVCAR-3 cells and implanted with a hormone pellet releasing regular-dose E2 (0.25 mg), low-dose E2 (0.05 mg), or placebo. Although the sample size was too small to examine the effect of E2 on survival time (N=1-2), mice were still allowed to progress to a loss-of-wellness endpoint to see whether any trend in survival time was observed. Mice injected with OVCA 432 cells did not show any difference in survival with E2 treatment; however, mice injected with OVCAR-3 cells showed a trend for shortened survival with regular-dose E2 treatment (Table 6). Surprisingly, GREB1 was not detectable in any of the tumours derived from either cell

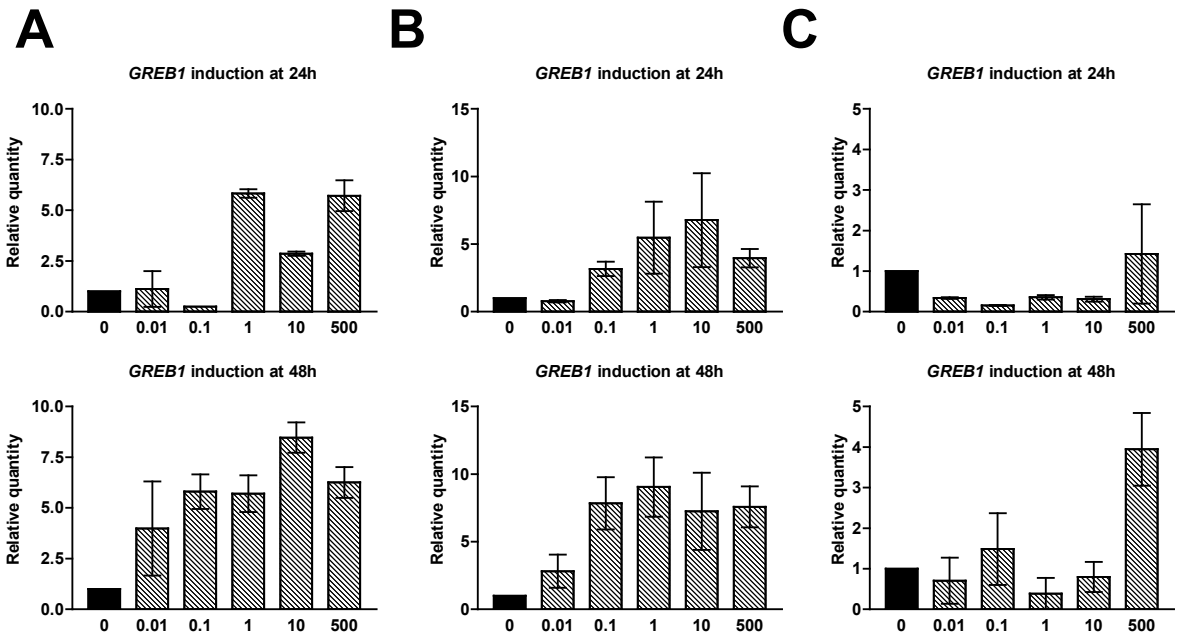

Figure 47. GREB1 upregulation by E2 in ovarian and cervical cancer cell lines. Cell lines were E2-deprived for at least 24h then treated with 0.01-500 nM E2 to determine the ideal dose to upregulate GREB1 (n=2). RNA was collected at 24h and 48h to examine *GREB1* by QPCR. A) OVCA 432 cells consistently upregulated GREB1 after 24h treatment with 1-500 nM E2 and after 48h with all doses. B) OVCAR-3 cells consistently upregulated GREB1 after 24h or 48h treatment with 0.1-500 nM E2. C) OV2008 consistently upregulated GREB1 only after a 48h treatment with 500 nM.

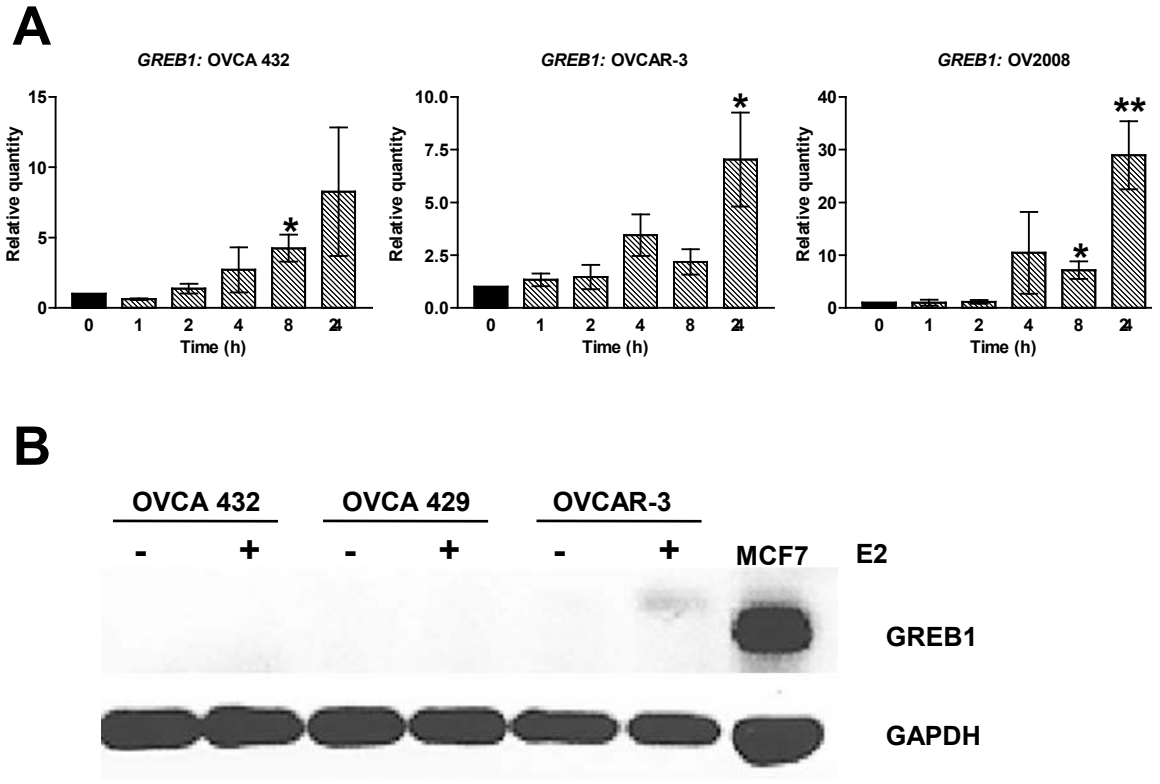

Figure 48. GREB1 induction by E2 over time in ovarian and cervical cancer cell lines. Cell lines were E2-deprived for 24-48h then treated with 500 nM E2. RNA was collected at 1-24h to examine *GREB1* by QPCR. Protein was collected at 30h to examine GREB1 by western blot. A) *GREB1* mRNA was induced consistently by 8h in OVCA 432 (24h p=0.0766) and OV2008 cells and by 24h in OVCAR-3 cells (n=3; *: $p<0.05$; **: $p<0.01$; one-sample t-test vs. control. B) GREB1 induction was faintly detected in OVCAR-3 cells but not in two other ovarian cancer lines (OVCA 432 and OVCA 429; n=1; positive control: MCF7 cells).

Table 6. Mouse survival after engraftment with human ovarian cancer cell lines.

Engrafted cell line	Survival - no E2 (days post surgery)	Survival - low dose E2 (days post surgery)	Survival - high dose E2 (days post surgery)
OVCAR-3	63,70	70	56,59
OVCA 432	82[1]	86,100	75,86

Mice were injected with 107 ovarian cancer cells (OVCAR-3 or OVCA 432) suspended in PBS, implanted with an E2 pellet (high: 0.25mg/60d; low: 0.05 mg/60d; N=1-2 per group), then monitored until loss of wellness required a humane endpoint.

[1]One additional mouse excluded from survival assessment because there were too few cells to inject the full amount.

line regardless of E2, although a faint band was observed above the putative GREB1 band in all OVCAR-3 xenografts and the MCF7 positive control, which could indicate a modified form of GREB1 (Figure 49).

3.5.2. GREB1 knockdown has similar but subtle effects in human ovarian cancer cells

To investigate GREB1 function in human ovarian cancer cell lines, the same lentiviral constructs used in MASE cells (Figures 3-4) were used to knock down and/or overexpress GREB1 in OVCAR-3 and OVCA 432 cells. Knockdown of *GREB1* was modest, with mRNA levels in OVCAR-3 cells decreasing by 25-50% with 3 shRNA constructs relative to cells expressing a non-silencing control (Figure 50A). Overexpression was more successful, with very high GREB1 expression in OVCA 432 cells and a faint but clear band in OVCAR-3 and HEY cells transduced with the overexpression construct (Figure 50B). GREB1 was detected by ICC in both the nucleus and cytoplasm of OVCA 432 cells transduced with a slightly different (LKO-based) lentiviral overexpression vector (Figure 50C). GREB1 knockdown did not alter proliferation of OVCAR-3 cells with either shRNA construct examined, although a trend for decreased proliferation was observed with one construct (shRNA #3; Figure 51A). Proliferation after GREB1 overexpression was not examined in OVCAR-3 cells due to the low expression levels observed. GREB1 knockdown and overexpression did not alter colony formation of OVCAR-3 cells (Figure 51B). GREB1 overexpression did not alter proliferation of OVCA 432 cells, although a trend for increased proliferation was seen (Figure 51C). Colony formation of OVCA 432 cells was not altered by GREB1 overexpression (Figure 51D). GREB1 overexpression increased proliferation of OVCA

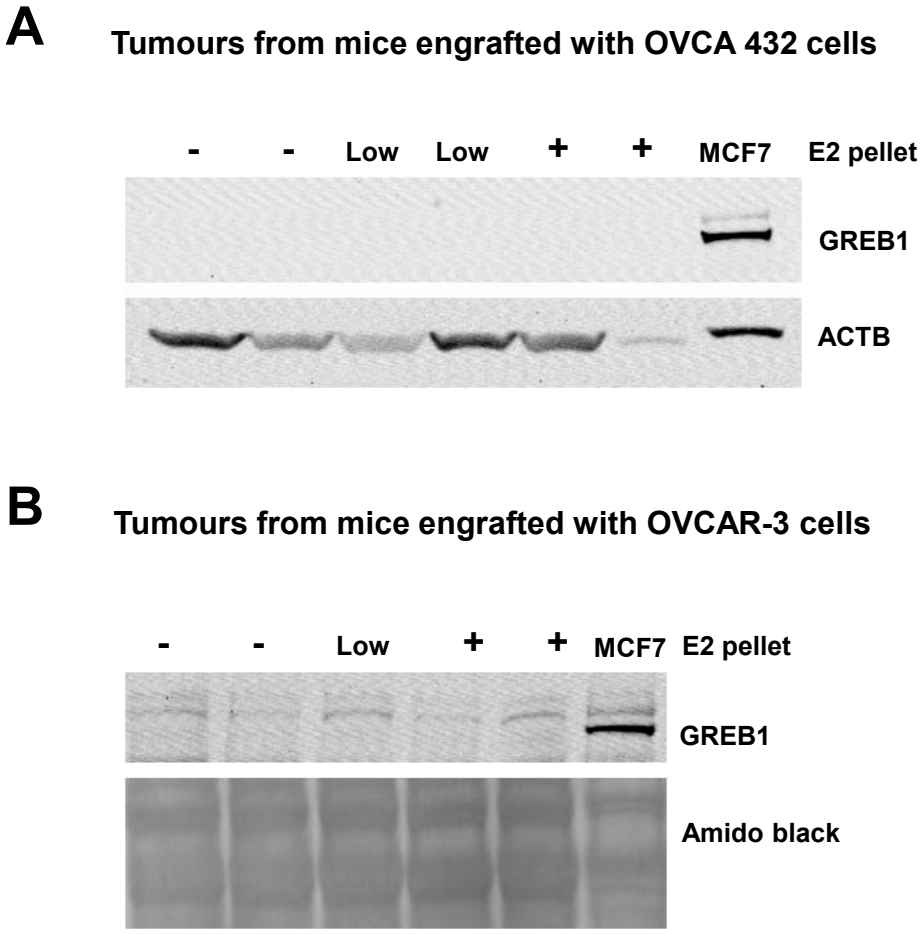

Figure 49. GREB1 expression in human ovarian cancer cells in vivo. To examine whether GREB1 is induced by E2 in human cell line xenografts, SCID mice were injected with 10^7 OVCA 432 or OVCAR-3 cells and implanted s.c. with a slow-release E2 pellet (0.05 mg low dose, "Low" or 0.25 mg higher dose, "+"). Mice were monitored until loss of wellness required a humane endpoint, then euthanized and tumours collected. GREB1 was measured by western blot, with MCF7 cells as a positive control. A) GREB1 was undetectable in OVCA 432-derived tumours regardless of E2 treatment. B) No GREB1 band was detected in OVCAR-3-derived tumours at the same level as the MCF7 positive control; however, a faint band above that band was seen in both the tumours and positive control, which could be caused by a post-translational modification of GREB1.

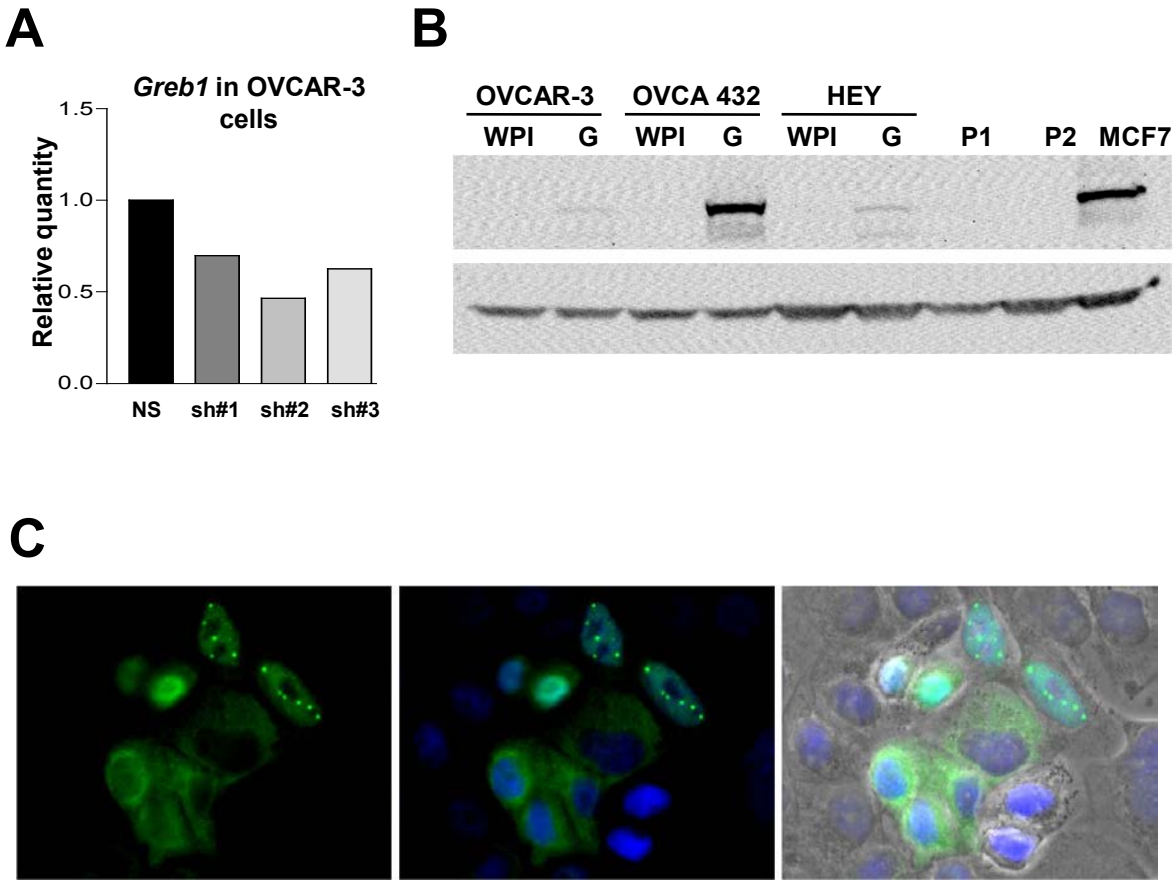

Figure 50. GREB1 knockdown, overexpression and localization in human ovarian cancer cells. A) GREB1 was knocked down in OVCAR-3 cells with the same GIPZ-based constructs used for mouse cells (Figure 4). Three short hairpin constructs (sh #1, sh #2, and sh #3) were compared to the non-silencing control. Maximum mRNA knockdown was about 50%. B) GREB1 was overexpressed in OVCAR-3, OVCA 432 and HEY cells with the same WPI-based constructs used for mouse cells (Figure 4). Strong GREB1 expression was seen in OVCA 432 cells transduced with the overexpression construct (G); faint GREB1 expression was seen in similarly transduced OVCAR-3 and HEY cells. P1, parental line 1 (OVCAR-3); P2, parental line 2 (OVCA 432). C) GREB1 was overexpressed in OVCA 432 cells with an alternative WPI-based construct expressing puromycin resistance instead of GFP. Following selection, GREB1 levels and localization were examined by ICC. GREB1 was seen in both nucleus and cytoplasm of transduced cells, but no fluorescence was seen in non-transduced cells (not shown).

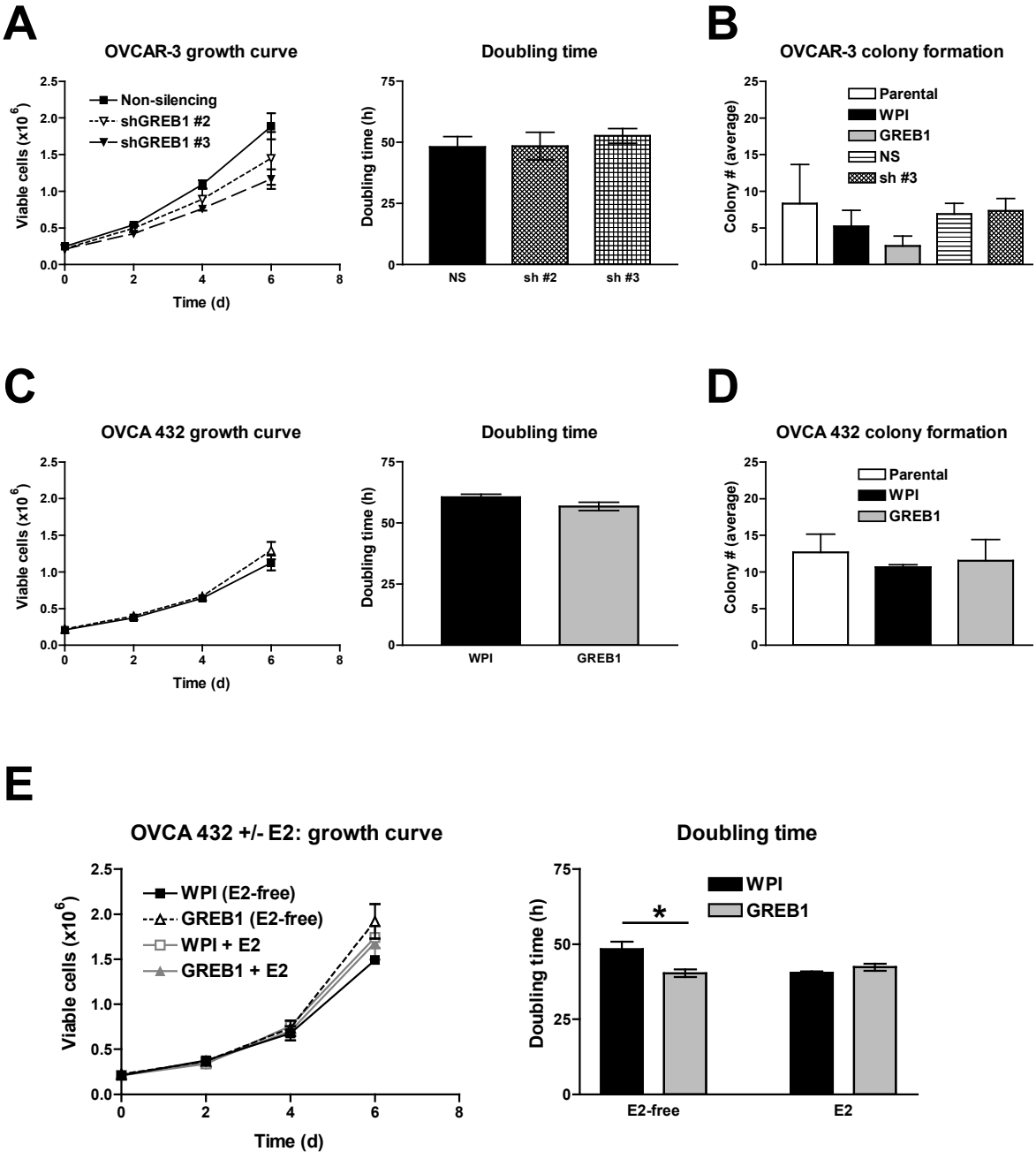

Figure 51. Effects of GREB1 on OVCAR-3 and OVCA 432 proliferation and colony formation. For proliferation assays, cells were grown in low-serum media and counted with a ViCell automated counter. For colony formation assays, cells were plated in E2-free media with 1% agarose and counted after 14d. A) GREB1 knockdown did not alter proliferation of OVCAR-3 cells. B) Colony formation was not changed by GREB1 knockdown or overexpression. C) GREB1 overexpression did not change OVCA 432 proliferation. D) Colony formation was not changed by GREB1 overexpression. E) GREB1 overexpression increased OVCA 432 proliferation under E2-free conditions, but not when 10 nM E2 was added (*: $p<0.05$, two-way ANOVA with Bonferroni post-test).

432 cells in E2-free conditions (doubling time decreased by 17%) but no difference was seen when 10 nM E2 was added to the media (Figure 51E).

3.5.3. GREB1 is expressed in the reproductive tract and several other normal tissues

GREB1 expression has been reported by others in normal breast and uterine tissues (Hnatyszyn et al. 2010, Pellegrini et al. 2012, Fung et al. 2015), but not in other tissues. We therefore examined GREB1 expression in public databases. RNA-sequencing data accessed through the EMBL-EBI Expression Atlas (based on data from 53 tissues in the GTEx Consortium 2013 and 32 tissues in The Human Protein Atlas) indicated that *GREB1* expression is highest in the ovary, with moderate expression in the prostate and female reproductive tissues and much lower but still detectable expression in all other tissues examined except tonsil and whole blood. GREB1 protein expression reported in The Human Protein Atlas was extremely inconsistent between the three antibodies examined and did not correlate well with gene expression data.

To examine GREB1 expression in normal tissues, a GREB1 antibody (Millipore) was optimized for IHC. GREB1 and ESR1 expression were examined in female reproductive tract tissue sections (ovary, cervix, and endometrium) obtained from The Ottawa Hospital and in a TMA panel of 50 normal tissues obtained from The Cooperative Human Tissue Network. In the reproductive tract sections, GREB1 was highly expressed in the ovarian stroma and was co-expressed with ESR1 in epithelial cells of follicular cysts and vestigial rete ovarii structures (Figure 52). In the endometrium and cervix, GREB1 and ESR1 were expressed in both the stroma and epithelial cells (Figure 53). The TMA showed similarly high GREB1 expression in the female reproductive tract (Figure 54A), including ovarian stroma, fallopian tube (stroma and epithelium), uterus (smooth

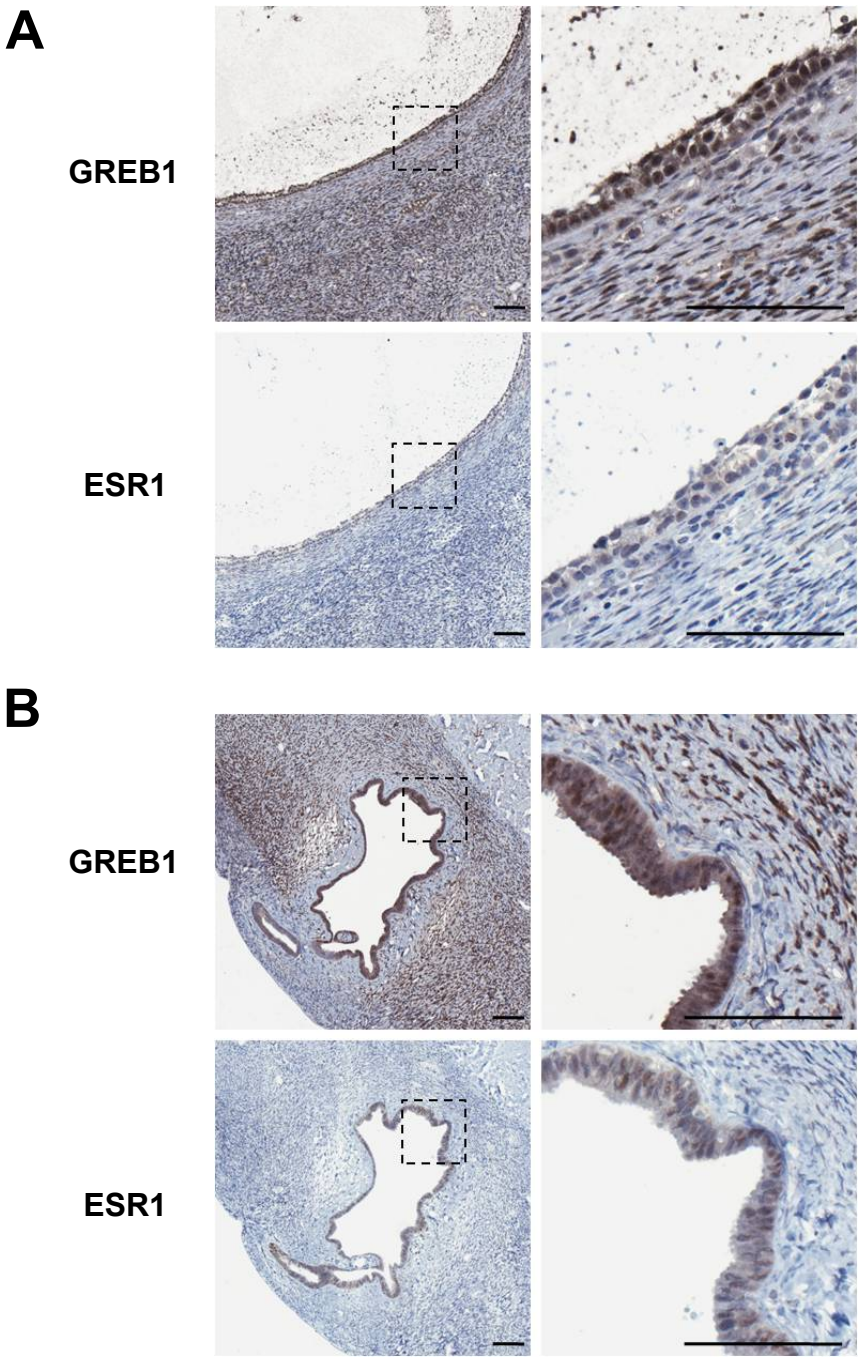

Figure 52. GREB1 and ESR1 expression in a normal ovary sample. Serial sections of a paraffin-embedded healthy ovary were stained for GREB1 and ESR1 by IHC. A) High GREB1 and low ESR1 expression are seen in the epithelial cells of a follicular cyst. Stromal cells were GREB1+ and ESR1-. B) A similar GREB1 and ESR1 expression pattern is seen in a vestigical rete ovarii structure elsewhere in the ovary. Scale bar: 100 µm.

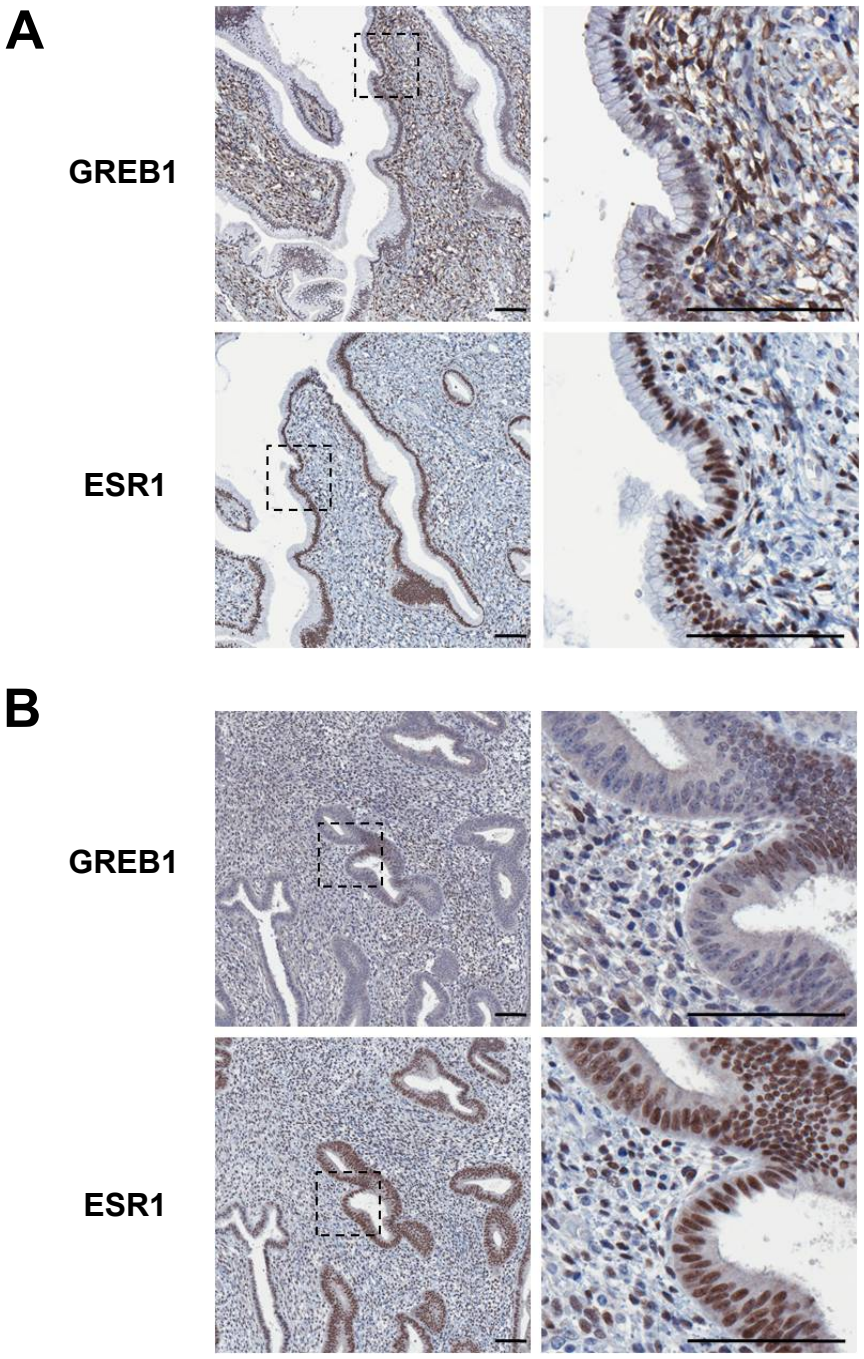

Figure 53. GREB1 and ESR1 expression in normal endometrium and cervix samples. Serial sections were stained for GREB1 and ESR1 by IHC. A) Most cells in the cervix were GREB1+. Epithelial cells were highly ESR1+; other cells were a mix of ESR1+ and ESR-. B) The endometrium had focal GREB1 expression. Epithelial cells were highly ESR1+; the stroma was a mix of ESR1+ and ESR- cells. Scale bar: 100 µm.

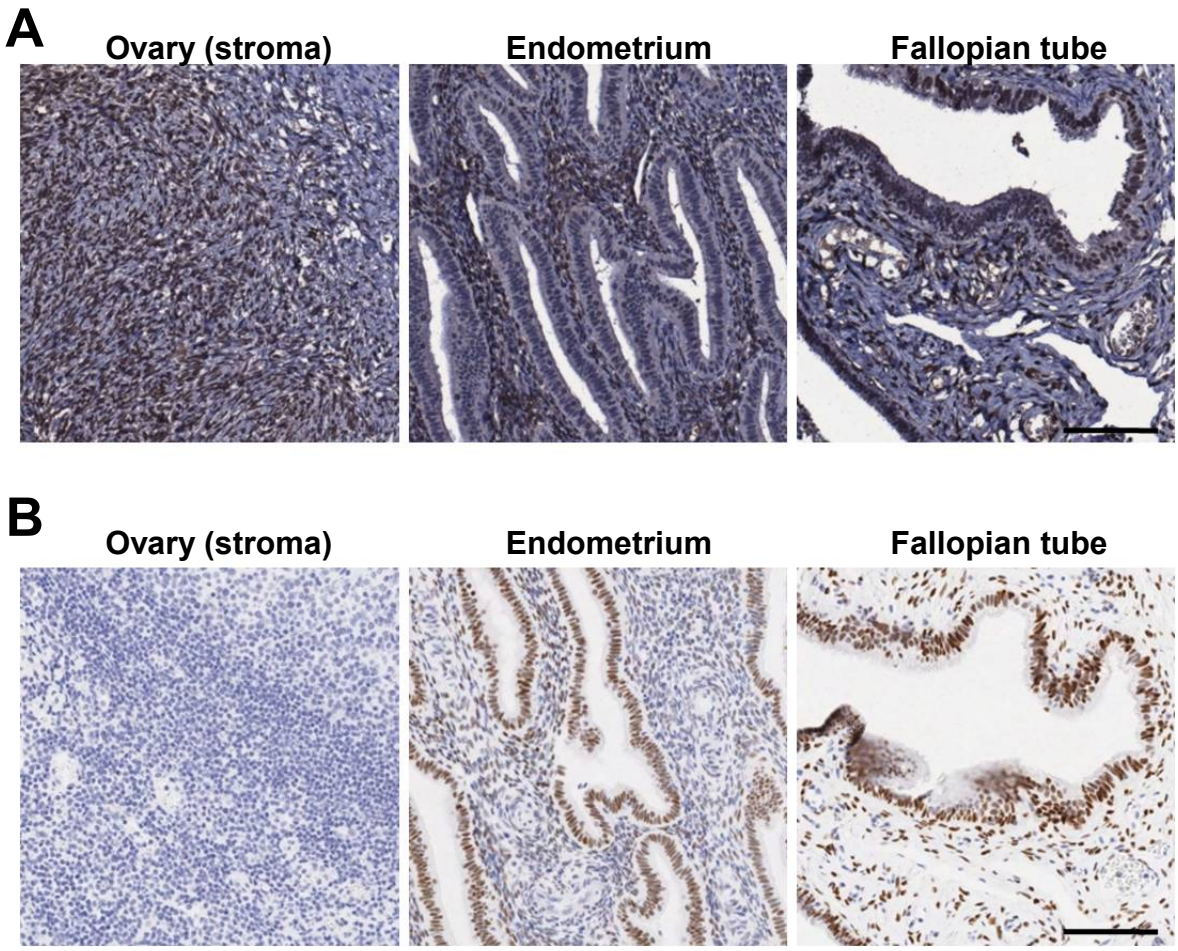

Figure 54. GREB1 and ESR1 expression in female reproductive tissues from a tissue microarray. A tissue microarray containing 50 normal tissues was stained for GREB1 and ESR1 by IHC. GREB1 and ESR1 expression was similar to staining observed previously in individual tissue sections (Figures 52-53). A) GREB1 was highly expressed throughout the female reproductive tract, including the ovary, endometrium, fallopian tube, and (not shown) cervix. GREB1 was expressed focally in the endometrial epithelium and consistently in the stroma. B) ESR1 was not expressed in the ovarian stroma and mixed expression was seen in the endometrial and fallopian tube stroma. Strong ESR1 staining was seen in the endometrial and fallopian tube epithelia. Scale bar: 100 μm.

muscle and endometrium), and cervix (ectocervix and endocervix), as well as breast epithelium. ESR1 was also expressed in many tissues throughout the females reproductive tract (examples shown in Figure 54B).

Other tissues with clear GREB1 expression included prostate, bronchus epithelium, thyroid, salivary gland, and kidney medulla (prostate, kidney and lung shown in Figure 55A). These tissues were almost all ESR1- (Figure 55B). Many of the other tissues had high background staining making interpretation difficult; however, clearly negative staining was observed in tonsil (squamous epithelium), hyperplastic parathyroid, small intestine villi, seminal vessicle, and lymph node (not shown). Lymphoid tissue (spleen, thymus) was also mainly negative with the exception of a few isolated high-staining cells. ESR1 was expressed exclusively in the female reproductive tract, epididymis (strongly ESR1+; GREB+, but with high background), thyroid (weakly ESR1+; GREB1+), and bladder epithelium (focally ESR1+; GREB1+, but with high background). In summary, ESR1+ tissues were all GREB1+, and many ESR1- tissues were also GREB1+.

3.5.4. GREB1 is expressed in all epithelial ovarian cancer subtypes

GREB1 expression had never been reported in ovarian cancer, so *GREB1* and *ESR1* expression were examined in a public database (TCGA; via cBioPortal). *GREB1* was highest in hormone-responsive cancers (ovarian, uterine, breast, prostate) as well as surprisingly, melanoma, whereas the lowest expression was seen in leukemia and cancers of the digestive tract. Similar expression patterns were seen for *ESR1*, with highest expression in breast, ovarian, and uterine cancers, and lowest expression in colorectal cancers. Notably, cBioPortal and similar databases focus on the most common subtype of

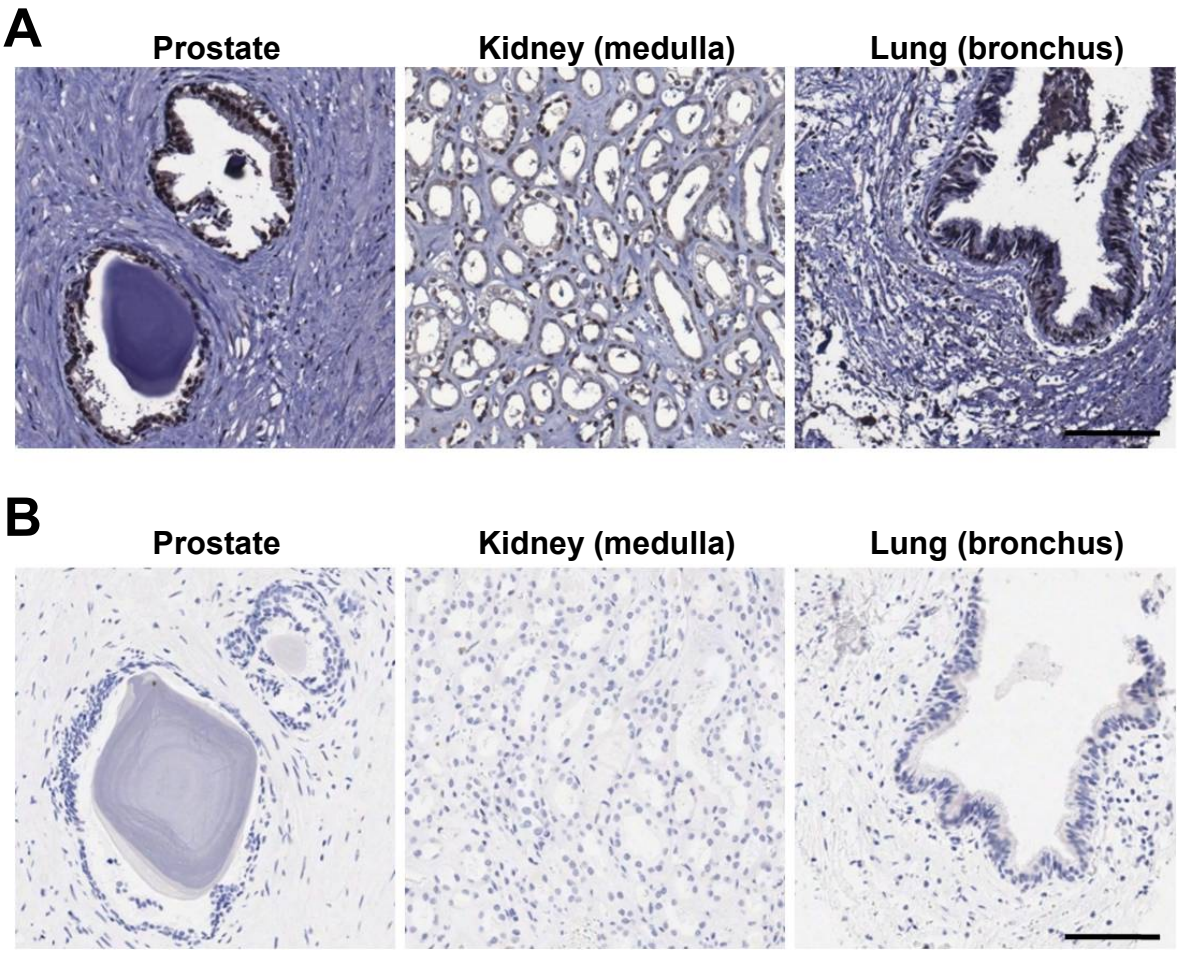

Figure 55. GREB1 and ESR1 expression in other tissues from a tissue microarray. A tissue microarray containing 50 normal tissues was stained for GREB1 and ESR1 by IHC. A) GREB1 was expressed in several tissues outside the female reproductive tract, including prostate, kidney, lung, and (not shown) breast, thyroid, and salivary gland. B) ESR1 was not detected in the prostate, kidney, or lung. Scale bar: 100 μm.

ovarian cancer (high-grade serous), and very little information is available for other EOC subtypes. We therefore investigated GREB1 expression by QPCR and IHC in tumours of all major histological subtypes.

GREB mRNA and protein were highly expressed in a small pilot study of EOC tumours from the Ottawa Ovarian Tumour Bank (4-5 each of low-grade serous, high-grade serous, endometrioid, and clear cell). *ESR1* and *GREB1* correlated at the mRNA level (Figure 56) and although only 1-2 tumours per subtype were examined by IHC, a similar pattern was observed in low-grade serous and endometrioid tumours (Figure 57). The mucinous tumour examined by IHC expressed high GREB1 but no detectable ESR1, whereas both high-grade serous tumours examined showed low, focal expression of both GREB1 and ESR1 (Figure 58). To confirm these results, a larger, unrelated group of ovarian tumours was examined in a TMA from The Cooperative Human Tissue Network (serous, mucinous, endometrioid, and clear cell; 20 cases per subtype). GREB1 was expressed in 75-85% of these EOC tumours, but surprisingly its expression did not correlate with ESR1 or any histological subtype (Table 7; Figure 59). In fact, 81% of ESR1- and 78% of ESR1+ tumours expressed GREB1. In the TMA, serous and endometrioid tumours were mainly ESR1+, whereas clear cell and mucinous tumours were mainly ESR1- (Table 7).

3.5.5. GREB1 may have potential as a diagnostic biomarker

To investigate if GREB1 could be used as a diagnostic marker to distinguish mucinous tumours of ovarian vs. gastrointestinal origin, a TMA was created by pathologist collaborators from The Ottawa Hospital Pathology department. In this TMA, GREB1 was expressed in most ovarian tumours but in only 16% of gastroinstestinal

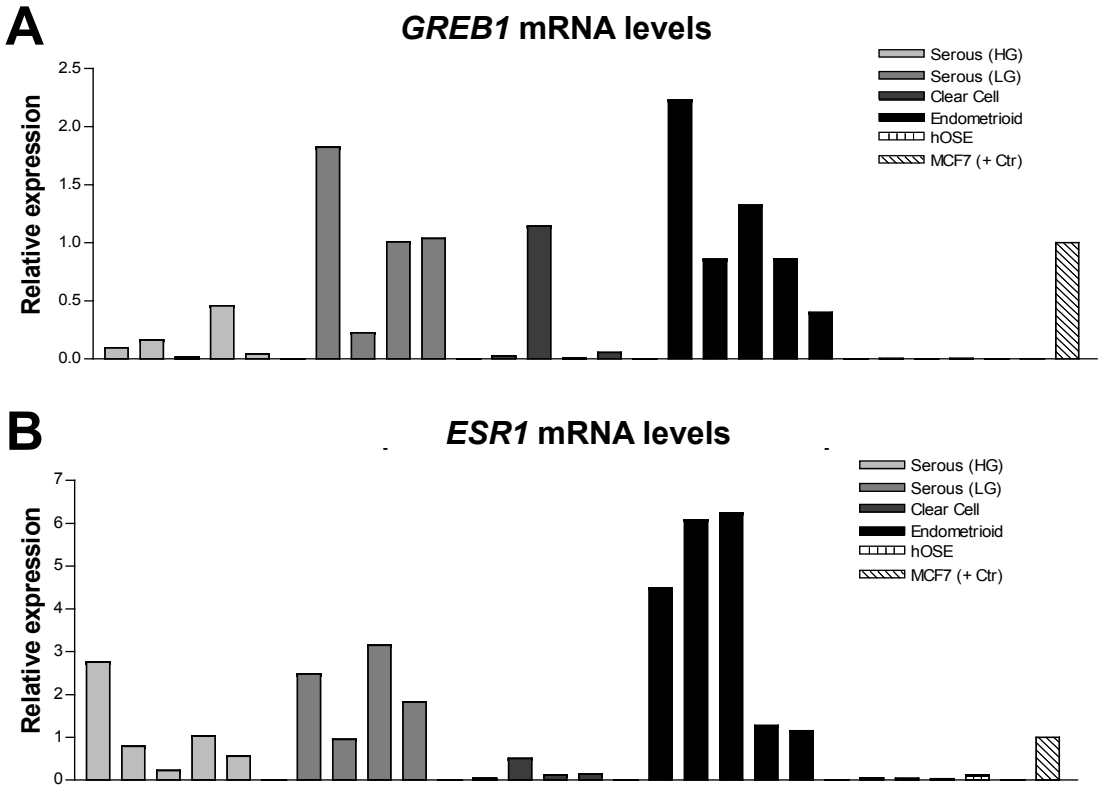

Figure 56. *GREB1* and *ESR1* expression in epithelial ovarian cancer. Snap-frozen ovarian tumours from surgical resection were obtained from the Ottawa Ovarian Tumour Bank with Research Ethics Board approval. *GREB1* and *ESR1* were examined by QPCR, with gene expression normalized to *PPIA* and quantified relative to the positive control (MCF7 cells). A) *GREB1* was expressed in all EOC samples examined, with the highest expression seen in endometrioid and low-grade serous tumours (N=4-5 per subtype). Very low expression was seen in normal ovarian surface epithelium cells (four early-passage hOSE cell lines). B) *ESR1* was also expressed in all EOC tumours and in all four hOSE lines. *ESR1* mRNA levels correlated with *GREB1* levels (R^2=0.589; p=0.0034; Pearson correlation analysis).

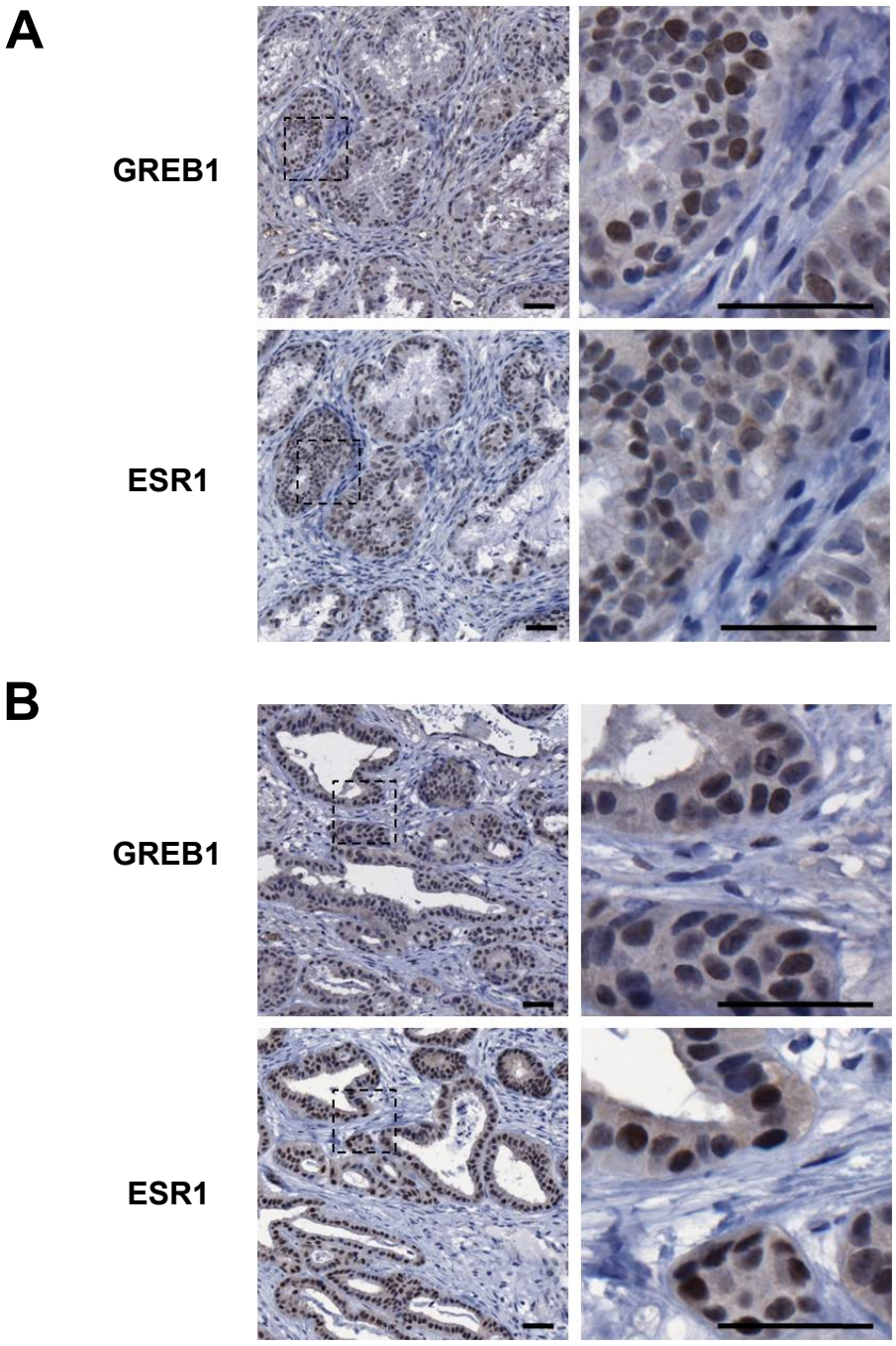

Figure 57. GREB1 and ESR1 expression in low-grade serous and endometrioid ovarian tumours. The tumours with highest *GREB1* and *ESR1* mRNA levels (Figure 56) were stained for GREB1 and ESR1 by IHC to validate the antibodies. The low-grade serous (A) and endometrioid (B) tumours co-expressed high GREB1 and ESR1, with low GREB1 and no ESR1 detected in the stroma (N=2/subtype). Scale bar: 100 μm.

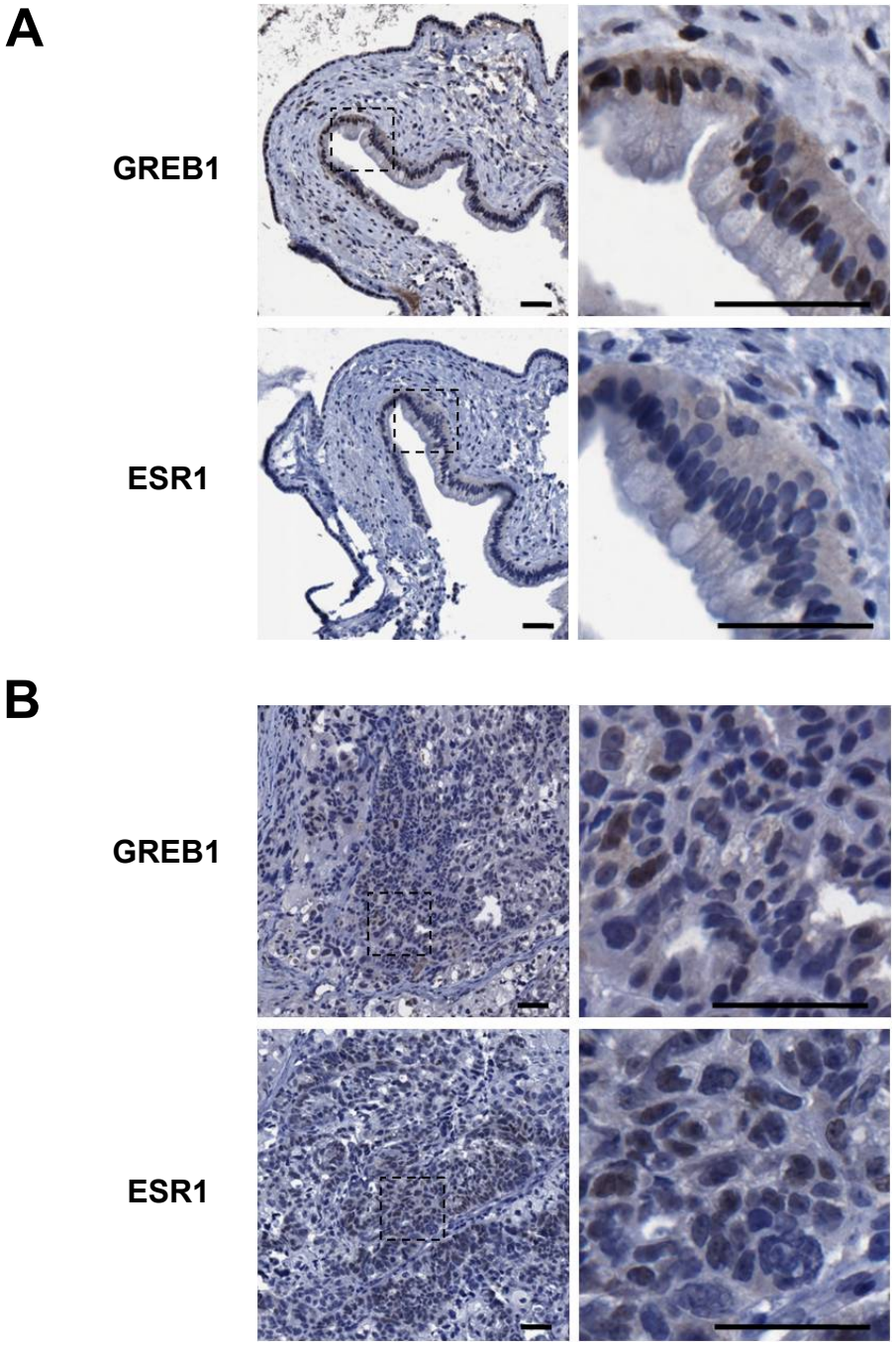

Figure 58. GREB1 and ESR1 expression in mucinous and high-grade serous ovarian tumours. A high-grade serous tumour with low *GREB1* and *ESR1* mRNA levels and a mucinous tumour with unknown GREB1 and ESR1 levels were stained for GREB1 and ESR1 by IHC. A) The mucinous tumour showed high GREB1 levels but no ESR1. B) The high-grade serous tumour showed focal expression of GREB1 and ESR1. Scale bar: 100 µm.

Table 7. GREB1 and ESR1 expression in tumours from the five major histological subtypes of ovarian cancer.

Histological subtype	GREB1+ ESR1-	GREB1+ ESR+	Total GREB1+	Total GREB1+ and/or ESR1+
Serous (low grade)	1/1	3/3	4/4 (100%)	4/4 (100%)
Serous (high grade)	3/3	10/13	13/16 (81%)	16/16 (100%)
Endometrioid	3/3	12/17	15/20 (75%)	20/20 (100%)
Clear cell	9/14	6/6	15/20 (75%)	15/20 (75%)
Mucinous	9/10	7/10	16/20 (80%)	19/20 (95%)

TMA sections obtained from the Cooperative Human Tissue Network (National Cancer Institute, USA). Scored by Dr. B. Djordjevic for predominant nuclear staining intensity (0,1,2,3) and % positive cells. GREB1 positivity was defined as ≥ 20% positive cells at intensity 1 or ≥ 1% positive cells at intensities 2 or 3.. ESR1 positivity was defined as ≥ 1% positive cells regardless of intensity.

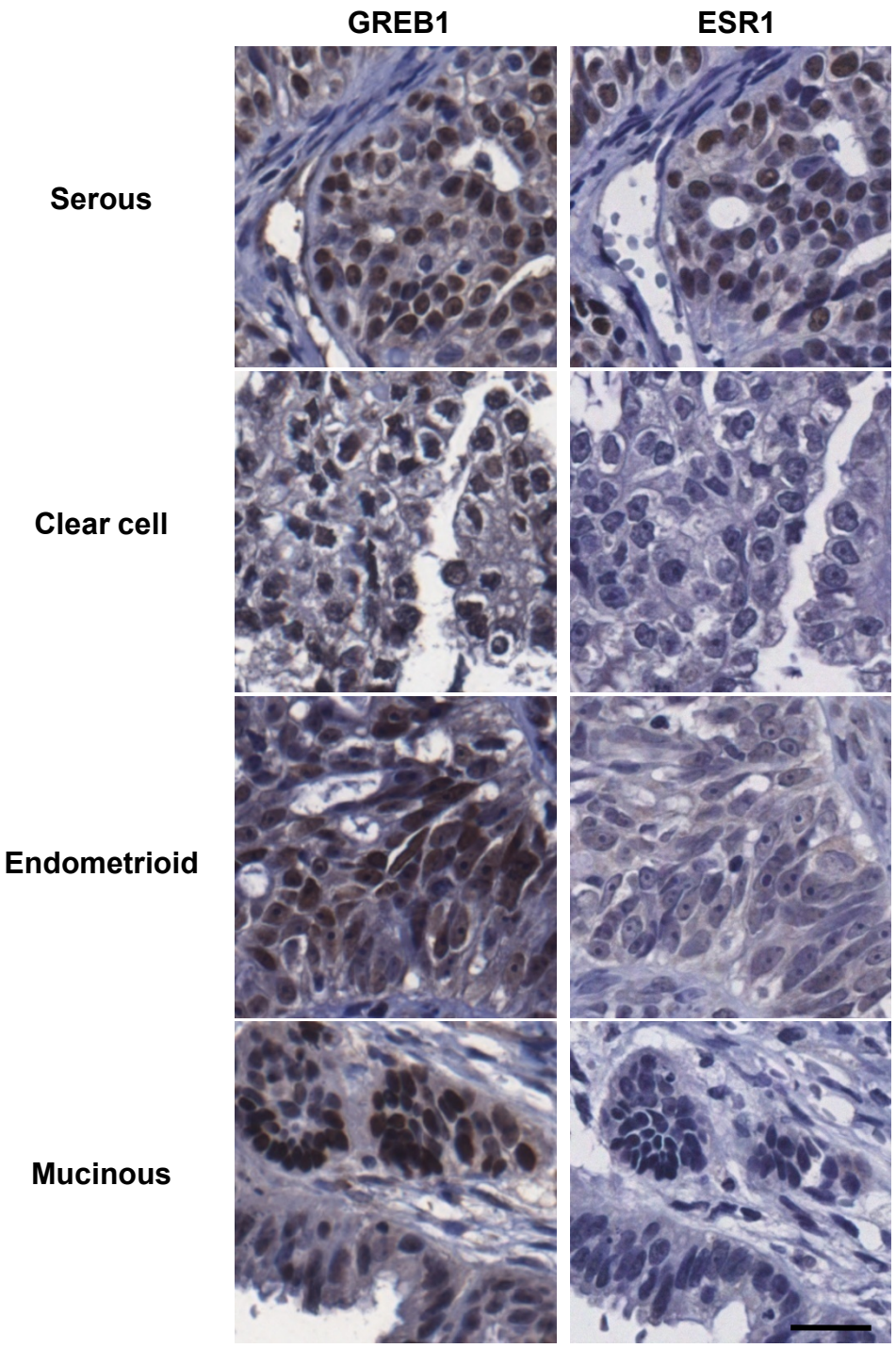

Figure 59. GREB1 and ESR1 expression by IHC in a tissue microarray of epithelial ovarian cancers. In a tissue microarray of four major EOC histological subtypes (N=20 each), GREB was expressed with similar proportions across all subtypes and did not correlate with ESR1 (see Table 6 for quantification). Scale bar: 25 μm.

tumours (both primary tumours and metastases to the ovary; Table 8). When combined with PAX8 expression, sensitivity to detect primary ovarian tumours in this set of tumours was increased to 93% (Table 8). This suggests that GREB1 may have utility as a diagnostic biomarker for mucinous tumours of unclear origin.

Table 8. GREB1 and PAX8 staining in mucinous cancers of ovarian vs. gastrointestinal origin.

Tumour type	GREB1+ (%)	PAX8+ (%)	GREB1+ *or* PAX8+ (%)	Total (N)
Ovarian primary	69	74	93	58
Gastrointestinal				
Primary	16	2	16	49
Metastasis to ovary	16	0	16	19

GREB1 and PAX8 were examined by IHC in a TMA of 60 primary mucinous ovarian neoplasms (19 cystadenomas, 21 borderline, and 20 adenocarcinoma), 49 primary mucinous gastrointestinal neoplasms (19 colorectal, 15 gastric, and 15 pancreatobiliary) and 19 metastases to the ovary (from a gastrointestinal primary tumour). TMA produced, scored and analyzed by Dr. B. Djordjevic and other pathologist collaborators at The Ottawa Hospital.

Chapter 4. Discussion

It has been known for decades that estrogen stimulates growth of breast and ovarian cancers. Although much has been learned since then, E2 signalling complexity and heterogeneity between model systems have made it difficult to determine the cellular and molecular mechanisms responsible for its tumour promoting actions. The main goal of this project was therefore to elucidate the mechanisms underlying E2-stimulated tumour growth in our mouse models of ovarian cancer and extrapolate the findings to human ovarian cancers.

4.1. Validation of the E2-responsiveness of our model systems

We first confirmed the accuracy of our model systems by showing that E2 accelerates tumour growth of OVX mice engrafted with mouse ovarian cancer cells, decreasing survival time. This supports earlier work by our lab (Laviolette et al. 2010) and others (Mullany et al. 2014, Armaiz-Pena et al. 2009, Spillman et al. 2010, Sawada et al. 1990) showing that E2 accelerates allograft and xenograft tumour growth. It also demonstrates that the MAS lines are not E2-dependent despite being E2-responsive. We also showed that E2 accelerates tumour growth in both young (8-10 week) and older (8 month) CAG-TAg mice with or without VCD-induced "menopause". As the majority of EOC occurs in postmenopausal women, it is important to know how physiological changes associated with menopause may alter E2 action. The consistency of E2 action regardless of reproductive status confirms that this model accurately reflects E2 action (e.g. HRT) in ovarian cancer developing after menopause.

Our lab has previously shown that E2 decreases survival time in transgenic mice by accelerating tumour initiation (Laviolette et al. 2010). Other immune-competent models have shown that E2 increases tumour growth and metastasis (Lee et al. 1992, Treviño et al. 2012, Mullany et al. 2014). Interestingly, E2 dependence was seen only after TP53 was disrupted in *LSL-Kras*^{G12D}; *Pten*$^{fl/fl}$*; Amhr2-Cre* mice (Mullany et al. 2014). In TP53-wildtype mice in that study and in a similar transgenic model (Romero et al. 2012), E2 did not alter tumour growth, metastases, or ascites. Although TP53 is not mutated in our mouse models, TAg binding stabilizes TP53 and impairs its function (Pipas 2009).

We found that MASE-derived tumours collected at endpoint were heavier in E2-treated mice; a similar trend was seen in mice engrafted with MASC cells. This supports the previously mentioned studies showing that E2 stimulates tumour growth, although it is unclear why E2-treated mice were not euthanized due to loss of wellness at the same tumour size as control-treated mice. E2 consistently decreased body weight in our allograft and transgenic models, which may have increased the harmful effects of the tumours. This is a well-known systemic E2 action mediated by SRC1 (Dubuc 1985, Zhu et al. 2013) but the implications on tumour progression, if any, have not been examined. Interestingly, mice with tumour-specific ESR1 deletion showed a small but consistent trend for increased body weight which was still decreased by E2, suggesting that E2 may decrease body weight both systemically and through ESR1-mediated effects in the tumour.

4.2. Mechanisms of E2 action in vivo

We have identified many E2-induced changes in gene expression that may mediate its tumour promoting effects in our models of EOC. This project has focused on our most promising candidate gene, *GREB1*, and we have shown that it has several cancer-promoting actions. However, we have also identified other genes that may contribute to E2 stimulation of tumour growth (Table 5). Several of these have been reported by others as E2-responsive, including *Pgr*, *Cyp11a1*, and *Stc2,* whereas others are novel targets. Only one other study has examined global gene expression changes after E2 treatment in an animal model of transplanted ovarian cancer cells (Spillman et al. 2010). They found that very few of the E2-regulated genes (including *GREB1*) in tumours derived from engrafted ESR1+ PE04 cells were similarly regulated in breast cancer, emphasizing the tissue specificity of E2 signalling. Two studies have examined E2-upregulated genes in human OSE or EOC lines in vitro (O'Donnell et al. 2005, Syed et al. 2005), but full lists of gene expression changes were not provided and few of their highlighted genes matched the gene expression changes we identified. These differences could be caused by various factors, but the most obvious explanation is that E2 differentially affects EOC cells growing in vitro vs. in vivo. In breast cancer, large changes in gene expression, including E2-regulated genes, have been reported between the same cancer cell lines growing in vitro vs. in xenografts (Thompson et al. 1990).

Although E2 upregulated angiogenesis-related genes in MASE tumours and cell lines, we found that it did not alter microvessel density in our allograft models. This suggests that angiogenesis is not a major mediator of E2 effects in our mouse models, and contradicts evidence that E2 promotes angiogenesis both in ESR1- breast and prostate cancer xenografts (Gupta et al. 2007) and in ESR1+ EOC xenografts (Armaiz-Pena et al. 2007). Interestingly, we found that E2 upregulated *Kdr*, *Ednra* and *Vegfa* in MASE cells

and tumours but downregulated them in MASC-derived tumours. The most obvious difference between MASE and MASC cell lines is ESR1 expression, suggesting that these genes are upregulated directly in the tumours through ESR1 rather than by systemic E2 actions. It is unclear why they are actually downregulated in MASC cells; this could be a compensatory response to other E2 actions or may signify E2 acting through alternative receptors. These opposing effects of E2 in MASE vs. MASC tumours may be related to the opposing trends seen in ascites formation, as tumour-secreted VEGFA is crucial for ascites development (Nagy et al. 1995). However, ascites volume was highly variable and no statistically significant differences were seen.

4.3. E2 action in ovarian cancer cell lines in vitro

Few actions of E2 were observed in our cell line models of ovarian cancer. Proliferation, migration, and colony formation were not changed by E2, suggesting that E2 may promote tumour progression through systemic and/or stroma-mediated effects. However, we have also accumulated considerable evidence that E2 acts directly on tumour cells. Three E2-upregulated genes identified in the microarray of MASE-derived tumours were also examined in vitro: *Greb1*, *Kdr* and *Ednra* were all upregulated within 48h by 10-500 nM E2 in MASE cells. KDR and GREB1 were also upregulated at the protein level, and IHC showed that KDR was expressed in tumour cells, not only in endothelial cells. Furthermore, ESR1 deletion in the tumour initiating cells prolonged survival and decreased E2 responsiveness of the CAG-TAg model.

Tumour cells in vivo may be more E2-responsive than the same cells in vitro due to various environmental differences (e.g. hypoxia, nutrient restriction, necrosis, three-dimensional growth, immune system interactions, extracellular matrix, endocrine and

paracrine factors). The tumour-promoting actions of E2 may be more easily observed in a growth-restricted environment, and E2 actions may affect tumour response to factors that are only seen in vivo. Furthermore, differences in E2 dose and length of treatment in vitro vs. in vivo are likely to alter response. We found that E2 upregulates *Greb1*, increases Ki67 staining, and stimulates cell proliferation only after long-term treatment, at which point many confluent areas had developed. This suggests that E2 is overriding cell cycle arrest signals to drive growth in suboptimal conditions. Reports of E2-responsiveness of EOC cell lines in vitro vary, even within a single cell line; for example, E2 has increased OVCAR-3 proliferation in some studies but not others.

4.4. Effects of P4 and menopause on tumour progression in the CAG-TAg model

P4 did not alter E2 actions in the CAG-TAg model, contrary to a previous report in SKOV3 cells (Armaiz-Pena et al. 2009). We also confirmed earlier findings by our lab that P4 does not alter CAG-TAg tumour progression by examining P4 in older mice (8 months) with and without VCD-induced "menopause", as well as testing a long-term (120d) P4 treatment and a PGR inhibitor (mifepristone). No changes in tumour progression or endpoint characteristics were seen with the 60d or 120d P4 treatments or with the PGR inhibitor. P4 action has not been thoroughly studied in mouse models of ovarian cancer, but two studies have shown a limited protective effect beyond the E2-antagonizing activity described earlier (Langdon et al. 1998, McDonnel et al. 2005) whereas several others have shown no effect (Laviolette et al. 2010, Sawada et al. 1990, Armaiz-Pena et al. 2009). Furthermore, a synthetic progestin reduced spontaneous EOC incidence in hens, although this effect was probably mainly caused by the inhibition of ovulation (Trevino et al. 2012).

4.5. Efforts to reduce E2-associated bladder problems with low-dose E2

Many of the E2-treated 8-month-old CAG-TAg mice developed bladder outlet obstruction requiring euthanasia. This has been occasionally observed by our lab (L. Laviolette et al. 2010) and others (Kuroda et al. 1985, Walker et al. 1992). In an attempt to reduce these bladder problems and simultaneously determine whether the effects of E2 are dose-dependent, we tested a lower E2 dose (0.05 mg rather than the previously used 0.25 mg). Serum E2 levels ranged from 0-10 pg/mL in serum from mice implanted with either 0.05 mg E2 (not shown) or placebo pellets. By contrast, serum E2 levels ranged from 100-200 pg/mL in mice collected 30d after implantation of a 0.25 mg pellet, and fell below 100 pg/mL in all mice collected 45d after implantation. This closely resembles E2 changes during pregnancy, where E2 slowly increases to a peak of 200-400 pg/mL at 20d in mice, then gradually returns to normal after giving birth (Wang et al. 2010). Serum E2 levels in humans are higher, ranging from 10-200 pg/mL throughout the menstrual cycle (Wright et al. 1999) and rising as high as 15 ng/mL during pregnancy (La Marca et al. 2005).

Surprisingly, none of the mice treated with either dose of E2 in this study developed bladder obstructions, so it is unclear whether the lower dose of E2 would have improved this problem. This problem may be more common in older mice. Furthermore, although a trend for intermediate survival was observed with low-dose E2 treatment in both ESR1-wildtype and ESR1-deleted mice, no significant survival differences were observed vs. control mice and tumour characteristics were similarly unchanged. Therefore, future studies should use E2 doses higher than 0.05 mg to ensure that survival is consistently decreased.

4.6. Effects of TAg hemizygosity and mouse strain on CAG-TAg tumour progression

TAg had a dose-dependent effect on tumour progression in the CAG-TAg model; hemizygous mice survived longer than homozygous mice. A similar effect has been observed in other TAg-driven mouse models of cancer, including prostate cancer (Perez-Stable et al. 1997), osteosarcoma (Wilkie et al. 1994), and melanoma (Larue et al. 1993). Furthermore, melanocytes isolated from TAg-hemizygous mice with low copy numbers of TAg were non-tumourigenic, unlike melanocytes from TAg-homozygous mice (Larue et al. 1993).

We also discovered a major effect of strain in this mouse model. When only one TAg allele was present, no mice with a mixed (F1 FVB/N x B6) background developed tumours within 400d, whereas 100% of FVB/N mice developed tumours with a median survival time of 219d. Strain differences have been shown previously in various mouse models of cancer, including spontaneous, chemical-induced, xenograft, and transgenic models (Dragani et al. 2003, Macleod and Jacks 1999). The B6 strain, including F1 mixed-background pups, has shown suppressed tumour growth in models of breast (Rose-Hellekant et al. 2002) and ovarian cancer (Garson et al. 2012). Despite various phenotypic differences including slower growth, tumours still developed in most or all B6 mice in these studies, so we were surprised to find complete inhibition of tumour development in F1 mixed-background pups in our model. Our discovery of a synergistic interaction between genetic strain and TAg hemizygosity indicates that TAg activity is highly dependent on genetic factors. This information will be critical when designing future studies using this model.

4.7. Importance of ESR1 in mediating E2 effects in our model systems

ESR1 is known to play a key role in tumour-promoting E2 signalling, but its importance relative to other estrogen receptors remains unclear. We have shown that in both our allograft and transgenic mouse models, ESR1 contributes to E2 action but is not the only factor. MASC cells express much lower ESR1 than the otherwise-similar MASE cell line, and are far less E2-responsive. In MASC cells, survival and tumour burden changes induced by E2 were smaller. In MASC-derived tumours, E2 downregulated angiogenesis-related genes that were upregulated by E2 in MASE cells and tumours. Furthermore, ESR1 deletion in tumours prolonged survival and decreased the response to E2. However, E2 still decreased survival in these mice. The ESR1-specific subset of E2 actions may be partially or entirely mediated by GREB1. ESR1 inhibition or deletion prevented GREB1 upregulation both in vitro and in vivo. Furthermore, *GREB1* is not induced by E2 in MASC cells in vitro, although induction was seen in MASC-derived tumours. Transfection of an ESR1- clear cell EOC cancer line (TOV21G) with ESR1 increased *GREB1* mRNA 2.5-fold (Yoffou et al. 2011). It would be interesting to see whether ESR1 transfection would similarly increase *GREB1* in MASC cells.

4.8. GREB1 induction and function in ovarian cancer models

When this project was started, little was known about GREB1 function beyond its essential role in hormone-stimulated breast and prostate cancer cell growth (Rae et al. 2005, Rae et al. 2006). Furthermore, GREB1 had never been examined in ovarian cancer or in mouse models. We have significantly expanded the knowledge of GREB1 activity by determining its role in several ovarian cancer model systems. We were also the first to

confirm that the mouse homolog of GREB1 has similar regulation and functions, supporting the relevance of our model systems for examining estrogen action.

In both mouse and human ovarian cancer cell lines, we detected GREB1 mRNA induction as early as 4h after adding E2, with the increased expression sustained for at least 48h. This time course resembles induction patterns described in MCF7 cells (Ghosh et al. 2000, Rae et al. 2005). GREB1 protein induction was seen in mouse cells at 48h, but little to no GREB1 protein was detectable in human cell lines despite comparable mRNA fold changes induced by E2. This may reflect lower baseline GREB1 levels and/or differences in posttranscriptional regulation of GREB1 levels in human vs. mouse tissues. We found that this induction by E2 was mediated by ESR1 binding to *Greb1* EREs in our mouse ovarian cancer cells, as shown previously in breast cancer cells (Sun et al. 2007, Deschenes et al. 2007). Others have shown that GREB1 can be upregulated by other steroid hormone receptor including ESR2, PGR and AR (Jacobsen et al. 2005, Rae et al. 2006); while these mechanisms may also be active in our cell lines, ESR1 inhibition and deletion experiments showed that ESR1 is required for GREB1 upregulation by E2 in MASE cells.

Intracellular localization can help clarify protein function. Reports in other hormone-responsive tissues and cancers suggest that GREB1 is located predominantly in the nucleus, which would support its identified role as an ESR1 cofactor. However, we discovered that GREB1 was more strongly expressed in the cytoplasm of mouse ovarian cancer cells. Interestingly, this expression was focal, with a very small fraction of cells expressing high levels of GREB1 but little to none in the majority of the population. The subpopulation of highly-expressing cells had very different morphology: cells were smaller, less flat, and more mesenchymal-looking than the main population. These cells

also had very bright, condensed DAPI staining, suggesting recent mitotic activity. It is unclear whether GREB1 is only ever expressed in a subpopulation of cells, or whether all MASE cells express GREB1 periodically (i.e. during mitosis). Regardless, this mitosis-linked expression pattern along with its ability to increase proliferation suggests that GREB1 is driving cell division.

By contrast, both human cell lines examined (MCF7 breast cancer cells and GREB1-overexpressing OVCA 432 ovarian cancer cells) showed high GREB1 in most cells, with strong expression in both the nucleus and cytoplasm. It is unclear what is causing differential localization in these human and mouse cell lines. GREB1 may have species-specific and/or tissue-specific regulatory mechanisms that result in high but transient cytoplasmic expression during mitosis in mouse ovarian cancer cells but more constant expression in human breast cancer cell lines. Further research is needed to clarify these expression patterns in human and mouse ovarian cancer cells and determine whether they are related to GREB1 function.

We were the first to show GREB1 promotes proliferation in ovarian cancer cell lines (Laviolette et al. 2014), as others have reported in breast (Rae et al. 2005) and prostate (Rae et al. 2006) cancer cell lines. These early reports focused on GREB1 interference, but we have shown that GREB1 overexpression and knockdown reciprocally alter proliferation. This indicates that GREB1 is not only an important link in proliferative pathways, it also directly stimulates proliferation of mouse ovarian cancer cells. The effects were more noticeable in low-serum media, suggesting that GREB1 is a particularly important driver of growth in unfavourable conditions. Supporting this theory, *Greb1* was induced by E2 in normal mOSE cells only after long-term treatment, when confluence had induced growth arrest in untreated mOSE cells (whereas E2-treated

cells continued to grow). However, GREB1 knockdown and overexpression did not alter colony formation of either mouse or human ovarian cancer cells plated in soft agar, suggesting that tumourigenicity is not affected by GREB1.

The effects of GREB1 knockdown and overexpression were subtle in human ovarian cancer cell lines. Although trends were seen for increased proliferation with GREB1 overexpression in OVCA 432 cells and decreased proliferation with GREB1 knockdown in OVCAR-3 cells, neither difference was significant. This suggests decreased E2-responsiveness and/or GREB1-responsiveness relative to our mouse ovarian cancer cell lines. Notably, GREB1 overexpression increased OVCA 432 cells in E2-free conditions but not when E2 was added. This could mean that endogenous GREB1 is already maximally active in regular media, which has low levels of estrogenic activity from phenol red and serum. Alternatively, GREB1 function may be influenced by other factors that are increased by E2 deprivation.

This research has also significantly expanded the knowledge of GREB1 action by exploring the effects of its altered expression on EMT and migration, which has never been reported. We noticed that GREB1 knockdown altered morphology, with a subpopulation of cells shifting to a more epithelial-looking phenotype. GREB1 overexpression had the opposite result, inducing a more mesenchymal-looking phenotype. These morphology changes corresponded with changes in cell size; GREB1 overexpression decreased cell volume and GREB1 knockdown showed a trend for increased cell volume.

To investigate the cause for these morphology changes, we examined EMT-related genes in a PCR array. Surprisingly, most genes were not altered by GREB1 knockdown or overexpression, suggesting that GREB1 does not affect EMT. The most

commonly reported markers of EMT are an increase in *Snai1* and an associated decrease in *Cdh1*. We found that neither gene changed with GREB1 overexpression or knockdown, although a trend for decreased *Snai1* was seen with GREB1 knockdown. Because morphology changes were only seen in a subpopulation of cells, it is possible that any EMT-related changes were masked by the main population. Furthermore, protein levels do not always correspond with mRNA levels. Therefore, CDH1 and SNAI1 should be examined by IF and correlated with morphology before concluding that the morphology differences are not EMT-related. Alternatively, the subpopulations with altered morphology could be isolated (e.g. by sorting for cell size) and immediately examined for EMT markers.

Based on the observed morphology changes, MASE cell migration was examined with scratch wound assays. We found that GREB1 overexpression promoted migration in all culture conditions, with the largest increases seen in low-serum and E2-free media conditions. This is significant because migration speed can be used to infer the propensity of a cell line to metastasize. Surprisingly, knockdown did not change migration in any culture condition. This implies that even E2-induced endogenous GREB1 levels are insufficient to promote migration of MASE cells in vitro. Alternatively, this could be a species-specific function of GREB1, as the overexpression construct encodes human GREB1.

Notably, we were the first to examine the role of GREB1 in tumour progression in vivo. We found that its proliferative effects in vitro translated to significant biological implications; GREB1 knockdown in MASE cells dramatically prolonged survival of engrafted mice. These findings were supported by a recent study showing that forced expression of miR-26, which targets *GREB1*, inhibited MCF7 xenograft tumour growth

(Tan et al. 2014). However, they predicted that miR-26 targets 695 genes, including three E2-regulated genes that partially mediated the proliferative response to E2 in vitro (*GREB1*, *CHD1* and *KPNA2*), so the relative contribution of GREB1 in this study was unclear.

We predicted that GREB1 knockdown would alter E2 response, but E2 dramatically decreased survival regardless of GREB1 knockdown. GREB1 knockdown was not detected in tumours of E2-treated mice, suggesting that the E2 dose used upregulated GREB1 sufficiently to overwhelm the shRNA being produced. E2 is also likely to be decreasing survival through GREB1-independent mechanisms. Therefore, it remains unclear how much the GREB1 upregulation we observed previously in E2-treated mice contributed to E2-accelerated growth. To elucidate the requirement for GREB1 in E2 action, a more consistent depletion or knockout of GREB1 would be required. This could be achieved through new CRISPR technology or by generating a GREB1-floxed mouse that could be crossed with our CAG-TAg model.

Surprisingly, we found that GREB1 overexpression did not alter survival of engrafted mice. Notably, tumours examined at endpoint showed no detectable GREB1, suggesting that the overexpression construct was no longer stably expressed. GFP intensity in these tumours was noticeably lower in tumours collected at longer survival times for both non-silencing and GREB1 knockdown groups, indicating fading construct expression over time in vivo. It is unclear why GREB1 knockdown altered survival but overexpression did not, if both constructs lost expression over time. Endogenous GREB1 levels in vivo may already be maximally promoting proliferation. Alternatively, the overexpression construct may have lost its expression more rapidly than the knockdown construct. Furthermore, GREB1 overexpression increased tumour burden at endpoint,

suggesting that it did promote tumour growth but alternative mechanisms drove disease progression in control mice, so overall survival time was unaffected by GREB1. These theories could be evaluated by collecting tumours at earlier time points and examining GREB1, Ki67, and tumour size to determine how rapidly the construct expression is lost in vivo and to evaluate the effects of GREB1 overexpression on tumour proliferation.

4.9. GREB1 expression in normal tissues and EOC

GREB1 expression has only been reported previously in breast (Hnatyszyn et al. 2010) and uterine (Pellegrini et al. 2012) tissues. In public databases, we found that *GREB1* mRNA levels are consistently highest in the reproductive tract. Protein expression data that is publically available is inconsistent; the three antibodies described in The Human Protein Atlas (Sigma HPA024616, HPA027843, and HPA028416) showed extreme differences in GREB1 expression in various tissues. Furthermore, intracellular localization was unclear; the Human Protein Atlas listed expression as cytoplasmic with a prediction of membrane localization, whereas GREB1 localization was reported as nuclear in breast cancer and normal breast tissue (Hnatyszyn et al. 2010). Uterine tissue showed mixed localization, with nuclear GREB1 expression in endometriotic lesions, but cytoplasmic expression in normal endometrial tissue (Pellegrini et al. 2012).

We found strongest GREB1 expression in the prostate and female reproductive tract, as predicted from mRNA expression data. GREB1 was also clearly expressed in several other tissues that were reported to have relatively low mRNA levels, including breast, lung, thyroid, salivary gland, and kidney. Tonsil, the only tissue type in the TMA with no mRNA expression detected by RNA sequencing, was completely negative for GREB1 with no background staining, supporting the specificity of the Millipore antibody

used. We detected both nuclear and cytoplasmic staining, although nuclear staining was more common and more clearly identifiable as specific staining. Like GREB1, ESR1 protein expression patterns resembled the mRNA patterns described in public databases, with strong expression in most tissues of the female reproductive tract but otherwise expressed only in the epididymis, thyroid and bladder epithelium, which were all GREB1+. GREB1 expression was seen in all ESR1+ tissues but also in many ESR1- tissues, suggesting that GREB1 is not solely regulated by ESR1, particularly in tissues outside of the female reproductive tract.

This is the first study to investigate GREB1 expression in EOC. We examined *GREB1* and *ESR1* expression in primary tumours listed in the cBioPortal database and found that both genes were most highly expressed in hormone-responsive cancers including high-grade serous EOC; the lowest expression was seen in cancers of the digestive tract. When we examined EOC tumours of all major histological subtypes by QPCR and IHC, we found that *GREB1* mRNA levels were highest in endometrioid and low-grade serous tumours; all EOC tumours examined showed high *GREB1* expression relative to four primary cultures of normal ovarian (hOSE) cells. At the protein level, GREB1 was frequently expressed with no major differences between histological subtypes. GREB1 expression was more frequent in low-grade tumours and in younger women, suggesting that it may be associated with less aggressive cancers and/or serum estrogen levels, but sample sizes were too low to draw clear conclusions.

At the mRNA level, *GREB1* correlated with *ESR1* levels, but no correlation was seen at the protein level. In contrast, GREB1 was rarely expressed in ESR1- breast cancers but frequently expressed in ESR1+ breast cancers (Hnatyszyn et al. 2010). As GREB1 is both downstream and upstream of ESR1 signalling in breast cancer cells

(Mohammed et al. 2013) and we have confirmed that GREB1 is also induced through ESR1 in ovarian cancer, it is surprising to see such frequent GREB1 expression in the absence of ESR1. In ESR1- tumours, GREB1 may have been induced by ESR1 that later degraded, or GREB1 may be regulated by alternative mechanisms. ESR1-independent GREB1 expression could be a mechanism for stimulating growth-promoting estrogen signalling pathways in the absence of E2 and/or ESR1. Interestingly, serous, mucinous, and endometrioid tumours were nearly always positive for GREB1 and/or ESR1; only 1/60 tumours was negative for both markers. Many more clear cell tumours (25%) were negative for both GREB1 and ESR1, suggesting that this subtype is less reliant on estrogen signalling pathways.

In high-grade serous ovarian tumours from the TCGA, *GREB1* did not correlate with *ESR1*; in fact, a trend for mutual exclusivity was observed. Surprisingly, the same study identified GREB1 as one of 409 genes upregulated in normal ovarian tissues relative to EOC, contrary to our findings that GREB1 is very low in hOSE cells. This is likely caused by the highly estrogenic environment of the functional ovary and/or the other cell types present in the whole ovary. The correlation we observed between *ESR1* and *GREB1* at the mRNA level in our samples may have been caused by including tumours of non-serous histotypes. If so, the lack of correlation at the protein level could be caused by posttranscriptional regulation. Alternatively, the mRNA correlation may be due to random chance, despite statistical significance; a larger sample size of non-serous tumours is needed to confirm these findings.

It is unclear why GREB1 correlated with ESR1 in breast cancer but not in ovarian cancer; GREB1 regulation may have tissue-specific differences. Furthermore, ovarian cancer is usually diagnosed after menopause, which could alter GREB1 regulation;

GREB1 in breast cancer biopsies correlated with serum E2 levels (Haakensen et al. 2011). Interestingly, Schaner et al. (2003) noted that several genes that are correlated with ESR1 in breast cancer (GATA-3, LIV-1 and X-box binding protein 1) did not show the same correlation in ovarian cancer. These differences in E2-responsive genes between breast and ovarian cancers could be related to E2-independence and response to antiestrogen therapies, which show limited efficacy in ovarian cancer. GREB1 loss has been linked to tamoxifen resistance in ESR1+ cell lines and breast cancer (Lippman et al. 2008, Mohammed et al. 2013); however, the effects of GREB1 expression in ESR1- cell lines have not been examined.

Metastatic mucinous ovarian tumours are frequently difficult to distinguish from metastatic gastrointestinal tumours. Because GREB1 is rarely expressed in gastrointestinal tissues, we investigated the potential of GREB1 as a diagnostic biomarker for differentiating tumour origin. We found that primary ovarian mucinous cancers were more likely to express GREB1 than secondary ovarian tumours (metastases from gastrointestinal cancers) or primary gastrointestinal tumours. When combined with PAX8, a current diagnostic biomarker, sensitivity for detecting ovarian tumours was improved to 93%. Therefore, GREB1 staining may be a useful diagnostic tool for mucinous cancers.

4.10. Conclusions

We have shown that E2 promotes tumour growth in our mouse models and have investigated potential mechanisms for its actions. Several previously reported mechanisms such as angiogenesis and upregulated *CCND1* were not altered by E2 in our model systems, emphasizing the heterogeneity of E2 action even within a single cancer

type. A microarray identified a highly E2-upregulated gene, *GREB1*, which promoted ovarian cancer cell proliferation and migration in vitro. In vivo, GREB1 knockdown prolonged survival of engrafted mice. Further experiments are needed to confirm the contribution of GREB1 to the accelerated tumour progression caused by E2 in our models. Several known effects of E2 were not examined in our study, including metabolite-induced DNA damage and altered stroma and immune cell recruitment. These actions may also contribute to the effects of E2 in our mouse models. However, we have shown that E2 acts directly on the tumour cells to promote disease progression through ESR1-mediated transcription of tumour-promoting genes including GREB1.

Future experiments will further elucidate the function of GREB1 by identifying its protein interactions with BioID and by determining whether ESR1 is required for GREB1 activity. The new MASE lines we generated will be an invaluable resource for these experiments, allowing GREB1 alteration in matched ESR1-deleted vs. wildtype cell lines. A drug screen is also planned to discover small molecules with GREB1-inhibiting activity in order to investigate potential therapeutic options.

Intriguingly, high GREB1 expression has been linked to antiestrogen sensitivity in breast cancer (Lippman et al. 2008, Mohammed et al. 2013), suggesting that increasing GREB1 activity may also be a viable strategy. Endocrine therapy is not used for most ovarian cancer patients due to limited overall efficacy; although some patients have responded to estrogen inhibition, biomarkers to identify these sensitive patients have not yet been validated. Further research is needed to determine whether GREB1 is related to antiestrogen sensitivity in ovarian cancer. If so, GREB1 may be useful as a predictive biomarker and/or therapeutic target to increase the efficacy of antiestrogen therapy.

References

Anglesio MS, Bashashati A, Wang YK, Senz J, Ha G, Yang W, Aniba MR, Prentice LM, Farahani H, Li Chang H, et al. 2015. Multifocal endometriotic lesions associated with cancer are clonal and carry a high mutation burden. J Pathol 236(2):201-9.

Antunes AA, Leite KR, Reis ST, Sousa-Canavez JM, Camara-Lopes LH, Dall'oglio MF, Srougi M. 2012. GREB1 tissue expression is associated with organ-confined prostate cancer. Urol Oncol 30(1):16-20.

Armaiz-Pena GN, Mangala LS, Spannuth WA, Lin YG, Jennings NB, Nick AM, Langley RR, Schmandt R, Lutgendorf SK, Cole SW, et al. 2009. Estrous cycle modulates ovarian carcinoma growth. Clin Cancer Res 15(9):2971-8.

Bai W, Oliveros-Saunders B, Wang Q, Acevedo-Duncan ME, Nicosia SV. 2000. Estrogen stimulation of ovarian surface epithelial cell proliferation. In Vitro Cell Dev Biol Anim 36(10):657-66.

Bareither ML and Verhage HG. 1981. Control of the secretory cell cycle in cat oviduct by estradiol and progesterone. Am J Anat 162(2):107-18.

Barnes MN, Berry WD, Straughn JM, Kirby TO, Leath CA, Huh WK, Grizzle WE, Partridge EE. 2002. A pilot study of ovarian cancer chemoprevention using medroxyprogesterone acetate in an avian model of spontaneous ovarian carcinogenesis. Gynecol Oncol 87(1):57-63.

Barry JA, Azizia MM, Hardiman PJ. 2014. Risk of endometrial, ovarian and breast cancer in women with polycystic ovary syndrome: A systematic review and meta-analysis. Hum Reprod Update 20(5):748-58.

Bast RC,Jr, Feeney M, Lazarus H, Nadler LM, Colvin RB, Knapp RC. 1981. Reactivity of a monoclonal antibody with human ovarian carcinoma. J Clin Invest 68(5):1331-7.

Bauerschlag DO, Ammerpohl O, Brautigam K, Schem C, Lin Q, Weigel MT, Hilpert F, Arnold N, Maass N, Meinhold-Heerlein I, et al. 2011. Progression-free survival in ovarian cancer is reflected in epigenetic DNA methylation profiles. Oncology 80(1-2):12-20.

Blagden SP. 2015. Harnessing pandemonium: The clinical implications of tumor heterogeneity in ovarian cancer. Front Oncol 5:149.

Boone JD, Dobbin ZC, Straughn JM,Jr, Buchsbaum DJ. 2015. Ovarian and cervical cancer patient derived xenografts: The past, present, and future. Gynecol Oncol 138(2):486-91.

Bossard C, Busson M, Vindrieux D, Gaudin F, Machelon V, Brigitte M, Jacquard C, Pillon A, Balaguer P, Balabanian K, et al. 2012. Potential role of estrogen receptor beta as a tumor suppressor of epithelial ovarian cancer. PLoS One 7(9):e44787.

Bourgeois DL, Kabarowski KA, Porubsky VL, Kreeger PK. 2015. High-grade serous ovarian cancer cell lines exhibit heterogeneous responses to growth factor stimulation. Cancer Cell Int 15:112,015-0263-4. eCollection 2015.

Braem MG, Onland-Moret NC, van den Brandt PA, Goldbohm RA, Peeters PH, Kruitwagen RF, Schouten LJ. 2010. Reproductive and hormonal factors in association with ovarian cancer in the netherlands cohort study. Am J Epidemiol 172(10):1181-9.

Cai W, Kramarova TV, Berg P, Korbonits M, Pongratz I. 2011. The immunophilin-like protein XAP2 is a negative regulator of estrogen signaling through interaction with estrogen receptor alpha. PLoS One 6(10):e25201.

Callahan MJ, Crum CP, Medeiros F, Kindelberger DW, Elvin JA, Garber JE, Feltmate CM, Berkowitz RS, Muto MG. 2007. Primary fallopian tube malignancies in BRCA-positive women undergoing surgery for ovarian cancer risk reduction. J Clin Oncol 25(25):3985-90.

Canadian Cancer Society. 2015. Canadian cancer Society's advisory committee on cancer statistics. Canadian Cancer Statistics .

Cancer Genome Atlas Research Network. 2011. Integrated genomic analyses of ovarian carcinoma. Nature 474(7353):609-15.

Cavalieri E, Chakravarti D, Guttenplan J, Hart E, Ingle J, Jankowiak R, Muti P, Rogan E, Russo J, Santen R, et al. 2006. Catechol estrogen quinones as initiators of breast and other human cancers: Implications for biomarkers of susceptibility and cancer prevention. Biochim Biophys Acta 1766(1):63-78.

Cekanova M and Rathore K. 2014. Animal models and therapeutic molecular targets of cancer: Utility and limitations. Drug Des Devel Ther 8:1911-21.

Celik C, Gezginc K, Aktan M, Acar A, Yaman ST, Gungor S, Akyurek C. 2004. Effects of ovulation induction on ovarian morphology: An animal study. Int J Gynecol Cancer 14(4):600-6.

Chakravarti S, Collins WP, Forecast JD, Newton JR, Oram DH, Studd JW. 1976. Hormonal profiles after the menopause. Br Med J 2(6039):784-7.

Chand AL, kConFab, Simpson ER, Clyne CD. 2009. Aromatase expression is increased in BRCA1 mutation carriers. BMC Cancer 9:148,2407-9-148.

Chand AL, Wijayakumara DD, Knower KC, Herridge KA, Howard TL, Lazarus KA, Clyne CD. 2012. The orphan nuclear receptor LRH-1 and ERalpha activate GREB1 expression to induce breast cancer cell proliferation. PLoS One 7(2):e31593.

Chao KC, Wang PH, Chang CC, Yen MS, Chi CW. 2013. The role of estrogen in the survival of ovarian tumors--a study of the human ovarian adenocarcinoma cell lines OC-117-VGH and OVCAR3. J Chin Med Assoc 76(2):63-70.

Chen X and Feng Y. 2003. Effect of progesterone combined with chemotherapy on epithelial ovarian cancer. Chin Med J (Engl) 116(3):388-91.

Chene G, Lamblin G, Le Bail-Carval K, Chabert P, Bakrin N, Mellier G. 2014. Early preinvasive lesions in ovarian cancer Biomed Res Int 2014:639252.

Chene G, Penault-Llorca F, Le Bouedec G, Mishellany F, Dauplat MM, Jaffeux P, Aublet-Cuvelier B, Pouly JL, Dechelotte P, Dauplat J. 2009. Ovarian epithelial dysplasia and prophylactic oophorectomy for genetic risk. Int J Gynecol Cancer 19(1):65-72.

Chien CH, Wang FF, Hamilton TC. 1994. Transcriptional activation of c-myc proto-oncogene by estrogen in human ovarian cancer cells. Mol Cell Endocrinol 99(1):11-9.

Chodankar R, Kwang S, Sangiorgi F, Hong H, Yen HY, Deng C, Pike MC, Shuler CF, Maxson R, Dubeau L. 2005. Cell-nonautonomous induction of ovarian and uterine serous cystadenomas in mice lacking a functional Brca1 in ovarian granulosa cells. Curr Biol 15(6):561-5.

Choi JH, Wong AS, Huang HF, Leung PC. 2007. Gonadotropins and ovarian cancer. Endocr Rev 28(4):440-61.

Choi KC, Kang SK, Tai CJ, Auersperg N, Leung PC. 2001. Estradiol up-regulates antiapoptotic bcl-2 messenger ribonucleic acid and protein in tumorigenic ovarian surface epithelium cells. Endocrinology 142(6):2351-60.

Cibula D, Widschwendter M, Zikan M, Dusek L. 2011. Underlying mechanisms of ovarian cancer risk reduction after tubal ligation. Acta Obstet Gynecol Scand 90(6):559-63.

Colgan TJ, Murphy J, Cole DE, Narod S, Rosen B. 2001. Occult carcinoma in prophylactic oophorectomy specimens: Prevalence and association with BRCA germline mutation status. Am J Surg Pathol 25(10):1283-9.

Collaborative Group on Epidemiological Studies of Ovarian Cancer, Beral V, Doll R, Hermon C, Peto R, Reeves G. 2008. Ovarian cancer and oral contraceptives: Collaborative reanalysis of data from 45 epidemiological studies including 23,257 women with ovarian cancer and 87,303 controls. Lancet 371(9609):303-14.

Collaborative Group On Epidemiological Studies Of Ovarian Cancer, Beral V, Gaitskell K, Hermon C, Moser K, Reeves G, Peto R. 2015. Menopausal hormone use and ovarian cancer risk: Individual participant meta-analysis of 52 epidemiological studies. Lancet 385(9980):1835-42.

Cramer DW and Welch WR. 1983. Determinants of ovarian cancer risk. II. inferences regarding pathogenesis. J Natl Cancer Inst 71(4):717-21.

Daly MB, Pilarski R, Axilbund JE, Berry M, Buys SS, Crawford B, Farmer M, Friedman S, Garber JE, Khan S, et al. 2016. Genetic/Familial high-risk assessment: Breast and ovarian, version 2.2015. J Natl Compr Canc Netw 14(2):153-62.

Deschenes J, Bourdeau V, White JH, Mader S. 2007. Regulation of GREB1 transcription by estrogen receptor alpha through a multipartite enhancer spread over 20 kb of upstream flanking sequences J Biol Chem 282(24):17335-9.

Diergaarde B and Kurta ML. 2014. Use of fertility drugs and risk of ovarian cancer. Curr Opin Obstet Gynecol 26(3):125-9.

Ding JX, Feng YJ, Yao LQ, Yu M, Jin HY, Yin LH. 2006. The reinforcement of invasion in epithelial ovarian cancer cells by 17 beta-estradiol is associated with up-regulation of snail. Gynecol Oncol 103(2):623-30.

Dinulescu DM, Ince TA, Quade BJ, Shafer SA, Crowley D, Jacks T. 2005. Role of K-ras and pten in the development of mouse models of endometriosis and endometrioid ovarian cancer. Nat Med 11(1):63-70.

Domcke S, Sinha R, Levine DA, Sander C, Schultz N. 2013. Evaluating cell lines as tumour models by comparison of genomic profiles. Nat Commun 4:2126.

Dragani TA. 2003. 10 years of mouse cancer modifier loci: Human relevance. Cancer Res 63(12):3011-8.

Dubuc PU. 1985. Effects of estrogen on food intake, body weight, and temperature of male and female obese mice. Proc Soc Exp Biol Med 180(3):468-73.

Dunbier AK, Anderson H, Ghazoui Z, Folkerd EJ, A'hern R, Crowder RJ, Hoog J, Smith IE, Osin P, Nerurkar A, et al. 2010. Relationship between plasma estradiol levels and estrogen-responsive gene expression in estrogen receptor-positive breast cancer in postmenopausal women. J Clin Oncol 28(7):1161-7.

Ebell MH, Culp MB, Radke TJ. 2016. A systematic review of symptoms for the diagnosis of ovarian cancer. Am J Prev Med 50(3):384-94.

Faber MT, Kjaer SK, Dehlendorff C, Chang-Claude J, Andersen KK, Hogdall E, Webb PM, Jordan SJ, Australian Cancer Study (Ovarian Cancer), Australian Ovarian Cancer Study Group, et al. 2013. Cigarette smoking and risk of ovarian cancer: A pooled analysis of 21 case-control studies. Cancer Causes Control 24(5):989-1004.

Falconer H, Yin L, Gronberg H, Altman D. 2015. Ovarian cancer risk after salpingectomy: A nationwide population-based study. J Natl Cancer Inst 107(2):10.1093/jnci/dju410. Print 2015 Feb.

Fathalla MF. 1971. Incessant ovulation--a factor in ovarian neoplasia? Lancet 2(7716):163.

Finch A, Beiner M, Lubinski J, Lynch HT, Moller P, Rosen B, Murphy J, Ghadirian P, Friedman E, Foulkes WD, et al. 2006. Salpingo-oophorectomy and the risk of ovarian, fallopian tube, and peritoneal cancers in women with a BRCA1 or BRCA2 mutation. Jama 296(2):185-92.

Flesken-Nikitin A, Choi KC, Eng JP, Shmidt EN, Nikitin AY. 2003. Induction of carcinogenesis by concurrent inactivation of p53 and Rb1 in the mouse ovarian surface epithelium. Cancer Res 63(13):3459-63.

Fung JN, Holdsworth-Carson SJ, Sapkota Y, Zhao ZZ, Jones L, Girling JE, Paiva P, Healey M, Nyholt DR, Rogers PA, et al. 2015. Functional evaluation of genetic variants associated with endometriosis near GREB1. Hum Reprod 30(5):1263-75.

Gaikwad NW, Yang L, Muti P, Meza JL, Pruthi S, Ingle JN, Rogan EG, Cavalieri EL. 2008. The molecular etiology of breast cancer: Evidence from biomarkers of risk. Int J Cancer 122(9):1949-57.

Garson K, Gamwell LF, Pitre EM, Vanderhyden BC. 2012. Technical challenges and limitations of current mouse models of ovarian cancer. J Ovarian Res 5(1):39,2215-5-39.

George SH and Shaw P. 2014. BRCA and early events in the development of serous ovarian cancer. Front Oncol 4:5.

Gery S, Xie D, Yin D, Gabra H, Miller C, Wang H, Scott D, Yi WS, Popoviciu ML, Said JW, et al. 2005. Ovarian carcinomas: CCN genes are aberrantly expressed and CCN1 promotes proliferation of these cells. Clin Cancer Res 11(20):7243-54.

Ghosh MG, Thompson DA, Weigel RJ. 2000. PDZK1 and GREB1 are estrogen-regulated genes expressed in hormone-responsive breast cancer. Cancer Res 60(22):6367-75.

Godwin AK, Testa JR, Handel LM, Liu Z, Vanderveer LA, Tracey PA, Hamilton TC. 1992. Spontaneous transformation of rat ovarian surface epithelial cells: Association with cytogenetic changes and implications of repeated ovulation in the etiology of ovarian cancer. J Natl Cancer Inst 84(8):592-601.

Goodman MT, McDuffie K, Kolonel LN, Terada K, Donlon TA, Wilkens LR, Guo C, Le Marchand L. 2001. Case-control study of ovarian cancer and polymorphisms in genes involved in catecholestrogen formation and metabolism. Cancer Epidemiol Biomarkers Prev 10(3):209-16.

Goodspeed A, Heiser LM, Gray JW, Costello JC. 2016. Tumor-derived cell lines as molecular models of cancer pharmacogenomics. Mol Cancer Res 14(1):3-13.

Gorski JJ, Kennedy RD, Hosey AM, Harkin DP. 2009. The complex relationship between BRCA1 and ERalpha in hereditary breast cancer. Clin Cancer Res 15(5):1514-8.

Gotfredson GS and Murdoch WJ. 2007. Morphologic responses of the mouse ovarian surface epithelium to ovulation and steroid hormonal milieu. Exp Biol Med (Maywood) 232(2):277-80.

Goyeneche AA, Caron RW, Telleria CM. 2007. Mifepristone inhibits ovarian cancer cell growth in vitro and in vivo. Clin Cancer Res 13(11):3370-9.

Green A, Purdie D, Bain C, Siskind V, Russell P, Quinn M, Ward B. 1997. Tubal sterilisation, hysterectomy and decreased risk of ovarian cancer. survey of women's health study group. Int J Cancer 71(6):948-51.

Gupta N, Grebhardt S, Mayer D. 2012. Janus kinase 2--a novel negative regulator of estrogen receptor alpha function. Cell Signal 24(1):151-61.

Gupta PB, Proia D, Cingoz O, Weremowicz J, Naber SP, Weinberg RA, Kuperwasser C. 2007. Systemic stromal effects of estrogen promote the growth of estrogen receptor-negative cancers. Cancer Res 67(5):2062-71.

Haakensen VD, Bjoro T, Luders T, Riis M, Bukholm IK, Kristensen VN, Troester MA, Homen MM, Ursin G, Borresen-Dale AL, et al. 2011. Serum estradiol levels associated with specific gene expression patterns in normal breast tissue and in breast carcinomas. BMC Cancer 11:332,2407-11-332.

Hales KH, Speckman SC, Kurrey NK, Hales DB. 2014. Uncovering molecular events associated with the chemosuppressive effects of flaxseed: A microarray analysis of the laying hen model of ovarian cancer. BMC Genomics 15:709,2164-15-709.

Hamilton TC, Young RC, McKoy WM, Grotzinger KR, Green JA, Chu EW, Whang-Peng J, Rogan AM, Green WR, Ozols RF. 1983. Characterization of a human ovarian carcinoma cell line (NIH:OVCAR-3) with androgen and estrogen receptors. Cancer Res 43(11):5379-89.

Han Z, Feng J, Hong Z, Chen L, Li W, Liao S, Wang X, Ji T, Wang S, Ma D, et al. 2013. Silencing of the STAT3 signaling pathway reverses the inherent and induced chemoresistance of human ovarian cancer cells. Biochem Biophys Res Commun 435(2):188-94.

Haynes BP, Viale G, Galimberti V, Rotmensz N, Gibelli B, A'Hern R, Smith IE, Dowsett M. 2013. Expression of key oestrogen-regulated genes differs substantially across the menstrual cycle in oestrogen receptor-positive primary breast cancer. Breast Cancer Res Treat 138(1):157-65.

Helzlsouer KJ, Alberg AJ, Gordon GB, Longcope C, Bush TL, Hoffman SC, Comstock GW. 1995. Serum gonadotropins and steroid hormones and the development of ovarian cancer. Jama 274(24):1926-30.

Hewitt SC, Kissling GE, Fieselman KE, Jayes FL, Gerrish KE, Korach KS. 2010. Biological and biochemical consequences of global deletion of exon 3 from the ER alpha gene. Faseb j 24(12):4660-7.

Hnatyszyn HJ, Liu M, Hilger A, Herbert L, Gomez-Fernandez CR, Jorda M, Thomas D, Rae JM, El-Ashry D, Lippman ME. 2010. Correlation of GREB1 mRNA with protein expression in breast cancer: Validation of a novel GREB1 monoclonal antibody. Breast Cancer Res Treat 122(2):371-80.

Ho SM. 2003. Estrogen, progesterone and epithelial ovarian cancer. Reprod Biol Endocrinol 1:73.

Hodgkinson KM and Vanderhyden BC. 2014. Consideration of GREB1 as a potential therapeutic target for hormone-responsive or endocrine-resistant cancers. Expert Opin Ther Targets 18(9):1065-76.

Hong H, Yen HY, Brockmeyer A, Liu Y, Chodankar R, Pike MC, Stanczyk FZ, Maxson R, Dubeau L. 2010. Changes in the mouse estrus cycle in response to BRCA1 inactivation suggest a potential link between risk factors for familial and sporadic ovarian cancer. Cancer Res 70(1):221-8.

Houghton SC, Reeves KW, Hankinson SE, Crawford L, Lane D, Wactawski-Wende J, Thomson CA, Ockene JK, Sturgeon SR. 2014. Perineal powder use and risk of ovarian cancer J Natl Cancer Inst 106(9):10.1093/jnci/dju208. Print 2014 Sep.

Hoyer PB and Sipes IG. 2007. Development of an animal model for ovotoxicity using 4-vinylcyclohexene: A case study. Birth Defects Res B Dev Reprod Toxicol 80(2):113-25.

Hu Y, Ghosh S, Amleh A, Yue W, Lu Y, Katz A, Li R. 2005. Modulation of aromatase expression by BRCA1: A possible link to tissue-specific tumor suppression. Oncogene 24(56):8343-8.

Hua K, Feng W, Cao Q, Zhou X, Lu X, Feng Y. 2008. Estrogen and progestin regulate metastasis through the PI3K/AKT pathway in human ovarian cancer. Int J Oncol 33(5):959-67.

Hua K, Din J, Cao Q, Feng W, Zhang Y, Yao L, Huang Y, Zhao Y, Feng Y. 2009. Estrogen and progestin regulate HIF-1alpha expression in ovarian cancer cell lines via the activation of akt signaling transduction pathway. Oncol Rep 21(4):893-8.

Hua W, Christianson T, Rougeot C, Rochefort H, Clinton GM. 1995. SKOV3 ovarian carcinoma cells have functional estrogen receptor but are growth-resistant to estrogen and antiestrogens. J Steroid Biochem Mol Biol 55(3-4):279-89.

Hughes P, Marshall D, Reid Y, Parkes H, Gelber C. 2007. The costs of using unauthenticated, over-passaged cell lines: How much more data do we need? Biotechniques 43(5):575, 577,8, 581-2 passim.

Ivarsson K, Sundfeldt K, Brannstrom M, Janson PO. 2001. Production of steroids by human ovarian surface epithelial cells in culture: Possible role of progesterone as growth inhibitor. Gynecol Oncol 82(1):116-21.

Jacobsen BM, Schittone SA, Richer JK, Horwitz KB. 2005. Progesterone-independent effects of human progesterone receptors (PRs) in estrogen receptor-positive breast cancer: PR isoform-specific gene regulation and tumor biology. Mol Endocrinol 19(3):574-87.

Jang JW, Boxer RB, Chodosh LA. 2006. Isoform-specific ras activation and oncogene dependence during MYC- and wnt-induced mammary tumorigenesis. Mol Cell Biol 26(21):8109-21.

Jazaeri AA, Bryant JL, Park H, Li H, Dahiya N, Stoler MH, Ferriss JS, Dutta A. 2011. Molecular requirements for transformation of fallopian tube epithelial cells into serous carcinoma. Neoplasia 13(10):899-911.

Johnson PA and Giles JR. 2013. The hen as a model of ovarian cancer. Nat Rev Cancer 13(6):432-6.

Jonsson JM, Skovbjerg Arildsen N, Malander S, Masback A, Hartman L, Nilbert M, Hedenfalk I. 2015. Sex steroid hormone receptor expression affects ovarian cancer survival. Transl Oncol 8(5):424-33.

Kampan NC, Madondo MT, McNally OM, Quinn M, Plebanski M. 2015. Paclitaxel and its evolving role in the management of ovarian cancer. Biomed Res Int 2015:413076.

Kappeler CJ and Hoyer PB. 2012. 4-vinylcyclohexene diepoxide: A model chemical for ovotoxicity. Syst Biol Reprod Med 58(1):57-62.

Kilkenny C, Browne WJ, Cuthill IC, Emerson M, Altman DG. 2010. Improving bioscience research reporting: The ARRIVE guidelines for reporting animal research. J Pharmacol Pharmacother 1(2):94-9.

Kim HS, Kim TH, Chung HH, Song YS. 2014. Risk and prognosis of ovarian cancer in women with endometriosis: A meta-analysis. Br J Cancer 110(7):1878-90.

Kim J, Coffey DM, Creighton CJ, Yu Z, Hawkins SM, Matzuk MM. 2012. High-grade serous ovarian cancer arises from fallopian tube in a mouse model. Proc Natl Acad Sci U S A 109(10):3921-6.

King SM, Hilliard TS, Wu LY, Jaffe RC, Fazleabas AT, Burdette JE. 2011. The impact of ovulation on fallopian tube epithelial cells: Evaluating three hypotheses connecting ovulation and serous ovarian cancer. Endocr Relat Cancer 18(5):627-42.

Kirilovas D, Schedvins K, Naessen T, Von Schoultz B, Carlstrom K. 2007. Conversion of circulating estrone sulfate to 17beta-estradiol by ovarian tumor tissue: A possible

mechanism behind elevated circulating concentrations of 17beta-estradiol in postmenopausal women with ovarian tumors. Gynecol Endocrinol 23(1):25-8.

Konecny GE, Wang C, Hamidi H, Winterhoff B, Kalli KR, Dering J, Ginther C, Chen HW, Dowdy S, Cliby W, et al. 2014. Prognostic and therapeutic relevance of molecular subtypes in high-grade serous ovarian cancer. J Natl Cancer Inst 106(10):10.1093/jnci/dju249. Print 2014 Oct.

Korch C, Spillman MA, Jackson TA, Jacobsen BM, Murphy SK, Lessey BA, Jordan VC, Bradford AP. 2012. DNA profiling analysis of endometrial and ovarian cell lines reveals misidentification, redundancy and contamination. Gynecol Oncol 127(1):241-8.

Kraemer S, Jaeger WH, Lang N. 2001. Growth regulation effects of gonadotropin induced steroidogenic response in human ovarian cancer. Anticancer Res 21(3B):2005-10.

Kramer S, Leeker M, Jager W. 1998. Gonadotropin levels in ovarian cyst fluids: A predictor of malignancy? Int J Biol Markers 13(3):165-8.

Kurman RJ and Shih I. 2011. Molecular pathogenesis and extraovarian origin of epithelial ovarian cancer--shifting the paradigm. Hum Pathol 42(7):918-31.

Kuroda H, Kohrogi T, Uchida N, Imai I, Terada N, Matsumoto K, Kitamura Y. 1985. Urinary retention induced by estrogen injections in mice: An analytical model. J Urol 134(6):1268-70.

La Marca A, Giulini S, Orvieto R, De Leo V, Volpe A. 2005. Anti-mullerian hormone concentrations in maternal serum during pregnancy. Hum Reprod 20(6):1569-72.

Langdon SP, Crew AJ, Ritchie AA, Muir M, Wakeling A, Smyth JF, Miller WR. 1994. Growth inhibition of oestrogen receptor-positive human ovarian carcinoma by anti-oestrogens in vitro and in a xenograft model. Eur J Cancer 30A(5):682-6.

Langdon SP, Gabra H, Bartlett JM, Rabiaz GJ, Hawkins RA, Tesdale AL, Ritchie AA, Miller WR, Smyth JF. 1998. Functionality of the progesterone receptor in ovarian cancer and its regulation by estrogen. Clin Cancer Res 4(9):2245-51.

Larue L, Dougherty N, Bradl M, Mintz B. 1993. Melanocyte culture lines from tyr-SV40E transgenic mice: Models for the molecular genetic evolution of malignant melanoma. Oncogene 8(3):523-31.

Lau KM, Mok SC, Ho SM. 1999. Expression of human estrogen receptor-alpha and -beta, progesterone receptor, and androgen receptor mRNA in normal and malignant ovarian epithelial cells. Proc Natl Acad Sci U S A 96(10):5722-7.

Laviolette LA, Hodgkinson KM, Minhas N, Perez-Iratxeta C, Vanderhyden BC. 2014. 17beta-estradiol upregulates GREB1 and accelerates ovarian tumor progression in vivo Int J Cancer 135(5):1072-84.

Laviolette LA, Ethier JF, Senterman MK, Devine PJ, Vanderhyden BC. 2011. Induction of a menopausal state alters the growth and histology of ovarian tumors in a mouse model of ovarian cancer. Menopause 18(5):549-57.

Laviolette LA, Garson K, Macdonald EA, Senterman MK, Courville K, Crane CA, Vanderhyden BC. 2010. 17beta-estradiol accelerates tumor onset and decreases survival in a transgenic mouse model of ovarian cancer. Endocrinology 151(3):929-38.

Lee KS, Sugiyama T, Kataoka A, Hirakawa N, Maruuchi T, Nishida T, Yakushiji M. 1992. A study of the role of sex hormones in rat ovarian cancer. Kurume Med J 39(4):285-90.

Leeper K, Garcia R, Swisher E, Goff B, Greer B, Paley P. 2002. Pathologic findings in prophylactic oophorectomy specimens in high-risk women. Gynecol Oncol 87(1):52-6.

Li HH, Zhao YJ, Li Y, Dai CF, Jobe SO, Yang XS, Li XF, Patankar MS, Magness RR, Zheng J. 2014. Estradiol 17beta and its metabolites stimulate cell proliferation and antagonize ascorbic acid-suppressed cell proliferation in human ovarian cancer cells. Reprod Sci 21(1):102-11.

Lim D and Oliva E. 2013. Precursors and pathogenesis of ovarian carcinoma. Pathology 45(3):229-42.

Lippman ME, Rae JM, Chinnaiyan AM. 2008. An expression signature of estrogen-regulated genes predicts disease-free survival in tamoxifen-treated patients better than progesterone receptor status. Trans Am Clin Climatol Assoc 119:77,90; discussion 90-2.

Liu H, Yan Y, Wen H, Jiang X, Cao X, Zhang G, Liu G. 2014. A novel estrogen receptor GPER mediates proliferation induced by 17beta-estradiol and selective GPER agonist G-1 in estrogen receptor alpha (ERalpha)-negative ovarian cancer cells. Cell Biol Int 38(5):631-8.

Lohff JC, Christian PJ, Marion SL, Arrandale A, Hoyer PB. 2005. Characterization of cyclicity and hormonal profile with impending ovarian failure in a novel chemical-induced mouse model of perimenopause. Comp Med 55(6):523-7.

Lu JJ, Zheng Y, Kang X, Yuan JM, Lauchlan SC, Pike MC, Zheng W. 2000. Decreased luteinizing hormone receptor mRNA expression in human ovarian epithelial cancer. Gynecol Oncol 79(2):158-68.

Lu Z, Zhang Y, Yan X, Chen Y, Tao X, Wang J, Jia N, Lyu T, Wang J, Ding J, et al. 2014. Estrogen stimulates the invasion of ovarian cancer cells via activation of the PI3K/AKT pathway and regulation of its downstream targets ecadherin and alphaactinin4. Mol Med Rep 10(5):2433-40.

Luan NN, Wu QJ, Gong TT, Vogtmann E, Wang YL, Lin B. 2013. Breastfeeding and ovarian cancer risk: A meta-analysis of epidemiologic studies. Am J Clin Nutr 98(4):1020-31.

Mabuchi S, Kuroda H, Takahashi R, Sasano T. 2015. The PI3K/AKT/mTOR pathway as a therapeutic target in ovarian cancer. Gynecol Oncol 137(1):173-9.

Mabuchi S, Ohmichi M, Kimura A, Nishio Y, Arimoto-Ishida E, Yada-Hashimoto N, Tasaka K, Murata Y. 2004. Estrogen inhibits paclitaxel-induced apoptosis via the phosphorylation of apoptosis signal-regulating kinase 1 in human ovarian cancer cell lines. Endocrinology 145(1):49-58.

Macleod KF and Jacks T. 1999. Insights into cancer from transgenic mouse models. J Pathol 187(1):43-60.

McCloskey CW, Goldberg RL, Carter LE, Gamwell LF, Al-Hujaily EM, Collins O, Macdonald EA, Garson K, Daneshmand M, Carmona E, et al. 2014. A new spontaneously transformed syngeneic model of high-grade serous ovarian cancer with a tumor-initiating cell population. Front Oncol 4:53.

McDaniel AS, Stall JN, Hovelson DH, Cani AK, Liu CJ, Tomlins SA, Cho KR. 2015. Next-generation sequencing of tubal intraepithelial carcinomas. JAMA Oncol 1(8):1128-32.

McDonnel AC, Van Kirk EA, Isaak DD, Murdoch WJ. 2005. Effects of progesterone on ovarian tumorigenesis in xenografted mice. Cancer Lett 221(1):49-53.

Medeiros F, Muto MG, Lee Y, Elvin JA, Callahan MJ, Feltmate C, Garber JE, Cramer DW, Crum CP. 2006. The tubal fimbria is a preferred site for early adenocarcinoma in women with familial ovarian cancer syndrome. Am J Surg Pathol 30(2):230-6.

Modugno F and Ovarian Cancer and High-Risk Women Symposium Presenters. 2003. Ovarian cancer and high-risk women-implications for prevention, screening, and early detection. Gynecol Oncol 91(1):15-31.

Mohammed H, D'Santos C, Serandour AA, Ali HR, Brown GD, Atkins A, Rueda OM, Holmes KA, Theodorou V, Robinson JL, et al. 2013. Endogenous purification reveals GREB1 as a key estrogen receptor regulatory factor. Cell Rep 3(2):342-9.

Mullany LK, Liu Z, Wong KK, Deneke V, Ren YA, Herron A, Richards JS. 2014. Tumor repressor protein 53 and steroid hormones provide a new paradigm for ovarian cancer metastases Mol Endocrinol 28(1):127-37.

Mullany LK, Fan HY, Liu Z, White LD, Marshall A, Gunaratne P, Anderson ML, Creighton CJ, Xin L, Deavers M, et al. 2011. Molecular and functional characteristics of ovarian surface epithelial cells transformed by KrasG12D and loss of pten in a mouse model in vivo. Oncogene 30(32):3522-36.

Mungenast F and Thalhammer T. 2014. Estrogen biosynthesis and action in ovarian cancer. Front Endocrinol (Lausanne) 5:192.

Murdoch WJ, Van Kirk EA, Isaak DD, Shen Y. 2008. Progesterone facilitates cisplatin toxicity in epithelial ovarian cancer cells and xenografts. Gynecol Oncol 110(2):251-5.

Nagy JA, Masse EM, Herzberg KT, Meyers MS, Yeo KT, Yeo TK, Sioussat TM, Dvorak HF. 1995. Pathogenesis of ascites tumor growth: Vascular permeability factor, vascular hyperpermeability, and ascites fluid accumulation. Cancer Res 55(2):360-8.

Nash JD, Ozols RF, Smyth JF, Hamilton TC. 1989. Estrogen and anti-estrogen effects on the growth of human epithelial ovarian cancer in vitro. Obstet Gynecol 73(6):1009-16.

Ness RB and Cottreau C. 1999. Possible role of ovarian epithelial inflammation in ovarian cancer. J Natl Cancer Inst 91(17):1459-67.

Ness RB, Cramer DW, Goodman MT, Kjaer SK, Mallin K, Mosgaard BJ, Purdie DM, Risch HA, Vergona R, Wu AH. 2002. Infertility, fertility drugs, and ovarian cancer: A pooled analysis of case-control studies. Am J Epidemiol 155(3):217-24.

Oka T and Schimke RT. 1969. Interaction of estrogen and progesterone in chick oviduct development. I. antagonistic effect of progesterone on estrogen-induced proliferation and differentiation of tubular gland cells. J Cell Biol 41(3):816-31.

Orsulic S, Li Y, Soslow RA, Vitale-Cross LA, Gutkind JS, Varmus HE. 2002. Induction of ovarian cancer by defined multiple genetic changes in a mouse model system. Cancer Cell 1(1):53-62.

Parrott JA, Doraiswamy V, Kim G, Mosher R, Skinner MK. 2001. Expression and actions of both the follicle stimulating hormone receptor and the luteinizing hormone receptor in normal ovarian surface epithelium and ovarian cancer. Mol Cell Endocrinol 172(1-2):213-22.

Parsanejad R, Fields WR, Morgan WT, Bombick BR, Doolittle DJ. 2008. The time course of expression of genes involved in specific pathways in normal human bronchial epithelial cells following exposure to cigarette smoke. Exp Lung Res 34(8):513-30.

Pearce CL, Chung K, Pike MC, Wu AH. 2009. Increased ovarian cancer risk associated with menopausal estrogen therapy is reduced by adding a progestin. Cancer 115(3):531-9.

Pellegrini C, Gori I, Achtari C, Hornung D, Chardonnens E, Wunder D, Fiche M, Canny GO. 2012. The expression of estrogen receptors as well as GREB1, c-MYC, and cyclin D1, estrogen-regulated genes implicated in proliferation, is increased in peritoneal endometriosis. Fertil Steril 98(5):1200-8.

Pennington KP, Walsh T, Harrell MI, Lee MK, Pennil CC, Rendi MH, Thornton A, Norquist BM, Casadei S, Nord AS, et al. 2014. Germline and somatic mutations in

homologous recombination genes predict platinum response and survival in ovarian, fallopian tube, and peritoneal carcinomas. Clin Cancer Res 20(3):764-75.

Pepin D, Sosulski A, Zhang L, Wang D, Vathipadiekal V, Hendren K, Coletti CM, Yu A, Castro CM, Birrer MJ, et al. 2015. AAV9 delivering a modified human mullerian inhibiting substance as a gene therapy in patient-derived xenografts of ovarian cancer. Proc Natl Acad Sci U S A 112(32):E4418-27.

Perets R, Wyant GA, Muto KW, Bijron JG, Poole BB, Chin KT, Chen JY, Ohman AW, Stepule CD, Kwak S, et al. 2013. Transformation of the fallopian tube secretory epithelium leads to high-grade serous ovarian cancer in brca;Tp53;pten models. Cancer Cell 24(6):751-65.

Perez-Stable C, Altman NH, Mehta PP, Deftos LJ, Roos BA. 1997. Prostate cancer progression, metastasis, and gene expression in transgenic mice. Cancer Res 57(5):900-6.

Perniconi SE, Simoes Mde J, Simoes Rdos S, Haidar MA, Baracat EC, Soares JM,Jr. 2008. Proliferation of the superficial epithelium of ovaries in senile female rats following oral administration of conjugated equine estrogens. Clinics (Sao Paulo) 63(3):381-8.

Pipas JM. 2009. SV40: Cell transformation and tumorigenesis. Virology 384(2):294-303.

Plaxe SC, Deligdisch L, Dottino PR, Cohen CJ. 1990. Ovarian intraepithelial neoplasia demonstrated in patients with stage I ovarian carcinoma. Gynecol Oncol 38(3):367-72.

Powell CB, Kenley E, Chen LM, Crawford B, McLennan J, Zaloudek C, Komaromy M, Beattie M, Ziegler J. 2005. Risk-reducing salpingo-oophorectomy in BRCA mutation carriers: Role of serial sectioning in the detection of occult malignancy. J Clin Oncol 23(1):127-32.

Prat J. 2012. New insights into ovarian cancer pathology. Ann Oncol 23 Suppl 10:x111-7.

Rabban JT, Garg K, Crawford B, Chen LM, Zaloudek CJ. 2014. Early detection of high-grade tubal serous carcinoma in women at low risk for hereditary breast and ovarian cancer syndrome by systematic examination of fallopian tubes incidentally removed during benign surgery. Am J Surg Pathol 38(6):729-42.

Rae JM, Johnson MD, Scheys JO, Cordero KE, Larios JM, Lippman ME. 2005. GREB 1 is a critical regulator of hormone dependent breast cancer growth Breast Cancer Res Treat 92(2):141-9.

Rae JM, Johnson MD, Cordero KE, Scheys JO, Larios JM, Gottardis MM, Pienta KJ, Lippman ME. 2006. GREB1 is a novel androgen-regulated gene required for prostate cancer growth Prostate 66(8):886-94.

Rahmioglu N, Nyholt DR, Morris AP, Missmer SA, Montgomery GW, Zondervan KT. 2014. Genetic variants underlying risk of endometriosis: Insights from meta-analysis of eight genome-wide association and replication datasets. Hum Reprod Update .

Reitsma W, de Bock GH, Oosterwijk JC, Bart J, Hollema H, Mourits MJ. 2013. Support of the 'fallopian tube hypothesis' in a prospective series of risk-reducing salpingo-oophorectomy specimens. Eur J Cancer 49(1):132-41.

Ribeiro JR and Freiman RN. 2014. Estrogen signaling crosstalk: Implications for endocrine resistance in ovarian cancer. J Steroid Biochem Mol Biol 143:160-73.

Risch HA. 1998. Hormonal etiology of epithelial ovarian cancer, with a hypothesis concerning the role of androgens and progesterone. J Natl Cancer Inst 90(23):1774-86.

Roby KF, Taylor CC, Sweetwood JP, Cheng Y, Pace JL, Tawfik O, Persons DL, Smith PG, Terranova PF. 2000. Development of a syngeneic mouse model for events related to ovarian cancer. Carcinogenesis 21(4):585-91.

Rodriguez GC, Walmer DK, Cline M, Krigman H, Lessey BA, Whitaker RS, Dodge R, Hughes CL. 1998. Effect of progestin on the ovarian epithelium of macaques: Cancer prevention through apoptosis? J Soc Gynecol Investig 5(5):271-6.

Romero IL, Gordon IO, Jagadeeswaran S, Mui KL, Lee WS, Dinulescu DM, Krausz TN, Kim HH, Gilliam ML, Lengyel E. 2009. Effects of oral contraceptives or a gonadotropin-releasing hormone agonist on ovarian carcinogenesis in genetically engineered mice. Cancer Prev Res (Phila) 2(9):792-9.

Rongvaux A, Willinger T, Martinek J, Strowig T, Gearty SV, Teichmann LL, Saito Y, Marches F, Halene S, Palucka AK, et al. 2014. Development and function of human innate immune cells in a humanized mouse model. Nat Biotechnol 32(4):364-72.

Rose-Hellekant TA, Gilchrist K, Sandgren EP. 2002. Strain background alters mammary gland lesion phenotype in transforming growth factor-alpha transgenic mice. Am J Pathol 161(4):1439-47.

Ruxton GD. 2006. The unequal variance t-test is an underused alternative to student's t-test and the mann-whitney U test Behav Ecol 17(4):688 <last_page> 690.

Sahambi SK, Visser JA, Themmen AP, Mayer LP, Devine PJ. 2008. Correlation of serum anti-mullerian hormone with accelerated follicle loss following 4-vinylcyclohexene diepoxide-induced follicle loss in mice. Reprod Toxicol 26(2):116-22.

Salazar H, Godwin AK, Daly MB, Laub PB, Hogan WM, Rosenblum N, Boente MP, Lynch HT, Hamilton TC. 1996. Microscopic benign and invasive malignant neoplasms and a cancer-prone phenotype in prophylactic oophorectomies. J Natl Cancer Inst 88(24):1810-20.

Salehi F, Dunfield L, Phillips KP, Krewski D, Vanderhyden BC. 2008. Risk factors for ovarian cancer: An overview with emphasis on hormonal factors. J Toxicol Environ Health B Crit Rev 11(3-4):301-21.

Savage KI, Matchett KB, Barros EM, Cooper KM, Irwin GW, Gorski JJ, Orr KS, Vohhodina J, Kavanagh JN, Madden AF, et al. 2014. BRCA1 deficiency exacerbates estrogen-induced DNA damage and genomic instability. Cancer Res 74(10):2773-84.

Sawada M, Terada N, Wada A, Mori Y, Yamasaki M, Saga T, Endo K. 1990. Estrogen- and androgen-responsive growth of human ovarian adenocarcinoma heterotransplanted into nude mice. Int J Cancer 45(2):359-63.

Schaner ME, Ross DT, Ciaravino G, Sorlie T, Troyanskaya O, Diehn M, Wang YC, Duran GE, Sikic TL, Caldeira S, et al. 2003. Gene expression patterns in ovarian carcinomas. Mol Biol Cell 14(11):4376-86.

Schlosshauer PW, Cohen CJ, Penault-Llorca F, Miranda CR, Bignon YJ, Dauplat J, Deligdisch L. 2003. Prophylactic oophorectomy: A morphologic and immunohistochemical study. Cancer 98(12):2599-606.

Schuler S, Ponnath M, Engel J, Ortmann O. 2013. Ovarian epithelial tumors and reproductive factors: A systematic review. Arch Gynecol Obstet 287(6):1187-204.

Seidman JD, Krishnan J, Yemelyanova A, Vang R. 2015. Incidental serous tubal intraepithelial carcinoma and non-neoplastic conditions of the fallopian tubes in grossly normal adnexa: A clinicopathologic study of 388 completely embedded cases. Int J Gynecol Pathol .

Shaw TJ, Senterman MK, Dawson K, Crane CA, Vanderhyden BC. 2004. Characterization of intraperitoneal, orthotopic, and metastatic xenograft models of human ovarian cancer. Mol Ther 10(6):1032-42.

Sherman-Baust CA, Kuhn E, Valle BL, Shih I, Kurman RJ, Wang TL, Amano T, Ko MS, Miyoshi I, Araki Y, et al. 2014. A genetically engineered ovarian cancer mouse model based on fallopian tube transformation mimics human high-grade serous carcinoma development. J Pathol 233(3):228-37.

Shi WF and Bartlett JS. 2008. Estrogen plays a critical role in AAV2-mediated gene transfer in ovarian cancer. Acta Pharmacol Sin 29(12):1440-50.

Shih IM and Kurman RJ. 2004. P63 expression is useful in the distinction of epithelioid trophoblastic and placental site trophoblastic tumors by profiling trophoblastic subpopulations. Am J Surg Pathol 28(9):1177-83.

Silva EG, Tornos C, Deavers M, Kaisman K, Gray K, Gershenson D. 1998. Induction of epithelial neoplasms in the ovaries of guinea pigs by estrogenic stimulation. Gynecol Oncol 71(2):240-6.

Singh S, Chakravarti D, Edney JA, Hollins RR, Johnson PJ, West WW, Higginbotham SM, Cavalieri EL, Rogan EG. 2005. Relative imbalances in the expression of estrogen-metabolizing enzymes in the breast tissue of women with breast carcinoma. Oncol Rep 14(4):1091-6.

Spillman MA, Manning NG, Dye WW, Sartorius CA, Post MD, Harrell JC, Jacobsen BM, Horwitz KB. 2010. Tissue-specific pathways for estrogen regulation of ovarian cancer growth and metastasis. Cancer Res 70(21):8927-36.

Stewart SL, Querec TD, Gruver BN, O'Hare B, Babb JS, Patriotis C. 2004. Gonadotropin and steroid hormones stimulate proliferation of the rat ovarian surface epithelium. J Cell Physiol 198(1):119-24.

Stossi F, Barnett DH, Frasor J, Komm B, Lyttle CR, Katzenellenbogen BS. 2004. Transcriptional profiling of estrogen-regulated gene expression via estrogen receptor (ER) alpha or ERbeta in human osteosarcoma cells: Distinct and common target genes for these receptors. Endocrinology 145(7):3473-86.

Sun J, Nawaz Z, Slingerland JM. 2007. Long-range activation of GREB1 by estrogen receptor via three distal consensus estrogen-responsive elements in breast cancer cells Mol Endocrinol 21(11):2651-62.

Sundar S, Neal RD, Kehoe S. 2015. Diagnosis of ovarian cancer. Bmj 351:h4443.

Syed V, Mukherjee K, Godoy-Tundidor S, Ho SM. 2007. Progesterone induces apoptosis in TRAIL-resistant ovarian cancer cells by circumventing c-FLIPL overexpression. J Cell Biochem 102(2):442-52.

Syed V, Ulinski G, Mok SC, Ho SM. 2002. Reproductive hormone-induced, STAT3-mediated interleukin 6 action in normal and malignant human ovarian surface epithelial cells. J Natl Cancer Inst 94(8):617-29.

Syed V, Ulinski G, Mok SC, Yiu GK, Ho SM. 2001. Expression of gonadotropin receptor and growth responses to key reproductive hormones in normal and malignant human ovarian surface epithelial cells. Cancer Res 61(18):6768-76.

Syed V, Zhang X, Lau KM, Cheng R, Mukherjee K, Ho SM. 2005. Profiling estrogen-regulated gene expression changes in normal and malignant human ovarian surface epithelial cells. Oncogene 24(55):8128-43.

Symeonides S and Gourley C. 2015. Ovarian cancer molecular stratification and tumor heterogeneity: A necessity and a challenge. Front Oncol 5:229.

Symonds DA, Merchenthaler I, Flaws JA. 2008. Methoxychlor and estradiol induce oxidative stress DNA damage in the mouse ovarian surface epithelium. Toxicol Sci 105(1):182-7.

Szabova L, Bupp S, Kamal M, Householder DB, Hernandez L, Schlomer JJ, Baran ML, Yi M, Stephens RM, Annunziata CM, et al. 2014. Pathway-specific engineered mouse allograft models functionally recapitulate human serous epithelial ovarian cancer. PLoS One 9(4):e95649.

Szabova L, Yin C, Bupp S, Guerin TM, Schlomer JJ, Householder DB, Baran ML, Yi M, Song Y, Sun W, et al. 2012. Perturbation of rb, p53, and Brca1 or Brca2 cooperate in inducing metastatic serous epithelial ovarian cancer. Cancer Res 72(16):4141-53.

Tan S, Ding K, Li R, Zhang W, Li G, Kong X, Qian P, Lobie PE, Zhu T. 2014. Identification of miR-26 as a key mediator of estrogen stimulated cell proliferation by targeting CHD1, GREB1 and KPNA2. Breast Cancer Res 16(2):R40.

Terry KL, Karageorgi S, Shvetsov YB, Merritt MA, Lurie G, Thompson PJ, Carney ME, Weber RP, Akushevich L, Lo-Ciganic WH, et al. 2013. Genital powder use and risk of ovarian cancer: A pooled analysis of 8,525 cases and 9,859 controls. Cancer Prev Res (Phila) 6(8):811-21.

Thompson AM, Steel CM, Foster ME, Kerr D, Paterson D, Deane D, Hawkins RA, Carter DC, Evans HJ. 1990. Gene expression in oestrogen-dependent human breast cancer xenograft tumours. Br J Cancer 62(1):78-84.

Tirodkar TS, Budiu RA, Elishaev E, Zhang L, Mony JT, Brozick J, Edwards RP, Vlad AM. 2014. MUC1 positive, kras and pten driven mouse gynecologic tumors replicate human tumors and vary in survival and nuclear grade based on anatomical location. PLoS One 9(7):e102409.

Tothill RW, Tinker AV, George J, Brown R, Fox SB, Lade S, Johnson DS, Trivett MK, Etemadmoghadam D, Locandro B, et al. 2008. Novel molecular subtypes of serous and endometrioid ovarian cancer linked to clinical outcome. Clin Cancer Res 14(16):5198-208.

Vercellini P, Crosignani P, Somigliana E, Vigano P, Buggio L, Bolis G, Fedele L. 2011. The 'incessant menstruation' hypothesis: A mechanistic ovarian cancer model with implications for prevention. Hum Reprod 26(9):2262-73.

Verhage HG, Mavrogianis PA, Boice ML, Li W, Fazleabas AT. 1990. Oviductal epithelium of the baboon: Hormonal control and the immuno-gold localization of oviduct-specific glycoproteins. Am J Anat 187(1):81-90.

Walker SE, McMurray RW, Besch-Williford CL, Keisler DH. 1992. Premature death with bladder outlet obstruction and hyperprolactinemia in new zealand black X new zealand white mice treated with ethinyl estradiol and 17 beta-estradiol. Arthritis Rheum 35(11):1387-92.

Walsh CS. 2015. Two decades beyond BRCA1/2: Homologous recombination, hereditary cancer risk and a target for ovarian cancer therapy. Gynecol Oncol 137(2):343-50.

Wang X, Huang C, Sun B, Gu Y, Cui Y, Zhao X, Li Y, Zhang S. 2010. The effect of high gravidity on the carcinogenesis of mammary gland in TA2 mice. Am J Reprod Immunol 63(5):396-409.

Wang Y, Mang M, Wang Y, Wang L, Klein R, Kong B, Zheng W. 2015. Tubal origin of ovarian endometriosis and clear cell and endometrioid carcinoma. Am J Cancer Res 5(3):869-79.

Wang Y, Qu Y, Zhang XL, Xing J, Niu XL, Chen X, Li ZM. 2014. Autocrine production of interleukin-6 confers ovarian cancer cells resistance to tamoxifen via ER isoforms and SRC-1. Mol Cell Endocrinol 382(2):791-803.

Wardell JR, Hodgkinson KM, Binder AK, Seymour KA, Korach KS, Vanderhyden BC, Freiman RN. 2013. Estrogen responsiveness of the TFIID subunit TAF4B in the normal mouse ovary and in ovarian tumors. Biol Reprod 89(5):116.

Webb PM. 2015. Environmental (nongenetic) factors in gynecological cancers: Update and future perspectives. Future Oncol 11(2):295-307.

Weroha SJ, Becker MA, Enderica-Gonzalez S, Harrington SC, Oberg AL, Maurer MJ, Perkins SE, AlHilli M, Butler KA, McKinstry S, et al. 2014. Tumorgrafts as in vivo surrogates for women with ovarian cancer. Clin Cancer Res 20(5):1288-97.

Wethington SL, Park KJ, Soslow RA, Kauff ND, Brown CL, Dao F, Otegbeye E, Sonoda Y, Abu-Rustum NR, Barakat RR, et al. 2013. Clinical outcome of isolated serous tubal intraepithelial carcinomas (STIC). Int J Gynecol Cancer 23(9):1603-11.

Whittemore AS, Harris R, Itnyre J. 1992. Characteristics relating to ovarian cancer risk: Collaborative analysis of 12 US case-control studies. IV. the pathogenesis of epithelial ovarian cancer. collaborative ovarian cancer group. Am J Epidemiol 136(10):1212-20.

Widschwendter M, Rosenthal AN, Philpott S, Rizzuto I, Fraser L, Hayward J, Intermaggio MP, Edlund CK, Ramus SJ, Gayther SA, et al. 2013. The sex hormone system in carriers of BRCA1/2 mutations: A case-control study. Lancet Oncol 14(12):1226-32.

Wilkie TM, Schmidt RA, Baetscher M, Messing A. 1994. Smooth muscle and bone neoplasms in transgenic mice expressing SV40 T antigen. Oncogene 9(10):2889-95.

Wollenhaupt K, Tomek W, Brussow KP, Tiemann U, Viergutz T, Schneider F, Nurnberg G. 2002. Effects of ovarian steroids and epidermal growth factor (EGF) on expression and bioactivation of specific regulators of transcription and translation in oviductal tissue in pigs. Reproduction 123(1):87-96.

Wright JV, Schliesman B, Robinson L. 1999. Comparative measurements of serum estriol, estradiol, and estrone in non-pregnant, premenopausal women; a preliminary investigation. Altern Med Rev 4(4):266-70.

Wright JW, Toth-Fejel S, Stouffer RL, Rodland KD. 2002. Proliferation of rhesus ovarian surface epithelial cells in culture: Lack of mitogenic response to steroid or gonadotropic hormones. Endocrinology 143(6):2198-207.

Wu CH. 1977. Plasma hormones in human gonadotropin induced ovulation. Obstet Gynecol 49(3):308-13.

Wu R, Hendrix-Lucas N, Kuick R, Zhai Y, Schwartz DR, Akyol A, Hanash S, Misek DE, Katabuchi H, Williams BO, et al. 2007. Mouse model of human ovarian endometrioid adenocarcinoma based on somatic defects in the Wnt/beta-catenin and PI3K/Pten signaling pathways. Cancer Cell 11(4):321-33.

Xing D and Orsulic S. 2006. A mouse model for the molecular characterization of brca1-associated ovarian carcinoma. Cancer Res 66(18):8949-53.

Yan Y, Jiang X, Zhao Y, Wen H, Liu G. 2015. Role of GPER on proliferation, migration and invasion in ligand-independent manner in human ovarian cancer cell line SKOV3. Cell Biochem Funct 33(8):552-9.

Yan Y, Liu H, Wen H, Jiang X, Cao X, Zhang G, Liu G. 2013. The novel estrogen receptor GPER regulates the migration and invasion of ovarian cancer cells. Mol Cell Biochem 378(1-2):1-7.

Yang J, Wang Y, Gao Y, Shao J, Zhang XJ, Yao Z. 2009. Reciprocal regulation of 17beta-estradiol, interleukin-6 and interleukin-8 during growth and progression of epithelial ovarian cancer. Cytokine 46(3):382-91.

Yoffou PH, Edjekouane L, Meunier L, Tremblay A, Provencher DM, Mes-Masson AM, Carmona E. 2011. Subtype specific elevated expression of hyaluronidase-1 (HYAL-1) in epithelial ovarian cancer. PLoS One 6(6):e20705.

Zahid M, Beseler CL, Hall JB, LeVan T, Cavalieri EL, Rogan EG. 2014. Unbalanced estrogen metabolism in ovarian cancer. Int J Cancer 134(10):2414-23.

Zhang L, Xiao H, Zhou H, Santiago S, Lee JM, Garon EB, Yang J, Brinkmann O, Yan X, Akin D, et al. 2012. Development of transcriptomic biomarker signature in human saliva to detect lung cancer. Cell Mol Life Sci 69(19):3341-50.

Zheng H, Kavanagh JJ, Hu W, Liao Q, Fu S. 2007. Hormonal therapy in ovarian cancer. Int J Gynecol Cancer 17(2):325-38.

Zheng J, Zhou J, Xie X, Xie B, Lin J, Xu Z, Zhang W. 2014. Estrogen decreases anoikis of ovarian cancer cell line caov-3 through reducing release of Bit1. DNA Cell Biol 33(12):847-53.

Zheng J, Mercado-Uribe I, Rosen DG, Chang B, Liu P, Yang G, Malpica A, Naora H, Auersperg N, Mills GB, et al. 2010. Induction of papillary carcinoma in human ovarian

surface epithelial cells using combined genetic elements and peritoneal microenvironment. Cell Cycle 9(1):140-6.

Zheng W, Magid MS, Kramer EE, Chen YT. 1996. Follicle-stimulating hormone receptor is expressed in human ovarian surface epithelium and fallopian tube. Am J Pathol 148(1):47-53.

Zhou H, Luo MP, Schonthal AH, Pike MC, Stallcup MR, Blumenthal M, Zheng W, Dubeau L. 2002. Effect of reproductive hormones on ovarian epithelial tumors: I. effect on cell cycle activity. Cancer Biol Ther 1(3):300-6.

Zhu J, Lu X, Hua KQ, Sun H, Yu YH, Feng YJ. 2012. Oestrogen receptor alpha mediates 17beta-estradiol enhancement of ovarian cancer cell motility through up-regulation of survivin expression. Arch Gynecol Obstet 286(3):729-37.

Zhu L, Yang Y, Xu P, Zou F, Yan X, Liao L, Xu J, O'Malley BW, Xu Y. 2013. Steroid receptor coactivator-1 mediates estrogenic actions to prevent body weight gain in female mice. Endocrinology 154(1):150-8.

Zhuge Y, Lagman JA, Ansenberger K, Mahon CJ, Daikoku T, Dey SK, Bahr JM, Hales DB. 2009. CYP1B1 expression in ovarian cancer in the laying hen gallusdomesticus. Gynecol Oncol 112(1):171-8.